FABRICATION OF ROBUST (BIO) INTERFACES BASED ON REACTIVE POLYMER FILMS:
SURFACE CONFINEMENT, REACTIVITY AND PATTERN FABRICATION ON MULTIPLE LENGTH SCALES

PROEFSCHRIFT

ter verkrijging van
de graad van doctor aan de Universiteit Twente,
op gezag van de rector magnificus,
prof. dr. W.H.M.Zijm,
volgens besluit van het College voor Promoties
in het openbaar te verdedigen
op donderdag 15 december 2005 om 13:15 uur,

door

Chuan Liang Feng
Geboren op 04 September 1972
te Henan, P. R. China

Dit proefschrift is goedgekeurd door:

Promotor:	Prof. G. J. Vancso
Assistent-promotor:	Dr. H. Schönherr

天道酬勤

This research has been financially supported by the Council for Chemical Sciences of the Netherlands Organization for Scientific Research (CW-NWO), grant 016.002.003.

Fabrication of Robust (Bio)interfaces Based on Reactive Polymer Films: Surface Confinement, Reactivity and Pattern Fabrication on Multiple Length Scales

Ph.D. Thesis
University of Twente
Enschede, the Netherlands

ISBN 90-365-2274-9

Printed by PrintPartners Ipskamp, Enschede, the Netherlands, 2005

Contents

概述

我们知道，生物界面研究的目的是对合成材料与天然生物种类界面的性质和进程的研究。此定义也包括对生物功能表面的设计和修饰。可控制设计的功能生物界面对诊断学、医学移植、人体组织工程和生物电子学和生物仿生学等领域起到了很重要的角色。例如，通过研究细胞在生物功能界面的运动和铺展，我们可以对细胞生物学进行新的研究，对药物输送的新动机和人体组织工程进行全新的调查。因为高灵敏度的生物界面对于基因治疗将是非常的重要，于是怎样寻找高灵敏度的生物界面将是一个很严峻的课题。

因此怎样用方便，重复性的表面修饰方法去得到强大的、功能性的生物界面对于新生物材料的实际应用至关重要。这样对所制成的生物界面提出了若干具体要求：生物分子的选择性地定向固定；被固定的生物分子的活性被高度保持；控制生物分子的非特异吸附；可利用的高密度生物分子固定的空间结构；垂直于界面分子之间间距的可控制性；可靠的基底机械特性；可控制的膜表面的粗糙度和形貌结构；经过修饰可以得到的生物膜图案等等。

在过去的研究中主要采用的是自组装单分子膜方法（SAMs）在各种各样的基底上去固定生物分子，该方法经常被用来发展新的生物界面。例如，由于 SAMs 可控制的结构和组成以及几乎拥有分子级别的分辨率，该方法已被用于仿生自然界分子之间的识别。但是，SAMs 很多内在的特性，比如环境中的稳定性和在各种各样的基底上不能控制的化学与形貌的图案等，将限制其在其它方面的应用。例如，细胞与界面相互作用的研究。此外，SAMs 的二维结构特性也是一个不利的因素，它将限制新的，高度灵敏的生物传感器的发展。

针对传统 SAMs 技术的种种问题，本课题中用聚合物材料替代 SAMs 在固体基底制备生物膜已经引起了极大的关注。这是因为相比于 SAMs 聚合物膜有很多的优点：强大、稳定、可定义的模量以及具有可同时引进形貌和化学图案的独特特征，经过修饰可以得到从 100 微米到 100 纳米范围之内的图案。此外，当生物分子固定时，聚合物中活性官能团的三维结构排列也克服了上面提到的 SAMs 很多内在的限制特性。

为了匹配复杂的生物体系的识别能力，真正的功能化生物界面要求先进的设计和制备，这包括把化学组成控制在100微米到100纳米范围之内的图案。尤其是为了能匹配纳米范围内蛋白质反应和细胞在10到100微米范围内的作用，把形貌和化学图案结合在一起是非常必须的，也是本课题的关键。人们已发现纳米级别的RGD功能化的细胞结合点决定了细胞在含有图案表面上的吸附和铺展。

现在发展小型化的图案主要依赖于“top – down”技术，例如，影印石板术和平板印刷术。在这些技术中，微米接触印刷术是非常有潜力的方法，它能在各种各样的基底上产生生物图案。此外，简单、低成本和灵活性使该技术更加有潜力。人们也意识到制备10到100纳米的图案对将来生物纳米或纳米生物技术领域将起到很重要的作用。这些包括电子、分析化学和纳米束的制

备。但是要制备大范围的纳米尺寸的结构仍旧存在挑战，它将限制纳米技术很多领域的前进。从这个意义上，“bottom-up” 技术在纳米修饰中，将是非常有潜力的工具。在这些方法中，嵌段聚合物在纳米范围之内可控制的自组装已经被利用，它们被广泛的认为是形成有序有机和无机纳米结构的先驱。这对于基础生物研究（例如，细胞生物学）和很多应用（比如高生产量的基因束及组合库扫描）将是有前景的。

在可预见的“bottom-up / top-down”组合方法中，嵌段聚合物的自组装形成的纳米级别有规律的图案及其独特的化学组成可以与扫描探针显微镜联合在一起去控制10到100 纳米之间的局部化学反应。从长远来看，利用聚合物作为平台，基于可控制的表面化学反应和界面有机化学反应，制备高密度的生物束和进行细胞与界面的研究将是有可能的。

针对以上的引用前景，本论文首次提出了反应活性微米平板印刷术的概念，该项技术将有着广泛的工业应用前景，尤其在生物芯片和生物传感器领域。在第六和七章对该方法进行了详细的描述。对必要的生物平台发展在生物技术的潜在应用作了研究，它包括：聚合物膜化学反应的详细分析和理解，限制反应的影响因素，从微米到纳米多重范围尺寸图案的制备。具体包括了对建立在有机和聚合物膜基础之上生物活性表面和界面的性质，表面反应和模板印刷术进行了概述 （第二章），超薄单一聚合物膜和二嵌段聚合物的界面反映的研究（第三章），生物分子在这些反应活性聚合物膜上的固定（第四和五章），利用反应活性微米平板印刷术在聚合物表面制备生物分子图案（第六和七章）。利用二嵌段聚合物的微相分离，对超薄聚合物膜上的纳米修饰进行了研究，用扫描探针技术，可以进行区域选择性修饰并且能够读出生物分子的信息（第八章）。

第二章主要对建立在有机和聚合物膜基础之上的生物活性表面、界面性质、表面反应和模板印刷进行了概述。尤其作为一种很灵活的技术，微米平板印刷术可以用来制备从微米到亚微米级尺寸的模板。这里作为一种“bottom-up”方法，由于利用嵌段聚合物的微相分离的特点可以制备纳米级尺寸的模板，所以对嵌段聚合物也进行了详细的介绍。

我们在第三章对含有虎伯酸基（NHS）单一聚合物在碱性水溶液中和二嵌段聚苯乙烯和丙酰基酯 (PS-b-PtBA)在3 M水溶液中的水解机理进行了系统的研究。结果表明从表面的位阻影响和转换能来分析, 相对于单分子膜来说聚合物膜表面的活性将是大大增加。此外，也详细的分析了聚合物膜表面的高度反应活性和功能团的高密度性。用傅立叶红外光谱学手段，本章队水解反应随着反应温度、膜厚度、热处理时间和聚合物表面化学组成的变化作了调研。结果表明二嵌段聚合物膜的厚度和表面的化学组成对反应速率常数没有影响。

在第四章报道了合成的单聚合物膜可以用来作为活性反应平台，用来高密度地固定生物分子。用傅立叶红外光谱学、X光电子谱(XPS)、荧光显微镜方法和椭圆光度法该聚合物与氨基修饰的各种分子的共价反应被详细的进行了研究。研究发现氨基修饰聚乙二醇（PEG_{500}-NH_2）在聚合物膜表面的共价反应速率要比在单分子膜表面的反应大。更重要的是，单位面积内在聚合物膜上共价的PEG_{500}-NH_2密度要3倍于单位面积内在单分子膜上共价的PEG_{500}-NH_2密度。用表面等离子共振技术，DNA在膜表面高密度的固定也进行了研究。它表明该聚合物对于研究生物分子的

固定提供了一个吸引人而又简单的平台。

为了得到可修饰的生物界面，对PS_{690}-b-$PtBA_{1210}$聚合物膜的详细研究在第五章进行了表述。用XPS和荧光光谱方法对虎伯酸基（NHS）活化的聚丙酰基酯(PtBA)的反应活性、可控制PEG_{500}-NH_2在该种膜上的嫁接密度和生物分子的固定进行了详细的研究。为了证明该二嵌段聚合物膜作为生物界面在将来可能的应用，我们对目标DNA分子和已经固定在膜表面的探针DNA分子的杂交、两种不同细胞 （K562和癌症细胞）与膜的相互作用作了阐述。

用反应活性微米平板印刷术，在含有虎伯酸基（NHS）单聚合物膜上修饰强大的生物分子微米束进行了研究 （第六章）。此方法结合了含有活性功能团的聚合物膜和平板印刷术的多样性及灵活性。用傅立叶红外光谱学，XPS， 荧光显微镜方法和椭圆光度法证明了PEG_{500}-NH_2被成功的从人造橡胶图章上通过共价反应转移到了聚合物膜上。在PEG_{500}-NH_2反应的地方可以阻止生物分子的非特异性吸附。而没有PEG_{500}-NH_2的区域可以被氨基修饰的生物分子有选择地发生化学反应。生物分子微米束制备因此很方便的在两个步骤可以完成。监测出的DNA在该聚合物膜上的成功杂交证明了反应活性微米平板印刷术是很实用的方法，它可为生物分子的固定和放映提供一个强有力的平台。

第七章介绍了用三种不同的平板印刷术方法在PS_{690}-b-$PtBA_{1210}$膜上制备化学修饰的图案, 该图案可以用来去制备(亚)微米级的生物分子的图案。本章也报道了从水溶液中制备多种生物分子共存的图案和生物分子区域选择性固定。用反应活性微米平板印刷术, 我们对区域水解的机理做了详细的调查。此外, 我们发现通过控制三氟丙酸的扩展, 蛋白质的图案尺寸可以很好的被控制.

选择性溶剂引起的PS_{690}-b-$PtBA_{1210}$聚合物膜表面结构的重新组合和生物分子在纳米尺寸选择性固定出现在第八章。用环己希作为选择性溶剂, 可以得到纳米尺寸的PtBA图案。用荧光光谱和原子力显微镜方法直接证明了生物分子在纳米尺寸选择性固定。用反应活性微米平板印刷术技术制备不同尺寸的图案和通过共价反应用扫描探针平板印刷术转移分子到聚合物膜上的可行性也作了详细的介绍。这些结果表明该聚合物膜可作为一种平台来发展高密度的生物束、高密度的信息存储和用来研究细胞与界面的相互作用。

Chapter 1

Reactive Platforms for Controllable Fabrication of Functional (Bio)interfaces

1.1 Scope of Surface Modification for (Bio)Reactive Platforms and Functional (Bio)interfaces

The objectives of biointerface research include investigations of properties of, and processes at, interfaces between synthetic materials on the one hand, and biological species and environments on the other hand. The discipline also includes the design and fabrication of biofunctional surfaces.[1] Well-designed functional biointerfaces play an important role in biosensors and biochips for diagnostics, in medical implants in the human body, in tissue engineering, and also in bioelectronics and in biomimetic materials.[2] For example, through investigating cell movement and spreading on tailored surfaces (biointerfaces), new insights into cell biology may be obtained[3] and new incentives for controlled drug delivery and also applications in the field of tissue engineering can be provided.[4] The search for methods and formats (platforms) for the sensitive detection of biomolecular interactions, such as hybridization reactions between a biosurface-attached single stranded catcher probe oligonucleotide and a complementary oligo- or polynucleotide strand from solution, currently attracts a lot of attention for a number of reasons, originating, e.g., from unsolved questions and problems in gene therapy.[5]

In this context convenient and reproducible surface modification procedures that yield robust, functional biointerfaces are highly desirable. The requirements for obtaining such interfaces include, among others, the orientation-selective immobilization (conjugation) of biomolecules, such as receptors, antibodies, proteins etc., the retention of the biological activity of these immobilized biomolecules, the control (elimination) of non-specific biomolecule (e.g. protein) adsorption, high molecular loading in bio-available configurations, the control of intermolecular distances in the substrate normal direction, defined mechanical properties of underlying substrates, as well as the control of roughness and topographical structures, patterns etc.

Self-assembled monolayer (SAM) approaches,[6] which can produce monomolecular films, have been applied to immobilize biological molecules on a variety of substrates. SAMs have also been successfully used for the development of (in vitro) biosurfaces that can, for instance, mimic naturally occurring molecular recognition processes due to the structural and compositional control in SAMs with almost molecular precision.[7] However, a number of inherent characteristics, such as environmental stability,[8] but also the absent independent control of chemical and topographical patterns *together* with variable substrate moduli, as deemed crucial for cell-surface interaction studies,[9] impose limitations for their application, e.g., in studies of cell-surface interactions. Similarly,

the molecular loading of these 2D systems is limited and thus impairs the development of new highly sensitive biosensors.

As an alternative, the deposition of polymeric materials onto solid substrates receives increasing attention.[10] Compared to SAMs, polymeric thin films have been shown to possess a number of important advantages, such as robustness and stability, and the unique possibility to introduce simultaneously topographic and chemical (compositional) patterns that span the 100 micrometer to sub-100 nm regime, as well as their defined mechanical modulus for various application areas. Thin films based on polymers that incorporate reactive functional groups also provide a quasi 3D geometry that can be further modified by chemical reactions with biomolecules and thereby overcome the mentioned intrinsic limitations of SAMs.[11]

1.2 Chemical and Topographical Pattern Fabrication from Micrometer to Nanometer Length Scales

Truly functional biointerfaces call for advanced design and preparation in order to match the sophisticated recognition ability of biological systems, which includes the control of chemical composition on length scales spanning the 100 micrometer to sub-100 nm regime. Specifically, combined topographic and chemical patterns on surfaces are required in order to match typical spacings of proteins on the nm scale and entire cells at the 10 to 100 micrometer scale. For example, it was found that the distance between RGD[12] functionalized cell-adhesive dots on the nanometer scale may determine cell attachment and spreading on patterned surfaces. These effects have been attributed to the corresponding cellular responses to restricted integrin clustering[13] rather than insufficient number of ligand molecules in the cell-matrix interface.[14]

Current developments to miniaturize patterns rely on “top-down” techniques, such as photolithography[15] and soft lithography.[16,17,18] Among these techniques, microcontact printing (μCP) is one of the promising approaches for producing (bio)chemical patterns on various solid substrates. In applications, such as the development of certain biosensors,[19] the simplicity of the method, as well as the low cost, the flexibility, and the possibility to pattern curved substrates make μCP a very attractive technique to fabricate chemical patterns. Alternative routes have also been opened by unconventional techniques,[20] such as microwriting,[21] micromachining,[22] and dip-pen nanolithography.[23]

It has been realized that the requirement to create patterns in 10 - 100 nm range for future applications is also highly relevant in many other fields outside the bionano- or nanobiotechnology area.[24] These areas include, among others, electronics,[25] analytical chemistry,[26], and preparation of nanoarrays,[27] where the large scale, routine formation of nanometer-sized structures remains a challenge that limits advances in many fields of nanotechnology.

In this sense, “bottom-up” self-assembly approaches are becoming increasingly a viable tool for nanofabrication. In these approaches the controlled, yet spontaneous assembly of complex structures of nanometer dimensions starting from molecular building blocks is being exploited. Among the

various promising materials, block copolymers are widely considered as ideal precursors for the formation of ordered organic, but also inorganic,[28] structures.

In particular, the nanometer scale patterns obtained from block copolymer films can be potentially used to spatially control the deposition of biomolecules in the future (Scheme 1.1), which can be critical for fundamental biological research involving cell biology[29] and for a number of applications, such as high-throughput genomic arrays and combinatorial library screening.[30]

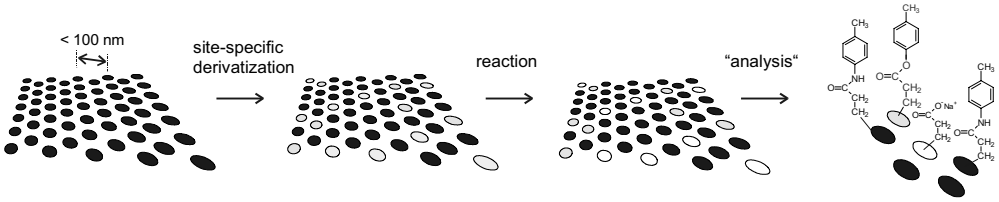

Scheme 1.1. Schematic of a block copolymer-based nanoperiodic array, which can be derivatized at predefined sites and analyzed to yield chemical / compositional information after a screening reaction.

In the envisioned combined bottom-up / top-down approach, the self-assembly of block copolymers and the encoded information regarding domain spacing and periodicity, as well as distinct chemical functionality, would be exploited in conjunction with, e.g., advanced scanning probe microscopy-based lithography approaches to control the local chemical composition of ordered 2D arrays on the 10 - 100 nm scale. Based on the full control of surface chemistry and interfacial organic coupling chemistry on these polymer-derived platforms, array-based screening formats with ultrahigh information content, as well as tailored biointerfaces for cell-surface studies would become possible in the long run.

1.3 Concept of This Thesis

The objective of this Thesis is to provide the necessary platform development, including the detailed analysis and understanding of the surface chemistry, confinement effects, and patterning on multiple length scales from the micrometer down to the sub-100 nm level, as a basis for a block copolymer-based nanometer scale screening array approach sketched in Scheme 1.1. Hence the work described in this Thesis aimed at the synthesis of suitable polymer systems, the investigation of interfacial reactions in confinement on ultrathin homopolymer and diblock copolymer polymer films, the immobilization of (bio)molecules, and the surface fabrication of biomolecular patterns by reactive microcontact printing on these reactive polymer films. Taking advantage of the micro-phase separation of diblock copolymer films, nanofabrication on ultrathin films was investigated to contribute to the future development of a model system that enables one to area-selectively deposit (write) and address (read out) biomolecules using, e.g., scanning probe lithography.

Chapter 2 presents an overview of (bio)reactive surfaces and biointerfaces based on organic and polymeric films, their characterization, as well as surface reactions, and patterning of organic and polymeric films. The μCP technique is introduced owing to its central role as flexible technique for the

production of micrometer and sub-micrometer scale patterns. Block copolymers are also introduced as materials used in a "bottom-up" approach to prepare nanometer scale patterns by exploiting the characteristic microphase separation.

In Chapter 3, the systematic investigation of the effect of confinement on the kinetics of the hydrolysis of poly(*N*-hydroxysuccinimidyl methacrylate) (PNHSMA) and polystyrene-*block*-poly(*tert*-butyl acrylate) (PS_n-b-$PtBA_m$) ultrathin films on oxidized silicon substrates will be treated. It was found that steric crowding in the surface-near region and tightness of the transition state, as concluded from the determination of the activation energies, is less pronounced in both types of polymer films compared to structurally related SAMs (Scheme 1.2). In addition, the polymer films were found to be characterized by a higher reactivity, as well as a higher density of reactive functional groups at and near their surface. By contrast, polymer film thickness, thermal pre-treatment of the films, block copolymer composition for PS_n-b-$PtBA_m$ and local surface composition did not affect the rate constants of hydrolysis.

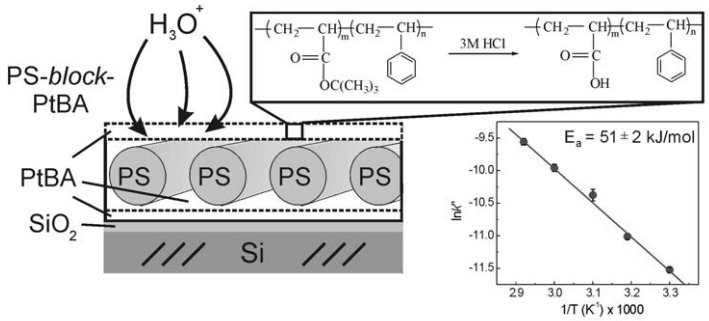

Scheme 1.2. The skin layer of PS_n-b-$PtBA_m$ films can be hydrolyzed under controlled conditions to provide a reactive platform with quasi-3D structure. Temperature controlled kinetics studies revealed the activation energies, among other useful parameters.[31]

Spin-coated ultrathin films of PNHSMA were subsequently investigated as reactive layers for (bio)molecule immobilization, as described in Chapter 4. The high molecular loading of PNHSMA with poly(ethylene glycol) (PEG) and enhanced rate constants were proved by ellipsometry, infrared spectroscopic, and surface plasmon resonance (SPR) measurements. These data indicated that the coupling reactions are not limited to the very surface of the polymer films, but proceed into the surface-near regions of the films in a quasi-3D environment. Thin films of PNHSMA showed robustness under aqueous processing conditions and were successfully applied in the construction of a model sensing surface for bacteria (listeria) and DNA hybridization (Scheme 1.3). Therefore PNHSMA films comprise an attractive and simple platform for the immobilization of biomolecules with high molecular loading.

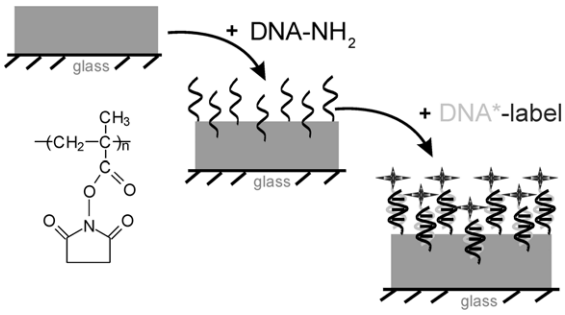

Scheme 1.3. PNHSMA films provide a platform for the immobilization of amino end-functionalized probe DNA with high molecular loading. Using fluorescence spectroscopic and microscopic approaches the hybridization of solution-borne target DNA can be conveniently assessed.[32]

The investigation of PS_{690}-b-$PtBA_{1210}$ films and their derivatization to obtain tailored biointerfaces is presented in Chapter 5. The reactivity of the hydrolyzed and subsequently NHS-activated PtBA skin layer, in particular the controllable loading with amino functionalized PEG, and the immobilization of biologically relevant molecules were studied by infrared, X-ray photoelectron spectroscopy (XPS), and fluorescence microscopy. To demonstrate possible applications of the PS_{690}-b-$PtBA_{1210}$ based platform as biointerfaces, hybridization of target DNA with immobilized probe DNA, as well as the interaction of two different types of cells, i.e. K562[33] and pancreatic cancer cells, on functionalized PS-b-PtBA films were investigated.

In Chapter 6, the fabrication of robust biomolecule microarrays by reactive μCP on spin-coated thin films of PNHSMA is described. Biomolecule microarrays were conveniently fabricated in a 2-step procedure that comprises the μCP transfer of amino functionalized PEG, followed by wet chemical derivatization from buffered solutions (Scheme 1.4). The hybridization of target DNA to immobilized complementary probe DNA in micropatterns proved the concept of reactive μCP on activated polymer films for obtaining robust patterned platforms for biomolecule immobilization and screening.

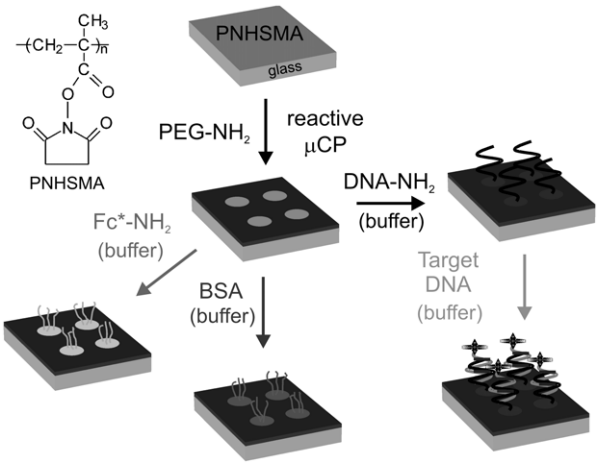

Scheme 1.4. Biomolecule microarrays can be fabricated by subsequent reactive μCP of amino functionalized PEG to yield a passivated matrix with incorporated reactive NHS ester dots, followed by wet chemical derivatization from buffered aqueous solutions.[34]

In Chapter 7, three complementary lithographic approaches to produce chemical patterns on thin PS_{690}-b-$PtBA_{1210}$ films are introduced, which can be expanded to obtain patterns of biomolecules with (sub)micrometer feature sizes. Patterning of multiple types of molecules and area-selective covalent coupling of biomolecules from aqueous media onto PEG-passivated micropatterns were demonstrated. A detailed study of the mechanism of the local hydrolysis using reactive μCP of trifluoroacetic acid showed that faithful pattern replication is only possible using oxidized PDMS stamps on which no liquid acid is present. In addition, it was found that protein patterns with micrometer scale dimensions could be fabricated by using stamps with 15 micrometer feature sizes by controlling the spreading of trifluoroacetic acid. Thus, ultrahigh density patterns can be conveniently fabricated.

The solvent induced reorientation of PS_{690}-b-$PtBA_{1210}$ ultrathin films and subsequently nanodomain-selective immobilization of (bio)molecules were studied in Chapter 8. Using cyclohexane as selective solvent, surfaces that expose PtBA domains in a PS matrix were obtained. The domain-selective immobilization of various (bio)molecules on hydrolyzed and subsequently NHS activated domains in these films was analyzed by fluorescence microscopy and atomic force microscopy force-volume measurements. The simultaneous patterning on multiple length scales by reactive μCP, as well as the demonstration of the feasibility of local delivery by scanning probe lithography and covalent coupling of molecules on chemically activated PS-b-PtBA were achieved. Therefore the groundwork for a future extension of these platforms for the development of array-based screening formats with ultrahigh information content, as well as tailored biointerfaces for cell-surface studies, has been laid.

1.4 References

1 Kasemo, B. *Surf. Sci*. **2002**, *500*, 656.

2 (a) Knoll, W.; Yu, F.; Neumann, T.; Schiller, S.; Naumann, R. *Phys. Chem. Chem. Phys*. **2003**, *5*, 5169. (b) Lynn, D. J.; Freeman, A. R.; Murray, C.; Bradley, D. G. *Genetics* **2005**, *170*, 1189. (c) Lockhart, D. J.; Winzeler, E. A. *Nature* **2000**, *405*, 827. (b) Berhane, B. T.; Limbach, P. A. *Anal. Chem*. **2003**, *75*, 1997. (d) Otsuka, H.; Nagasaki, Y.; Kataoka, K. *Curr. Opin, Coll. Inter. Sci.* **2001**, *6*, 3. (c) Prime, K. L.; Whitesides, G. M. *Science* **1991**, *252*, 1164.

3 Lehnert, D.; Wahrel-Haller, B.; David, C.; Weiland, U.; Ballestrem, C.; Imhof, B. A.; Bastmeyer, M. *J. Cell Sci*. **2004**, *117*, 41.

4 Castner, D.G.; Ratner, B.D. *Surf. Sc.* **2002**, *500*, 28.

5 Agrawel, S.; Iyer, R. P. *Curr. Opin. Biotechnol*. **1995**, *6*, 12.

6 (a) Smith, R. K.; Lewis, P. A.; Weiss, P. S. *Progr. Surf. Sci*. **2004**, *75*, 1. (b) Ulman, A. *Chem. Rev*. **1996**, *96*, 1533.

7 Revell, D. J.; Knight, J. R.; Blyth, D. J.; Haines, A. H.; Russell, D. A. *Langmuir* **1998**, *14*, 4517.

8 Clegg, R. S.; Reed, S. M.; Smith, R. K.; Barron, B. L.; Rear, J. A.; Hutchison, J. E. *Langmuir* **1999**, *15*, 8876.

9 Chen, C. S.; Mrksich, M.; Huang, S.; Whitesides, G. M.; Ingber, D. E. *Science* **1997**, *276*, 1425.

10 (a) Delamarche, E.; Michel, B.; Biebuyck, H. A.; Gerber, C. *Adv. Mater*. **1996**, *8*, 719. (b) Lang, P.; Mekhalif, Z.; Rat, B.; Garnier, F. *J. Electroanal. Chem*. **1998**, *441*, 83. (c) Huseman, M.; Morrisson, M.; Benoit, D.; Frommer, J.; Mate, C. M.; Hinsberg, W. D.; Hedrick, J. L.; Hawker, C. L. *J. Am. Chem. Soc*. **2000**, *122*, 1844.

11 a) Bruening, M. L.; Zhou, Y.; Aguilar, G.; Agee, R.; Bergbreiter, D. E.; Crooks, R. M. *Langmuir* **1997**, *13*, 770. b) Chance, J. J.; Purdy, W. C. *Langmuir* **1997**, *13*, 4487.

12 RGD (Arg-Gly-Asp) is a tripeptide recognition motif that is important in cellular adhesive properties. The tripeptide recognition sequence of arginine, glycine and aspartic acid is found in the binding domain of many extracellular matrix proteins. Interest in this sequence has increased due to its binding to specific receptors. The processes the binding controls include are hemostasis, cell proliferation, cellular transduction and tumorgenesis. (Muller, A.; F. Schuman; Koksch, M.; Sewald, N. *Lett Peptide Sci.* **1997**, *4*, 275).

13 Integrins are a large family of heterodimeric transmembrane glycoproteins that attach cells to extracellular matrix proteins of the basement membrane or to ligands on other cells. Integrins contain large (α) and small (β) subunits of sizes 120-170 kDa and 90-100 kDa, respectively.

14 Micoulet, A.; Spatz, J. P.; Ott, A. *ChemPhysChem* **2005**, *6*, 663.

15 Geppert, L. *IEEE Spectrum* **1996**, *33*, 33.

16 Xia, Y. N.; Whitesides, G. M. *Angew. Chem., Int. Ed.* **1998**, *37*, 551.

17 Michel, R.; Lussi, J. W.; Csucs, G.; Reviakine, I.; Danuser, G.; Ketterer, B.; Hubbell, J. A.; Textor, M.; Spencer, N. D. *Langmuir* **2002**, *18*, 3281.

18 Falconnet, D.; Koenig, A.; Assi, F.; Textor, M. *Adv. Func. Mater*. **2004**, *14*, 749.

19 Crooks, R. M.; Ricco, A. J. *Acc. Chem. Res*. **1998**, *31*, 219.

20 Xia, Y.; Rogers, J. A.; Paul, K. E.; Whitesides, G. M. *Chem. Rev*. **1999**, *99*, 1823.

21 Kumar, A.; Abbott, N. L.; Kim, E.; Biebuyck, H. A.; Whitesides, G. M. *Acc. Chem. Res*. **1995**, *28*, 219.

22 Abbott, N. L.; Kumar, A.; Whitesides, G. M. *Chem. Mater*. **1994**, *6*, 596.

23 (a) Piner, P. D.; Zhu, J.; Hong, S.; Mirkin, C. A. *Science* **1999**, *283*, 661. (b) Auletta, T.; Dordi, B.; Mulder, A.; Sartori, A.; Onclin, S.; Bruinink, C.M.; Nijhuis, C.A.; Bijleveld, H.; Peter, M.; Schönherr, H.; Vancso, G.J.; Casnati, A.; Ungaro, R.; Ravoo, B.J.; Huskens, J.; Reinhoudt, D.N. *Angew. Chem. Int. Ed.*, **2004,** *43*, 369-373.

24 Niemeyer, C. M.; Mirkin, C. A. *Nanobiotechnology*, Wiley-VCH. 2000.

25 Chen, J.; Reed, M. A.; Rawlett, A. M.; Tour, J. M. *Science* **1999**, *286*, 1550.

26 (a) Service, R. E. *Science* **1995**, **268**, 26. (b) Manz, A. *Chimia* **1996**, *59*, 140. (c) Day, P. *Chem. Br*. **1996**, *29*,

27 Gimzewski, J. K.; Joachim, C. *Science* **1999**, *283*, 1683.

28 (a) Thurn-Albrecht, T.; Schotter, J.; Kastle, C. A.; Emley, N.; Shibauchi, T.; Krusin-Elbaum, L.; Guarini, K.; Black, C. T.; Tuominen, M. T.; Russell, T. P. *Science* **2000**, *290*, 2126. (b) Park, M.; Harrison, C.; Chaikin, P. M.; Register, R. A.; Adamson, D. H. *Science* **1997**, *276*, 1401. (c) Ulrich, R.; Du Chesne, A.; Templin, M.; Wiesner, U. *Adv.*

Mater. **1999**, *11*, 141. (b) Templin, M.; Franck, A.; Du Chesne, A.; Leist, H.; Zhang, Y. M.; Ulrich, R.; Schadler, V.; Wiesner, U. *Science* **1997**, *278*, 1795.

29 Kane, R. S.; Takayama, S.; Ostuni, E.; Ingber, D. E.; Whitesides, G. M. *Biomaterials* **1999**, *20*, 2363.

30 (a) Macbeath, G.; Schreiber, S. L. *Science* **2000**, *289*, 1760. (b) Mrksich, M.; Whitesides, G. M. *Trends Biotechnol*. **1995**, *13*, 228. (c) Yadavalli, V. K.; Koh, W. G.; Lazur, G. J.; Pishko, M. V. *Sens. Actuators* **2004**, *97*, 290.

31 Feng, C. L.; Vancso, G. J.; Schönherr, H. *Langmuir* **2005**, *21*, 2356.

32 Feng, C. L.; Zhang, Z.; Förch, R.; Knoll, W.; Vancso, G. J.; Schönherr, H. *Biomacromolecules* **2005**, *6*, 3243.

33 K562 cells are probably the most widely used experimental model of chronic phase of chronic myelogenous leukemia (CML) (Kuželová, K.; Grebeňová, D.; Marinov, I.; Hrkal, Z. *J. Cellular Biochem*. **2005**, *95*, 268).

34 Feng, C. L.; Vancso, G. J.; Schönherr, H. *Adv. Funct. Mater.* **2006**, *in press*.

Chapter 2

Surface Reactions and Fabrication of Bioreactive Platforms Based on Organic and Polymeric Films: From Micrometer to Nanometer Length Scales

2.1 Introduction: Bioreactive Platforms and Biointerfaces via Organic and Polymeric Films

Biointerfaces refer to interfaces in biological systems. The interaction between biomolecules and surfaces and the behavior of complex macromolecular systems at materials interfaces play very important roles in the fields of biology, biotechnology, diagnostics, and medicine. Similar to biointerfaces, interfacial reactions at organic or polymeric surfaces are becoming an increasingly important subject also for biochemical and biological studies. Controlling the chemical and structural properties of surfaces is furthermore crucial for advancements in selective and environmentally friendly catalysis,[1] chemical sensing,[2] and many other applications.[3] To understand the rules that govern surface reactions at organic or polymeric surfaces provides ultimately very important tools and platform approaches that expand this knowledge from fundamental studies to applications in chemistry and biochemistry.[4]

While reactivity and kinetics of organic chemical reactions in solution phase represent an established field for many decades, it has been found that the chemical reactivity in ultrathin organic or polymeric films, such as Langmuir-Blodgett films[5] and self-assembled films,[6] can be distinctively different from reactions occurring in solution. Very often reaction rates are found to be reduced. Only in isolated cases enhanced rates have been reported. These observations can be attributed to confinement effects in the ultrathin organic films because the functional groups or molecules involved in these reactions are packed densely at the surface.[7] Steric effects, among others, may therefore result in higher apparent energy barriers than found in solution.

A diversity of organic or polymeric surfaces has been investigated as bio-functional interfacial architectures for their use as affinity coatings in genomics,[8] proteomics,[9] and biosensors[10] for biomedical purposes.[11] With respect to the structural and functional properties of the organic or polymeric films surface, biomimetic films can be constructed such as so called-tethered bilayer membranes, which can mimic a biomembrane to the extent that functional units, e.g., membrane channels or receptors can be incorporated, as mono or multilayers, or in the form of thin (polymeric) films.[12] These different surface coatings allow, e.g., for the construction of microarrays for the fabrication of gene and protein chips.[13]

Organic or polymeric surfaces can also be designed to serve as biointerfaces between the biological environment and man-made materials, which is central to biology and medicine and crucial in research relating to implants, biosensors, drug delivery, proteomics, and many other fields.[14] In particular, biointerfaces play an important role in cell engineering on microfabricated surfaces,[15] cell adhesion, and cell activity in terms of metabolism (Figure 2.1a). Based on organic and polymeric surfaces, it is also possible to develop robust biosensors for detection of infectious and toxigenic bacterias, as shown in Figure 2.1b,[16] or for microarray sensing platforms.

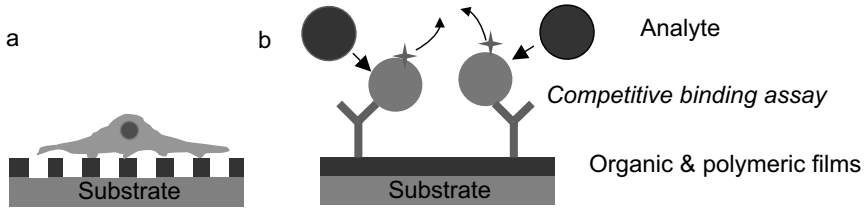

Figure 2.1. Schematic of (a) cells on structured surface and (b) biosensors based on organic or polymeric thin films.

In this context convenient and reproducible surface modification procedures that yield robust, functional biointerfaces would be highly desirable. The requirements for obtaining such biointerfaces include, among other factors:

- orientation-selective immobilization of biomolecules (receptors, proteins, antibodies, cofactors etc.) - "bioconjugation";
- protein immobilization without denaturation or folding of the protein (i.e. retention of biological activity);
- immobilization of biomolecules in defined, biologically relevant surface coverages and in an accessible configuration;
- control (elimination) of non-specific biomolecule (e.g. protein) adsorption;
- defined modulus of underlying substrate (for cell - surface interactions);
- control of roughness and topographical structures / patterns etc.

For example, phospholipid polymers were reported to show excellent biological properties at the biointerface.[17] Protein adsorption induced by hydrophobic interactions between the phospholipid polymer surface and proteins was suppressed.[18] Furthermore, cell adhesion via a protein adsorption layer was clearly inhibited, which provided a good surface environment for cell adhesion. Other approaches, which are based on monolayers and polymer thin films, will be discussed in more detail in the following sections. The essential elements of bioconjugation, as summarized in Table 2.1, remain very similar in all cases.

Table 2.1 Summary of immobilization approaches for biomolecules on surfaces to generate functional biointerfaces.

Immobilization approaches	Materials / Reactions	
Physical adsorption	Proteins or nucleic acids on nitrocellulose, nylon membranes, polystryrene, metal oxide surfaces such as palladium, aluminum oxide	19
Metal complexation	Ni-histidine tag mediated binding	20
Protein-mediated coupling	Avidin/streptavidin-biotin complexation	21
Antibody-antigen interactions	Various antibody - antigene pairs	22
Covalent attachment	Reaction of carboxylic acid functionalities with primary amine (using coupling agents); *N*-hydroxy succimidyl ester with amine; thiols with malimides; etc.	23

2.1.1. Organic and Polymeric Films

Among the various approaches to fabricate functional thin films, self-assembled monolayer (SAM) approaches[24] provide powerful tools to generate monomolecular films of biological molecules on a variety of substrates. SAMs can be conveniently formed by the adsorption of long-chain, alkylthiols or alkylchlorosilanes etc. onto gold and oxides, such as silica.[25] SAMs are very versatile as their functionality and structure can be controlled and varied with molecular precision, which can be used for the development of (in vitro) bio-surfaces that can, for instance, mimic naturally occurring molecular recognition processes.[26] Being in intimate contact with the support surface, SAMs do not exhibit problems associated with mass transport, which provides the advantage of a faster and potentially more intense response of the layers when exposed to external stimuli. SAMs presenting functional groups exhibit various packing and ordering phenomena, which have also been applied in a broad range of fundamental studies for evaluating modern theories of wetting,[27] spreading,[28] adhesion,[29] and corrosion.[30] The interfacial properties of the layers are primarily determined by the terminal groups exposed at the surface.

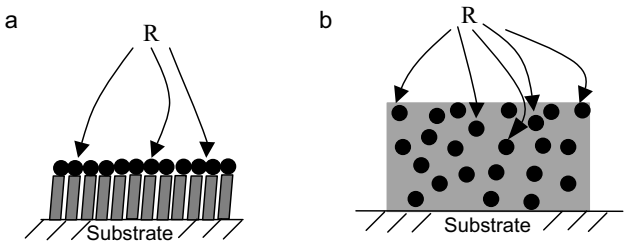

Figure 2.2. Scheme of surface reactions on (a) self-assembled monolayer; (b) polymer films on a solid substrate.

It is clear that SAMs are intrinsically 2D in nature and therefore the maximum number of functional groups per unit area is limited (~ 4.5 molecules / nm^2 for SAMs on gold).[31] However, it has been shown frequently that the use of 2-component binary SAMs may be required if biologically active species are being immobilized with the aim to exploit interactions between these and solution-borne (bio)molecules.[32]

As an alternative, the deposition of polymeric materials onto solid substrates also receives increasing attention.[33] Using electrografting, Jérôme et al. have prepared reactive surfaces bearing activated ester groups, which are highly reactive towards nucleophiles. This reactivity makes the electrografted coating appropriate for anchoring of a large variety of molecules.[34] Other polymer-based systems and approaches[35] to overcome the briefly mentioned intrinsic limitations of 2-D platforms comprise hydrogels,[36,37] dendrimers,[38,39,40] hyperbranched polymers,[41] chemical vapor deposition approaches,[42] self-assembled polyelectrolyte mutilayers,[43] plasma polymers,[44] and polymer brushes based on grafting to approach.[45]

2.1.2 Pattern Fabrication on Organic and Polymeric Films

Since miniaturization and parallelization offer considerable practical and technical advantages, increasingly smaller structures with controllable biochemical properties at organic or polymeric surfaces are sought, such as micro- and nanoarrays of proteins and oligonucleotides.[46] Soft lithographic methods (also see section 2.3.1)[47] are well known to be versatile techniques for the generation of patterns of proteins[48] or various mammalian cells,[49] however, commercial products in the area of high throughput genetic screening rely on photolithography[50] or contact spotting.[51]

In general, micro- and nanoarray analyses require high-quality surfaces. The reproducible preparation of these surfaces can be a demanding process as they determine in parts how well the molecules attach to them, as well as the efficiency of the subsequent biochemical reactions, the precision of the detection steps, and the quality of the resulting data.[52] In studies of cell biology and implant-host response, a detailed understanding of how surface structures of biomaterials translate into specific cellular responses[53] is another important area of investigation that benefits from well-defined

patterns containing biological functionality at length scales comparable to those of substructures present on the surfaces of cells, i.e., from the micrometer to the sub-100 nm range.

As mentioned, the spatially controlled deposition of proteins and other biomolecules on reactive substrates on the nanometer scale is critical for basic biological research involving cell biology[54] and for a number of applications, such as high-throughput genomic arrays (e.g. microarrays) and combinatorial library screening.[55] Genomic arrays comprise ordered array of elements on a planar substrate on the scale of 10 - 100 μm, which allows the specific binding of genes or gene products.[56] For example, chips containing thousands of genes may be used to examine fluorescently labeled DNA samples prepared by labeling target DNA molecules from cells, tissues, and other biological sources as shown in Figure 2.3. The huge capacity of these miniature devices allows one to effectively analyze the entire human genome in a single experiment by measuring fluorescence emission, which can provide enormous information on human disease, mental illness, and many other clinical matters. Genomic arrays can also be used to find changes in gene sequences, which pave the way for genetic screening, testing, and diagnostics.

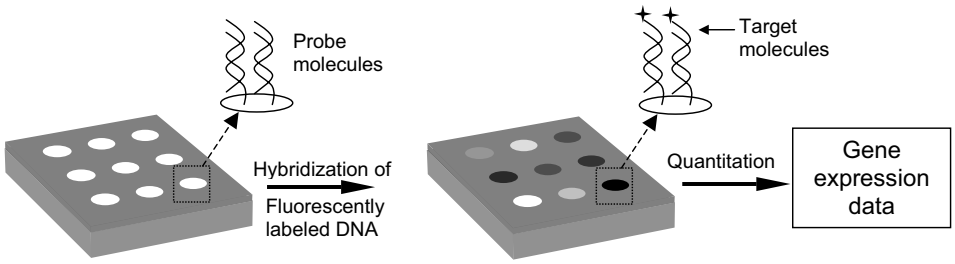

Figure 2.3. Scheme of biomicroarray for high throughput genomic screening.

The possibility to create structures at organic or polymeric surfaces in the 10 - 100 nm range is widely recognized as a requirement for future applications in many fields, such as electronic devices,[57] analytical chemistry,[58] and nanobiotechnology.[59] In order to be able to fabricate and surface-engineer the corresponding platforms for, e.g., biosensors or nanoarrays of multicomponent systems, surface chemistry must be performed locally on the nanometer scale. As described in this Thesis, we have tackled the first steps in this direction by a combination of surface chemistry and soft lithography on the one hand and block copolymer reactive films on the other hand (see also below).

2.2 Surface Reactions of Organic and Polymeric Films

In this part, the surface reactivity of organic and polymeric films will be introduced. The effects of confinement on, for example, reaction rates, degrees of conversion, as well as temperature effects, will also be treated.

2.2.1 Self-Assembled Monolayers

2.2.1.1 Reactions in Self-Assembled Monolayers

General Reactions of Monolayers in Solution: Reactions in liquid media, i.e. in the presence of a solvent, show several advantages compared to cases where there is no solvent present, such as simple operation and easily controlled reaction conditions. Simple organic reactions, such as nucleophilic substitutions, free radical halogenations, oxidation/reduction etc. can also be performed on surfaces in a solution.[60] In practice, however, most synthetically useful reactions are performed on monolayers terminated by carboxyl, amino, or hydroxyl groups. This is mainly due to surface purification issues. While any soluble contaminants can be easily removed from surface by rinsing off the solid support, monolayers cannot be purified from by-products or unreacted materials that are attached to the surface. This becomes especially complex when monolayers are subjected to a number of successive reactions, as formation of surface-attached by-products at each step leads to accumulation of defects. This situation is partly alleviated by the fact that, because of a very small amount of surface-immobilized material, bulk reagents are always present in large excess with respect to the monolayer.[61]

Reactions of Monolayers in the Absence of Solvents: A unique property of SAMs is that the tail groups are generally in contact with the ambient environment. Reactions in the absence of solvents have also been studied between monolayers and gas-phase reagents. Hydroxy- and amine-terminated monolayers react with volatile silyl chlorides to produce silyl ethers and silylamines, respectively.[62] Hydroxyl terminal groups are quantitatively converted to trifluoroacetic by exposure to the vapors of trifluoroacetic anhydride. Interestingly, even carbodiimide coupling can be performed in the gas phase by direct exposure of the acid-terminated monolayer to the mixed vapor of a carbodiimide, an alcohol, and a base.[63] Reactivity of OH-terminated monolayers towards acylating reagents in solution and the gas phase was found to be quite similar, although in some instances gas-phase processes also did not lead to complete functionalization.[64] The viability of gas-phase reactions makes them promising for industrial fabrication of mono- and multilayers.

"Intrafilm" Reactions: The proximity of the adjacent chains or functional groups in SAMs makes it possible to perform chemical reactions between them, a phenomenon conceptually similar to intramolecular reactions in solution chemistry. An obvious type of such reactions is polymerization of surface-attached unsaturated compounds. For instance, diacetylenes were successfully polymerized in SAMs.[65] Similarly, mercaptomethyl styrene was photopolymerized on a gold surface, all monomer being consumed during the reaction.[66] Another type of polymerization reaction between adjacent chains combines the chemistry of gold-thiol and silane monolayers. Hydrolysis of the monolayers of (3-mercaptopropyl)-trimethoxysilane assembled on a gold surface produces a siloxane polymer.[67] In addition to polymerization, many other reactions can be performed between adjacent chains in monolayers. A recent study described the formation of an interchain anhydride from the monolayer of mercaptohexadecanoic acid. Reaction with trifluoroacetic anhydride in dimethylformamide in the presence of triethylamine probably leads first to formation of a mixed anhydride intermediate, which then reacts with the adjacent carboxylate group to produce the interchain product.[68]

2.2.1.2 Functionalization of Monolayers

To control the surface properties of a SAM, a variety of functional groups have been introduced. Attachment of the targeted functional molecules to a gold surface has been achieved mostly by self-assembly of the appropriate ω-functionalized thiol or disulfide, leading to the desired function in a single step. Some functional groups can only be introduced via a corresponding surface reaction from a suitable precursor. As mentioned, most useful surface reactions are done on halogen-bearing,[69] amino-,[70] hydroxyl-,[71] and carboxyl-[72] terminated SAMs because of quantitative yields of the reaction.

Carboxylic Acid- and Anhydride-terminated SAMs:

An activation step is necessary for these SAMs if chemical modification is performed, for example, by treatment with carbodiimides, such as dicyclohexylcarbodiimide (DCC) or 1-ethyl-3-(3-dimethylaminopropyl) carbodiimide (EDC).[73] Alternatively, conversion to a mixed anhydride can be effected by reaction of a carboxyl-terminated film with ethyl chloroformate.[74] Exposure of the surface to gaseous $SOCl_2$ has been reported to produce carboxyl chloride groups.[75] Hydroxyl terminal groups are quantitatively converted to trifluoroacetates by exposure to the vapors of trifluoroacetic anhydride.[76] These activated acid derivatives then react smoothly with amino groups functionalized bio(molecules) to form esters or amides (Figure 2.4).

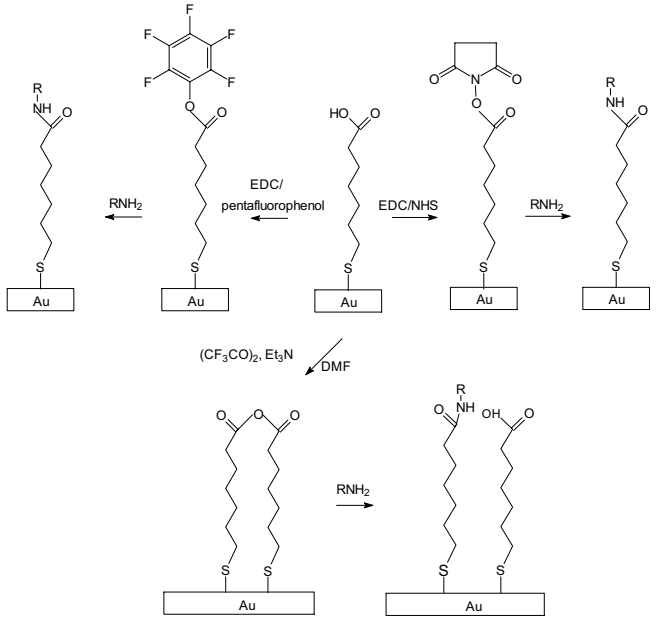

Figure 2.4. Schematic of the functionalization, covalent coupling of amino functionalized (bio)molecules on SAMs.

Amino-terminated SAMs: Amidation is one of the mostly used surface reactions on SAMs. Surface amino groups can be easily converted to amides by coupling with a carboxylic acid as shown in Figure 2.5. The active amino-terminated monolayer can also react with N-hydroxysuccinimidyl groups functionalized molecule through amidation reaction (Figure 2.5), which can be used for the further attachment of biomolecules onto gold surfaces.[77]

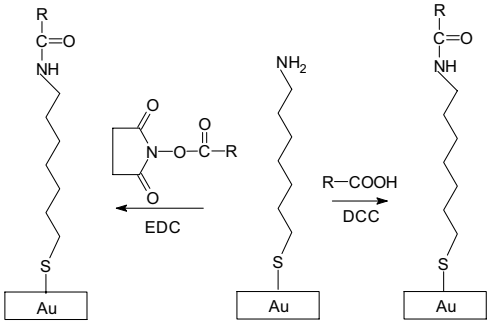

Figure 2.5. Amidation on amino groups functionalized monolayer.

In addition, hydroxyl-terminated SAMs and halogen-bearing SAMs have also been studied. In general, hydroxyl-terminated SAMs are more difficult to derivatize as compared to amino- or carboxylic acid-terminated ones because of the higher activation energies. The terminal hydroxyl groups of the SAMs can be functionalized by both solution- and vapor-phase reactions. Pan et al. reported on the esterification of SAMs of 16-mercapto-1-hexadecanol with trifluoroacetic anhydride.[78]

The reaction of halogen-bearing SAMs was found to be also difficult; here the rate of reaction was much slower on a monolayer compared to reactions carried out in solution. In a separate study, the electrophilicity of halogen was shown to possess a significant influence on the reactivity of the monolayer.[79] The higher the electropholicity, the easier the reaction of the monolayer was found.

2.2.1.3 Application of SAMs to Generate Biointerfaces

The immobilization of biomolecules on SAMs can be achieved via various routes as summarized in section 2.1. In the subsequent sections we focus on the covalent attachment of biomolecules on SAMs owing to the robustness of the attachment and the relevance for the remainder of this thesis.

Protein immobilization on SAMs:

Biosurfaces can be obtained by the covalent immobilization of proteins on reactive or activated SAMs.[80] For example, the chemical modification of the protein using the commercially available 2-iminothiolane has been reported.[81] Through reaction of 2-iminothiolane with the ω- amino group of lysine amino acid residues, the protein was covalently immobilized. After reaction in solution, the modified protein was self-assembled onto gold-coated surfaces (Figure 2.6).

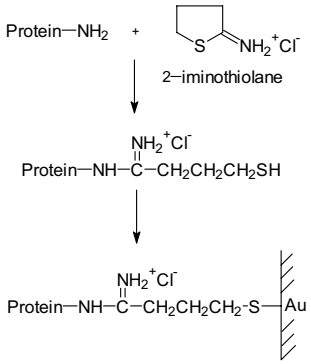

Figure 2.6 Attachment of protein on gold-coated surfaces.

In turn, proteins can also be covalently immobilized onto carboxylate-terminated alkanethiols SAMs, such as 3-mercaptopropanoic acid and 11-mercaptoundecanoic acid (11-MUA).[82] The 11-MUA monolayer was activated with NHS activation, then the enzyme was bound to the SAM via formation of an amide bond between the ester groups and the exposed ω- amino groups of lysine amino acid residues (Figure 2.7).

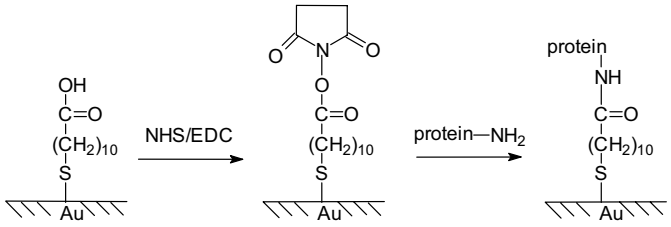

Figure 2.7 The immobilization of protein on SAMs.

The successful immobilization of proteins on monolayers makes it possible to prepare monolayer-based protein chips for proteomics applications. It is known that almost all proteins contain amino groups, so the NHS ester functionalized molecules in the monolayer can covalently bind proteins, as shown in Figure 2.7. However, during adsorption or coupling on the film, protein refolding of the secondary structure has been observed.[83] Protein denaturation is commonly defined as any change in the structure of a protein. This change, which may alter the secondary, tertiary or quaternary structure of the molecules,[84] should be of course circumvented. By depositing dendrimers on monolayers to obtain activated surfaces, very high activity of the immobilized proteins were observed in the case of higher generation dendrimers, which renders the fabrication of highly functional surfaces for protein chips possible.[85]

DNA immobilization on SAMs: Recent advances in nucleic acid probe-based biosensors have led to the development of genosensor technology for gene sequence analysis and for nucleic acid-ligand binding studies (see above). In these applications, it is desirable to covalently attach nucleic acids to a surface by a linker attached to one of the ends of the nucleic acid chain (Figure 2.8), which can lead to probe

structure flexibility with respect to change in its conformation once hybridization has taken place, without being removed from the sensor surface. A lot of work has been described in this area from attachment of the hydroxyl or phosphate groups to carboxyl residues based on various celluloses using carbodiimide derivatives.[86] Cyanuric chloride and cyanogen bromide[87] have been used to react oligonucleotides to a variety of materials. Further, carboxylic acid and aldehyde-modified nucleic acids have been attached to latex spheres via hydrazide or Schiff-base type linkages.[88] Since many biosensor surfaces are based on silica or metal oxide, the sensor must be first modified with some type of adhesive agent. Organosilanes such as aminopropyltriethoxysilane (APTES) [89] 3-mercaptopropyltriethoxysilane (MPTS)[90] and glycidoxypropyltriethoxysilane (GOPS)[91] have been used to create functionalized surfaces on a broad range of substrates. The silanes hydrolyze onto the surface to form a robust siloxane bond with surface silanols, and also crosslink themselves to further increase robustness. In the case of APTES, succinnic anhydride is often used to change the amino functionality to carboxylic acid that is then attached to an amino-linked nucleic acid via carbodiimide coupling. MPTS can be used to form disulfide linkages with thiol-containing biomolecules. GOPS has been employed in schemes using long polyether chains to provide greater distance and flexibility between the surface and the nucleic acid probe, which is very important for the preparation of biosensors.

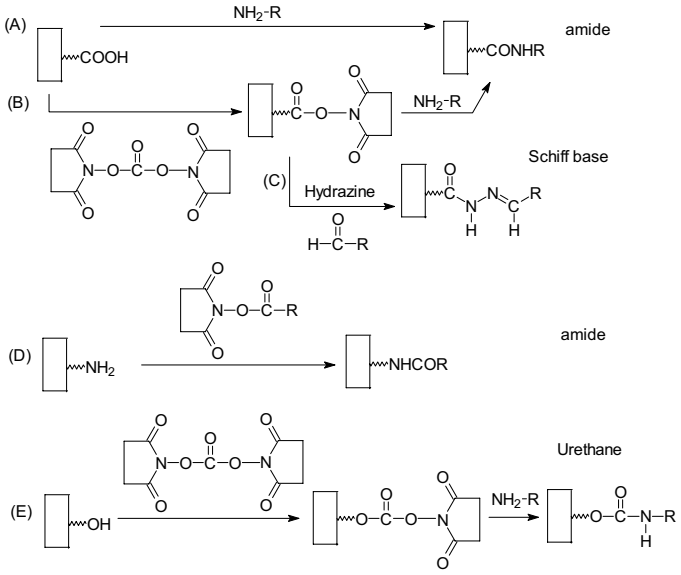

Figure 2.8. Surface immobilization of nucleic acid by covalent binding. Coupling of carboxylic acid functionalities with primary amine to produce amide linkages using, (A) 1-(3-dimethylaminopropyl)-3-ethyl carbodiimide hydrochloride; (B) N,N'-disuccimidyl carbonate (via N-hydroxysuccimidyl ester). Activation of N-hydroxysuccimidyl ester with hydrazine followed by Schiff-base formation with an aldehyde (C). Reaction of amine surface with N-hydroxysuccimidyl ester to form amide linkage (D). Alcohol group reaction with N,N'-disuccimidyl carbonate followed by treatment with primary amine to produce an amide-type linkage (E).

Antibody immobilization on SAMs: SAMs provide an unprecedented opportunity to engineer sensor surfaces with a wide spectrum of designed properties,[92] in particular by conjugating suitable antibodies or fragments thereof. This strategy enables one to conveniently tune molecular recognition via structurally well-defined functional assemblies and the control of functional groups density. Yu et al. have prepared mixed SAMs comprising ethylene glycol (EG)-terminated thiols and biotin-terminated thiols with various molar ratios on gold surfaces.[93] Monoclonal antibodies against biotin and a secondary antibody were used as free analytes in bulk solution. Specific-antibody-antigen interactions were observed for anti-biotin antibody solutions passing over the surfaces by surface plasmon field-enhanced fluorescence spectroscopy, as shown in Figure 2.9.

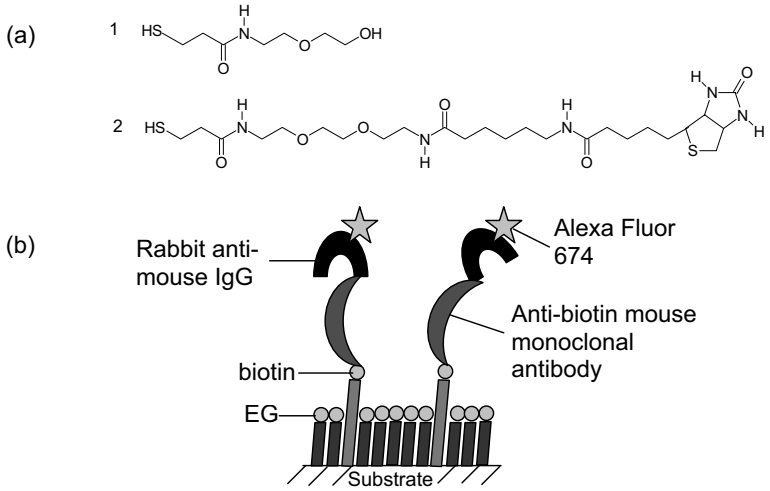

Figure 2.9. (a) Structure formula of (1) ethylene glycol-terminated thiol and (2) the biotin terminated thiol employed for the mixed SAM preparation. (b) A schematic drawing of the interfacial molecular architectures for direct and indirect fluorescence detection schemes.

Biomolecules deposition on SAMs in a non-covalent way: In addition, biomolecules (e.g. proteins) can also be deposited on SAMs by controlling the hydrophobicity of the surface. SAMs can present different functional groups, such as alkyl, perfluoroalkyl, amine, alcohol, nitrile, carboxylic acid, phosphonic acid, boric acid, heterocycle groups, which has significant influence on the surface hydrophobicity. For example, the adsorption of proteins on hydrophobic surface was achieved on mixed SAMs, which leads to the formation of a monolayer of protein.[94]

2.2.1.4 Confined Reactions of Monolayers

Thanks to their well-defined structure, low defect density, and chemical stability, SAMs offer unique opportunities to probe the mechanistic details of reactions at interfaces. However, there are various factors that result from the structure and highly ordered arrangement of SAMs and related systems that have an impact on the reactivity observed.

Steric effects: The decreased reactivity of SAMs as has been studied in most mechanistic studies is ascribed to partially blocked access of an external reagent to the monolayer-embedded reaction center. Houseman and Mrksich found for enzyme-based reactions that the extent of reaction drops dramatically if the surface concentration of functional groups is higher than a certain threshold (70%). Low yields at high coverage were ascribed to steric crowding at the surface, which inhibits the enzymatic reaction.[95] The reactivity in monolayers deposited on gold colloids was also studied as a function of size of the incoming nucleophile and steric crowding around reaction center. Steric effects were reported to be important in these reactions, and that the reaction rate was substantially diminished with bulky nucleophiles or in short-chain monolayers on gold colloids, where the density of the reaction centers is the highest.[96]

Stirling and co-workers studied the reactivity of surface-attached esters towards base-catalyzed hydrolysis. They showed that the carbonyl groups buried well below the surface [$HS(CH_2)_{10}OCO(CH_2)_8CH_3$] of well-packed monolayers of aliphatic esters are very resistant to hydrolysis, while the closer the esters are with their carbonyl function to the monolayer surface [$HS(CH_2)_{10}OCOCH_3$], the more rapid the hydrolysis progresses.[97] In such systems, the reaction is thought to start at defect sites and domain boundaries because access of an external reagent is blocked. The reaction can then grow and coalesce as the reaction proceeds. For these reactions, the initial induction of hydrolysis will be a slow reaction at scarce defect sites and be followed by a more rapid process with the leaving of the blocking groups from the monolayer by increased conversion.[98]

Dordi et al. have investigated the reactivity of NHS esters in SAMs of the corresponding disulfides on gold systematically as a function of chain length.[99] A markedly different reactivity of the NHS monolayers with different chain lengths was found, which was attributed to differences in orientation, packing, and conformational order of the molecules confined in the monolayers. By IR spectroscopy and contact angles measurements it was found that SAMs with short chain length exhibited increased disorder and a more facile reorientation of functional groups at the surface of the SAMs. Increasing disorder, reduced steric hindrance and reduced crowding at the SAM surface was argued to release the constraint of the local environment and to facilitate the attack of the hydroxide ions and thus increase the rate of the reaction.

Ryswyk and co-workers reported on the influence of surface density of the isonicotinate ester groups on the reactivity on the mixed monolayers of isonicotinate esters and alkanethiols. The rates of reactions on monolayers with pure isonicotinate ester were extremely slowly because of the blocked access to the carbonyl functional group (see Figure 2.10). However, with increasing surface coverage of isonicotinate groups, the monolayer becomes susceptible to hydroxide-mediated hydrolysis. Kinetic plots of this reaction showed clean first-order behavior,[100] which implies that access of hydroxide to the reaction center in disordered layers is not hindered.

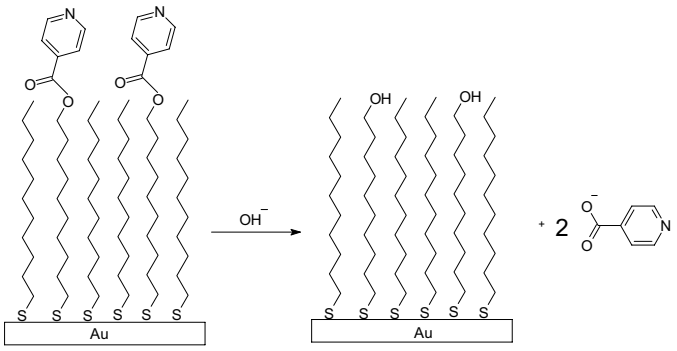

Figure 2.10. Schematic of the reaction of SAMs presenting isonicotinate ester groups with hydroxide in aqueous environment.

By contrast, Chechik and Stirling found faster reaction in monolayers, which was tentatively assigned to the higher local concentration of the amine in the vicinity of monolayer as compared to the bulk solution in the study of aminolysis of surface-confined p-nitrophenyl esters.[101]

The nucleophilic reactivity of amino groups in monolayers on gold was reported to be significantly suppressed in both inter- and intramolecular reactions as compared to the bulk reactions.[102] Failure of the amino-terminated monolayers on the surface of gold colloids to react with isothiocyanate compounds was reported.[103] This unusually low reactivity of the amino group was tentatively assigned to its interactions with the gold surface. Well-packed monolayers with Br terminal groups readily underwent substitution with small nucleophiles, while the reaction did not go to completion with bulky nucleophiles. By contrast, the sterically undemanding reaction with tin radicals proceeded rapidly and quantitatively.[104]

Solvent effects: Solvation of functional groups embedded in a monolayer may differ from the bulk. The local concentration of dissolved reagents near the surface can also be different. This is especially true for charged surfaces.[105] For example, ionization of the SAMs surfaces leads to accumulation of charge and formation of a double layer at the surface. So the pH in the vicinity of a monolayer is different from the bulk solution due to the presence of the double layer. Thus, the apparent reactivity of the charged surfaces is inherently different from bulk because of the very existence of the double layer.[106]

Accumulation of charges at an interface leads to unfavorable interactions between incipient ionized groups. Contact angle titrations of mixed monolayers of ionizable compounds and appropriate alkanethiols showed that the acid groups become less acidic with a decreased concentration of acidic groups in the monolayer. Formation of hydrogen bonds between adjacent acid or base groups in the monolayers may also have some effect on their ionization properties.[107]

Mrksich and co-workers studied a Diels-Alder reaction between surface-attached quinone and cyclopentadiene. They found substantial deviations from the second-order kinetics[92] for reactions at hydrophobic surfaces. This led to the suggestion that the diene partitions between the monolayer and the bulk solvent, thus changing its local concentration in the vicinity of the reaction center.[108]

Temperature effects: Himmel et al.[109] studied the surface derivatization of OH and COOH terminated SAMs with phenyl isocyanate (C6H5NCO, PIC). In both cases the reactivity to gas phase PIC was very slow for the samples at room temperature. However, most reaction rates can increase rapidly once the reaction temperature is increased. This is consistent with the space requirement of phenyl rings with respect to the packing of alkyl chains in SAMs, according to previous reported theoretical studies on SAMs with phenyl sulfone groups.

Depending on the temperature, considerable changes of the reactivity behavior of *16,16´-dithiobis(N-hydroxysuccinimidylhexadecanoate)* (NHS-C_{15}) monolayers have been observed.[110] These changes of the rate law (sigmoid kinetics at low temperatures, pseudo-first order kinetics at higher temperatures) have been attributed to the formation of a more disordered layer due to untilting of the chains. By increasing the temperature, the number of defects increased and rendered the reactive centers more accessible to the external reagent as also alluded to above.

2.2.2 Surface Modification with Polymers

The adsorption of polymers and reactions on (thin) polymer films comprise alternative ways to functionalize surfaces and to obtain bioreactive platforms. While the degree of order and definition does not rival those of SAMs, there are a number of advantages, depending on the requirements of the particular system, which render polymeric platforms viable alternatives.

2.2.2.1 The Adsorption of Polymers onto Solid Surfaces

The modification of surfaces with thin polymer films is widely used to tailor surface properties, such as wettability, biocompatibility, corrosion resistance, colloidal stabilization, and friction.[111] Such thin polymer films can be applied by deposition or spraying a polymeric coating from solution. One key feature of polymer deposition is the range of configurations allowable at the solid-liquid interface. As macromolecules adhere to a solid surface, they leave large loops and tails dangling into solution. The structure is intimately related to the important properties of such surface, such as stability, adhesion, or lubrication. A typical chain configuration is illustrated in Figure 2.11.

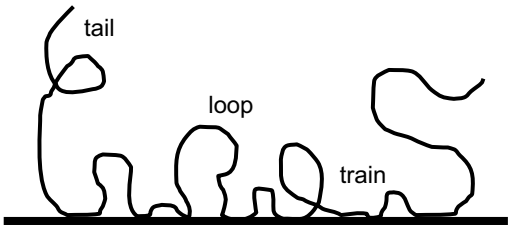

Figure 2.11. Schematic diagram of possible structures of an adsorbed polymer chain. Segments are distributed into trains directly attached to the surface, as well as loops and tails that extend into solution.

Upon adsorption, a polymer loses both translational and configurational entropy. This energetic cost is balanced by the gain in energy of segment surface contacts.[112] Polymers typically exhibit a high-affinity adsorption isotherm, which can be modeled with the Langmuir equation. The study of the polymer configurations at the solid-liquid interface has been paid particular interest.

Because the mean field produces concentration profiles that decay exponentially with distance from the surface[113] Here a chain of length N at a bulk concentration of ϕ_b in an approximate solution has a loop profile that can be estimated by

$$\phi(z) = A \exp[-(24B/N)^{1/2} z] \quad (1)$$

with

$$A = (\chi_s - 1)/(2 - 4\chi) \quad (2)$$

and

$$B = \ln (AN/(6\phi_b \ln(1/\phi_b))) \quad (3)$$

where $\phi(z)$ is the segment concentration. A is an integration constant; B is a polymer-solvent interaction parameter. The stronger the interaction between polymer and solvent, the smaller is the value of B. z is normalized to the segment size, which can be big, or small, or equal to zero in different cases. χ_s is the Silberberg adsorption energy parameter, which is defined as $\chi_s = -\Delta E_{ads}$. χ is the Flory-Huggins interaction parameter reflecting the solution conditions; $\chi = 0.5$ for an ideal or "theta" solution and $\chi = 0$ for a good solvent. While limited to values of $A \leq 1$, this expression provides helpful insight into adsorbed polymer layer structure.[114]

The thickness of an adsorbed polymer layer is important for many applications. The adsorbed polymer thickness increases with the adsorbed amount and the polymer molar mass and scales as power law function of the molecular mass with an exponent varying from 0.4 to 0.7.[115]

Many more complex polymers are receiving attention because of their technological importance. The adsorption of polyelectrolytes combines the interesting features of polymer configurational statistics with the added complexity of electrostatics,[116] requiring characterization of such features as

the charge on the polymer and surface and the effect of counter ions on adsorption. In addition, the adsorption of polymer through layer-by-layer deposition has been studied by controlling the counter ions.[117] Polymer based capsules also were studied for immobilizing proteins as application for diagnostic assays.[118]

In contrast to adsorbed homopolymers, diblock copolymers show an adsorbed layer thickness increasing linearly with the molecular mass of the soluble block, making them attractive for colloidal stabilization.[119] In addition, diblock copolymers can combine the different properties together from different blocks, which will make them much broad application.

Proteins adsorbing to solid surfaces are a ubiquitous feature of medicine, biotechnology, food processing, and environmental engineering.[120] Some flexible proteins behave much the same as water-soluble polymers, most are globular in structure and exhibit different adsorption behavior. Globular proteins lose entropy on folding and are held in place by intramolecular forces between residues.[121] Many proteins unfold upon adsorption to surfaces to regain some configurational entropy, while maximizing contacts with the surface.[122] This effect is of course unwanted in sensors and other related applications. A very important interaction is due to the hydrophobic interaction between parts of the protein and polymeric surfaces, although electrostatic interactions are also important.[123]

2.2.2.2 Polymer Brushes

A polymer brush is a system of polymer chains that are densely end-tethered or end-grafted onto a surface. The attachment can be made either by end-grafting of a homopolymer or by the selective adsorption of one of the blocks of a diblock copolymer.[124] Grafting has been utilized as an important technique to modify the chemical and physical properties of polymers. The advantage of polymer brushes over other surface modification methods (e.g. self-assembled monolayers) is their mechanical and chemical robustness, coupled with a high degree of synthetic flexibility towards the introduction of a variety of functional groups (also via brush copolymerization, see below). There is also an increasing interest of using functional or diblock copolymer brushes for “smart” or responsive surfaces, which can change a physical property upon stimulation.[125] Depending on the nature of their backbone and side chains, besides the molecular mass and molecular mass distribution and other grafting parameters, they can be used for a wide variety of applications, such as surfactants, compatibilization agents in polymer blends, additives in high impact materials, enhanced tensile strength, adhesives, improved metal adhesion, controlled wettability, better pigment dispersion, enhanced thermal stability, thermoplastic elastomers, etc.[126]

Ionic polymerization techniques permit a very good control of the graft copolymer structure although they require stringent conditions, such as, complete absence of moisture and other acidic impurities. Most graft polymers are prepared by free radical polymerization. There are two graft polymerization methods, “grafting to” and “grafting from”.[127]

Grafting to approach: Polymer chains can be covalently tethered to the surface using the so-called "grafting to" approach. [128] The "grafting to" approach refers to covalently linking an end-functionalized polymer to a surface that presents complementary reactive groups. This approach results in low grafting density (e.g. in the range of ~ 10 - 40 mg/mm^2). because the immobilized polymer chains sterically hinder the diffusion of polymer molecules from solution to the reactive sites at the surface. Furthermore, depending upon the surface density of the polymer and the interaction forces between the polymer and underlying surface, the thickness and density of the polymer graft is difficult to control due to the various conformations of the polymer at the surface. This limitation is especially important in the fabrication of a non-fouling surface using poly(ethylene glycol) (PEG) that is grafted from solution, because protein resistance of grafted PEG depends on both the surface density and the chain length of the PEG chains.[129]

Grafting from: An alternative approach to grafting surfaces with polymers is the "grafting from" approach as shown in Figure 2.12. In this approach, a surface is activated to present an initiator, and a polymer of interest is grown from the surface. Firstly, the substrate of choice is modified with initiator-bearing self-assembled monolayers. These monolayers can be formed on almost any surface, as long as an appropriate functionality is chosen (for example: thiols on gold, silanes on glass, Si/SiO_2 and plasma oxidized polymers). The initiator surfaces are then exposed to solutions containing catalyst and monomer (plus solvent if necessary). Ideally, the polymerization is not only surface-initiated but also surface-confined, i.e. no polymerization occurs in solution. [130]

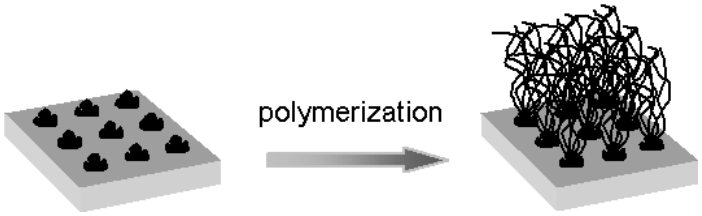

Figure 2.12. Scheme of grafting from approach.

To achieve maximum control over brush density, polydispersity, and composition, a controlled polymerization is highly desirable. During the last few years, this field has rapidly evolved and all the major controlled polymerization strategies have been used to grow polymer brushes. Of these, controlled radical polymerizations have become the most popular routes, mostly because of their tolerance to a wide range of functional monomers and less stringent experimental conditions. The different controlled polymerizations for brush growth have been used. It includes living ring opening polymerization, living anionic polymerization, living cationic polymerization, ring opening metathesis polymerization, nitroxide-mediated polymerization (NMP), reversible addition-fragmentation chain transfer polymerization, and atom transfer radical polymerization (ATRP).[131]

In recent years ATRP has become the most widely employed technique for the formation of polymer brushes via surface initiated polymerization. ATRP is compatible with a variety of

functionalized monomers, and the living/controlled character of the ATRP process yields polymers with a low polydispersity that are end functionalized and so can be used as macroinitiator for the formation of di- and triblock copolymers. Equally important, surface-initiated ATRP is experimentally more accessible than for example, the living anionic, which require rigorously dry conditions. The synthesis of thiol and silane derivatized surface-bound initiators is easier that the AIBN-silane derivative or the nitroxide silane derivative for free radical and NMP polymerization. The controlled nature of ATRP is due to the reversible activation-deactivation reaction between the growing polymer chain and a copper-ligand species.[132]

The most widely used monomer for the formation of polymer brushes via surface initiated ATRP is methyl methacrylate. PS-b-poly(*tert*-butyl acrylate) (PS-b-PtBA) brushes were also synthesized by ATRP. It was found that the PtBA block grown from PS films produced a decrease in the water contact angle (90° to 86°).[133] PtBA can be regarded as precursor for carboxylic acid functionalities, as shown by Mengel et al. who hydrolyzed PtBA in LB films.[134]

Ma et al. synthesized an alkanethiol functionalized with a terminal ATRP initiator and prepared a SAM of this ATRP initiator-functionalized thiol on gold.[135] The initiator-functionalized SAM on gold was then used to carry out surface initiated ATRP of poly(OEGMA) (POEM) on gold, as shown in Figure 2.13.

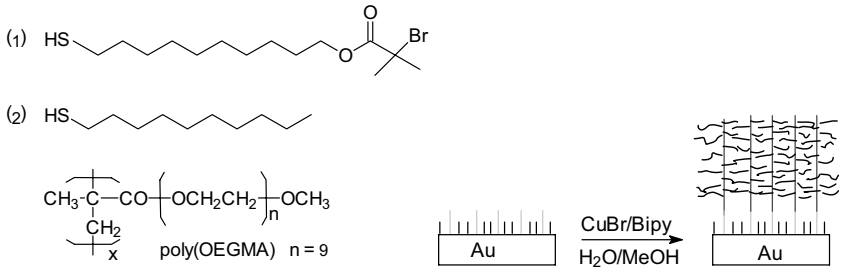

Figure 2.13. Surface-initiated ATRP. Molecular structure of the ATRP initiator-functionalized thiol (1), diluent thiol (2), and a repeat unit of a tethered "bottle" brush of POEM grown from a mixed SAM of (1) and (2).

In summary, "*grafting from*" has several attractive features: (a) very high surface density of up to 85 mg/mm^2 of a polymer can be obtained.[136] (b) A linear increase in the polymer thickness with polymer molecular mass is observed because the high surface density of the polymer forces the polymer chains into a brush conformation to minimize steric constraints. (c) The procedure is easy, because the synthesized polymer is solely localized at the interface, so that the need for extraction of loosely physisorbed polymer is eliminated.[137]

2.2.2.3. Reactive Polymer Coatings

Reactive polymer coatings, as a platform for immobilization of bioactive molecules, proteins, or cells, are becoming very important for several technologies such as the development of certain biosensors,[138] and for fundamental studies of cell biology.[139] For many applications polymer substrates are more desirable compared to metal substrates.[140] In principle, polymers may be deposited as thin films by different techniques, such as dipping, spin-coating, electrografting, and chemical vapor deposition, to provide suitable interfaces for further surface modification.

Spin-coating has been widely used to prepare substrate-supported polymer films with defined thickness, among these thin and ultrathin (d < 100 nm) films of block copolymers.[141] For example, for potential nanoelectronic research, spin coated triblock copolymer films of polystyrene-polybutadiene-polystyrene has been used to pattern barium titanate precursor with nanoscale modulations.[142] The reorganized thin films of polymer are selectively OH-functionalized in situ on the unsaturated carbon bonds in the polybutadiene matrix. The regioselective deposition of the barium titanium alkoxide on the original polybutadiene matrix of the polymer thin films was achieved. Selective decoration of a phase-separated diblock copolymer prepared by spin-coating with thiol-passivated gold nanocrystals also has been reported.[143]

As an appropriate technique to improve the adhesion to organic coatings, electrochemistry has been used to irreversibly deposit polymeric materials onto conductive solid inorganic surface.[144] It was found that electrografting of (meth)acrylates is a very powerful approach for the chemisorption of synthetic polymers onto conductive substrates.[145] For example, epoxy and fluorinated groups have been immobilized at the conductive surface by the electrografting of poly(glycidyl methacrylate) and poly(trifluoroethylacrylate), respectively. Using electrografting technique, reactive polymer surfaces containing highly activated N-succinimidyl acrylate (NHSA) ester groups have been prepared (Figure 2.14). These activated groups make the electrografted surface appropriate to immobilize of a number of amino functionalized molecules, e.g. proteins.[146]

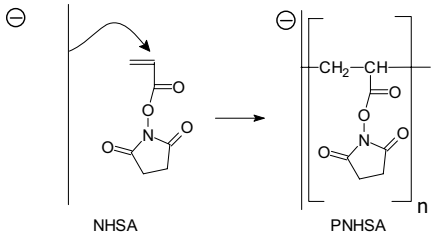

Figure 2.14 The preparation procedure of PNHSA by electrografting.

Alternatively, chemical vapor deposition (CVD) polymerization, which is a substrate-independent method for surface modification, has been used to deposit polymer films.[147] Compared to the deposition of polymer films by solvent-based methods, CVD has several advantages. For instance,

CVD provides a wide range of functional groups, excellent adhesion to various substrates, and is applicable to devices with three-dimensional geometries.[148] Using this approach, functionalized p-xylylene has been prepared for the study of protein attachment and for patterning of polymer brushes.[149] Recently, this approach was extended by deposition of reactive coatings, that is, poly(p-xylylene carboxylic acid pentafluorophenolester-co-p-xylylene) (PPX-PPF) as shown in Figure 2.15.[150] Without the need for further activation, the high chemical reactivity of their functional groups supported the conversion with biological ligands or proteins and was used for surface patterning using microcontact printing. The potential impact of this technology in surface engineering may depend on how variable reactive coatings with different functional groups can be prepared, which enable different binding modes for biomolecules.

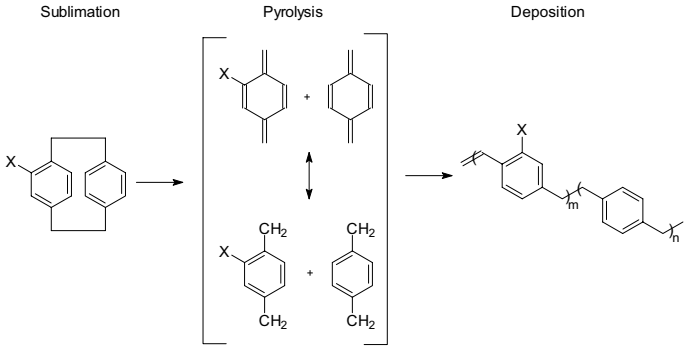

Figure 2.15: Chemical vapor deposition polymerization of reactive coatings, such as PPX-PPF.

Plasma polymerization has been studied intensively since the 1950s.[151,152] Plasma polymers can be applied successfully in the surface modification of solids (mainly conventional polymers) as protective layers, in electronic devices, and in the biological field.[153] Many different organic compounds could be applied as monomer for plasma polymerization, such as di(ethylene glycol) vinyl ether (EO_2), allylamine (AA), and maleic anhydride (MA), etc. Because of the complex nature of the plasma deposition process, the functional groups of the monomers are often lost during polymerization. The physical and chemical properties of the plasma polymerized films for given feed gases and the deposition rate of plasma polymerization depend on many factors, which are feed gas composition, reactor type, frequency and power of the excitation signal, flow rate of feed gases, plasma pressure, substrate position, substrate temperature, and so on.[154]

Since the application of plasma polymers as biomaterials has to be investigated in solvent environment,[155] the variation of the chemical structure, the swelling behavior, the optical properties,[156] and the morphology have been studied in detail by XPS, FTIR spectroscopy and AFM.[157] The property changes play an important role for understanding the behavior of proteins, cells, and DNA on platforms based on plasma polymer films.

For example, Zhang et al.[158] has described the fabrication, characterization, and optimization of amino groups derivatized polymer coatings prepared by pulsed-plasma polymerization for applications as adhesion layers in DNA immobilization. The successful DNA attachment on amino functionalized surfaces was found to depend on the macromolecular architecture of the plasma films and on the amino group densities. The data appear to suggest that the oligonucleotides are able to penetrate into the polymer network and are able to interact with reactive sites to an effective film thickness of up to approximately 40 – 50 nm due to the swelling of the plasma polymer films shown as in Figure 2.16.

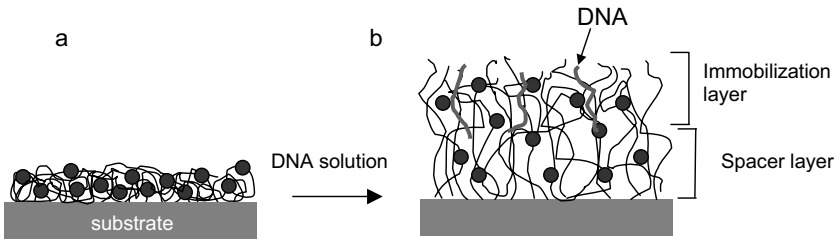

Figure 2.16. (a) Scheme of plasma polymer film in the unswollen state. (b) DNA interacts with the plasma film in a certain film depth, the remaining film acts as a spacer layer.

2.3 Patterned Organic and Polymeric Films for Tailored (Bio)interfaces

Controlling the selective immobilization of (bio)molecules in defined positions of a surface is very important for the development of biosensors and high-throughput biomolecule screening assays.[159] In the development of rapid, robust screening microarrays several patterning strategies have been successfully applied. These comprise, among others, robot-based high-precision contact-printing[160] and multistep photolithography, [161] as well as more recently selective molecular assembly patterning, [162] soft lithographic approaches, [163] and scanning probe lithography (dip pen nanolithography (DPN) etc.[164]

2.3.1 Microcontact Printing

The microcontact printing (μCP) technique developed by Whitesides et al.[165] is widely used for the fabrication of monolayer-based micrometer and sub-micrometer scale patterns. Using μCP one can transfer a variety of molecules with sub-micrometer resolution to reactive substrates without the need for dust-free environments or harsh chemical treatments.[166] Molecules can be patterned normally through physical interaction (including electrostatic and hydrophobic interactions),[167] or covalent coupling[168] with the substrate. In applications, such as the development of certain biosensors,[169] the simplicity of the method, as well as the low cost, flexibility, and possibility to pattern curved substrates make μCP very attractive.

2.3.1.1 Procedure of Microcontact Printing

μCP is a technique relevant to creating patterned substrates resulting in binary-component organic films arranged in simple spatial patterns for the purpose of organized attachment of biomolecules or cells, or to use such printed films as sacrificial layers for complex fabrication of nanoscale materials,

to name a few applications.[170] The most commonly used materials as stamp is poly(dimethylsiloxane) (PDMS). This PDMS stamp is used to transfer molecules of the "ink" to the surface of the substrate by contact. The patterned organic or polymeric layer can be transferred (Figure 2.17).[171] Binary-component films are then formed by backfilling the non-patterned areas with a different adsorbate.

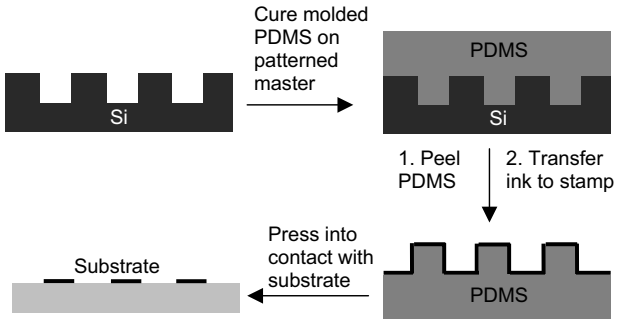

Figure 2.17. Schematic of the microcontact printing process. The relief patterns of the silicon master are transferred as negative to the PDMS stamp.

The μCP technique is attractive because it is inherently rapid and can be performed in parallel, i.e. many features can be printed simultaneously with one stamp application.

2.3.1.2 Limitations of Microcontact Printing

The resolution, reproducibility and stability of features produced using soft lithography depend partly on the properties of the elastomeric stamp and partly on the behavior of the molecular ink during transfer. The desired conformal contact during stamping benefits from a low Young's modulus of the stamp material and moderate, yet sufficient, work of adhesion. The stability of small patterns, however, requires a stiff material. Hence it is essential to achieve the appropriate balance of materials properties of the elastomer for the desired structure. Further challenges associated with using an elastomer such as PDMS include capillary forces that cause the pattern to spread after conformal contact, as well as gravitational or adhesion forces that can cause unintentional contact between the stamp or mold and the substrate.

Owing to the central importance of the stamps' materials properties, conformal and adhesion properties of elastomeric materials have been investigated.[172] It was found that reliable and repeatable conformal contact and defect-free separation demand and following three features:

1) a relatively low and defined Young's modulus and high toughness to avoid local overload and defects caused by brittle failure of vulnerable features;

2) a rubber elastic behavior to allow stamps to recover their original shape even after having undergone significant strain (> 25%);

3) a low work of adhesion to allow the stamp to separate from the substrate at low force and to prevent the sticking of particles to the substrate.

All of these requirements presuppose a sound understanding of the mechanics of stamps in order to optimize the system for soft-lithography applications.[173]

Microcontact printing of alkanethiols on gold was the first soft-lithography process reported.[174] "Inking" of the stamp was done by placing a drop of ink solution onto the stamp for a duration of 30 seconds. The ink solution was then removed under a stream of nitrogen, leaving a reproducible amount of ink on and in the stamp. This method only allowed control over the average amount of ink transferred.

Miccrocontact printing relies on ink transfer (by diffusion) from stamp to substrate, and this imposes limitations on the resolution that can be attained. Accurate reproduction of patterns realized in PDMS stamps on gold substrates was found to be problematic on a scale smaller that 500 nm due to the diffusion of ink molecules from the site of contact to the noncontacted area.[175] Delamarche et al. described several different diffusion pathways for the molecules in a microcontact-printed SAM as shown in Figure 2.18.[176] Firstly, the inking solution can spread from the surface of the stamp to areas of the substrate not intended for patterning. Secondly, it is possible that ink transfers from the stamp to the substrate in non-contacting areas via the vapor phase, which is directly related to the vapor pressure of the inking molecule (i.e., molecules having a high vapor pressure will have a higher chance of this type of diffusion). Thirdly, the molecules can diffuse along the substrate after the stamping procedure, forming areas of ordered or semiordered monolayers. These effects can be reduced by a lower concentration inking solution, thereby reducing the number of molecules available for diffusion. In order to form a complete monolayer, it is then necessary to increase the printing time (>1 s). Obviously, it is necessary to find the proper balance between alkanethiol length, solution concentration, and printing time. Using larger molar mass inks, such diffusion can be restricted.[177] Macromolecules (e.g. proteins), nanoparticles, and catalytic nanoparticles have been used as ink.[178] As a result, patterns can be faithfully transferred with high edge resolution.[179]

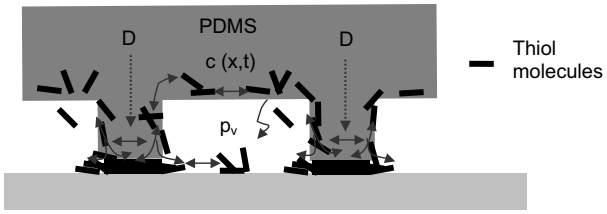

Figure 2.18. The scheme above identifies various pathways for dispersal of ink through the stamp and along its surface and that of the substrate. Characteristic parameters are the concentration of the thiols on the stamp, c(x,t), the diffusion coefficient D, and the vapor pressure p_v of the thiols.

2.3.1.3 Applications of Films Prepared by Microcontact Printing

Patterned Adsorption of Proteins on Surfaces: Many applications require control over the spatial distribution of proteins or other biomolecules adsorbed on surface. The μCP technique has been used to pattern a SAM into regions terminated with methyl- and $(EG)_6$ groups with dimensions down to 1 μm. Exposure of the patterned substrate to a protein-containing solution resulted in the irreversible adsorption of protein to the hydrophobic regions of the SAM.[180] By using μCP, biotin was also transferred onto mixed SAMs of alkanethiolates on gold, which were made from thiols presenting terminal tri(ethylene glycol) groups and terminal hexa(ethylene glycol) groups. The formation of patterned SAMs presenting biotin ligands was detected by fluorescence microscopy of substrates that were incubated with a solution of fluorescently labeled antibiotin antibody.[181]

Pattering biotin and streptavidin on an polymer surfaces by physical adsorption has been studied using reactive μCP by Hyun et al.[182] They demonstrate that polyethylene, polystyrene, poly(methyl methacrylate), and poly(ethylene terephthalate) films have been successfully patterned using biotin. By exploiting molecular recognition between biotin and streptavidin, streptavidin adsorbed on the micropatterned biotin surfaces, as detected by fluorescence microscopy.

Microarrays containing up to three different proteins were also fabricated by μCP technique and tested as a detection system for specific antibodies.[183] After fabrication, immunoassays were successfully performed using the patterned protein microarrays. The developed immunoassays were characterized by fluorescence microscopy as shown in Figure 2.19. The characterization revealed the quality of the protein deposition and indicated a high degree of selectivity for the targeted antigen-antibody interactions. The results of this study suggest that μCP is an inexpensive and effective way to fabricate biologically active substrates that can be of use for multiple reagentless immunosensor applications.

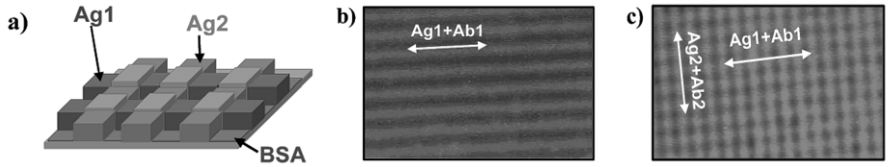

Figure 2.19 (a) Substrate design to detect three proteins. For this experiment, two printed antigens were used, mouse IgG (Ag1) and human IgG (Ag2). The regions between the IgGprinted areas were blocked with BSA. (b) Fluorescence image of the detection array after incubation only in a solution of FTIC-labeled anti-mouse IgG (Ab1). The image shows optical activity only in the Ag1 + Ab1 direction (bright areas) and no activity in the Ag2 direction (image size, 30 × 45 μm^2). (c) Fluorescence image of the same substrate after incubation in a solution of FTIC-labeled anti-human IgG (Ab2). Now optical activity can be seen in both the Ag1 + Ab1 and Ag2 + Ab2 directions. These data indicate that only specific protein binding occurred (image size, 30 × 56 μm^2).

In addition, μCP combined with microfluidic networks has been introduced by Bernard et al.[184] These authors used a stamp inked by means of a microfluidic network. Thus 16 different proteins have been successfully patterned onto the polystyrene surface. It is important to explore and expand the scope of applications of this patterning method and it may prove necessary to increase the number of different proteins that a stamp can convey simultaneously.

Patterned Cell Attachment: Micropatterning of localized chemical or biochemical domains has the potential to become a powerful tool to control the behavior of anchorage dependent cells. Control of cell-substrate contact area,[185] cell attachment and growth,[186] and cell-cell interactions[187] on the microscale have been demonstrated using microfabricated metal templates, self-assembled monolayers, biopolymers, extracellular matrix proteins, cell-adhesive peptides, and membranes. Kleinfeld et al. prepared siloxane SAMs, containing regions terminated in methyl and amino groups.[188] Cerebellar cells plated in media containing serum attached and grew only on the ionic, rather than the hydrophobic, regions of the surface, whereas cells plated in the absence of serum attached to all regions of the surface. Presumably, there is a kinetic preference for serum proteins that do not promote attachment of cells to adsorb on the hydrophobic regions.

Hyun et al. report a simple and genetic method to micropattern surfaces with an amphiphilic comb polymer (poly(ethylene glycol methacrylate)) presenting short oligoethylene glycol side chains that enable long-term, spatially resolved attachment and growth of mammalian cells in a biologically relevant milieu on a variety of substrates.[189] In the first step, PDMS is inked with a comb polymer, which was then transferred onto substrate. In a second step, incubation of the patterned surface in a protein-containing solution (fibronectin (FN) because of its role in promoting cell adhesion)[190] allows back-filling of only the unstamped regions with the protein via adsorption, because the micropatterned comb polymer is protein resistant. Incubation of micropatterns of the comb polymer on FN-pre-adsorbed polymer surfaces with fibroblasts resulted in the formation of cellular micropatterns that were confined to the underlying fibronection pattern, indicating the affinity of cells for fibronectin and the ability of the comb polymer to repel cells.

2.3.2 Selective Molecular Assembly Patterning (SMAP)

To address the limitations in biomolecular patterning by μCP using PDMS, a novel patterning approach, selective molecular assembly patterning (SMAP), has been developed by the Textor group (see Figure 2.20).[191] This approach comprises a simple and versatile patterning technique based on selective adsorption from aqueous media of multifunctional organic molecules onto oxide substrate pre-patterned by lithographic methods (also called molecular-assembly patterning by lift-off).[192] The preparation of cell-adhesive patterns of arbitrary geometry has been reported. Using this patterned films, Textor and co-workers investigated the relationship between pattern geometry and the organization of elements of the cell adhesion apparatus, namely focal contacts and stress fibers. The molecular assembly system is based on a polycationic copolymer: poly(lysine)-graft-poly(ethylene glycol) (PLL-g-PEG), which can spontaneously adsorbs from aqueous solutions onto negatively charged surfaces.[193] The subsequent layer can resist the biomolecular adsorption on the films due to

the existence of a PEG brush.[194] The PLL-g-PEG adlayers also show long term stability while still retain the resistance to protein adsorption.[195] In addition, another advantage is that the PEG can be further functionalized with bioactive molecules (ligands). Since the fraction of PEG chain can be adjusted during polymerization, the density of ligand end functionalized PEG can also be controlled.[196]

Using SMAP, protein patterns of arbitrary geometry can be prepared under a wide range of length scales in a confident and reproducible way, which may be used to study the interactions between cells and surface. This approach can be used as a generic platform for the biotechnology field. Through producing biologically relevant 2 dimensional as well as 3 dimensional surface structures, a surface with biological functionalities at geometrically well-defined interfacial architectures can be achieved. SMAP combines the advantages from the top-down approach with the bottom-up approach at the same time, that is, it can not only produce large scale pattern but also benefit from the gentle and cost-effective self-organization of chemical and biological moieties from aqueous solution at room temperature. One disadvantage of this approach is that the resolution is diffraction limited.

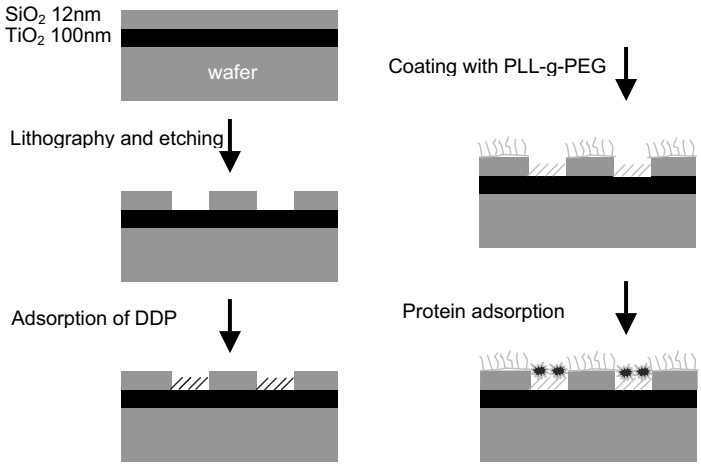

Figure 2.20. Schematic illustration of the SMAP method. Step 1: Two thin layers of oxide, TiO_2 and subsequently SiO_2, were coated onto a substrate. Step 2: Using lithographic and etching techniques, the desired geometrical pattern with different physical and chemical properties was obtained. Step 3: An oriented dodecyl phosphate (DDP) self-assembled monolayer on TiO_2 was prepared from aqueous solution. Step 4: After rinsing with water, polylysine-graft-poly(ethylene glycol) adsorbs onto the bare SiO_2 from a buffered solution, which repels proteins completely. Step 5: The obtained pattern surface with the chemical contrast between hydrophobic and hydrophilic was used to selectively deposit proteins on it. Cell culture experiment can then be performed on such patterned surfaces.

2.3.3 Embossing and Nano-imprinting

In the previous sections, a number of selected lithographic approaches have been discussed that are directly relevant for the understanding of the remainder of this thesis. These approaches allow one to introduce (bio)chemical patterns at various length scales on organic thin films. For interfacing cells with man-made artificial surfaces in studies of cellular processes and cell behavior it was found that cells react, in addition to chemical patterns, to two other types of external cues: (a) topographic patterns, (b) different substrate modulus. In the subsequent section we will therefore focus on the topographic patterning using embossing-type approaches.

Conventional embossing uses a rigid master (e.g. a master made of nickel or SiO_2) to imprint relief structures into a thermoplastic polymer (for example, polycarbonate or PMMA) that has been thermally softened.[197] The master, containing the pattern to be transferred, is then placed on top of the polymer with the surface to be embossed in contact with the polymer. Next the temperature is increased above the glass transition temperature of the polymer, and the master is forced into the polymer under pressure. After reduction of the temperature, the pressure is released, and the polymer containing the added superficial structures can be removed from the master. A schematic of the hot embossing/nano-imprinting process is given in Figure 2.21.

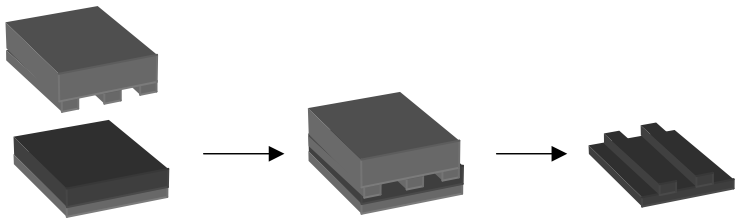

Figure 2.21: A scheme of the hot embossing/nano-imprinting process.[198]

Compared to conventional lithographic techniques, such as photolithography,[161] electrochemical micromachining,[199] and injection molding,[200] the advantages of this technique are its comparatively low costs and low complexity of the replication mechanism. It is remarkable that large areas over 3 cm^2 can be generated[201] and a given master can be used several times.[202] These features render this approach appealing for the production of multiple polymeric replicas. These fabricated surfaces can then be utilized in a variety of applications, such as supports for biomedical experimentation[203] or for fluidic devices.[204]

Poly(ethylene-2,6-naphthalate) (PEN) that was microstructured by hot embossing was found to be biocompatible, therefore structuring of the polymer surface could be used to investigate topography effects on cell growth.[205] Osteoblast-like MG63 cells were used to test the biocompatibility of the PEN surfaces used in this work. Using optical microscopy, it was found that the seeded cells attach to the PEN surface. The cells started to elongate from the beginning and until completely cover the surface area of the polymer with long time incubation. This proves that the PEN used is culture compatible, and non-toxic towards MG63 cells.

2.3.4 Self-Assembled Block Copolymer Patterns

As mentioned above, length scales in the mm to sub-μm range are covered by established optical lithography and soft lithography approaches. However, the fabrication of structures at organic or polymeric surfaces in the 10 - 100 nm range, which is difficult to access in a highly parallel manner, is widely recognized as a requirement for future applications in many fields. While serial lithographic processes, such as e-beam lithography, can in principle provide access to biologically relevant patterns, the fabrication of the corresponding platforms would benefit from new approaches to address this issue at least in parts in a highly parallel manner. In this context, nanometer scale patterns based on self-assembly have been considered as alternatives to replace or complement high resolution lithographic technologies, such as X-ray, electron beam and interference lithography to enable a variety of nano(bio)technologies. In particular, block copolymers have recently received much attention not only thanks to the scale of the microdomains, their various chemical and physical properties, but also due to the convenient size and shape tenability of microdomains afforded by simply changing their molecular masses and compositions.[206]

2.3.4.1 Definition of Block Copolymers

Block copolymers, for example, diblock copolymers, consist of two chemically different, yet covalently linked, polymer chains (i.e., blocks) typically referred to as block A and block B as shown in Figure 2.22.

Figure 2.22: Scheme of AB diblock copolymers.

The A and B blocks have a relative repulsive energy of $k_b\chi T$ per monomer pair and would macroscopically phase separate if they were not joined (here χ is the Flory-Huggins interaction parameter and T is temperature).[207] Due to the incompatibility between the two blocks and connectivity constraints, diblock copolymers with a narrow polydispersity and $\chi N > 10$ spontaneously microphase-separate into nanometer sized domains that exhibit ordered morphological equilibrium, where N is the number of monomers per chain. The periodicity and the size of the microstructures are controlled by synthesizing the appropriate polymer chain length, the ratio between blocks, and the molecular mass. In a given block copolymer system, the resulting morphology of the microstructures is largely determined by the relative chain lengths (volume fraction) of blocks A and B. Commonly observed microdomain morphologies in bulk samples of diblock copolymer are periodic arrangements of lamellae, cylinders, and spheres (see below). The sizes of these microdomain structures are governed by the chain dimensions and are typically on the order of 10 - 30 nm. For a given diblock molecular mass, the more incompatible the species, the more stretched the chains and therefore the larger the spacing of the structure. In the case of strongly segregated monodisperse diblock copolymers, Semenov et. al.[208] derived a relation between the structure spacing d, the number of monomers per chain N, and the Flory parameter χ: $d_0 \propto N^{2/3}\ \chi^{1/6}$.[209] While the dependence with N can be easily verified through controlling degree of polymerization, the dependence with χ has been

checked in very few cases due to the very limited variations obtained through temperature modulation, a method usually chosen to change the value of χ. The variations of structure spacing and object size accessible through the tuning of χ are thus quite limited, which makes the independent choice of molecular weight and microstructure sizes almost impossible, once the chemical natures of the blocks are imposed.[210] Structures smaller than 10 nm are also obtainable if one chooses appropriate blocks with a high Flory-Huggins interaction parameter[209] and decreases the block lengths. However, the synthesis of block copolymers with very large molecular mass is not possible because of the high viscosity of the reaction medium, so there were no limitations to obtain structures with very larger spacing.

Each block of the copolymer can be chosen for a specific application and selective processing of one block relative to the other is possible by use of chemical or physical dissimilarities between the two blocks. According to this idea, certain patterns with a periodicity less than 50 nm have been obtained successfully.[211] By contrast, a similar periodic patterning by electron beam lithography would be limited in three aspects. First, routine production of patterns with feature sizes below 30 nm is difficult to achieve with commercial electron beam systems. Second, the obtainable minimum periodicity of features is still not much below 100 nm. Third, as with any serial technique, large area lithography would be very time consuming because the processing is serial. This has led to the prospect that diblock copolymers will become promising materials in nanotechnology in the future.[212]

An artificial topographic pattern on a substrate has been used to orient the growth of a thin film in a process known as graphoepitaxy.[213] Recently, similar schemes have been used for orienting block copolymer systems. Long-range alignment of cylindrical domains in polystyrene-*block*-polyisoprene thin films has been observed following directional solidification of a polymer solution on a patterned substrate.[214] Patterned substrates were also employed to improve the in-plane order of polystyrene-*block*-poly(2-vinylpyridine) (PS/PVP) thin films by floating precast, 1-monolayer-thick polymer films onto patterned substrates, followed by annealing.[215] The PS/PVP block copolymer formed single grains with very low defect levels over lengths of up to 5 μm adjacent to substrate steps. By combining block copolymer self-assembly with long range ordering methods would allow nanostructures to be lithographically fabricated in precise positions on a substrate. Cheng et al. presented a graphoepitaxy method for orienting self-assembled block copolymers using substrates patterned by interference lithography over areas of several cm^2.[216] They transfer the resulting patterns into an underlying layer of silica to form an ordered array of high-aspect-ratio silica posts with a hierarchical structure. This method can be generalized to the patterning of a wide range of materials using graphoepitaxy processes.

2.3.4.2 Phase Behavior of Diblock Copolymers

The blocks of diblock copolymers are usually mutually immiscible because they consist of blocks of chemically distinct immiscible polymers.[217] As a result microphase separation can often be observed in the bulk and on the surface of films of this kind of polymers. Typically, the temperature,

the composition, the chemical nature of the phases and the molar mass will influence the morphology of the diblock copolymers.[218] A diblock copolymer phase diagram is plotted in Figure 2.23, with the order-disorder transitions (ODT) and the order-order (OOT) between the different morphologies as a function of temperature and composition.[219]

These quantities can be described as mentioned above by the Flory-Huggins interaction parameter χ, the number of statistical segments in the block copolymer N and the fraction composition f. In a diblock copolymer phase diagram, the product χN is plotted as function of composition f.[220] The parameter χN can be regarded as a measure for the degree of segregation. For higher $(\chi N)_{ODT} > 10$ a symmetric diblock copolymer is expected to form a lamellar bulk morphology in equilibrium and the order to disorder transition for the diblock copolymer can be predicted.[219] Normally, the domain interfaces are sharp in the strong segregation limit ($(\chi N)_{ODT} > 10$) and more diffuse in the weak segregation limit. The morphologies of microphase separation formed by diblock copolymers are well-understood by now.[221] Typical examples for the morphologies of diblock copolymers are depicted in Figure 2.23. These include alternating lamellae (LAM), Hexagonally packed cylinders (HEX), bicontinuous gyroid, and body centered cubic packed spheres (BCC). Here, the bicontinuous gyroid phase will appear especially near the order-disorder transition.[222] In the strong segregation limit, i.e. at large values for xN, the volume fractions for the transitions between the different ordered phases are almost independent of χN or temperature.

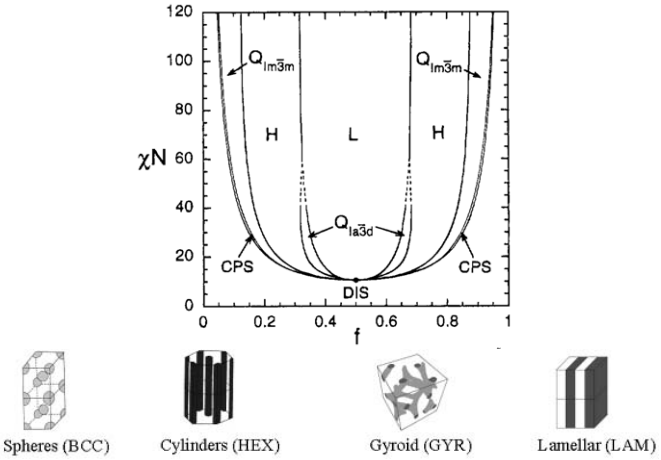

Figure 2.23. Phase diagram and scheme of morphologies predicted and observed for linear diblock copolymers. Theory predicts four equilibrium morphologies: spherical (S), cylindrical (C), gyroid (G) and lamellar (L), depending on the composition f and the combination parameter χN (image reproduced from reference 223).

2.3.4.3 Applications

Block copolymers are complex, soft materials that have been used in diverse scientific and technological applications. They have been employed to understand interesting and broadly important physical phenomena in ordered soft materials.[224] Predictable self-assembly and the wide array of

accessible block structures have further enabled scientific and technologically relevant advances using these materials. With respect to the latter materials, block copolymers are arguably ideal precursors for the formation of ordered nanoporous organic polymers. The preparation of ordered nanoporous polymers from block copolymer precursors was established in 1988 by Nakahama.[225] Nanoporous polymers can be prepared by several routes, such as controlled phase separation, etching, and molecular imprinting. These materials with nanometer periodic patterning of block polymers are important due to their potential and established utility as patterned media,[226] catalysts[227] transistor, nanowire and template for the growth of nanoscopic materials,[228] lithography templates,[229] polymeric electrolytes,[230] cell growth control, sensors and biomaterials.[231]

Nanopatterns by diblock copolymers: Lammertink, Vacso et al. have described the microphase separated structures of organometallic poly(styrene-block-ferrocenylsilane) (PS-*b*-PFS) diblock copolymers, which are attractive materials because of the formation of metal-containing nanostructures upon phase separation.[232] They studied the phase separated structures of (PS-*b*-PFS) copolymers as a function of their block composition. By increasing the volume of PFS blocks in the copolymer, the different morphologies from cylindrical to lamellar have been observed by TEM.

Morkved et al. have demonstrated the use of an in plane electric field to uniformly orient the cylindrical microdomains of PS-*b*-PMMA diblock copolymer film and the clear observation of field induced orientation in a large area thin film of asymmetric PS-*b*-PMMA diblock copolymer from small angle neutron scattering data.[233] The method uses a shear apparatus with certain frequency and amplitude to shear the film along a certain direction, which can control anisotropic molecular orientations inside the ordered block copolymer mesophases. It will be potentially significant for novel technological applications.[234] Using this method, Zhu et al.[235] have discussed nanoconfined polymer crystallization in a complex hexagonally perforated layer (HPL) phase in a poly(styrene-block-ethylene oxide) (PS-*b*-PEO) diblock copolymer. Microdomain patterns can also be obtained from epitaxy. In crystalline materials, control of the solidification process is central to many technologies that rely on the features of the resultant microstructure for achieving optimum properties. A vertically oriented lamellar structure has been achieved[236] by utilizing crystallization from the microphase separated state of a low molecular mass diblock copolymer adjacent to boundaries formed by dewetting from the substrate. Self-organization of hollow spherical micelles from a rod-coil diblock copolymer system in a selective solvent for the flexible coil block and their long range, close packed self ordering into iridescent, ordered microporous solids is another method to get ordered patterns.[237]

Biomaterials based on block copolymers: Block copolymers have a tendency to self-assemble at surfaces and into micelles in a selective solvent. At an aqueous interface, the amphiphilic property of block copolymers composed of hydrophilic and hydrophobic segments can cause the distal end of the hydrophilic chain to extend into the bulk aqueous solution, anchoring the hydrophilic block to the substrate surface through hydrophobic segments.[238] In an aqueous solution, micelles with core-shell structure and formed through the segregation of insoluble blocks into the core, which is surrounded by a hydrophilic shell composed of hydrophilic blocks.[239] This interfacial activity of amphiphilic block

copolymers provides their high utility in the biomedical field as colloidal dispersants, surface modifiers and drug carriers, and characterization of micelle properties.[240]

Otsuka et al. have described the recent progress in the field of block copolymer assembly on the surface and in the solution, focusing on the biological and biomedical application of poly(ethylene glycol) (PEG)-based block copolymers.[241] Otsuka et al. designed block copolymer (PEG-*b*-PLA) having an end-functionalized PEG (acetal-PEG) segment. Reactive block copolymers of acetal-PEG-PLA can be utilized as surface modifiers of biodegradable PLA to provide the reactive sites on the PEGylated surface. PEG chains tethered on a surface or forming the corona of nanometer scaled micelle exhibit the ability to sterically exclude other macromolecules and particles, which is related to high flexibility and the large exclusion volume of PEG strands in water. This property is particularly useful for preventing the adsorption of proteins and adhesion of cells. In this regard, these supramolecular structures involving PEG-based block copolymers should be of substantial importance for the development of blood contraction biomaterials, which are expected to play a key role in such fields as cell and tissue engineering, bio-sensing and drug delivery systems.

Biomolecules patterning on block copolymer films: By using self-assembly of diblock copolymer, the function behind molecular arrangement of single integrins[191] in cell adhesion has been studied.[242] A separation of ≥ 73 nm between the adhesive dots results in limited cell attachment and spreading and dramatically reduces the formation of focal adhesion and actin stress fibres. It has been attributed these cellular responses to restricted integrin clustering rather than insufficient number of ligand molecules in cell-matrix interface since micro-nanopatterned substrates consisting of alternating fields with dense and no nano-dots support cell adhesion.

Spin-coated block copolymers have also been used to control deposition of proteins and other biomolecules on the nanometer scale because of their ability to produce periodical functional patterns via phase separation. Very recently, Kumar et al.[243] have reported a technique to immobilize various protein molecules including bovine immunoglobulin G (IgG), fluorescein isothiocyanate conjugated anti-bovine IgG, and protein G through physical adsorption using the microphase-separated domains of polystyrene-b-poly(methyl methacrylate) diblock copolymer ultrathin films. These proteins can selectively self-segregate on the microdomain regions of polystyrene due to their preferential interactions with polystyrene. By using the phase separation of diblock copolymer, such method represents a step towards nanometer-spaced protein immobilization with high areal density. However, there are drawbacks of this method, including self-segregation of the proteins on the polymer films by physical adsorption, which will lead to instable adsorption of the proteins on the films.

Phase separation of block copolymers can offer several advantages. In small volumes, biochemical reactions may not be diffusion-limited and may thus be more efficient; less reagent and sample solution are used, lowering the costs per test.[244] Miniaturized assays can be achieved and carried out simultaneously in large numbers on phase separated block copolymer; small scales can be the key to the realization of certain types of assays.[245] In addition, it is also possible to deposit a variety of

different biomolecules onto copolymers with nanometer films scale periodical patterns and then read them out by using scanning force microscopy techniques. This can provide a platform for preparing high-throughput biosensors in future applications (Figure 2.24). Such nanopatterned polymer films can also be used to study interactions between cells and designed surfaces, thus providing new insights into vital processes in cell biology.

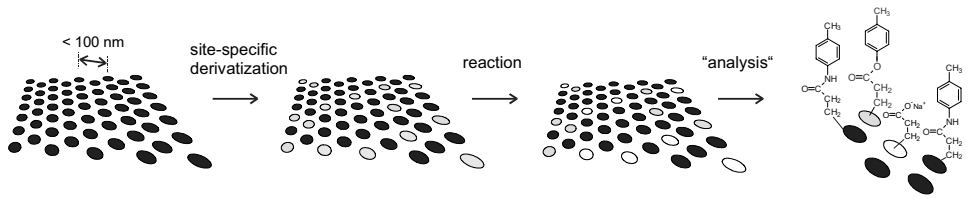

Figure 2.24. Scheme of a periodic array, which can be derivatized at predefined sites and after a screening reaction analyzed to yield chemical/compositional information. Using block copolymer thin films as reactive platforms, the principle of parallel array-based screening can be extended to a sub-micrometer level. Thereby one could potentially study and elucidate reactivity on a nanometer scale. One can identify three requirements for a successful approach: (1) a known, preferably periodic arrangement of chemically well-defined domains, (2) domain-selective functionalization (i.e. controlled derivatization of individual domains), and (3) some means of data read out. In this Thesis unconventional patterning routes, the surface reactivity of polymer-based platforms, as well as the application of block copolymer thin films, were explored as a first step towards realization of the depicted approach.

2.4 References

1 Clark, J. H. D.; Macquarrie, J. *Chem. Soc. Rev*. **1996**, *25*, 303.

2 (a) Ricco, A. J.; Crooks, R. M.; Osbourn, G. C. *Acc. Chem. Res.* **1998**, *31*, 289. (b) Paolesse, R.; Dinatale, C.; Macagnano, A.; Davide, F.; Boschi, T.; Damico, A. *Sens. Actuators B* **1998**, *47*, 70. (c) Everhart, D. S. *Chemtech* **1999**, *4*, 30. (d) Wessa, T.; Goepel, W. *Fresenius J. Anal. Chem.* **1998**, *361*, 239.

3 (a) Ulman, A. *An Introduction to Ultrathin Organic Films: From Langmuir Blodgett to Self-Assembly, Academic*, New York **1991**. (b) Ulman, A. *Chem. Rev*. **1996**, *96*, 1533. (c) Allara, D. L. *Biosens. Bioelectron*. **1995**, *10*, 771.

4 (a) Mrksich, M. *Curr. Opin. Colloid Interface Sci.* **1997**, *2*, 83. (b) Mrksich, M.; Whitesides, G. M. *Ann. Rev. Biomol. Struct.* **1996**, *25*, 55.

5 (a) Roberts, G. *LB Films*; Plenum Press: New York, **1990**. (b) see also reference 3.

6 (a) Schönherr H.; Feng C. L.; Shovsky A. *Langmuir* **2003**, *19*, 10843. (b) Shovsky, A.; Schönherr, H. *Langmuir* **2005**, *21*, 4393.

7 (a) Ahmad, J.; Astin, K. B. *Langmuir* **1990**, *6*, 1797 and references therein. (b) Chechik, V.; Crooks, R. M.; Stirling, C. J. M. *Adv. Mater*. **2000**, *12*, 1161.

8 Lynn, D. J.; Freeman, A. R.; Murray, C.; Bradley, D. G. *Genetics* **2005**, *170*, 1189.

9 (a) Lockhart, D. J.; Winzeler, E. A. *Nature* **2000**, *405*, 827. (b) Berhane, B. T.; Limbach, P. A. *Anal. Chem*. **2003**, *75*, 1997.

10 Knoll, W.; Yu, F.; Neumann, T.; Schiller, S.; Naumann, R. *Phys. Chem. Chem. Phys*. **2003**, *5*, 5169.

11 (a) Bergstrom, K.; Holmberg, K.; Safranj, A. S.; Edgell, A. S.; Kozlowski, A.; Hovanes, B. A.; Harris, J. M. *J. Biomed. Mater. Res*. **1992**, *26*, 779. (b) Otsuka, H.; Nagasaki, Y.; Kataoka, K. *Curr. Opin, Coll. Inter. Sci.* **2001**, *6*, 3. (c) Prime, K. L.; Whitesides, G. M. *Science* **1991**, *252*, 1164.

12 Yu, F.; Demirgöz, D.; Knoll, W. *Laborwelt* **2003**, *3*, 19.

13 Liebermann, T.; Knoll, W. *Langmuir*, **2003** *19*, 1567.

14 Kasemo, B. *Surf. Sci*. **2002**, *500*, 656.

15 Biran, I.; Walt, D. R. *Anal. Chem*. **2002**, *74*, 3046.

16 Deisingh, A. K.; Thompson, M. *Analyst* **2002**, *127*, 567.

17 (a) Oki, A.; Adachi, S.; Takamura, Y.; Ishihara, K.; Ogawa, H.; Ogawa, Y.; Ichiki, T.; Horiike, Y. *Electrophoresis* **2001**, *22*, 341. (b) Yoneyama, T.; Sugihara, K.; Ishihara, K.; Iwasaki, Y.; Nakabayashi, N. *Biomaterials* **2002**, *23*, 1445.

18 (a) Kitano, H.; Sudo, K.; Ichikawa, K.; Ide, M.; Ishihara, K. *J. Phys. Chem. B* **2000**, *104*, 11425. (b) Kitano, H.; Imai, M.; Mori, T.; Gommei-Ide, M.; Yokoyama, Y.; Ishihara, K. *Langmuir* **2003**, *19*, 10260.

19 Ausubel, F. M.; Brent, R.; Kingston, R. E. *DNA sequencing; in Current Protocols in Molecular Biology*, John Wiley, New York, **1993**.

20 Tang, A. J.; Wang, C.; Stewart, R.; Kopecek, J. *Bioconjugate Chem*. **2000**, *11*, 363.

21 (a) Ebersole, R. C.; Miller, J. A.; Moran, J. R. Ward, M. D. *J. Am. Chem. Soc*. **1990**, *112*, 3239. (b) Wilchek, M.; Bayer, E. A. *Avidin-Biotin Technology; Methods in Enzymology* **1990**, *184*.

22 Haha, M. A.; Tabb, J. S.; Krauss, T. D. *Anal. Chem*. **2005**, *77*, 4861.

23 (a) Yang, M.; McGovern, M. E.; Thompson, M. *Anal. Chimi. Acta* **1997**, *346*, 295. (b) Shiokawa, S.; Ohta, T.; Nozoe, S. *Chem. Pharmaceut. Bulletin* **1992**, *40*, 1398. (c) Iwanami, K.; Hinakubo, Y.; Oriyama, T. *Tetrahedron Lett*. **2005**, *46*, 5881.

24 (a) Smith, R. K.; Lewis, P. A.; Weiss, P. S. *Progr. Surf. Sci*. **2004**, *75*, 1. (b) Ulman, A. *Chem. Rev*. **1996**, *96*, 1533.

25 (a) Giancarlo, L. C.; Flynn, G. W. *Ann. Rev. Phys. Chem*. **1998**, *49*, 297. (b) Kesmodel, L. L.; Dubois, L. H.; Somorjai, G. A. *Chem. Phys. Lett*. **1978**, *56*, 267.

26 Revell, D. J.; Knight, J. R.; Blyth, D. J.; Haines, A. H.; Russell, D. A. *Langmuir* **1998**, *14*, 4517.

27 Laibinis, P. E.; Whitesdes, G. M.; Allara, D. L.; Tao, Y. T.; Parikh, A. N.; Nuzzo. R. G. *J. Am. Chem. Soc*. **1991**, *113*, 7152.

28 Bain, C. D.; Whitesides, G. M. *Science* **1998**, *240*, 62.

29 Ostuni, E.; Chapman, R. G.; Liang, M. N.; Meluleni, G.; Pier, G.; Ingber, D. E.; Whitesides, G. M. *Langmuir* **2001**, *17*, 6336.

30 Zamborini, F. P.; Crooks, R. M. *Langmuir* **1998**, *14*, 3279.

31 Giz, M. J.; Duong, B.; Tao, N. J. *J. Electroanal. Chem*. **1999**, *465*, 72.

32 Liebermann, T.; Knoll, W.; Sluka, P.; Herrmann, R. *Colloids Surf. A*, **2000**, *169*, 337.

33 (a) Delamarche, E.; Michel, B.; Biebuyck, H. A.; Gerber, C. *Adv. Mater*. **1996**, *8*, 719. (b) Lang, P.; Mekhalif, Z.; Rat, B.; Garnier, F. *J. Electroanal. Chem*. **1998**, *441*, 83. (c) Huseman, M.; Morrisson, M.; Benoit, D.; Frommer, J.; Mate, C. M.; Hinsberg, W. D.; Hedrick, J. L.; Hawker, C. L. *J. Am. Chem. Soc*. **2000**, *122*, 1844.

34 Jérôme, J.; Gabriel, S.; Voccia, S.; Detrembleur, C.; Ignatova, M.; Gouttebaron, R.; Jérôme, R. *Chem. Comm*. **2003**, 2500.

35 Falconnet, D.; Koenig, A.; Assi, F.; Textor, M. *Adv. Funct. Mater*. **2004**, *14*, 749.

36 Malmqvist, M.; Karlsson, R. *Curr. Opin. Chem. Bio*. **1997**, *1*, 378.

37 (a) Sigal, G. B.; Bamdad, C.; Barberis, A.; Strominger, J.; Whitesides, G. M. *Anal. Chem*. **1996**, *68*, 490, (b) Toomey, R.; Freidank, D.; Rühe, J. *Macromolecules* **2004**, *37*, 882.

38 (a) Niemeyer, C. M.; Blohm, D. *Angew, Chem., Int. Ed, Engl*. **1999**, *38*, 2865. (b) Schulze, A.; Downward, J. *Nat. Cell Biol*. **2001**, *3*, E190.

39 (a) Benters, R.; Niemeyer, C. M.; Drutschmann, D.; Blohm, D.; Wöhrle, D. *Nul. Acid Res*. **2002**, *30(e10)*, 1. (b) Pathak, S.; Singh, A. K.; McElhanon, J. R.; Dentinger, P. M. *Langmuir* **2004**, *20*, 6076.

40 Degenhart, G. H.; Dordi, B.; Schönherr, H.; Vancso, G. J. *Langmuir* **2004**, *20*, 6216.

41 Rowan, B.; Wheeler, M. A.; Crooks, R. M. *Langmuir* **2002**, *18*, 9914.

42 Lahann, J.; Balcells, M.; Rodon, T.; Lee, J.; Choi, I. S.; Jensen, K. F.; Langer, R. *Langmuir* **2002***, 18*, 3632.

43 Zhou, X.; Wu, L.; Zhou, J. *Langmuir* **2004**, *20*, 8877.

44 (a) Zhang, Z.; Chen, Q.; Knoll, W.; Foerch, R.; Holcomb, R.; Roitman, D. *Macromolecules* **2003**, *36*, 7689. (b) Zhang, Z.; Knoll, W.; Foerch, R.; Holcomb, R.; Roitman, D. *Macromolecules* **2005**, *38*, 1271.

45 Zhao, B.; Brittain, W.J. *Progress in Polymer Science* **2000**, *25*, 677.

46 (a) Peluso, P.; Wilson, D.S.; Do, D.; Tran, H.; Venkatasubbaiah, M.; Quincy, D.; Heidecker, B.; Poindexter, K.; Tolani, N.; Phelan, M.; Witte, K.; Jung, L.S.; Wagner, P.; Nock, S. *Anal. Biochem*. **2003**, *312*, 113. (b) Emili, A.Q.; Cagney, G.; *Nat. Biotechnol*. **2000**, *18*, 393. (c) Vrana, K.E.; Freeman, W.M.; Aschner, M.; *Neurotoxicology* **2003**, *24*, 321.

47 Xia, Y.; Rogers, J. A.; Paul, K. E.; Whitesides, G. M. *Chem. Rev.* **1999**, *99*, 1823.

48 (a) Kane, R. S.; Takayama, S.; Ostuni, E.; Ingber, D. E., Whitesides, G. M. *Biomaterials* **1999**, *20*, 2363. (b) Bernard, A.; Renault, J. P.; Michel, B.; Bosshard, H. R.; Delamarche, E. *Adv. Mater.* **2000**, *12*, 1067.

49 Mrksich, M.; Dike, L. E.; Tien, J.; Ingber, D. E.; Whitesides, G. M. *Exp. Cell Res.* **1997**, *235*, 305.

50 Yang, L. J.; Qu, Y. C. *LabChip* **2005**, *5*, 979.

51 Schwobeck, S.; Krause-Griepe, A.; Gajovic-Echelmann, A.; Ehrentreich-Foster, E.; Meinl, W.; Glatt, H. Bier, F. F. *Biosens. Bioelectron*. **2004**, *20*, 956.

52 Schena, M. *Microarray Analysis*, Wiley-Liss, **2002**, p 95.

53 (a) Boyan, B.D.; Lohmann, C.H.; Dean, D.D.; Sylvia, V.L.; Cochran, D.L.; Schwartz, Z. *Ann. Rev. Mater. Res*. **2001**, *31*, 357. (b) Kasemo, B. *Surf. Sci.* **2002**, *500*, 656. (c) Craighead, H.G.; James, C.D.; Turner, A.M.P. *Curr. Opin. Solid State Mater. Sci*. **2001**, *5*, 177. (d) Huang, S.; Ingber, D.E.; *Exp. Cell Res*. **2000**, *261*, 91.

54 Kane, R. S.; Takayama, S.; Ostuni, E.; Ingber, D. E.; Whitesides, G. M. *Biomaterials* **1999**, *20*, 2363.

55 (a) Macbeath, G.; Schreiber, S. L. *Science* **2000**, *289*, 1760. (b) Mrksich, M.; Whitesides, G. M. *Trends Biotechnol*. **1995**, *13*, 228. (c) Yadavalli, V. K.; Koh, W. G.; Lazur, G. J.; Pishko, M. V. *Sens. Actuators* **2004**, *97*, 290.

56 Schena, M. *Microarray Analysis*, Wiley-Liss, **2002**, chapter 1.

57 Chen, J.; Reed, M. A.; Rawlett, A. M.; Tour, J. M. *Science* **1999**, *286*, 1550.

58 (a) Service, R. E. *Science* **1995**, *268*, 1698. (b) Manz, A. *Chimia* **1996**, *59*, 140. (c) Day, P. *Chem. Br*. **1996**, *29*,

59 Nanobiotechnology is a field that concerns the utilization of biological systems optimized through evolution, such as cells, cellular components, nucleic acids, and proteins, to fabricate functional nanostructured and mesoscopic architectures. Nanobiotechnology also concerns the refinement and application of instruments, originally designed to generate and manipulate nanostructured materials, to basic and applied studies of fundamental biological processes, such as bottom-up approach and Dip-pen nanolithography. ((a) Niemeyer, C. M.; Mirkin, C. A. Nanobiotechnology, Wiley-VCH. 2000, p 10. (b) Gimzewski, J. K.; Joachim, C. *Science* **1999**, *283*, 1683. (c) Mirkin, C. A.; Hong, S.; Levine, R. D. *ChemPhysChem* **2001**, *2*, 37.)

60 (a) Fryxell, G. E.; Rieke, P. C.; Wood, L. L.; Engelhard, M. H.; Williford, R. E.; Graff, G. L.; Campbell, A. A.; Wiacek, R. J.; Lee, L.; Halverson, A. *Langmuir* **1996**, *12*, 5064. (b) Baker, M. V.; Watling, J. D. *Langmuir* **1997**, *13*, 2027. (c) Balachander, N.; Sukenik, C. N. *Langmuir* **1990**, *6*, 1621.

61 Feng, C. L.; Schönherr, H.; Vancso, G. J. *Langmuir* **2005**, *21*, 2356.

62 Sun, L.; Thomas, R. C.; Crooks, R. M.; Ricco, A. J. *J. Am. Chem. Soc*. **1991**, *113*, 8550.

63 Hutt, D. A.; Leggett, G. J. *Langmuir* **1997**, *13*, 2740.

64 Sabapathy, R. C.; Crooks, R. M. *Langmuir* **2000**, *16*, 1777.

65 Prucker, O.; Naumann, C. A.; Ruhe, J.; Knoll, W.; Frank, C. W. *J. Am. Chem. Soc*. **1999**, *121*, 8766.

66 Ford, J. F.; Vickers, T. J.; Mann, C. K.; Schlenoff, J. B. *Langmuir* **1996**, *12*, 1944.

67 Thompson, W. R.; Cai, M.; Ho, M. K.; Pemberton, J. E. *Langmuir* **1997**, *13*, 2291.

68 Yan, L.; Marzolin, C.; Terfort, A.; Whitesides, G. M. *Langmuir* **1997**, *13*, 6704.

69 Koloski, T. S.; Dulcey, C. S.; Haralson, Q. J.; Calvert, J. M. *Langmuir* **1994**, *10*, 3122.

70 Whitsell, J. K.; Chang, H. K. *Science* **1993**, *261*, 73.

71 (a) Pan, S.; Castner, D. G.; Ratner, B. D. *Langmuir* **1998**, *14*, 3545. (b) Hutt, D. A.; Leggett, G. J. *Langmuir* **1997**, *13*, 2740.

72 Leggett, G. J.; Roberts, C. J.; Williams, P. M.; Davies, M. C.; Jackson, D. E. ; Tendler, S. J. B. *Langmuir* **1993**, *9*, 2356.

73 Duan, C. M.; Meyerhoff, M. E. *Mikrochim. Acta* **1995**, *117*, 195.

74 Wells, M.; Crooks, R. M. *J. Am. Chem. Soc*. **1996**, *118*, 3988.

75 (a) Duevel, R. V.; Corn, R. M. *Anal. Chem*. **1992**, *64*, 337. (b) Baker, M. V.; Landau, J.; *Aust. J. Chem*. **1995**, *48*, 1201.

76 Hutt, D. A.; Leggett, G. J. *Langmuir* **1997**, *13*, 2740.

77 (a) Fox, M. A.; Whitesell, J. K.; McKerrow, A. J. *Langmuir* **1998**, *14*, 816. (b) Yu, H. Z.; Zhao, J. W.; Wang, Y. Q.; Cai, S. M.; Liu, Z. F. *J. Electroanal. Chem*. **1997**, *438*, 221.

78 Pan, S.; Castner, D. G.; Ratner, B. D. *Langmuir* **1998**, *14*, 3545.

79 Lee, Y. W.; Reed-Mundell, J.; Sukenik, C. N.; Zull, J. E. *Langmuir* **1993**, *9*, 3009.

80 Ferretti, S.; Paynter, S.; Russell, D. A.; Sapsford, K. E. *Thends Anal. Chem*. **2000**, *19*, 530.

81 Kenny, J. W.; Fanning, T. G.; Lambert, J. M.; Traut, R. R. *J. Mol. Biol*. **1979**, *135*, 151.

82 Patel, N.; Davies, M. C.; Hartshorne, M.; Heaton, R. J.; Roberts, C. J.; Tendler, S. J. B.; Williams, P. M. *Langmuir* **1997**, *13*, 6485.

83 Sethuraman, A.;HVedantham, GH.; HImoto, TH.; HPrzybycien, TH.; HBelfort, GH. *Proteins-Structure Function and Bioinformatic* **2004**, *56*, 669.

84 The primary structure of a segment of a polypeptide chain or of a protein is the amino-acid sequence of the polypeptide chain without regard to spatial arrangement. The secondary structure of a segment of polypeptide chain is the local spatial arrangement of its main-chain atoms without regard to the conformation of its side chains or to its relationship with other segments. The tertiary structure of a protein molecule, or of a subunit of a protein molecule, is the arrangement of all its atoms in space, without regard to its relationship with neighbouring molecules or subunits. The quaternary structure of a protein molecule is the arrangement of its subunits in space and the ensemble of its intersubunit contacts and interactions, without regard to the internal geometry of the subunits (IUPAC-IUB, 1970).

85 Pathak, S.; Singh, A. K.; McElhanon, J. R.; Dentinger, P. M. *Langmuir* **2004**, *20*, 6077.

86 Schott, H.; Affinity Chromatography: *Template Chromatography of Nucleic Acids and Proteins*, 1984.

87 Biagioni, S.; Sisto, R.; Ferraro, A.; Caiafa, P.; Turano, C. *Anal. Biochem*. **1978**, *89*, 616.

88 Kremsky, J. N.; Wooters, J. L.; Dougherty, J. P.; Meyers, R. E.; Collins, M.; Brown, E. L. *Nucleic Acids Res*. **1987**, *15*, 2891.

89 Wu, T.; Wang, H.; Au, L. *Chinese J. Microbiol. Immunol*. **1990**, *23*, 147.

90 Bhatia, S. K.; Shriver-Lake, L. C.; Prior, K. J. *Anal. Biochem*. **1989**, *178*, 408.

91 Maskos, U.; Southern, E. M. *Nucleic Acids Res*. **1992**, *20*, 1679.

92 (a) Sigal, G. B.; Bamdad, C.; Barberis, A.; Strominger, J.; Whitesides, G. M. *Anal. Chem*. **1996**, *68*, 490. (b) Spinke, J.; Liley, M.; Guder, H. J.; Angermaier, L.; Knoll, W. *Langmuir* **1993**, *9*, 121. (c) Hodneland, C. D.; Lee, Y. S.; Min, D. H.; Mrksich, M. *Proc. Natl. Acad. Sci. U. S. A*. **2002**, *99*, 5048.

93 Yu, F.; Yao, D.; Knoll, W. *Anal. Chem*. **2003**, *75*, 2610.

94 Mrksich, M.; Whitesides, G. M. *Tibtech* **1995**, *13*, 228.

95 Houseman, B. T.; Mrksich, M. *Angew. Chem. Int. Ed*. **1999**, *38*, 782.

96 Templeton, A. C.; Hostetler, M. J.; Kraft, C. T.; Murray, R. W. *J. Am. Chem. Soc*. **1998**, *120*, 1906.

97 Neogi, P.; Neogi, S.; Stirling, C. J. M. *J. Chem. Soc., Chem. Commun*. **1993**, 1134.

98 Schönherr, H.; Chechik, V.; Stirling, C. J. M.; Vancso, G. J. *J. Am. Chem. Soc*. **2000**, *122*, 3679.

99 Dordi, B.; Schönherr, H.; Vancso, G. J. *Langmuir* **2003**, *19*, 5780.

100 $-d[C]/dt = k''[OH^-][C] = k'[C]$; where [C] and [$OH^-$] denote the concentration of isonicotinate ester and hydroxide ions, respectively, k'' and k' are the second order and pseudo-first-order rate constants, respectively ([OH^-] ≈ constant; $k' = k''$ [OH^-]).

101 Chechik, V.; Stirling, C. J. M. *Langmuir* **1998**, *14*, 99.

102 Chechik. V.; Stilring, C. J. M. *Langmuir* **1997**, *13*, 6354.

103 Buining, P. A.; Humbel, B. M.; Philipse, A. P.; Verkleij, A. J. *Langmuir* **1997**, *13*, 3921.

104 Fryxell, G. E.; Rieke, P. C.; Wood, L. L.; Engelhard, M. H.; Williford, R. E.; Graff, G. L.; Campbell, A. A.; Wiacek, R. J.; Lee, L.; Halverson, A. *Langmuir* **1996**, *12*, 5064.

105 Chechik, V.; Crooks, R. M.; Stirling, C. J. M. *Adv. Mater*. **2000**, *12*, 1161.

106 (a) White, H. S.; Peterson, J. D.; Cui, Q. Z.; Stevenson, K. J. *J. Phys. Chem. B* **1998**, *102*, 2930. (b) Smalley, J. F.; Chalfant, K.; Feldberg, S. W.; Nahir, T. M.; Bowden, E. F. *J. Phys. Chem. B* **1999**, *103*, 1676.

107 Godinez, L. A.; Castro, R.; Kaifer, A. E. *Langmuir* **1996**, *12*, 5087.

108 Yousaf, M. N.; Mrksich, M. *J. Am. Chem. Soc*. **1999**, *121*, 4286.

109 Himmel, H. J.; Weiss, K.; Jäger, B.; Dannenberger, O.; Grunze, M.; Wöll, Ch. *Langmuir* **1997**, *13*, 4943.

110 Dordi, B. University of Twente, *PhD thesis*, **2003**, Chapter 4.

111 (a) Fleer, G. J.; Lyklema, J. *Adsorption from Solution at the Solid/Liquid Interface*, Academic Press, Orlando, FL. **1983**, Chapter 4, p.153-220. (b) Di Marzio, E. A. *Physics of Polymer Surfaces and Interfaces*, Butterworth-Heinemann, London, **1992**, Chapter 4, p. 73-96.

112 Van der Beek, G. P.; Cohen Stuart, M. A.; Fleer, G. J.; Hofman, J. E. *Langmuir* **1989**, *5*, 1180.

113 Char, K.; Frank, C. W.; Gast, A. P. *Langmuir* **1989**, *5*, 1096.

114 Ploehn, H. J.; Russel, W. B. *Macromolecules* **1989**, *22*, 266.

115 (a) Cohen Stuart, M. A.; Waajen, F. H. W. H.; Cosgrove, T.; Vincent, B.; Crowley, T. L. *Macromolecules* **1984**, *17*, 1825. (b) Mckenzie, P. F.; Kapur, V.; Anderson, J. L. *Colloid Surf*. **1994**, *A86*, 263.

116 (a) Berndt, P.; Kurihara, K.; Kunitake, T. *Langmuir* **1992**, *8*, 2486. (b) Biggs, S.; Healy, T. W. *J. Chem. Soc., Faraday Trans*. **1994**, *90*, 3415.

117 Kapas, A.; Grzeszczuk, M. *J. Electroanal. Chem*. **2005**, *582*, 209.

118 Bousalem, S.; Benabderrahmane, S.; Sang, Y. Y. C.; Manqeney, C.; Chemini, M. M. *J. Mater. Chem*. **2005**, *15*, 3109.

119 (a) Dahlgren, M. A. G.; Claesson, P. M.; Audebert, R. *J. Colloid Interface Sci*. **1994**, *166*, 343. (b) Dahlgren, M. A. G. *Langmuir* **1994**, *10*, 1580.

120 (a) Lyklema, J. *Colloids Surf*. **1984**, *10*, 33. (b) Andrade, J. D. *Surface and Interfacial Aspects of Biomedical Polymers*, Vol. 2, *Protein Adsorption*, Plenum, **1985**.

121 Dill, K. A.; Bromberg, S.; Yue, K.; Fiebig, D. M. Yee, D. P. Thomas, P. D. Chan, H. S. *Protein Sci*. **1995**, *4*, 561.

122 Norde, W.; Lyklema, J. *J. Colloid Interf. Sci*. **1978**, *66*, 257.

123 Stahlberg, J.; Jonsson, B.; Horvath, C. *Anal. Chem*. **1992**, *64*, 3118.

124 Whitmore, M. D.; Noolandi, J. *Macromolecules* **1990**, *23*, 3321.

125 Konradi, R.; Ruhe, J. *Macromolecules* **2005**, *38*, 6140.

126 (a)Turi, E. A., Editor. *Thermal Characterization of Polymer Materials*, 2nded. California: Academic Press, **1997**. (b) Satas D. Acrylic Adhesives. In: Satas D, Editor. *Handbook of Pressure Sensitive Adhesive Technology*. New York: Van Nostrand Reinhold, **1982**.

127 Fernández García, M.; de la Fuente, J. L.; Cerrada, M. L.; Madruga, E. L. *Polymer* **2002**, *43*, 3173.

128 Currie, E.P.K.; Norde, W.; Stuart, M.A.C. *Advances in Colloid and Interface Science* **2003**, *100*, 205.

129 Feng, C. L.; Zhang, Z.; Förch, R.; Knoll, W.; Vancso, G. J.; Schönherr, H. *Biomacromolecules*, **2005**, *6*, 3243.

130 Edmondson, S.; Osborne, V. L.; Huck, W. T. S. *Chem. Soc. Rev*. **2004**, *33*, 14.

131 (a) Jaworek, T.; Neher, D.; Wegner, G.; Wieringa, R. H.; Schouten, A. J. *Science*, **1998**, *279*, 57. (b) Jordan, R.; Ulman, A.; Rafailovick, M. H.; Sokolov, J.; *J. Am. Chem. Soc.* **1999**, *121*, 1016. (c) Zhao, B.; Brittain, W. J. *Macromolecules* **2000**, *33*, 342. (d) Kim, N. Y.; Jeon, N. L.; Choi, I. S.; Takami, S.; Harada, Y. K.; Finnie, R.; Girolami, G. S.; Nuzzo, R. G.; Whitesides, G. M.; Laibinis, P. E. *Macromolecules* **2000**, *33*, 2793. (e) Blomberg, S.;

Ostberg, S.; Harth, E.; Bosman, A. W.; Van Horn, B.; Hawker, C. J. *J. Polym. Sci., Part A: Polym. Chem.* **2002**, *40*, 1309. (f) Baum, M.; Brittain, W. J. *Macromolecules* **2002**, *35*, 610. (f) Matyjaszewski, K.; Miller, P. J. *Macromolecules* **1999**, *32*, 8716.

132 Ejaz, M.; Yamamoto, S.; Ohno, K.; Tsujii, Y.; Fukuda, T. *Macromolecules* **1998**, *31*, 5934.

133 Mengel, C.; Esker, A. R.; Meyer, W. H.; Wegner, G. *Langmuir* **2002**, *18*, 6365.

134 Mengel, C.; Esker, A. R.; Meyer, W. H.; Wegner, G. *Langmuir* **2002**, *18*, 6365.

135 Ma, H.; Hyun, J.; Stiller, P.; Chilkoti, A. *Adv. Mater.* **2004**, *16*, 338.

136 Prucker, O.; Ruhe, J. *Macromolecules* **1998**, *31*, 602.

137 Nath, N.; Hyun, J.; Ma, H.; Childoti, A. *Surf. Sci*. **2004**, *570*, 98.

138 Crooks, R. R.; Ricco, A. J. *Acc. Chem. Res*. **1998**, *31*, 219.

139 Chen, C. S.; Mrksich, M.; Huang, S.; Whitesides, G. M.; Ingber, D. E. *Biotechnol. Prog*. **1998**, *14*, 356.

140 Ulman, A. *Chem. Rev*. **1996**, *96*, 1533.

141 (a) Siegel, R. W. *Phys. Today* **1993**, *46*, 64. (b) Nijhara, K. *J. Cram. Soc. Jpn*. **1991**, *99*, 974.

142 Lee, T.; Yao, N.; Aksay, I. A. *Langmuir* **1997**, *13*, 3866.

143 Zehner, R. W.; Lopes, W. A.; Morkved, T. L.; Jaeger, H.; Sita, L. R. *Langmuir* **1998**, *14*, 241.

144 Koutsos, V.; Van Der Vegte, E. W.; Hadziiannou, G. *Macromolecules* **1999**, *32*, 1233.

145 Baute, N.; Martinot, T. L.; Mertens, M.; Dubois, P.; Jérôme, R. *Eur. J. Inorg. Chem*. **1998**, 1711.

146 Jérôme, C.; Gabriel, S.; Voccia, S.; Detrembleur, C.; Ignatova, M.; Gouttebaron, R.; Jérôme, R. *Chem. Comm*. **2003**, 2500.

147 Lahann, J.; Klee, D.; Höcker, H. *Macromol. Rapid Commun*. **1998**, *19*, 441.

148 Lahann, J.; Balcells, M.; Rodon, T.; Lee, J.; Choi, I. S.; Jensen, K. F.; Langer, R. *Langmuir* **2002**, *18*, 3632.

149 Lahann, J.; Langer, R. *Macromolecules* **2002**, *35*, 4380.

150 Lahann, J. Balcells, M.; Lu, H.; Rodon, T.; Jensen, K. F.; Langer, R. *Anal. Chem*. **2003**, *75*, 2117.

151 Schmellenmeier, H. *Exp. Techn. Phys.* **1953**, *1*, 49.

152 Goodmann, J. *J. Polym. Sci.* **1960**, *44*, 551.

153 Biederman, H.; Slavinska, D. *Surface and Coating Technology* **2000,** *125*, 375.

154 (a) Biederman, H.; Slavinska, D. *Surface and coating Technology* **2000,** *125*, 371. (b) Foerch, R.; Mcintyre, N. S.; Hunter, D. H. *J. Polym. Sci. A*. **1990**, *28*, 803.

155 Schönherr, H.; van Os, M.T.; Förch, R.; Timmons, R. B.; Knoll, W.; Vancso, G. J. *Chem. Mater.* **2000**, *12*, 3689.

156 Jacobsen, V.; Menges, B.; Förch, R.; Mittler, S.; Knoll, W. *Thin Solid Films* **2002**, *409*, 185.

157 Jacobsen, V.; Menges, B. Förch, R.; Mittler, S.; Knoll, W. *Thin Solid Films* **2002**, *30*, 185.

158 Zhang, Z.; Chen, Q.; Knoll, W.; Förch, R.; Holcomb, R.; Roitman, D. *Macromolecules* **2003**, *36*, 7689.

159 (a) Singhvi, R.; Kumar, A.; Lopez, G. P.; Stephanopoulos, G. N.; Wang, D. I.; Whitesides, G. M. *Science* **1994**, *264*, 696. (b) Lopez, G. P.; Biebuyck, H. A.; Harter, A. R.; Kumar, A.; Whitesides, G. M. *J. Am. Chem. Soc*. **1993**, *115*, 10774. (c) Ostuni, E.; Kane, R.; Chen, C. S.; Ingber, D. E.; Whitesides, G. M. *Langmuir* **2000**, *16*, 7811. (d) Yousaf, M. N.; Houseman, B. T.; Mrksich, M. *Proc. Natl. Acad. Sci. U.S.A*. **2001**, *98*, 5992.

160 MacBeath, G.; Schreiber, S. L. *Science* **2000**, *289*, 1760.

161 Brack, H. P.; Padeste, C.; Slaski, M.; Alkan, S.; Solak, H. H. *J. Am. Chem. Soc*. **2004**, *126*, 1004.

162 Lussi, J. W.; Michel, R.; Reviakine, I.; Falconnet, D.; Goessl, A.; Csucs, G.; Hubbell, J. A.; Textor, M. *Prog. Surf. Sci.* **2004**, *76*, 55.

163 (a) Kumar, A.; Abbott, N. A.; Kim, E.; Biebuyck, H. A.; Whitesides, G. M. *Langmuir* **1995**, *28*, 219. (b) C. Wang, Y. Zhang, *Adv. Mater*. **2005**, *17*, 150.

164 Piner, R. D.; Zhu, J.; Xu, F.; Hong, S.; Mirkin, C. A. *Science* **1999**, *283*, 661.

165 Kumar, A.; Whitesides, G. M. *Appl. Phys. Lett*. **1993**, *63*, 2002.

166 Quake, S. R.; Scherer, A. *Science* **2000**, *290*, 1536.

167 (a) Renault, J. P.; Bernard, A.; Juncker, D.; Michel, B.; Bosshare, H. R.; Delamarche, E. *Angew. Chem.; Int. Ed.* **2002**, *41*, 2320. (b) Bruckbauer, A.; Zhou, D. J.; Ying, L. M.; Korchev, Y. E.; Abell, C.; Klenerman, D. *J. Am. Chem. Soc*. **2003**, *125*, 9834.

168 Anzai, J.; Kobayashi, Y.; Nakamura, N.; Nishimura, M.; Hoshi, T. *Langmuir* **1999**, *15*, 221.

169 Crooks, R. M.; Ricco, A. J. *Acc. Chem. Res*. **1998**, *31*, 219.

170 (a) Ostuni, E.; Yan, L.; Whitesides, G. M. *Coll. Surf., B.* **1999**, *15*. 3. (b) Maoz, R.; Frydma, E.; Cohen, S. R.; Sagiv, J. *Adv. Mater*. **2000**, *12*, 725. (c) Ito, H. *IBM J. Res. Dev*. **1997**, *41*, 119.

171 Xia, Y. N.; Whitesides, G. M. *Angew. Chem., Int. Ed.* **1998**, *37*, 551.

172 Bietsch, A.; Michel, B. *J. Appl. Phys*. **2004**, *88*, 4310.

173 Michel, B. Bernard, A.; Bietsch, A.; Delamarche, E.; Geissler, M.; Juncker, D.; Kind, H.; Renault, J. P.; Rothuizen, H.; Schmid, H.; Schmidt-Winkel, P.; Stutz, R.; Wolf, H. *IBM. J. RES. Dev*. **2001**, *45*, 697.

174 Schmid, H.; Michel, B. *Macromolecules* **2000**, *33*, 3042.

175 Libioulle, L.; Bietsch, A.; Schmid, H.; Michel, B.; Delamarche, E. *Langmuir* **1999**, *15*, 3000.

176 Delamarche, E.; Schmid, H.; Bietsch, A.; Larsen, N. B.; Rothuizen, H.; Michel, B.; Biebuyck, H. *J. Phys. Chem. B* **1998**, *102*, 3324.

177 Liebau, M.; Huskens, J.; Reinhoudt, D. N. *Adv. Funct. Mater*. **2001**, *11*, 147.

178 (a) Hidber, P. C.; Helbig, W.; Kim, E.; Whitesides, G. M. *Langmuir* **1996**, *12*, 1375. (b) Hidber, P. C.; Healey, P. F.; Helbig, W.; Kim, E.; Whitesides, G. M. *Langmuir* **1996**, *12*, 5209.

179 Degenhart, G. H.; Dordi, B.; Schönherr, H.; Vancso, G. J. *Langmuir* **2004**, *20*, 6261.

180 Lopez, G. P.; Biebuyck, H. A.; Harter, R.; Kumar, A.; Whitesides, G. M. *J. Am. Chem. Soc*. **1993**, *115*, 10774.

181 Lahiri, J.; Ostuni, E.; Whitesides, G. M. *Langmuir* **1999**, *15*, 2055.

182 Hyun, J.; Zhu, Y.; Liebmann-Vinson, A.; Beebe, T. P.; Jr.; Chilkoti, A. *Langmuir* **2001**, *17*, 6358.

183 Inerowicz, H. D.; Howell, S.; Regnier, F. E.; Reifenberger, R. *Langmuir* **2002**, *18*, 5263.

184 Bernard, A.; Renault, J. P.; Michel, B.; Bosshard, H. R.; Delamarche, E. *Adv. Mater*. **2000**, *12*, 1067.

185 (a) Carter, S. B. *Exp. Cell Res*. **1967**, *48*, 189. (b) Liu, V. A.; Jastromb, W. E.; Bhatia, S. N. *J. Biomed. Mater*. *Res*. **2002**, *60*, 126. (c) Singhvi, R.; Kumar, A.; Lopez, G. P.; Stephanopoulos, G. N.; Wang, D. I.; Whitesides, G. M.; Ingber, D. E. *Science* **1994**, *264*, 696. (d) Thomas, C. H.; Lhoest, J. B.; Castner, D. G.; McFarland, C. D.; Healy, K. E. *J. Biomech. Eng*. **1999**, *121*, 40.

186 Saneinejad, S.; Schoichet, M. S. *J. Biomed. Mater. Res*. **1998**, *42*, 13.

187 (a) Bhatia, S. N.; Yarmush, M. L.; Toner, M. *J. Biomed. Mater. Res*. **1997**, *34*, 189. (b) Bhatia, S. N.; Balis, U. J.; Yarmush, M. L.; Toner, M. *Biotechnol. Prog*. **1998**, *14*, 378.

188 Kleinfeld, D.; Kahler, K. E.; Hockberger, P. E. *J. Neurosci.* **1988**, *8*, 4098.

189 Hyun, J.; Ma, H.; Zhang, Z.; Beebe, T. P.; Jr.; Chilkoti, A. *Adv. Mater*. **2003**, *15*, 576.

190 RGD (Arg-Gly-Asp) is a tripeptide recognition motif that is important in cellular adhesive properties. The tripeptide recognition sequence of arginine, glycine and aspartic acid is found in the binding domain of many extracellular matrix proteins. Interest in this sequence has increased due to its binding to specific receptors. The processes the binding controls include are hemostasis, cell proliferation, cellular transduction and tumorgenesis. (Muller, A.; F. Schuman;Koksch, M.; Sewald, N. *Lett Peptide Sci.* **1997**, *4*, 275).

191 Michel, R.; Lussi, J. W.; Csucs, G.; Reviakine, I.; Danuser, G.; Ketterer, B.; Hubbell, J. A.; Textor, M.; Spencer, N. D. *Langmuir* **2002**, *18*, 3281.

192 Falconnet, D.; Koenig, A.; Assi, F.; Textor, M. *Adv. Func. Mater*. **2004**, *14*, 749.

193 VandeVondete, S.; Vörös, J.; Hubbbell, J. A. *Biotechnol. Bioeng*. **2003**, *82*, 784.

194 Pasche, S.; De Paul, S. M.; Vörös, J.; Spencer, N. D.; Textor, M. *Langmuir* **2003**, *19*, 9216.

195 Faraasen, S.; Vörös, J.;Csucs, G.; Textor, M.; Merkle, H. P.; Walter, E. *Pharm. Res*. **2003**, *20*, 237.

196 Huang, N. P. Vörös, J.; De Paul, S. M.; Textor, M.; Spencer, N. D. *Langmuir* **2002**, *18*, 220.

197 Emmelius, M.; Pawlowski, G.; Vollmann, H. W. *Angew. Chem. Int. Ed.* **1989**, *28*, 1445.

198 Mills, C. A.; Escarré, J.; Engel, E.; Martinez, E.; Errachid, A.; Bertomeu, J.; Andreu, J.; Planell, J. A.; Samitier, J. *Nanotechnology* **2005**, *16*, 369.
199 Datta, M. *J. Electrochem. Soc.* **1995**, *142*, 3801.
200 Michaeli, W.; Bielzer, R. *Adv. Mater*. **1991**, *3*, 260.
201 Heidari, B.; Maximov, I.; Montelius, L. *J. Vac. Sci.Technol. B* **2002**, *18,* 3557.
202 Chou, S. Y.; Kraus, P. R.; Renstrom, P. J. *J. Vac. Sci. Technol. B* **1996**, *14*, 4129.
203 Kasemo, B. *Surf. Sci.* **2002,** *500,* 656.
204 (a) Becker, H.; Locascio, L. E. *Talanta* **2002**, *56,* 267. (b) Jakeways, R.; Klein, J. L.;Ward, I. M. *Polymer* **1996**, *37,* 3761.
205 Curtis, A.; Wilkinson, C. *Biomaterials* **1997**, *18,* 1573.
206 Park, C.; Yoon, J.; Thomas, E. L. *Polymer* **2003**, *44*, 6725.
207 (a) Suess-Fink, G.; Meister, G. *Adv. Organomt. Chem*. **1993**, *35*, 41; (b) Muetterties, E. L.; Krause, M. J. *Angew. Chem. Int. Ed. Engl*. **1983**, *22*, 135.
208 Semenov, A. N. *Sov. Phys. JETP* **1985**, *61*, 733.
209 Ren, Y.; Lodge, T. P.; Hillmyer, M. A. *Macromolecules* **2002**, *35*, 3889.
210 Bendejacq, D.; Ponsinet, V.; Joanicot, M.; Vacher, A.; Airiau, M. *Macromolecules* **2003**, *36*, 7289.
211 Park, M.; Harrison, C.; Chaikin, P. M.; Register, R. A.; Adamson, D. H. *Science* **1997**, *276*, 1401.
212 Park, C.; Yoon, J. Thomas, E. L. *Polymer* **2003**, *22*, 6725.
213 Smith, H. I.; Geis, M. W.; Thompson, C. V.; Atwater, H. A. *J. Cryst. Growth* **1983**, *63*, 527.
214 Flanders D. C.; Shaver, D. C.; Smith, H. I. *Appl. Phys. Lett*. **1978**, *32*, 597.
215 Segalman, R. A.; Yokoyama, H.; Kramer, E. J. *Adv. Mater*. **2001**, *13*, 1152.
216 Cheng, J. Y.; HRoss, C. AH.; HThomas, E. LH.; HSmith, H. IH.; HVancso, G. JH. *Appl. Phys. Lett*. **2002**, *81*, 3657.
217 Bates, F. S.; Fredrickson, G. H. *Annu. Rev. Phys. Chem*. **1990**, *41*, 525.
218 Bates, F. S. *Science* **1991**, *251*, 887.
219 Andersen, T. H.; Tougaard, S.; Larsen, N. B.; Almdal, K.; Johannsen, I. *J. Electron. Spectrosc. Rel. Phenom*. **2001**, *121*, 93.
220 (a) Leibler, L. *Macromolecules* **1980**, *13*, 1602; (b) Frederickson, G. H.; Helfand, E. *J. Chem. Phys*. **1987**, *87*, 697; (c) Matsen, M. W.; Bates, F. S. *Macromolecules* **1996**, *29*, 1091.
221 Bates, F. S.; Rosedale, J. H.; Frederickson, G. H. *J. Chem. Phys*. **1990**, *92*, 6255.
222 Seul, M.; Andelman, D. *Science* **1995**, *267*, 476.
223 Matsen, M. W.; Bates, F. S. *Macromolecules* **1996**, *29*, 1091.
224 Hamley, I. W. *The Physics of Block Copolymers; Oxford University Press*: Oxford, **1998**.
225 Lee, J.; Hirao, A.; Nakahama, S. *Macromolecules* **1988**, *21*, 274.
226 Miroslav, J.; Sykora, D.; Svec, F.; Frechet, J. M. J.; Scheweer, J.; Holm, R. *J. Polym. Sci., Part A: Polym. Chem*. **2000**, *38*, 2767.
227 (a) Deng, H.; Gin, D. L.; Smith, R. C. *J. Am Chem. Soc*. **1998**, *120*, 3522; (b) Gu W.; Zhou, W. J.; Gin, D. L., *Chem. Mater*. **2001**, *13*, 1949.
228 Martin, C. R. *Science* **1994**, *266*, 1961.
229 (a) Morkved, T. L.; Wiltzius, P.; Jaeger, H. M.; Grier, D. G.; Witten, T. A. *Appl. Phys. Lett*. **1994**, *64*, 422; (b) Mansky, P.; Harrison, C. K.; Chaikin, P. M.; Register, R. A.; Yao, N. *Appl. Phys. Lett.* **1996**, *68*, 2586.
230 (a) Ruzette, A. V. G.; Soo, P. P.; Sadoway, D. R.; Mayes, A. M., J. *Electrochem. Soc*. **2001**, *148*, A537; (b) Matsumi, N.; Sugai, K.; Ohno, H. *Macromolecules* **2002**, *35*, 5731.
231 (a) Zhao, B.; Brittain, W. J. *Prog. Polym. Sci*. **2000**, *25*, 677; (b) Aksay, I. A.; Trau, M.; Manne, S.; Honma, I.; Yao, N.; Zhou, L.; Fenter, P.; Eisenberger, P. M.; Gruner, S. M. *Science* **1996**, *273*, 892; (c) Yang, X. G.; Shi, J.; Johnson, S.; Swanson, B. *Langmuir* **1998**, *14*, 1505.
232 Lammertink, R. G. H.; Hempenius, M. A.; Thomas, E. L.; Vancso, G. J. *J. Polym. Sci.: Part B: Polym. Phys*. **1999**, *37*, 1009.

233 Mansky, P.; Derouchey, J.; Russell, T. P.; Mays, J.; Pitsikalis, M.; Morkved, T.; Jaeger, H. *Macromolecules* **1998**, *31*, 4399.

234 Ni, Y.; Rulkens, R.; Manners, I. *J. Am. Chem. Soc*. **1996**, *118*, 4102.

235 Zhu, L.; Cheng, S. Z. D.; Huang, P.; Ge, Q.; Quirk, R. P.; Thomas, E. L.; Lotz, B.; Hsiao, B. S.; Yeh, F.; Liu, L. *Adv. Mater*. **2002**, *14*, 31.

236 Reiter, G.; Castelein, G.; Hoerner, P.; Riess, G.; Blumen, A.; Sommer, J. U. *Phys. Rev. Lett*. **1999**, *83*, 3844.

237 (a) McConnell, G. A.; Gast, A. P.; Huang, J. S.; Smith, S. D. *Phys. Rev. Lett*. **1993**, *71*, 2102; (b) McConnell, G. A.; Lin, M. Y., Gast, A. P. *Macromolecules* **1995**, *28*, 6754; (c) McConnell, G. A.; Gast, A, A. P. *Macromolecules* **1997**, *30*, 435. (d) Webber, S. E.; Munk, P.; Tuzar, Z.; Eds., *Solvents and Self Organization of Polymers* (Kluwer Academic, Dordrecht, 1996); Webber, S. E. *J. Phys. Chem. B* **1998**, *102*, 2618; (e) Halperin, A.; Tirrell, M.; Lodge, T. P. *Adv. Polymer Sci*. **1992**, *100*, 31; (f) Förster, S.; Antonietti, M. *Adv. Mater*. **1998**, *10*, 195.

238 (a) Tuzar, Z.; Kratochvil, P. *Surf. Colloid Sci*. **1993**, *15*, 1; (b) Aleen, C.; Mayinger, D.; Eisenberg, A. *Colloids Surf*. **1999**, *16*, 3.

239 (a) Won, Y. Y.; Davis, T. H.; Bates, F. S., Agamalian, M.; Wignall, G. D. *J. Phys. Chem. B* **2000**, *104*, 7134; (b) Cammas-Marion, S.; Okano, T.; Kataoka, K. *Colloids Surf. B* **1999**, *16*, 207; (c) Bergbreiter, D. E. *Angew. Chem. Int. Ed*. **1999**, *38*, 2870.

240 Otsuka, H.; Nagasaki, Y.; Kataoka, K., *Curren. Opin. Colloid. Interf. Sci*. **2001**, *6*, 3.

241 (a) Holmberg, K.; Bergstrom, K.; Brink, C.; Osterberg, E.; Tiberg, F.; Harris, J. M. *J. Adhes. Sci. Technol*. **1993**, *7*, 530; (b) Ista, L. K.; Fan, H.; Baca, O.; Lopez, G. P. *FEMS Microbiol. Lett*. **1996**, *142*, 59.

242 Micoulet, A. Spatz, J. P.; Ott, A. *ChemPhysChem* **2005**, *6*, 663.

243 Kumar, N.; Hahm, J. *Langmuir* **2005**, *21*, 6652.

244 Freemantle, M. *Chem. Eng. News* **1999**, *77 (Feb.) 22*.

245 Weigl, B. H.; Yager, P. *Science* **1999**, *283*, 346.

Chapter 3

Confinement Effects on the Reactivity in Ultrathin Polymer Films: Kinetics and Temperature Dependence of the Hydrolysis of NHS and tBA Esters*

The effect of spatial confinement of the reactants on the kinetics of the hydrolysis of poly(N-hydroxysuccinimidyl methacrylate) (PNHSMA) and polystyrene-block-poly(tert-butyl acrylate) (PS_n-b-$PtBA_m$) ultrathin films (~90 nm) on oxidized silicon substrates was systematically investigated. The activation energies determined according to the Arrhenius equation, and in particular the activation entropies calculated according to the transition state theory, revealed that steric crowding in the surface-near region and tightness of the transition state is less pronounced in polymer films compared to self-assembled monolayers (SAMs) that expose the same reactive ester groups. Apparent rate constants calculated according to infrared (IR) spectroscopy and contact angle (CA) data for both polymers and SAMs directly demonstrated that polymer films are characterized by higher reactivity, as well as a high density of reactive functional groups at and near the polymer surface. However, the reactivity of polymer films was reduced compared to reactivity in solution because of restricted access and reduced mobility of the ester functional groups in these films. Finally, it was found that polymer film thickness, thermal pre-treatment of the films, block copolymer composition for PS_n-b-$PtBA_m$ and local surface composition did not affect the rate constants of hydrolysis.

3.1 Introduction

The ability to control the chemical and structural properties of surfaces is crucial for advancements in selective and environmentally friendly catalysis,[1] electronics,[2] chemical sensing,[3,4,5,6,7] bio-chemistry,[8] and applications in many other areas.[9,10] Studies of chemical reactions of surfaces may provide new routes to tailored surface properties. Such reactions allow, for example, the tethering of biologically important molecules to surfaces, which can be of significant importance in chemical biology and microarray technology.[11] In addition, chemical reactions occurring on organic or polymeric surfaces play a crucial role in many applications, ranging from the mentioned array technologies to biosensors,[12] nanoclusters,[13] anchoring of proteins,[14] nanoreactors,[15] and drug delivery[16] (see Chapter 2).

Self-assembled monolayers (SAMs) are perhaps the most popular model systems for studies of chemistry at interfaces under controlled conditions. In the last decade, countless studies have been performed that involve the chemical modification of monolayers.[17,18,19,20,21,22] However, the reactivity of functional groups placed in an ordered monolayer environment will be influenced by many factors,

---

* Part of the work described in this Chapter has been published in: Schönherr H.; Feng C. L.; Shovsky A. *PMSE Prepr.* **2003**, *89*, 250-251. Schönherr H.; Feng C. L.; Shovsky A. *Langmuir*, **2003**, *19*, 10843-10851; Feng C. L.; Vancso G. J.; Schönherr H. *Langmuir* **2005**, *21*, 2356-2363.

such as solvent, steric and electronic effects.[23] Thus, the chemical reactivity can be affected by confinement effects, which leads to reduced reactivity and incomplete conversions.[24] For typical applications in, e.g., the areas of sensors, however, rapid reactions and full conversion are desirable to optimize throughput and to minimize reaction times.

Compared to SAMs,[18,23] polymer films may offer the advantage of a quasi-3-D structure (high loading per unit surface area) and the possibility to exploit the rich structural hierarchy of ordering on different length scales. In particular, block copolymers can be regarded as ideal candidates in this respect. Block copolymers can self-assemble into well-defined microphase-separated morphologies that have tremendous potential in different application areas (see Chapter 2).[25] By varying film thickness,[26] controlling interfacial interactions,[27] as well as applying external fields,[28] diblock copolymer domains, which exhibit characteristic dimensions on the nanoscale, can be readily oriented in thin films.

In addition to thin polymer films,[29] dendrimers,[30] and hyperbranched polymers,[31,32] *N*-hydroxy succinimide (NHS) ester polymer brushes prepared, e.g., by grafting-from procedures[33] have been reported as a viable alternative in screening assays. The physical behavior of polymers in confinement, such as in substrate-supported ultrathin films,[34] differs considerably from the behavior observed in the bulk and is often governed by interfacial effects.[35] Depending on the thickness of ultrathin films (film thickness < 100 nm), the glass transition temperature[36], surface composition[37] (see also this Chapter), or the crystallization kinetics[38] may be altered, among other properties. In particular, the topmost layer of substrate-supported ultrathin polymer films can be considered to possess properties different from the bulk, which may affect surface reactivity.[39,40] As a result, surface chemical reactions may be different compared to reactions in solution or in the gas phase (see also Chapter 5).

In this Chapter, two different polymer thin film model systems, i.e. poly(N-hydroxysuccinimidyl methacrylate) (PNHSMA) and polystyrene-block-poly(tert-butyl acrylate) (PS_n-b-$PtBA_m$) were studied, which possess different hydrolysis behavior and were exploited in the fabrication of bioreactive platforms in subsequent Chapters. The reaction kinetics of the hydrolysis of NHS ester groups in PNHSMA and tBA ester groups in PS_n-*b*-$PtBA_m$ films were investigated as a function of temperature, film thickness, thermal pre-treatment and relative ester surface coverage to unravel the impact of confinement on the kinetics of the surface hydrolysis. Based on the understanding of the factors that govern reactivity in thin substrate-supported reactive polymer films, optimized procedures for surface functionalization with high loading (see Chapters 4, 5) and sub-micrometer local patterning strategies can be developed (Chapters 5-7).

3.2 Ultrathin PNHSMA Polymer Films

Firstly, the reaction kinetics of the hydrolysis of NHS ester groups in PNHSMA films was studied as a function of temperature. The analysis was mainly based on by IR and CA and yielded apparent rate constants and activation energies.

3.2.1 Characterization of the Hydrolysis of PNHSMA Films

The reaction of PNHSMA film in base solution to form the corresponding carboxylate is shown in Scheme 3.1.

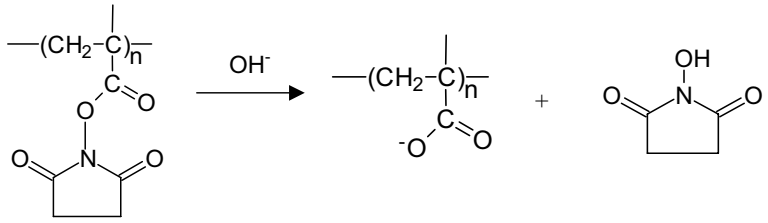

Scheme 3.1. Schematic of hydrolysis of PNHSMA copolymer to yield poly(methacrylic acid) (PMAA).

Smooth films of the NHS ester methacrylate polymer PNHSMA on oxidized silicon with a thickness of 40 ± 5 nm were obtained by spin-coating from DMF. Tapping mode atomic force microscopy (TM-AFM) images acquired in air showed almost featureless films with a rms roughness of 0.5 ± 0.2 nm assessed from 1 μm^2 images (Figure 3.1a). Tapping mode AFM data (Figure 3.1b) provided evidence for the integrity of the films. After a treatment time of 17 hours the rms roughness was virtually unchanged (0.7 ± 0.2 nm), however, the TM-AFM height images revealed a granular texture, in which small protrusions was observed. The change in morphology can be attributed to the swelling of the PMMA exposed at the surface as a result of water uptake from the ambient atmosphere and formation of PMAA globules (Chapter 4). Hydrolysis was carried out in base solution (concentration $[OH^-] = (1.8 \pm 0.2) \times 10^{-2}$ M) for different reactions times.

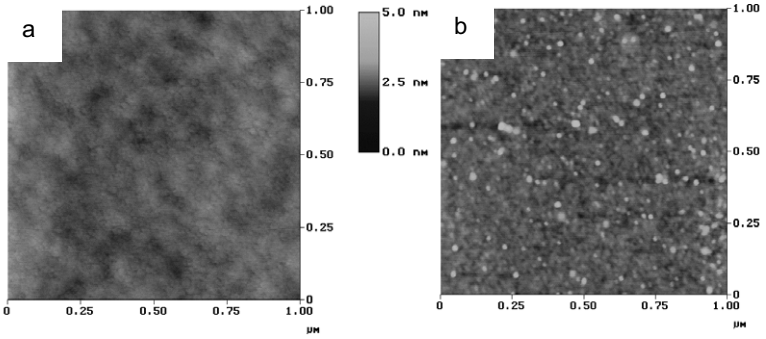

Figure 3.1. Tapping mode AFM height images of PNHSMA on SiO_2 (a) prior to and (b) after hydrolysis for 17 hours.

The thin film transmission FTIR spectrum of PNHSMA on SiO_2 did not differ from bulk spectra of the polymer obtained in KBr as shown in Figure 3.2. The most important bands are those of the succinimide carbonyl C=O stretching vibration (ν (C=O), 1737 cm^{-1}), the split ester carbonyl C=O stretching vibration (ν (C=O), 1810 cm^{-1}, 1780 cm^{-1}) and the C-O stretching vibration (ν (C-O), 1205 cm^{-1}). Transmission mode FTIR spectra, in which transition dipoles in the plane of the polymer films

are sampled, and complementary p-polarized grazing incidence reflection spectra were virtually identical indicating the absence of a preferred molecular orientation.

For the analysis of hydrolyzed films (*vide infra*), the absorbance of the relevant carbonyl bands was normalized to the C-O vibration associated with the carboxyl group of the ester at 1205 cm^{-1} (Figure 3.2).

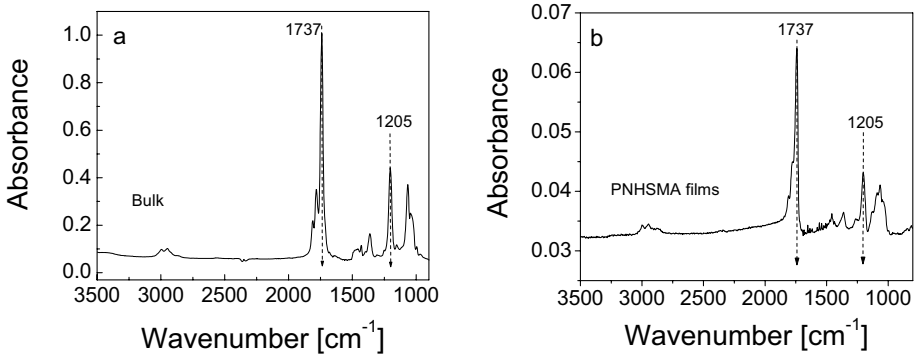

Figure 3.2. Transmission mode FTIR spectrum of (a) bulk and (b) ultrathin film of PNHSMA (film thickness: ~40 nm) supported on oxidized silicon. The absorption bands of the succinimide carbonyl C=O stretching vibration (ν (C=O), 1737 cm^{-1}) and the C-O stretching vibration (ν (C-O), 1205 cm^{-1}) are indicated.

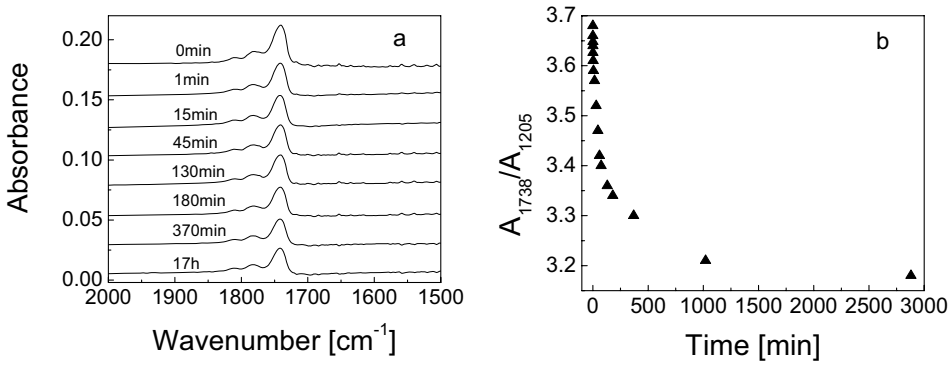

Figure 3.3. (a) Transmission FTIR spectra of films of PNHSMA on SiO_2 following hydrolysis at 21ºC for the indicated reaction time; (b) integrated absorbance for succinimide carbonyl band (ν (C=O), 1737 cm^{-1}) normalized to the absorbance of the C-O stretching vibration (ν (C-O), 1205 cm^{-1}).

The progress of the reaction was assessed in FTIR measurements (Figure 3.3), as well as by CA measurements (Figure 3.4). After an initial rapid decrease in normalized absorbance of the succinimide ester band (Figure 3.3b), the reaction slows down progressively. Considering the penetration depth of IR irradiation into organic material, it is evident that IR samples the *entire* depth of the ultrathin film.[41] From the FTIR data (Figure 3.3a) it can be concluded that the reaction does not

proceed through the entire film. The initial rapid decrease in NHS ester coverage may be attributed to the reaction at the surface of the polymer film, while at longer times the surface-near region of the film is more slowly hydrolyzed. This latter observation can be explained in part by the presence of deprotonated carboxyl groups in the surface region of the film that may repel diffusing hydroxide ions.

The course of the reaction can be quantified by analyzing the changes in absorbance of the succinimidyl carbonyl band. The absence of possible carboxylate was confirmed in the region of 1540 - 1560 cm^{-1}, the presence of dimeric carboxylic acids (1704 cm^{-1}) is not pronounced.[42] The absorbance of monomeric acid (1710 - 1720 cm^{-1}), as measured in addition to the mentioned dimeric carboxylic acids (1704 cm^{-1}) in independent IR experiments on spin-coated films of poly(methacrylic acid), would overlap partially with the succinimidyl carbonyl band at 1737 cm^{-1}. Since the contribution of the bands of the monomeric and dimeric acid can be expected to be very small compared to the changes in absorbance of the succinimidyl carbonyl band and to be approximately equal to the decrease in absorbance of the ester carbonyl bands, we have estimated the changes in film composition by analyzing the integrated absorbance of the entire carbonyl region. This procedure takes the decrease of both the ester and the succinimidyl carbonyl bands, as well as the increase of the carboxylic acid band, into account.[43]

The initial course of the reaction, as followed by both FTIR and CA measurements, is summarized in Figure 3.4a. It is evident that the reaction, as sampled by CA, seems to proceed more rapidly than sampled by IR spectroscopy. This difference can be attributed to the different information depth of the methods. While the water droplets in the CA measurements probe the outermost 5 - 10 Å,[44] IR spectroscopy probes all chromophores in the irradiated area throughout the entire depth of the film. Since the reaction must start at the polymer - solution interface and IR spectroscopy is not very surface-sensitive, IR provides information about the reaction at the surface only at the beginning of the reaction.

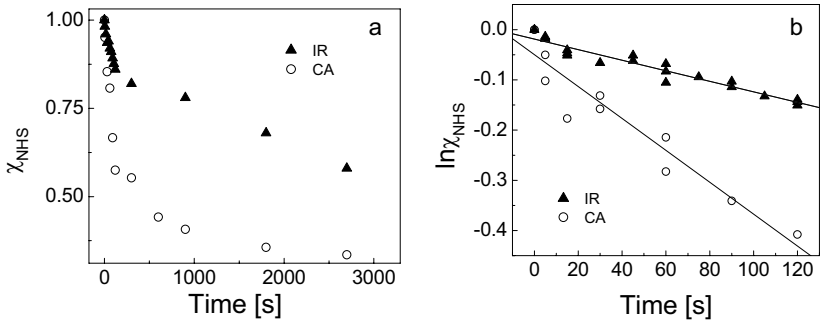

Figure 3.4. (a) Comparison of the early stages of the hydrolysis as probed by CA measurements and FTIR spectroscopy at 21°C. The coverage of NHS groups was calculated from the CA data by applying the Cassie equation: [45] $\cos\theta_{exp} = \chi_{NHS}\cos\theta_{NHS} + \chi_{COOH}\cos\theta_{COOH}$ *where χ_{NHS} and χ_{COOH} are the surface coverages of the two components and θ_{NHS} and θ_{COOH} are 60° and 35°, respectively. (b) Linearization of the kinetic data shown in Figure 3.4a for short reaction times according to pseudo-first-order kinetics. The solid lines correspond to linear least squares fits of the IR and CA data, respectively.*

For short reaction times (< 120 s) we observe an exponential decrease of the NHS ester coverage (Figure 3.4b). This behavior is consistent with a pseudo-first-order reaction kinetics at the early stage of the reaction and the presence of a homogeneous reaction (*vide supra*). From the slopes of the linearized plot in Figure 3.4b we can estimate the apparent pseudo-first-order rate constants k' of the hydrolysis at 21°C, which can then be converted to concentration-independent second order rate constants. The rate of the reaction is described by:

$$-\frac{d[NHS]}{dt} = k''[OH^-][NHS] = k'[NHS] \qquad (1)$$

where [NHS] and [OH^-] denote the concentration of NHS ester and hydroxide ions, respectively, k'' and k' are the second order and pseudo-first-order rate constants, respectively ([OH^-] ≈ constant; $k' = k''$ [OH^-]).

For comparison, we show previously reported data for the hydrolysis of 11,11`-dithiobis(*N*-hydroxysuccinimidylundecanoate) (NHS-C10) films in 1.00×10^{-2} M aqueous solution of NaOH on gold at 21°C in Scheme 3.2. Similar to PNHSMA films, the progress of the reaction was conveniently and rapidly followed by CA measurements at 20ºC.

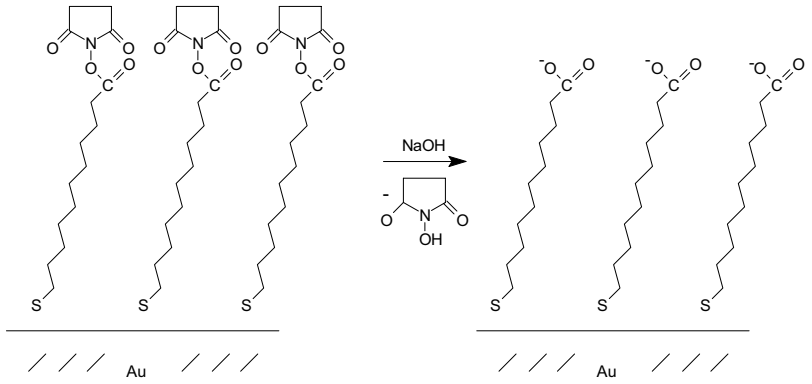

Scheme 3.2. Schematic of the hydrolysis of terminal NHS-esters in SAMs of NHS-C10 on gold in aqueous sodium hydroxide.[46]

The corresponding rate constants for both SAMs and PNHSMA films are summarized in Table 3.1. The apparent rate constant for the SAMs (5×10^{-2} L/mol s) is five times smaller than that for the surface of the polymer films (26×10^{-2} L/mol s). However, the rate constants for both systems are much smaller compared to similar reactions in solution. These results indicate that the reaction is affected by confinement effects both in the SAMs and the ultrathin polymer films.

Table 3.1. Rate constants of base-catalyzed hydrolysis of different NHS esters.

sample	k'' [L/mol s]
NHS ester (solution); T = 25°C*	8700×10^{-2} [a]
NHS-C10 (CA, IR); T = 20°C	5×10^{-2}
PNHSMA (IR); T = 21°C	7×10^{-2}
PNHSMA (CA); T = 21°C	26×10^{-2}

[a] data taken from reference 47.

3.2.2 Temperature Dependence of Reaction Kinetics

The reaction was further studied systematically at different temperatures. We observed consistently that the early stages of the hydrolysis could be described as pseudo-first-order reaction (Figure 3.5). The apparent second order rate constants, calculated from the linear least squares fits shown in Figure 3.5 for the hydrolysis of the NHS groups in the polymer films obey the Arrhenius equation (Figure 3.6) (equation 2).

$$\ln k'' = \ln A - \frac{E_a}{RT} \qquad (2)$$

The value of the apparent activation energy determined at the surface by CA measurements ($E_{a\,(CA)}$ = 61 ± 2 kJ/mol) is smaller than in the surface-near region, as probed by IR spectroscopy ($E_{a\,(IR)}$ = 99 ± 2 kJ/mol). This finding can be understood since the surface region of the polymer film can be

expected to be more mobile than the surface-near region owing to more open structure at and very close to the film solution interface.

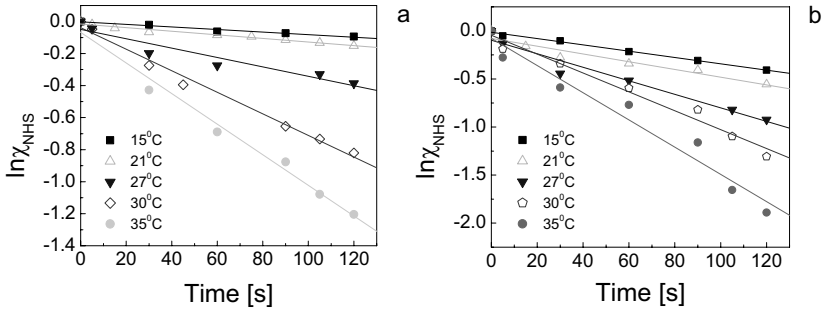

Figure 3.5. Linearization of the NHS ester surface coverages determined from (a) the CA data and (b) the FTIR data acquired at various reaction temperatures according to pseudo-first-order kinetics. The solid lines correspond to linear least squares fits of the data.

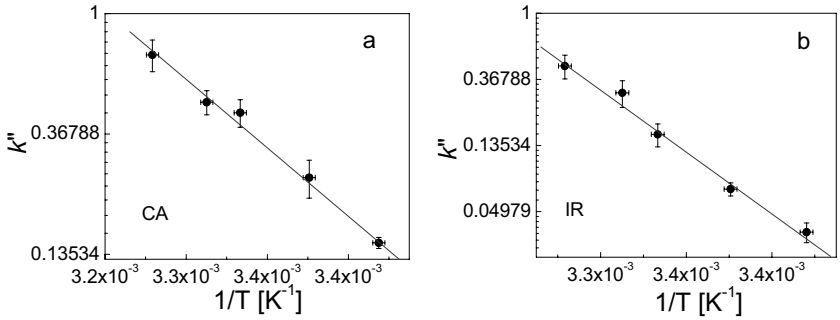

Figure 3.6. Logarithmic plots of second order rate constants obtained from the linear fits in Figure 3.5 vs. inverse temperature according to the Arrhenius equation for (a) CA data and (b) IR data. The solid lines correspond to linear least squares fits of the data.

Table 3.2. Apparent activation energies and estimated parameters characterizing the transition state.

sample	E_a [kJ/mol]	A [(M s)$^{-1}$]	$\Delta S^{\neq}$ [J/mol K][a,*]	$\Delta H^{\neq}$ [kJ/mol][b,*]	$\Delta G^{\neq}$ [kJ/mol][c,*]
NHS-C10	30 ± 1	2.1 x 10^4	- 176	28	80
PNHSMA (CA)	61 ± 2	1.2 x 10^{10}	- 59	59	76
PNHSMA (IR)	99 ± 2	2.0 x 10^{16}	+ 54	97	81

* calculated for T = 298 K

[a] calculated according to $\Delta S^{\neq} = R(\ln A/T - \ln k_b/h - 1)$ (3)
where k_b denotes the Boltzmann constant and h denotes Planck's constant

[b] calculated according to $\Delta H^{\neq} = E_a$ - RT with gas constant R (4)

[c] calculated according to $\Delta G^{\neq} = \Delta H^{\neq}$ - T $\Delta S^{\neq}$ (5)

For NHS-C10 monolayers, the second order rate constants also obey the Arrhenius equation (equation 2).[48] The activation energies and the parameters characterizing the transition state of the

activated complex are summarized in Table 3.2 for both the reactions in SAMs and the reactions of the ultrathin polymer films.

3.2.3 Comparison of Surface Reactions in SAMs and Ultrathin Polymer Films

Both self-assembled monolayer and ultrathin homopolymer film systems studied show pseudo-first order surface hydrolysis kinetics and obey the Arrhenius equation. A comparison with the hydrolysis of low molar mass NHS esters in solution (Table 3.1) indicates that the reactivity is significantly reduced in the SAMs (decrease of k'' by three orders of magnitude compared to solution), as well as the surface of the ultrathin polymer films (decrease of k'' by two orders of magnitude compared to solution). Hence, we can attribute this general observation to the strong confinement effects present.

The reduced apparent second order rate constants seem to reflect both the order of the system, the accessibility of the carbonyl carbons attacked by the hydroxide ions in the reaction (Table 3.2), and possibly the difference in local polarity.[49] At the surface of the polymer films, the reactivity of the NHS esters is higher than in the SAMs owing to the absence of a near-closed packing of the ester groups and an increase in free volume of the polymer (Scheme 3.3.). For the reaction in the surface-near region of the polymer film, where a more bulk-like polymer structure can be expected, the rate constant decreases and is comparable to the SAMs (Table 3.1). This observation may also be attributed to a lower effective concentration of hydroxide ions in the corresponding region of the film, as well as in and out diffusion of reactants and reaction products.

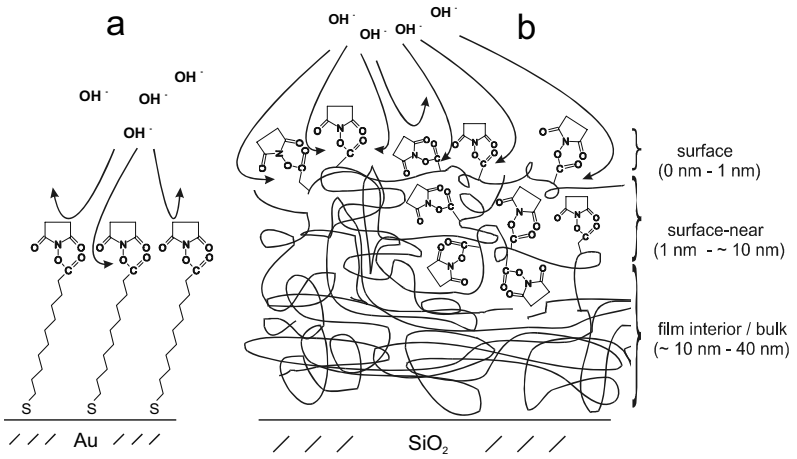

Scheme 3.3. Schematic of base-catalyzed hydrolysis reaction in (a) SAMs of NHS-C10 and (b) ultrathin films of PNHSMA on oxidized silicon together with definition of surface and surface-near regions of the polymer film. The approximate depths in this tentative model were assigned based on (1) the information depth of the techniques (CA: 1 nm, IR: the entire film, i.e. 40 nm), (2) the fact that only 25% of the NHS ester groups can be hydrolyzed, and (3) on the assumption that the reaction can be expected to start at the film-solution interface and proceeds homogeneously into the amorphous film.

The activation energies show a different trend than the rate constants. For the surface reaction of PNHSMA, the activation energies are significantly higher than observed for SAMs of NHS-C10. The surface-near region of PNHSMA shows the highest activation energy. These observations can be attributed to an increase in mobility and flexibility in the polymer films compared to the SAMs. $\Delta G^{\neq}$ does not vary significantly, whereas the activation entropies $\Delta S^{\neq}$ increase in the same order as the activation energies. For the surface-near region of PNHSMA the activation entropies become positive. While the hydrolysis of NHS-C10 is characterized by a very tight and sterically demanding transition state, as judged by the magnitude of $\Delta S^{\neq}$,[47] the transition state is less crowded for PNHSMA and even becomes favorable in the case of the interior of the polymer. This latter result can be attributed to swelling effects of the hydrolyzation product poly(methacrylic acid)**.**

In summary, the quantitative elucidation of the hydrolysis kinetics for reactive polymer confined into ultrathin films suggests that the surface of this polymer film is more reactive in a simple hydrolysis reaction compared to the structurally related NHS-C10 SAMs. Since the reaction at the polymer film surface is significantly less confined than in the SAMs, the reaction can also be much more efficiently affected by temperature. This feature makes the use of polymer surface reactions an attractive avenue for localized thermal reactions.[50]

As an alternative polymer system, PS_n-*b*-$PtBA_m$ was also studied. Reactive tBA groups can be hydrolyzed under acidic conditions. In addition, the absence of background fluorescence (detected for PNHSMA in feasibility experiments for single molecule optical studies), the ease of topographical patterning, and microphase separation of PS_n-*b*-$PtBA_m$ films render this system attractive for various application (see Chapters 6, 7, 8). In the following sections, the hydrolysis and reactivity of PS_n-*b*-$PtBA_m$ will be discussed in detail.

3.3 Ultrathin PS_n-b-$PtBA_m$ Polymer Films

In order to unravel the impact of confinement on the kinetics of the surface hydrolysis of PtBA containing block copolymers, the composition and structure of the surface and the surface-near region of polystyrene-*block*-poly(*tert*-butyl acrylate) (PS_n-*b*-$PtBA_m$) films were characterized first. Subsequently, the hydrolysis kinetics of thin films on oxidized silicon in aqueous hydrochloric acid and its dependence on various parameters were addressed.

3.3.1 Characterization of Polymer Thin Film Surface Composition

The reactivity of the *t*-butyl ester groups in thin films of PS_n-*b*-$PtBA_m$ (shown in Scheme 3.4) is potentially influenced by the local chemical composition and structure of the surface of the films. A skin layer of PtBA can be expected for microphase separated block copolymer films owing to the lower surface tension of PtBA compared to PS (γ_{PtBA} = 31.2 mN/m; γ_{PS} = 40.7 mN/m).[34] To validate the existence of a skin layer, the surfaces of spin-coated films were investigated by CA and angle-dependent X-photoelectron spectroscopy (XPS) measurements.

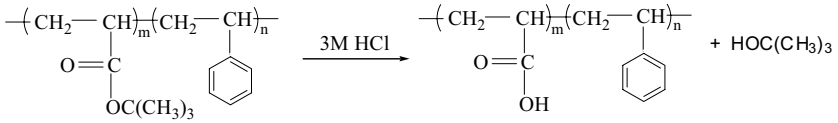

Scheme 3.4. Schematic of hydrolysis of PS_n-b-$PtBA_m$ diblock copolymer to yield PS_n-b-PAA_m.

Static CA were measured with water (H_2O) and diiodomethane (CH_2I_2) as probe liquids on PS_n-*b*-$PtBA_m$ films (thickness ~ 90 nm). The values obtained for PtBA and PS_{690}-*b*-$PtBA_{1210}$, as well as PS_{2091}-*b*-$PtBA_{1054}$, were identical within the experimental error, while neat PS films showed lower CA. These data agree well with the differences in surface tension of the blocks and indicate that PtBA is exposed on the PS_{690}-*b*-$PtBA_{1210}$ and PS_{2091}-*b*-$PtBA_{1054}$ block copolymer films. By contrast, films of PS_{88}-*b*-$PtBA_{35}$, which do not exhibit microphase separation (see below), showed intermediate CA values.

Table 3.3. Static CA measured with water and diiodomethane as probe liquids on spin-coated films of various polymers on oxidized silicon (film thickness ~ 90 nm).

	θ_{H_2O} [deg]	$\theta_{CH_2I_2}$ [deg]
PS_{690}-*b*-$PtBA_{1210}$	89 ± 2	23 ± 2
PS_{2091}-*b*-$PtBA_{1054}$	89 ± 2	23 ± 2
PS_{88}-*b*-$PtBA_{35}$	88 ± 2	20 ± 2
PtBA	89 ± 2	23 ± 2
PS	86 ± 2	15 ± 2

More definite evidence for skin layer formation, in particular for films of PS_{690}-*b*-$PtBA_{1210}$, was obtained in XPS scans with a take-off angle of 45° (Figure 3.7). We observed only the expected elements, i.e. carbon and oxygen (except for PS homopolymer, which showed only carbon). The C_{1s} peak corresponding to neutral carbon was observed at 284.0 eV. The C_{1s} peak observed at 287.8 eV for the PtBA containing polymers was assigned to the carbonyl carbon. For PS also the C_{1s} shake-up peak corresponding to π-π* transition of the benzene ring was observed at 290.2 - 291.0 eV.

The oxygen/carbon ratio for PS_{690}-*b*-$PtBA_{1210}$ derived from the integrated intensities of the corresponding O_{1s} and C_{1s} peaks, as summarized in Table 3.4, is within the experimental error equal to that obtained on PtBA homopolymer films, indicating the presence of a PtBA skin layer for this polymer.

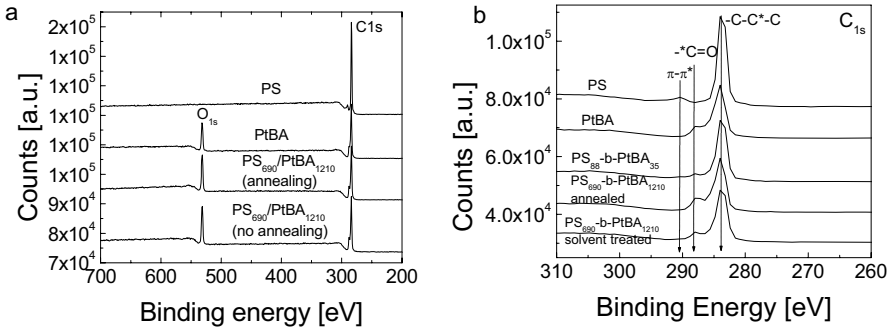

Figure 3.7. (a): XPS survey scans of different thin polymer films; (b): XPS C_{1s} core-level spectra of different polymer films on SiO_2 substrates (film thickness ~ 90 nm). All neutral C_{1s} peaks were assigned to a binding energy of 284.0 eV to correct for the charging energy shift.

Table 3.4. Carbon / oxygen ratios determined by XPS at take-off angles of 45 °.

	Experimental value C/O ratio	Theoretical value C/O ratio[b]
PtBA	3.6 ± 0.4	3.5
PS	-[a]	-
PS_{88}-*b*-$PtBA_{35}$	10.3 ± 1.2	12.5
PS_{2091}-*b*-$PtBA_{1054}$ annealed	4.2 ± 0.4	10.9
PS_{2091}-*b*-$PtBA_{1054}$ annealed + solvent	9.5 ± 1.1	10.9
PS_{690}-*b*-$PtBA_{1210}$ annealed	3.5 ± 0.3	6.1
PS_{690}-*b*-$PtBA_{1210}$ annealed + solvent	6.0 ± 0.7	6.1

[a] no oxygen detected; [b] values calculated based on the stoichiometry of the corresponding block copolymer.

Films of PS_{2091}-*b*-$PtBA_{1054}$ showed a slight carbon enrichment in the depth probed using a take-off angle of 45° (ca. 7 nm, see below), since the C/O ratio exceeds the theoretical value for PtBA. This observation is consistent with a thinner skin layer for the PS rich block copolymer thin films. For the non-microphase separated film of PS_{88}-*b*-$PtBA_{35}$, we observe a near-stoichiometric ratio of C/O indicating the absence of a skin layer.

A solvent treatment with cyclohexane, similar to the procedure discussed in reference 51 combined with soft lithography, was used to obtain an enrichment of PS in the surface-near region of the films (see also Chapter 8). The observed C/O ratios of 6.0 ± 0.7 and 9.5 ± 1.1 indicate a coexistence of both

blocks in the sampled depth of the film surface for solvent-treated PS_{690}-*b*-$PtBA_{1210}$ and PS_{2091}-*b*-$PtBA_{1054}$, respectively.

The thickness of the skin layer on PS_{690}-*b*-$PtBA_{1210}$ films was estimated by variable-angle XPS experiments. The take-off angle α was varied systematically to control the information depth and thus to obtain chemical composition vs. depth profile.[52] The data for four different take-off angles are shown in Table 3.5. Up to an angle of 45°, which corresponds to an estimated information depth of 7 nm,[38] the value of the surface composition was equal to that found for PtBA homopolymer films. For angles exceeding 60° (information depth of 8.7 nm),[38] an increase of the C/O ratio was observed, which is consistent with a contribution of PS from the underlying microphase separated PS_{690}-*b*-$PtBA_{1210}$ to the detected XPS signal. Based on this experiment, the thickness of the skin layer of PS_{690}-*b*-$PtBA_{1210}$ film is estimated as 8 ± 1 nm.

Table 3.5. Theoretical and experimental C/O ratios obtained for different take-off angles and estimated information depths by angle-dependent XPS for 90 nm thin films of PS_{690}-b-$PtBA_{1210}$.

	theoretical C/O ratio (PtBA)	experimental C/O ratio (30º, 5 nm)	experimental C/O ratio (45º, 7 nm)	experimental C/O ratio (60º, 9nm)	experimental C/O ratio (90º, 10 nm)
PS_{690}-*b*-$PtBA_{1210}$	3.5	3.5	3.5	3.7	3.8

3.3.2. Characterization and Kinetics of the Hydrolysis of PS_m-b-$PtBA_n$ Films

The changes of CA of PS_{690}-*b*-$PtBA_{1210}$ with reaction time for a reaction temperature of 25°C in 3 M HCl are shown in Figure 3.8. Since a reorientation of the created PAA-rich surface region may occur, which would lead to an exposure of unhydrolyzed PtBA at the surface to lower the free surface energy,[53] the CA measurements can be anticipated to yield an underestimate of the extent of the surface hydrolysis reaction. Considering the depth information for the transmission FTIR measurements, it is obvious that the IR active chromophores throughout the entire depth of the thin film will contribute to the measured signal.[54] Therefore the kinetics was determined via FTIR measurement.

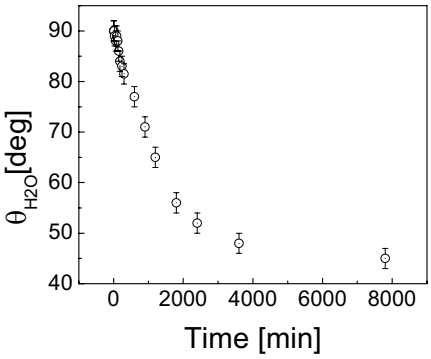

Figure 3.8: Static water contact angle of PS_{690}-b-$PtBA_{1210}$ measured as function of hydrolysis time.

The vibrational assignments and peak wavenumbers of the major absorptions in the spectra of unhydrolyzed PS_n-*b*-$PtBA_m$ before and after hydrolysis are listed in Table 3.6. Compared to the spectra of PS_{690}-*b*-$PtBA_{1210}$, the acid functionality is clearly visible as broad band at > 3000 to 3500 cm^{-1} (ν(COOH) *after* hydrolysis in Figure 3.9.[55] The intense absorption of PtBA (ν(C=O) at 1733 cm^{-1} was replaced by a broad peak at 1710 cm^{-1} assigned to the absorbance of carboxylic acids[41] in the PAA block. The intense band of the methyl group $\nu_{as}(CH_3)$ at 2978 cm^{-1}, $\nu_s(CH_3)$ at 2875 cm^{-1} and a doublet at 1392/1368 cm^{-1} from the symmetric methyl deformation mode disappeared. Some absorption bands related to the methylene groups did not show changes for the two blocks, for example, $\nu_{as}(CH_2)$ at 2926 $cm^{-1}$and $\nu_s(CH_2)$ at 2852 cm^{-1}.

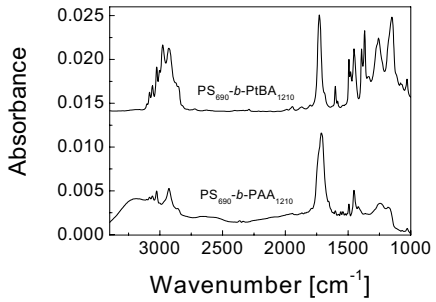

Figure 3.9. Transmission IR spectra of PS_{690}-b-$PtBA_{1210}$ and PS_{690}-b-PAA_{1210} block copolymers.

Table 3.6: Peak assignments and wavenumbers for infrared spectra of PS-b-PtBA and PS-b-PAA films on oxidized silicon.[39,56]

Vibration	PS block (cm^{-1})	PtBA block (cm^{-1})	PAA block (cm^{-1})
$\nu(CH)_{aromat.}$	3083		
	3062		
	3061		
$\nu_{as}(CH_3)$		2978	
$\nu_{s}(CH_3)$		2875	
$\nu_{as}(CH_2)$	2924	2926	2926
$\nu_{s}(CH_2)$	2850	2852	2852
$\nu(C=O)$		1733	1710
$\nu(CC)_{aromat.}$	1493		
	1453		
$\delta_{s}(CH_3)$		1392	
		1368	
$\nu(C\text{-}O\text{-}C)$		1257	
		1145	
$\nu(C\text{-}O)_{COOH}$			1245
			1170

The completely different IR absorption for the PtBA and PAA blocks, in particular, the presence or absence of the absorption of *tert*-butyl groups, makes it possible to follow the reaction kinetics of the hydrolysis by investigating the integrated absorbance of the *tert*-butyl groups. Figure 3.10a shows typical spectra of the *tert*-butyl ester bands used for the estimation of the progress of the reaction. The absorbance of the $\nu_{as}(CH_3)$ band can be observed to decrease with progressing hydrolysis at 25ºC. For the analysis of hydrolyzed films, we normalized the absorbance of this band to the absorbance of the $\nu_{as}(CH_2)$ band at 2926 cm^{-1}, which is constant before and after hydrolysis. The normalized absorbance shown in Figure 3.10b decreases rapidly initially, then the reaction slows down progressively.

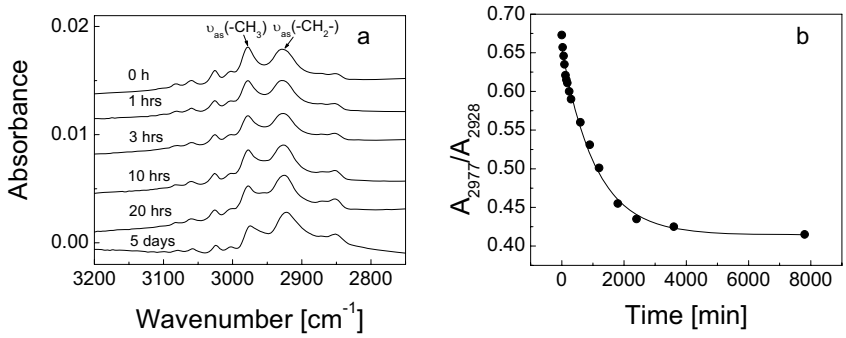

Figure 3.10. (a) Transmission FTIR spectra of films of PS-b-PtBA on oxidized silicon after various hydrolysis times (25°C, 3M HCl); (b) integrated absorbance for the $\nu_{as}(CH_3)$ vibration at 2978 cm^{-1} normalized to the absorbance of the $\nu_{as}(CH_2)$ vibration at 2926 cm^{-1}. The solid line corresponds to a fitted exponential decay.

Simultaneous tapping mode AFM height/phase imaging was used to investigate the changes of the surface morphology following hydrolysis on the nanometer scale (Figure 3.11). The equilibrium bulk morphology of the PS_{690}-*b*-$PtBA_{1210}$ block copolymer used is cylindrical (PS (35%) cylinders inside a PtBA matrix phase).[57] Using AFM we observed a morphology that is consistent with in-plane cylindrical structures in height images acquired on the untreated films of PS_{690}-*b*-$PtBA_{1210}$ on oxidized Si (film thickness 90 nm).[58]

AFM data acquired after different hydrolysis times are shown in Figure 3.11 c – f. Compared to untreated films (Figure 3.11 a,b), some small particle-like and worm-like features appeared on the surface after 1 hour hydrolysis (Figure 3.11 c,d). The small particles almost disappeared and surface coverage of "worms" increased on the surface with further progress of the reaction (Figure 3.11 e,f). Typical diameter of these worm-like features were ~13 nm. The mean roughness (R_a)[59] assessed from 1 μm^2 topographical images changed from 0.8 nm, 1.0 nm to 1.4 nm with increasing treatment time of 0, 60, and 120 minutes. The features observed in the height images were also clearly recognized in the phase images. The pronounced changes of phase contrast suggest that domains with different adhesive and likely different surface mechanical properties appeared.[60]

It is known that the PAA block is hydrophilic as the water CA of PAA is below 10°.[61] The surface coverage of exposed PAA will increase with the progress of the reaction on the top surface of the film, which will result in swelling of the surface owing to uptake of water from the reaction solution. Hence we attribute the observed particle and worm-like features to swollen PAA-rich globules on the film surface.

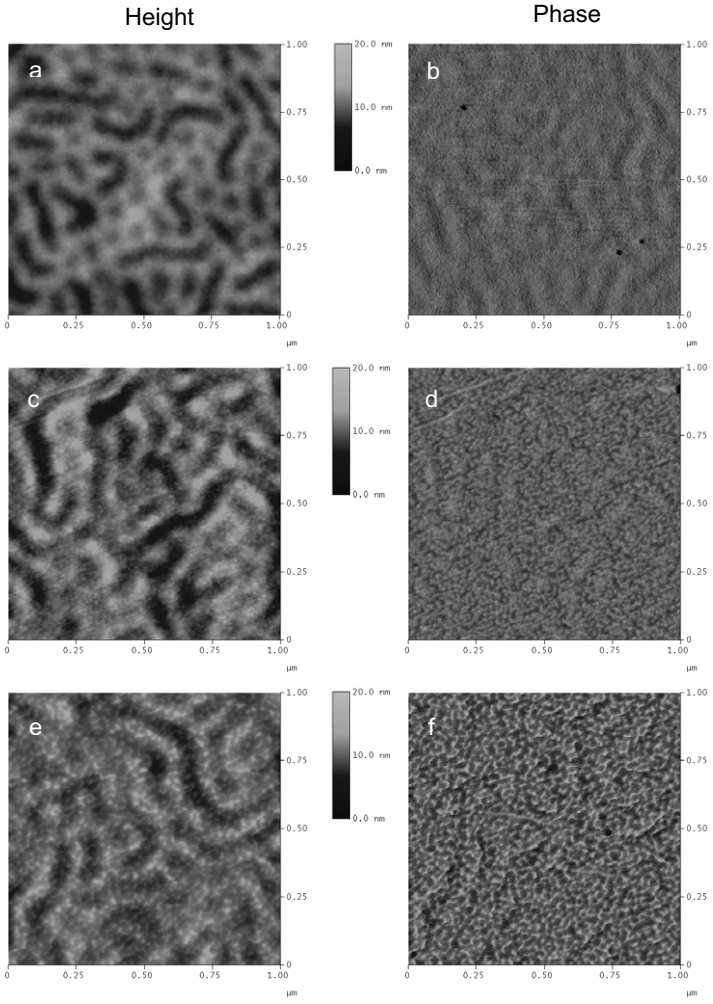

Figure 3.11. Tapping mode AFM height (left) and phase (right) images of PS_{690}-b-$PtBA_{1210}$ on oxidized Si following hydrolysis in 3M HCl at 60ºC for 0 min (a)(b), for 60 min (c)(d), and for 120 min (e)(f).

3.3.3 Investigation of the Temperature Dependence of Reaction Kinetics

Using FTIR spectroscopy, we observed an exponential decrease of the *t*-butyl ester surface coverage for reaction time shorter than 2 hrs. This behavior is consistent with pseudo-first-order reaction kinetics at the early stage for a homogeneous reaction. The kinetics was studied systematically at different temperatures. The IR and CA data acquired for shorter reaction times are shown in Figure 3.12. Due to reorientation effects of the film surface, the CA data (and application of, e.g., the Cassie equation)[45] lead to an underestimate of the extent of the reaction, as mentioned above. Thus, the quantitative analysis will be based on the IR data.

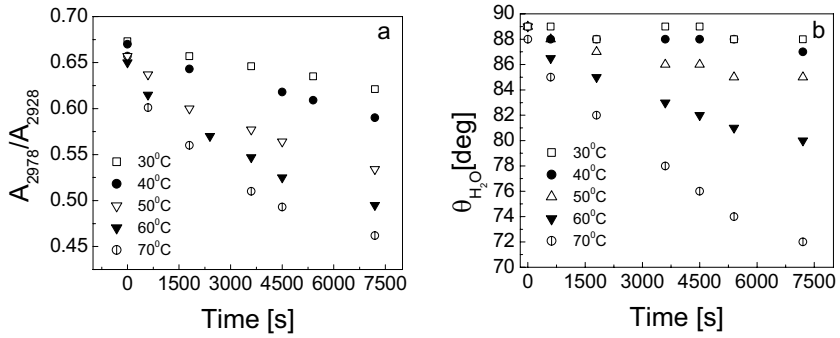

Figure 3.12. The early stages of the hydrolysis at five different temperatures as probed by (a) FTIR spectroscopy and (b) CA measurements.

Linearization of the tBA ester surface coverages, which are directly related to the conversion or extent of reaction, according to pseudo-first-order kinetics is shown in Figure 3.13a. From the slopes of the linearized plot, the different apparent pseudo-first-order rate constants k′ of the hydrolysis at different temperatures can be estimated. The second-order rate constants obey the Arrhenius equation, as shown in Figure 3.13b. The value of the apparent activation energy (E_a) was determined from these data as 51 ± 2 kJ/mol. In addition, other parameters characterizing the transition of the activated complex can be determined (see below).

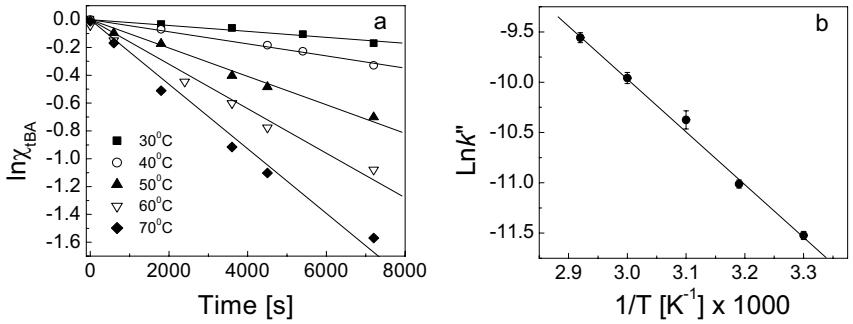

Figure 3.13. (a) Linearization of the tBA ester surface coverages determined from the FTIR data acquired according to pseudo-first-order kinetics for various reaction temperatures. The solid lines correspond to linear least-squares fits of the data. (b) Arrhenius plot of second-order rate constants obtained from the linear fits in (a). The solid line corresponds to a linear least-squares fit of the data.

3.3.4 Effects of Film Thickness and Thermal Pre-Treatment on Reaction Rates

As the morphology of block copolymer films may depend on film thickness[62] and hence may affect the properties of the exposed PtBA skin layer, a number of films with different thicknesses were investigated to unravel the possible influence of the film thickness of PS_n-*b*-$PtBA_m$ films on the rate of hydrolysis. We performed the hydrolysis for all the films under identical conditions (3M HCl, 60°C, 1hr). Due to the different film thicknesses, the calculation for the hydrolysis rate is replaced by the net

decrease of the integrated absorbance of the absorption band at 2978 cm^{-1} ($\nu_{as}(CH_3)$). *No* dependence of film thickness for the hydrolysis for these systems was observed, as shown in Figure 3.14.

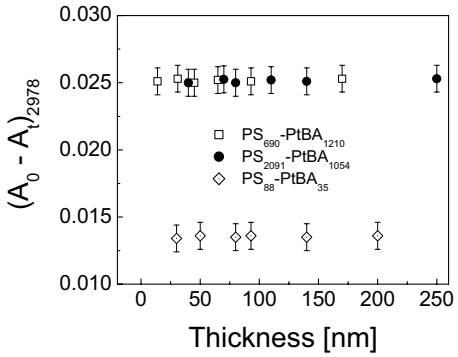

Figure 3.14: FTIR Investigation of conversion during the hydrolysis reaction in 3M HCl for PS-b-PtBA diblock copolymers for different film thicknesses. Microphase separation occurs for both PS_{690}-b-$PtBA_{1210}$ and PS_{2091}-b-$PtBA_{1054}$ diblock copolymers, but not for PS_{88}-b-$PtBA_{35}$. Each point corresponds to the net decrease of integrated area of the absorption band at 2978 cm^{-1} ($\nu_{as}(CH_3)$) after hydrolysis in 3M HCl for 60 minutes (T = 60ºC).

For both PS_{690}-b-$PtBA_{1210}$ and PS_{2091}-b-$PtBA_{1054}$ diblock copolymer films, identical results were obtained, as shown in Figure 3.14. Thus, the presence of a skin layer appears to be film thickness independent and also block ratio independent for films, in which microphase separation occurs (for additional XPS evidence, see above).

By contrast, the PS_{88}-*b*-$PtBA_{35}$ block copolymer does *not* show microphase separation due to the low molar mass and the low Flory-Huggins parameter of $\chi \approx 0.03$ ($\chi N = 2.48$).[63] The reaction of PS_{88}-*b*-$PtBA_{35}$ films with different thickness was also checked using the same experimental conditions. Also in this case *no* thickness dependence of the hydrolysis kinetics was found. However, a significant difference for this block copolymer is that the apparent rate of hydrolysis is lower than that of the other two block copolymers. This effect can be attributed to a smaller PtBA fraction exposed at the surface (Table 3.4) as will be explained in the next section.

3.3.5 Dependence of Hydrolysis Kinetics on Surface Composition

PS_{88}-*b*-$PtBA_{35}$ and PS_{690}-*b*-$PtBA_{1210}$ showed significantly different reaction rates under the same reaction conditions, which may be attributed to different fractional coverage of the PtBA block on the surface in different films. This becomes evident from the investigation of the surface composition dependent hydrolysis of PS_n-*b*-$PtBA_m$.

The apparent second order rate constants for films of block copolymers with different surface composition (coverage of PtBA, χ_{PtBA}), achieved either by choice of molar mass or surface treatment (see above), were determined at 60° C in 3M HCl solutions (Figure 3.15). The apparent rate constants

were found to depend linearly on the surface composition. This observation is an important result because it directly proves that the reactive groups in the PtBA at the surface reside in very similar environments in all the different systems studied. The presence of PS does not affect the reactivity (corrected second order rate constant k''_c obtained from the slope) to a measurable extent for PS_{88}-*b*-$PtBA_{35}$.

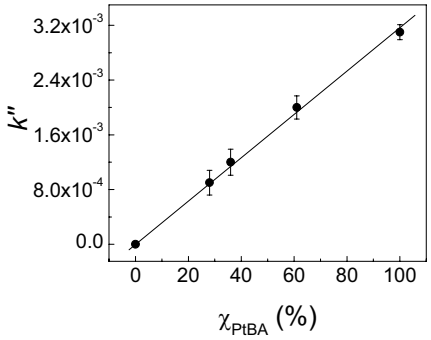

Figure 3.15. Apparent second-order rate constants (calculated from the IR data) vs. surface coverage χ_{PtBA} determined by XPS measurements. The surface coverages of 0, 28, 36, 61, and 100 % were observed for samples of neat PS, PS_{88}-b-$PtBA_{35}$, PS_{2091}-b-$PtBA_{1054}$ (cyclohexane-treated), PS_{690}-b-$PtBA_{1210}$ (cyclohexane-treated) and PS_{690}-b-$PtBA_{1210}$, respectively. The corrected rate constant k''_c is obtained from the slope of the plot.

3.3.6 Comparison of Reactivity of t-Butyl Esters in PS_n-b-$PtBA_m$ Thin Films and in Solution

Compared to solution, the reactivity of the *t*-butyl ester groups was found to be significantly reduced in the substrate supported thin polymer films studied here. A comparison of the thin film data with known hydrolysis data of low molar mass *t*-butyl acetate in solution is shown in Table 3.7.[64,65] The values for k' (for 3M HCl, 25ºC) indicate that the reactivity is obviously reduced on the surface of the thin polymer films by two orders of magnitude compared to the reactivity in solution. We can attribute this result in part to hindered access of the acid to the reactive centers in the polymer films.

Strikingly, the activation energies are lower for the surface reaction of PS_{690}-*b*-$PtBA_{1210}$ polymer compared to the reaction of the low molar mass model compound, which may be related to a decrease in degrees of freedom of the ester functional group attached to the polymer chains. For the reaction in solution, the activation entropy $\Delta S^{\neq}$ is positive compared to the substantially negative value of polymer films, which suggests that the transition state of PtBA during hydrolysis is tight. All our data suggest that the reduced reactivity (compared to solution) of *t*-butyl ester groups at the surface of thin polymer films can be attributed to the confinement of the groups in the film. A comparison with the data for related SAMs (t-BuC10) on Au shows that the reaction in these SAMs is more confined, as judged by $\Delta S^{\neq}$.

Table 3.7. Pseudo-first-order rate constants, activation energies and activation entropies.

Sample	E_a [kJ/mol]	$\Delta S^{\neq}_{298}$ [J/(mol K)]
t-butyl acetate in solution	115 [a]	14.2 [a]
t-Bu-C10	35 ± 2	-211± 11[b]
PS-b-PtBA film (IR)	51 ± 2	-103 ± 3 [c]

[a]data taken from reference 65. [b]data taken from reference 47.

In summary**,** the surface reactivity of homo and diblock polymers at different reaction temperatures was systematically investigated. It was found that both spin-coated PNHSMA films and PS_n-*b*-$PtBA_m$ diblock copolymer films are more reactive compared to related SAMs due to reduced confinement. Since the confinement on both polymer systems is less severe than found for related self-assembled monolayers and is in principle controllable via structural modifications on different length scales (copolymerization or higher order architectures), reactive organic surfaces with optimized reactivity and loading can be designed based on reactive polymers. These approaches can also be extended to be compatible with sub- or micrometer chemical and topographical patterning strategies (see Chapters 6,7). Such reactive polymers may be used to prepare robust, high throughout biosensor and bioarray platforms in the future.

3.4 Experimental Section

Materials. 11,11`-dithiobis(*N*-hydroxysuccinimidyl undecanoate) (NHS-C10, see Scheme 1) was synthesized according to the procedure reported previously [66] . Poly(*N*-hydroxysuccinimidyl-methacrylate) (PNHSMA) was synthesized following a procedure adapted from reference 67 (by AIBN-initiated free radical polymerization of *N*-hydroxysuccinimidyl-methacrylate in toluene at 75°C under argon. The monomer was synthesized and purified according to reference 68.

Characterization data of monomer: ^{1}H-NMR ($CDCl_3$, δ in ppm): 6.36 (*s*, 1 H, C=CHH), 5.8 (*s*, 1 H, C=CHH), 2.81 (*s*, 4 H, CH_2CH_{2cycl}), 1.94 (*s*, 3 H, CH_3) IR [cm^{-1}]: 2940 (CH), 1794 (C=O), 1759 (C=O), 1735 (C=O), 1632, 1535, 1207, 1682.

Characterization data of polymer: IR [cm^{-1}]: 2947, 2984 (CH), 1809, 1782, 1738, (C=O), 1454, 1362, 1202, 1065, ^{1}H-NMR ($CDCl_3$, δ in ppm): 2.75 (*s*, 4 H, CH_2CH_{2cycl}), 1.8-2.0 (*b*, 2 H, CH_2), 0.75-1.1 (*b*, 2 H, CH_3); following gel permeation chromatography (Waters model 410 GPC) using polystyrene standards, a M_n of 3650 g/mol and a polydispersity index M_w / M_n of 1.30 were determined. The glass transition temperature of the polymer was 140°C as measured by differential scanning calorimetry (Perkin Elmer DSC 7).

Two PS_n-*b*-$PtBA_m$ diblock copolymers with different block ratio (the repeat units were: n_1 = 690, m_1=1210; n_2 = 2091, m_2 = 1054, where n_i and m_i correspond to the degree of polymerization of the respective blocks of the block copolymers) were purchased from Polymer Source Company (Dorval, Canada) and were used as received. The molar masses for two block copolymers were 202.4 kg/mol (PS: minority) and 352.5 kg/mol (PS: majority) and the polydispersity indices were 1.03 and 1.08, respectively. A PS-*b*-PtBA diblock copolymer with lower molar mass was synthesized according to

the procedure reported previously by Davis and Matyjaszewski.[69] The ^{1}H NMR and IR spectroscopic data agreed with the reported literature data. The synthesized block copolymer PS_{88}-*b*-$PtBA_{35}$ had a molar mass of 13 kg/mol and a polydispersity index of 1.20, as determined by GPC measurements in THF. For the determination of molar mass values PS standards and the universal calibration approach were used.

Concentrated HCl (37%), cyclohexane, ammonium hydroxide (28-30%) were purchased from Aldrich and used as received. Toluene (99.7%) and N,N-Dimethylformamide (DMF) (99.8%) were purchased from Biosolve (the Netherlands) and used as received.

Preparation of Thin Films. All glassware used to prepare monolayers was immersed in piranha solution (solution of 1 : 3 (vol. : vol.) 30% H_2O_2 and concentrated H_2SO_4) for 15 minutes, then rinsed with copious amounts of high purity water (Millipore Milli-Q water). ***Caution: Piranha solution should be handled with extreme caution; it has been reported to detonate unexpectedly.*** Gold substrates (200 nm gold on 2 nm Ti primer on glass) were acquired from SSENS BV (Hengelo, The Netherlands). The gold substrates were cleaned by oxygen plasma, subsequently immersed in ethanol for 10 minutes to remove any possible oxide layer[70] and immersed with minimal delay into 1.0 mM solutions of **NHS-C10** in ethanol. The substrates were removed from solutions after > 16 hours assembly time and rinsed extensively with ethanol and water to remove any physisorbed material. Finally, the samples were dried in a stream of nitrogen.

Polymer thin films were prepared by spin-coating polymer solutions in DMF (for PNHSMA) and toluene (for PS_n-b-$PtBA_m$) (typical concentration between 4 and 30 mg/ml) onto silicon wafers, which were cleaned by an oxygen plasma treatment (Elektrotech PF 340 apparatus). The samples were spun at 3000 rpm for 30 s using a P6700 spin-coater (Specialty Coating Systems Inc). All spin-cast samples were annealed at 150°C (for PNHSMA) or 135°C (for PS_n-b-$PtBA_m$) for 24 hours in vacuum before analysis. Mean film thicknesses were determined using a custom-built spectroscopic ellipsometer using a He-Ne laser (λ = 632.8 nm). The refractive index used for PNHSMA film was 1.50 and for the block polymer films 1.513, while for PtBA and PS we used 1.464 and 1.590, respectively.[71]

Hydrolysis: The hydrolysis of NHS ester NHS-C10 monolayers and polymer films was carried out by incubation of the corresponding sample for different reaction times in 1.00×10^{-2} M NaOH and in 25×10^{-2} M aqueous NH_3 (PNHSMA), respectively. The concentration of hydroxide ions in the aqueous NH_3 solution was calculated based on tabulated values of the corresponding equilibrium constant and its dependence on temperature.[72] The films of PS_n-b-$PtBA_m$ were immersed in 3M aqueous HCl acid solutions in closed beakers for different times or at different temperatures. The temperature was controlled between 25°C and 70°C using an oil bath. After the reaction, the samples were thoroughly rinsed three times using Mill-Q water and dried in vacuum.

Solvent Treatment of Thin Films. Cyclohexane was used to enrich the surface in PS by placing a cross-linked poly(dimethylsiloxane) (PDMS) slab previously soaked in cyclohexane onto the polymer surface.[73] After 3 hrs contact treatment, the PDMS was removed and the samples were stored overnight in vacuum.

Atomic Force Microscopy (AFM). The tapping mode AFM measurements were carried out with a NanoScope III multimode AFM (Digital Instruments / Veeco, Santa Barbara, CA) using a 10 μm

scanner and microfabricated silicon tips / cantilevers (Nanosensors, Wetzlar, Germany) in ambient atmosphere (ca. 30 % relative humidity, 24ºC temperature) as described previously (ref CC18).

Contact Angles Measurement. Static and dynamic CA were measured on a CA microscope (Data Physics, OCA 15Plus) with Millipore water or CH_2I_2 (99.9%, Fluka) as probe liquids at room temperature and ambient humidity. Data were obtained at least at three different locations and was averaged per polymer sample.

Fourier Transform Infrared (FTIR) Spectroscopy. Transmission mode FTIR spectra (spectral resolution of 4 cm^{-1}, 1024 scans) were obtained using a BIO-RAD model FTS575C FTIR spectrometer equipped with a liquid nitrogen-cooled cryogenic mercury cadmium telluride (MCT) detector. Background spectra were obtained using oxygen plasma-cleaned silicon wafers.

X-ray Photoelectron Spectroscopy (XPS). XPS spectra were recorded on a PHI Quantum 2000 Scanning ESCA microprobe using a monochromated X-ray beam (Al-anode); 100 μm diameter / 25 Watt X-ray beam scanned over 700 μm × 300 μm area at a variable take-off angle of between 30 and 90º. Atomic concentrations were determined by numerical integration of the relative peak areas using the Multipak software with supplied sensitivity factors (C1s: 0.314; O1s: 0.733).[74]

3.5 References

1. Ding, L. M.; Lu, Z. X.; Egbe, D. A. M.; Karasz, F. E. *Macromolecules* **2004**, *37*, 10031.
2. Mirkin, C. A.; Patner, M. A. *Ann. Rev. Phys. Chem*. **1992**, *43*, 719.
3. Wang, Z. Y.; Heflin, J. R.; Stolen, R. H.; Ramachandran, S. *Appl. Phys. Lett*. **2005**, *86*, 223104.
4. Paolesse, R.; Dinatale, C.; Macagnano, A.; Davide, F.; Boschi, T.; Damico, A. *Sens. Actuators B* **1998**, *47*, 70.
5. Everhart, D. S. *Chemtech.* **1999**, *4*, 30.
6. Wessa, T.; Goepel, W. *Fresenius J. Anal. Chem*. **1998**, *362*, 239.
7. Storri, S.; Santoni, T.; Minunni, M.; Mascini, M. *Biosens, Bioelectron*. **1998**, *13*, 347.
8. Allara, D. L. *Biosens. Bioelectron*. **1995**, *10*, 771.
9. Ulman, A. *An Introduction to Ultrathin Organic Films: From Langmuir-Blodgett to Self-Assembly*, Academic, New York **1991**.
10. Pawlowski, D.; Tieke, B. *Langmuir* **2003**, *19*, 6498.
11. (a) Pirrung, M. C. *Angew. Chem. Int. Ed.* **2002**, *41*, 1276. (b) Sawant, P. D.; Watson, G. S.; Nicolau, D.; Myhra, S.; Nicolau, D, V. *J. Nanosci. Nanotech*. **2005**, *5*, 951.
12. *Biosensors and Chemical Sensors*, Wang, J. *ACS Symp. Ser*. *487*, ACS: Washinton, D. C. 1992.
13. Tannenbaum, R.; Hakanson, C.; Zeno, A.; Tirrell, M. *Langmuir* **2002**, *18*, 5592.
14. Jérôme, C.; Gabriel, S.; Voccia, S.; Detrembleur, C.; Ignatova, M.; Gouttebaron, R.; Jérôme, R. *Chem. Commun*. **2003**, 2500
15. Han, W. Q.; Fan, S. S.; Li, Q. Q.; Hu, Y. D. *Science* **1997**, *277*, 1287
16. Godwin, A.; Hartenstein, M.; Müller, A. H. E.; Brocchini, S. *Angew. Chem. Int. Ed*. **2001**, *40*, 549
17. (a) Ferretti, S.; Paynter, S.; Russell, D. A.; Sapsford, K. E.; Richardson, D. J. *TrAC* **2000**, *19*, 530. (b) Mrksich, M. *Chem. Soc. Rev*. **2000**, *29*, 267. (c) Ostuni, E.; Yan, L.; Whitesides, G. M. *Coll. Surf., B*. **1999**, *15*, 3.
18. (a) Schönherr, H.; Chechik, V.; Stirling, C. J. M.; Vancso, G. J. *J. Am Chem. Soc*. **2000**, *122*, 3679. (b) Schönherr, H.; Chechik, V.; Stirling, C. J. M.; Vancso, G. J. *ACS Symp. Ser*. **2001**, *781*, 36.
19. (a) Prucker, O.; Rühe, J. *Macromolecules* **1998**, *31*, 592. (b) Prucker, O.; Rühe, J. *Macromolecules* **1998**, *31*, 602. (c) Smith, R. K.; Lewis, P. A.; Weiss, P. S. *Progr. Surf. Sci*. **2004**, *75*, 1.
20. Evans, S. D.; Johnson, S. R.; Ringsdorf, H.; Williams, L. M.; Wolf, H. *Langmuir* **1998**, *14*, 6436.

21. Lockhart, D. J.; Winzeler, E. A. *Nature* **2000**, *405*, 827.
22. Zhu, H.; Snyder, M. *Curr. Opin. Chem. Biol*. **2001**, *5*, 40.
23. Chechik, V.; Crooks, R. M.; Stirling, C. J. M. *Adv. Mater*. **2000**, *12*, 1161.
24. Bertilsson, L.; Liedberg, B. *Langmuir* **1993**, *9*, 141.
25. (a) Park, P.; Harrison, C. K.; Chaikin, P. M.; Register, R. A.; Adamson, D. H. *Science* **1997**, *276*, 1401.; (b) Heier, J.; Genzer, J.; Kramer, E. J.; Bates, F. S.; Walheim, S.; Krausch, G. *J. Chem. Phys*. **1999**, *111*, 11101.; (c) Jeong, U.; Kim, H. C.; Rodriguez, R. L.; Tsai, I. Y.; Stafford, C. M.; Kim, J. K.; Hawker, C. J.; Russell, T. P. *Adv. Mater*. **2002**, *14*, 274.; (d) Thurn, A. T.; Schottter, J.; Kästle, G. A.; Emley, N.; Shibauchi, T.; Krusin, E. L.; Guarini, K.; Black, C. T.; Tuominen, M. T.; Russell, T. P. *Science* **2000**, *290*, 2126.; (e) Li, R. R.; Dapkus, P. D.; Thompson, M. E.; Joeng, W. G.; Harrison, C.; Chaikin, P. M.; Register, R. A.; Adamson, D. H. *Appl. Phys. Lett*. **2000**, *76*, 1689.; (f) Mansky, P.; Harrison, C. K.; Chaikin, P. M.; Register, R. A.; Yao, N. *Appl. Phys. Lett*. **1996**, *68*, 2586.; (g) Turner, M. S. *Phys. Rev. Lett*. **1992**, *69*, 1788.
26. Lamboy, P.; Russell, T. P.; Kellogg, G. J.; Mayes, A. M.; Gallacher, P. D.; Satija, S. K. *Phys. Rev. Lett*. **1994**, *72*, 2899.
27. Mansky, P.; Liu, Y.; Huang, E.; Russell, T. P.; Hawker, C. *Science* **1997**, *275*, 1458.
28. Morkved, T. L.; Lu, M.; Urbas, A. M.; Ehrichs, E. E.; Jaeger, H. M.; Mansky, P.; Russell, T. P. *Science* **1996**, *273*, 931.
29. Dequaire, M.; Heller, A. *Anal. Chem.* **2002***, 74,* 4370.
30. (a) Benters, R.; Niemeyer, C. M.; Drutschmann, D.; Blohm, D.; Wöhrle, D. *Nucl. Acids Res.* **2002***, 30,* e10. (b) Benters, R.; Niemeyer, C. M.; Wöhrle, D. *Chembiochem. 2001, 2,* 686.
31. (a) Zhou, Y. F.; Bruening, M. L.; Bergbreiter, D. E.; Crooks, R. M.; Wells, M. *J. Am. Chem. Soc.* **1996***, 118,* 3773. (b) Dermody, D. L.; Peez, R. F.; Bergbreiter, D. E.; Crooks, R. M. *Langmuir* **1999***, 15,* 885. (c) Cosulich, M. E.; Russo, S.; Pasquale, S.; Mariani, A. *Polymer* **2000***, 41,* 4951.
32. Rowan, B.; Wheeler, M. A.; Crooks, R. M. *Langmuir* **2002***, 18,* 9914.
33. Golze, S. Ph. D. thesis; 2001; University of Mainz.
34. Frank, C. W.; Rao, V.; Despotopoulou, M. M.; Pease, R. F. W.; Hinsberg, W. D.; Miller, R. D.; Rabolt, J. F. *Science* **1996**, *273*, 912 and references cited.
35. (a) Rühe, J.; Kuan, S.; Blackman, G.; Novotny, V.; Clarke, T.; Street, G. B. *ACS Symp. Series 485*, **1992**, pp. 156. (b) Fryer, D. S.; Nealey, P. F.; de Pablo, J. J. *Macromolecules* **2000**, *33*, 6439; (c) Torres, J. A.; Nealey, P. F.; dePablo, J. J. *Phys. Rev. Lett.* **2000**, *85*, 3221.
36. (a) Keddie, J. L.; Jones, R. A. L.; Cory, R. A. *Europhys. Lett*. **1994**, *27*, 59. (b) Forrest, J. A.; Mattsson, J. *Phys. Rev. E* **2000**, *61*, R53 and references cited.
37. Feng, C. L.; Vancso, G. J.; Schönherr, H. *Langmuir* **2005**, *21*, 2356.
38. (a) Schönherr, H.; Frank, C. W. *Macromolecules* **2003,** *36,* 1188. (b) Schönherr, H.; Frank, C. W. *Macromolecules* **2003,** *36,* 1199.
39. Gopferich, A. *Biomat.* **1996***, 17,* 103.
40. (a) Lenhart, J. L.; Jones, R. L.; Lin, E. K.; Soles, C. L.; Wu, W. L.; Fischer, D. A.; Sambasivan, S.; Goldfarb, D. L.; Angelopoulos, M. *J. Vac. Sci. Technol. B* **2002**, *20*, 2920. (b) Somorjai, G. A. *J. Phys. Chem. B* **2002***, 106,* 9201.
41. *Surface Infrared and Raman Spectroscopy : Methods and Applications*, Suetaka, W.; Yates, J. T. Jr.; Plenum Press; New York; 1995.
42. Mengel, C.; Esker, A. R.; Meyer, W. H.; Wegner, G. *Langmuir* **2002**, *18*, 6365.
43. The decrease in integrated absorbance of the ν(C-H) bands of the methylene groups of the NHS ester shows very similar results, however, due to the relatively minute changes as a result of interfacial hydrolysis, these data are less accurate.
44. Laibinis, P. E.; Bain, C. D.; Nuzzo, R. G.; Whitesides, G. M. *J. Phys. Chem.* **1995,** 99*,* 7663.
45. Israelachvili, J. N.; Gee, M. L. *Langmuir* **1989**, *5*, 288.

46 Dordi B.; Schönherr, H.; Vancso, G. J. *Langmuir* **2003**, *19*, 5780.

47. Pan, S.; Castner, D. G.; Ratner, B. D. *Langmuir* **1998***, 14,* 3545.

48 Schönherr H.; Feng C. L.; Shovsky A. *Langmuir*, **2003**, *19*, 10843.

49. Besselink, G. A. J.; Beugeling, T.; Bantjes, A. *Appl. Biochem. Biotech.* **1993**, *43*, 227.

50. Shovsky, A.; Schönherr, H. *Langmuir* **2005**, *21*, 4393.

51. Elbs, H.; Fukunaga, K.; Stadler, R.; Sauer, G.; Magerle, R.; Krausch, G. *Macromolecules* **1999**, *32*, 1204.

52. Liu, Z.; Pappacena, K.; Cerise, J.; Kim, J.; Durning, C. J.; O´Shaughnessy, B.; Levicky, R. *Nanoletters* **2002**, *2*, 219.

53. Matyjaszewski, K.; Miller, P. J.; Shukla, N.; Immaraporn, B.; Gelman, A.; Luokala, B. B.; Siclovan, T. M.; Kickelbick, G.; Vallant, T.; Hoffmann, H.; Pakula, T. *Macromolecules* **1999**, *32*, 8716.

54. Camillone, N.; Chidsey, C. E. D.; Liu, G. Y.; Putvinski, T. M.; Scoles, G. *J. Chem. Phys*. **1991**, *94*, 8493.

55. Fernández-García, M.; de la Fuente, J. L.; Cerrada, M. L.; Madruga, E. L. *Polymer* **2002**, *43*, 3173.

56. Lu, Z.; Liu, G.; Duncan S. *Macromolecues* **2004**, *37*, 174.

57. Bates, F. S.; Frederickson, G. H. *Physics Today*, February **1999**, *52*, 32.

58. The film thickness of ~ 90 nm, determined by ellipsometry, exceeds the equilibrium domain spacing by ~ 7 nm for this microphase separated block copolymer (see: Fasolka, M. J.; Banerjee, P.; Mayes, A. M.; Pickett, G.; Balazs, A. C. *Macromolecules* **2000**, *33*, 5702).

59. Schönherr, H.; Vancso, G. J. *J. Polym. Sci. B, Polym. Phys*. **1998**, *36,* 2483.

60 (a) Magonov, S. N.; Elings, V.; Whangbo, M.-H. *Surf. Sci.* **1997**, *372*, L385. (b) Bar, G.; Thomann, Y.; Whangbo, M. H. *Langmuir* **1998,** *14*, 1219 and references cited.

61. Mengel, C.; Esker, A. R.; Meyer, W. H.; Wegner, G. *Langmuir* **2002**, *18*, 6365.

62. Andersen, T. H.; Tougaard, S.; Larsen, N. B.; Almdal, K.; Johannsen, I. *J. Electron Spectro. Related Phenom*. **2001**, *121*, 93.

63. Kim, J. H.; Park, D. S.; Kim, C. K. *J. Polymer Science B. Polymer Phys*. **2000**, *38*, 2666.

64. Bunnett, J. F. *J. Am. Chem. Soc*. **1961**, *83*, 4956.

65. Solomaa, P. *Suomen Kemi*, **1959**, *B32*, 145.

66 Dordi, B.; Schönherr, H.; Vancso, G. J. *Langmuir* **2003**, *19,* 5780.

67. Batz, H. G.; Franzmann, G.; Ringsdorf, H. *Makromol. Chem*. **1973**, *172*, 27.

68. Batz, H. G.; Koldehoff, J. *Makromol. Chem*. **1976**, *177*, 683.

69. Davis, K, A.; Matyjaszewski, K. *Macromolecules* **2000**, *33*, 4039.

70 Ron, H.; Rubinstein, I. *Langmuir* **1994**, *10,* 4566.

71. *Polymer Handbook*, 3rd ed. Brandrup, J.; Immergut, E. H. John Wiley & Sons: New York, **1989**.

72. $K_1/K_2 = 434.9\ (1/T_1 - 1/T_2)$ (*Handbook of Chemistry and Physics*, Weast, R. C. 57th Edition; 1976-1977, p. D67.

73. (a) Lee, J. N.; Park, C.; Whitesides, G. M. *Anal. Chem*. **2003**, *75*, 6544. (b) Hillborg, H.; Tomczak, N.; Olàh, A.; Schönherr, H.; Vancso, G. J. *Langmuir* **2004,** *20*, 785.

74. Reilman, R. F.; Msezane, A.; Manson, S. T. *J. Electron Spectroscopy* **1976**, *8*, 389.

Chapter 4

Reactive Thin Polymer Films as Platforms for the Immobilization of Biomolecules*

Spin-coated thin films of poly(N-hydroxysuccinimidyl methacrylate) (PNHSMA) were investigated as reactive layers for obtaining platforms for biomolecule immobilization with high molecular loading. The surface reactivity of PNHSMA films in coupling reactions with amino-functionalized poly(ethylene glycol) (M_n: 500 g/mol) (PEG_{500}-NH_2) was determined by FTIR spectroscopy, X-ray photoelectron spectroscopy (XPS), fluorescence microscopy and ellipsometry measurements, respectively. The PEG_{500}-NH_2 loading observed was about three times higher for the polymer thin films compared to self-assembled monolayers (SAMs) of 11,11´-dithiobis(N-hydroxysuccinimidyl-undecanoate) (NHS-C10) on Au. These data indicated that the coupling reactions are not limited to the outermost surface layer of the polymer films, but proceed into the surface-near regions of the films. An increased loading was also observed by surface plasmon resonance (SPR) measurements for the covalent immobilization of amino-functionalized probe DNA. Hybridization of fluorescently labeled target DNA was successfully detected by fluorescence microscopy and surface plasmon resonance-enhanced fluorescence spectroscopy (SPFS), thereby demonstrating that thin films of PNHSMA show robustness and comprise an attractive and simple platform for the immobilization of biomolecules with high densities. Finally, the successful application of PNHSMA films as platform for biosensors for pathogen detection was demonstrated using a protein G mediated antibody-based detection of bacteria (listeria).

4.1 Introduction

Considerable effort has been invested recently to create robust high throughput biosensors with improved detection sensitivity.[1] A biosensor can be defined as a device that can convert binding events between an analyte of interest and complementary binding into an electronic signal.[2] The detection of the binding event is in many cases based on electronic/electrochemical detection principles or employs optical techniques. However, an important part of the biosensor design is the (bio)chemical nature of the interfacial layer at the sensor surface, which affords specific bio-recognition reactions with high affinity binding sites. Surface chemical reactions are similarly important for various biological applications,[3] such as the fabrication of gene[4,5] or protein chips.[6]

Self-assembled monolayers (SAMs)[7] have been successfully applied as platform for the fabrication of sensing surfaces in biosensors.[8] The limitation of these films is that they can only provide a 2-D architecture of affinity-binding sites on the surface and hence limited surface coverages (see Chapter 2). In these and related approaches, the ability to introduce versatile chip interfaces and to control the

* Part of the work described in this Chapter has been published in: Schönherr H.; Feng C. L.; Shovsky A.; Degenhart G.; Dordi B.; Zhang Z.; Förch R.; Knoll W.; Vancso G. J. *PMSE Prepr*. **2004**, *90*, 689-690. Feng, C. L.; Zhang, Z.; Förch, R.; Knoll, W.; Vancso, G. J.; Schönherr, H. *Biomacromolecules* **2005**, *6,* 3243.

immobilization of biomolecules, represents a crucial point due to the interplay of organization on the molecular scale and reactivity in the confinement of organized organic thin films.[9] These effects result in difficulties to achieve high densities of immobilized biomolecules in their functional[10] or optimized oriented form.[11]

As an alternative method to obtain reactive platforms, the deposition of polymeric materials onto solid substrates receives increasing attention.[12] Using electrografting, Jérôme et al. have prepared reactive surfaces bearing activated ester groups, which are highly reactive towards nucleophiles. This reactivity makes the electrografted coating appropriate for anchoring of a large variety of molecules.[13] Other polymer-based systems and approaches[14] to overcome the mentioned intrinsic limitations of 2-D platforms comprise hydrogels,[15,16] dendrimers,[17,18,19] hyperbranched polymers,[20] chemical vapor deposition approaches,[21] self-assembled polyelectrolyte mutilayers,[22] plasma polymers,[23] and polymer brushes obtained by grafting-from approaches.[24]

In Chapter 3, the analysis of hydrolysis reactions of simple reactive PNHSMA ultrathin films and related SAMs showed that the reaction proceeds also into the surface-near region of the polymer films (< 10 nm depth) implying an enhanced coverage of immobilized guest molecules in coupling reactions compared to SAMs. In addition, the reaction kinetics may be significantly retarded for SAMs due to more pronounced confinement. Hence reactive coatings based on PNHSMA may allow one to couple many more (bio)molecules per unit area compared to a monolayer (Scheme 4.1). PNHSMA and related polymer films, such as polystyrene-*b*-poly(*tert*-butyl acrylate) (see Chapters 3 and 5), can be easily obtained, for example, by spin-coating. The film thickness of such polymer films can be precisely adjusted (via concentration of the polymer solution and / or the spinning speed) so that quenching of fluorescence due to energy transfer to the underlying metal substrate[25] can be avoided during signal detection. Thus an optimum sensitivity enhancement in, e.g., surface plasmon resonance-enhanced fluorescence spectroscopy (SPFS), can be achieved.[26]

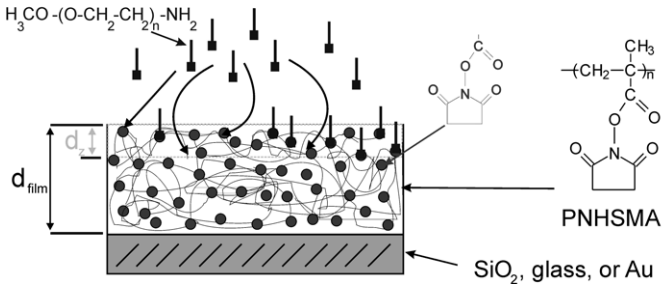

Scheme 4.1. Schematic structure of substrate-supported thin film of PNHSMA (with tunable thickness d_{film}) reacting with PEG_{500}-NH_2. The reactive NHS ester groups, which can be converted to amides, are located in a surface-near region with depth d_z. The PEG_{500}-NH_2 molecules and reactive NHS ester moieties are schematically depicted as bars and dots, respectively.

In this Chapter, the investigation of thin PNHSMA films as platforms for the coupling of biomolecules for potential application in robust, high loading biosensors is discussed. The coupling of PEG_{500}-NH_2, proteins (BSA), and probe DNA, as well as its hybridization with target DNA, were studied to confirm an increased (bio)molecular loading on the one hand and controlled swelling and layer stability on the other hand. These properties render PNHSMA and related polymer films suitable for applications involving the immobilization of biomolecules with high molecular loading and controlled substrate - biomolecule spacing. To demonstrate the concept of a biosensor architecture for pathogen detection based on the PNHSMA platform, anti-listeria antibodies, immobilized via strong interactions with covalently coupled and correctly oriented protein G, were shown to selectively recognize listeria. By contrast, PEG_{500} layers grafted to PNHSMA were shown to be effective to suppress non-specific adsorption of proteins and bacteria.

4.2 Investigation of the Reactivity of PNHSMA

A well-known strategy for rendering surfaces biomolecule (e.g. protein) - resistant involves incorporation of PEG both into polymers and as surface-grafted chains.[27] The resistance of PEG to the adsorption of proteins is generally considered as steric repulsion effect, where the polymer prevents the protein from reaching the substrate surface to adsorb. It was found that the net force determining the adsorption of the PEG-presenting surface depends on the thickness of the grafted layers and their surface coverage.[27] Hence the reaction of the activated NHS ester groups at and near the surface of PNHSMA films with PEG_{500}-NH_2 from aqueous solution will be discussed first, followed by the covalent immobilization of various (bio)molecules.

4.2.1 Coupling of PEG_{500}-NH_2

The FTIR spectra of PNHSMA films before and after reaction with PEG_{500}-NH_2 are shown in Figure 4.1 In both spectra, the succinimide carbonyl band at 1737 cm^{-1} (attributed to the succinimide C=O stretching vibration) is clearly observed. This observation suggests that the reacted films contain a significant fraction of unreacted NHS ester groups. After immobilization of PEG_{500}-NH_2 several new bands can be distinguished. In addition to the prominent band at 1107 cm^{-1}, attributed to the C-O vibration of the PEG, the C-H stretching vibrations at ca. 2851 and 2920 cm^{-1}, the amide I and amide II bands are observed at 1653 cm^{-1} and 1538 cm^{-1}, respectively.[28] These amide bands are a result of the covalent bond formation between the primary amine terminus of the PEG and the NHS ester groups of the reactive polymer films because there are no amide bonds present in the PNHSMA polymer. In addition, a new peak is observed at 1263 cm^{-1}. This characteristic band is attributed to the PEG backbone, namely the EG CH_2 twist vibration.[28] The band position of the twisting vibration of 1263 cm^{-1}, is indicative of an amorphous PEG layer grafted onto the PNHSMA polymer films.[27,29]

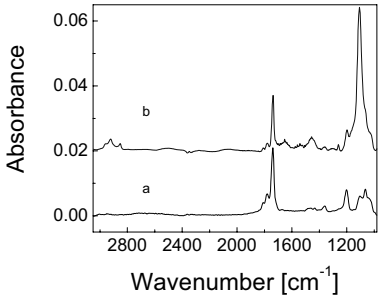

Figure 4.1. FTIR spectra of (a) PNHSMA on oxidized Si; (b) PNHSMA on oxidized Si after the grafting reaction with PEG_{500}-NH_2 (3hrs) from PB buffer (pH = 7.4).

The kinetics of the PEG immobilization was followed by ex situ FTIR spectroscopy for different concentrations of PEG_{500}-NH_2. As mentioned above, the band attributed to the EG CH_2 twist vibration was pronounced after covalent PEG_{500}-NH_2 attachment and was completely absent for PNHSMA film. This peak can thus be conveniently used without any peak deconvolution as reference peak to determine the thickness increase following the coupling reaction. Further, the integrated absorbance of the EG CH_2 twist band in spin-coated films of PEG_{500}-NH_2 was calibrated with respect to thickness as determined by ellipsometry (see inset in Figure 4.2a). Figure 4.2a shows the PEG surface coverage and PEG layer thickness for coupling reactions carried out using different PEG_{500}-NH_2 concentrations. The surface coverage of PEG (χ_{PEG}) increased rapidly in the early stages of reaction and finally saturates. For all concentrations studied, a limiting grafting thickness of 1.8 nm was reached. Linearization according to pseudo-first-order kinetics afforded the corresponding apparent rate constants k' (Table 4.1).[30]

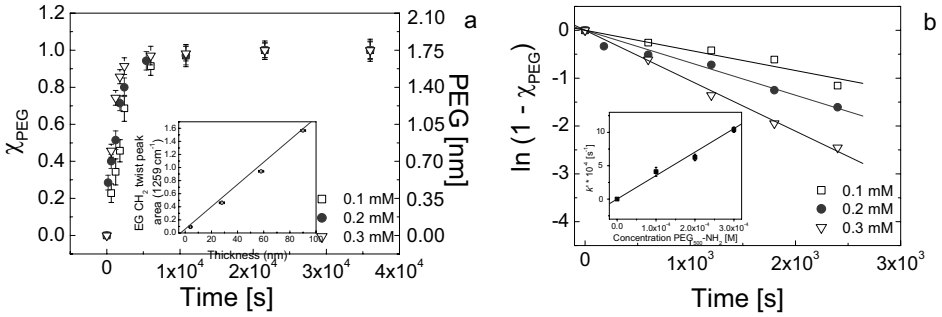

Figure 4.2. (a) Surface coverage and grafting thickness of PEG_{500}-NH_2 following covalent coupling to PNHSMA films (inset: IR peak area (1263 cm^{-1}) vs. PEG film thickness determined by ellipsometry). (b) Linearization of the data shown in Figure 4.2a according to pseudo-first-order kinetics (the solid lines correspond to linear least squares fits; inset: dependence of k' on concentration of PEG_{500}-NH_2).[30]

The early stages of PEG_{500}-NH_2 coupling on PNHSMA film can hence be described as a pseudo-first-order reaction. The apparent pseudo-first-order rate constants k' were found to increase proportional to the PEG_{500}-NH_2 concentration (see inset in Figure 4.2b). From the slope, the concentration independent second order rate constant k'' of 3.5 ± 0.1 $M^{-1}s^{-1}$ was estimated.

Table 4.1. Pseudo-first-order rate constants k' for coupling reaction of PEG_{500}-NH_2 to PNHSMA determined by FTIR spectroscopy and ellipsometry.

Concentration of PEG_{500}-NH_2 [mM]	k' [s^{-1}]
0.1	$4.1 \times 10^{-4} \pm 6.6 \times 10^{-5}$
0.2	$6.2 \times 10^{-4} \pm 4.9 \times 10^{-5}$
0.3	$10.5 \times 10^{-4} \pm 3.9 \times 10^{-5}$

4.2.2 Coupling of Fluoresceinamine and BSA to PNHSMA Films

The reactivity of PNHSMA films was also investigated by fluorescence microscopy using fluoresceinamine as a label. Figure 4.3 shows fluorescence microscopy images of PNHSMA films reacted with the dye in aqueous medium for various times. It can be noted that the intensity and the homogeneity of the fluorescence emission increased with increasing reaction time. After 90 minutes reaction time, very homogeneous fluorescence emission and the absence of the granular texture, which was observed at shorter reaction times (Figures 4.3b and 4.3c), were detected (Figure 4.3d). These observations indicate that the reaction has proceeded to completion. The kinetics of the coupling was estimated by an integration of the fluorescence intensity; the normalized surface coverage of dye molecules on PNHSMA films is shown in Figure 4.3e. The rate constant of the reaction obtained is comparable to the value determined for PEG_{500}-NH_2 by FTIR measurements under the same conditions; the second order rate constant k'' was calculated as 4.3 ± 0.2 $M^{-1}s^{-1}$.

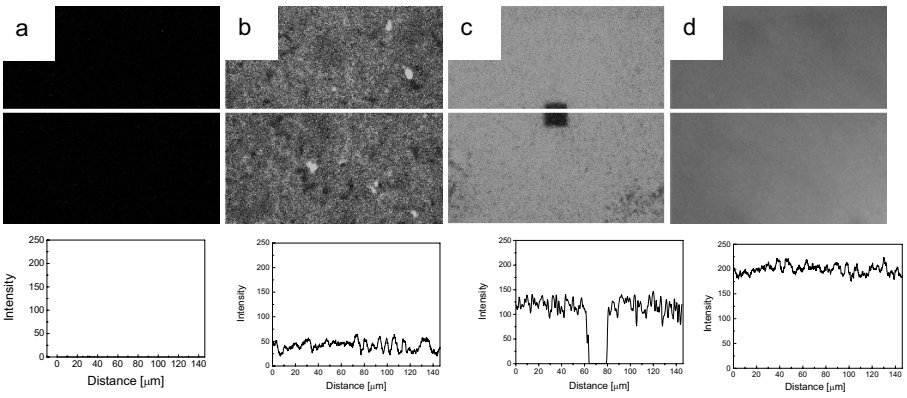

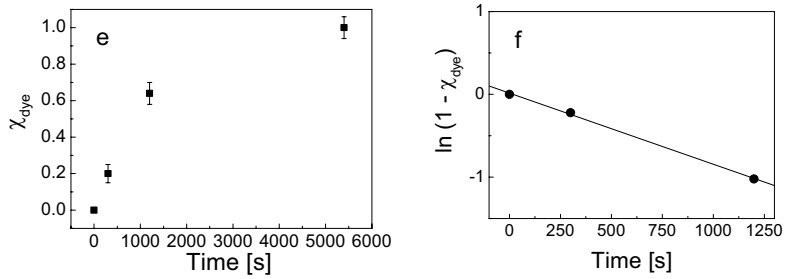

Figure 4.3. Fluorescence microscopy images (top) and corresponding cross sectional intensity plots (bottom) (image size: 146 × 146 μm^2) of (a) unreacted PNHSMA film and (b) - (d) PNHSMA film after grafting with fluoresceinamine for 5, 20, and 90 minutes, respectively. The central area in (c) has been photo-bleached on purpose. (e) Fluoresceinamine surface coverage vs. grafting time. (f) linearized data in (e). All fluorescence emission data was normalized to the maximum fluorescence emission observed for 5500s coupling time.

The reactivity of PNHSMA films to biomolecules (e.g. dye-labeled bovine serum albumin, BSA) was followed by fluorescence microscopy. As a reference experiment, a PNHSMA film was studied first. No fluorescence emission was detected, as shown in Figure 4.4a. BSA was then reacted with a PNHSMA film in PB buffer. The detected fluorescence emission of BSA functionalized films in Figure 4.4b suggests that PNHSMA can be used as reactive layer to immobilize proteins. The demonstration of the working principle and architecture of a biosensor for the detection of pathogens will be discussed in section 4.5 of this Chapter.

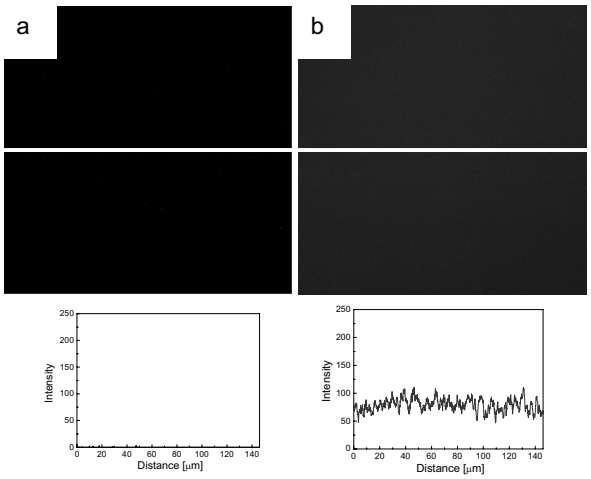

Figure 4.4. Fluorescence microscopy images (top) and corresponding cross sectional intensity plots (bottom) (image size: 146 × 146 μm^2) of (a) unreacted PNHSMA film and (b) PNHSMA film after grafting with BSA for 90 minutes, respectively.

4.2.3 Comparison of Surface Reactions on PNHSMA Films and NHS-C10 Monolayers

To quantify the differences in PEG_{500}-NH_2 loading on SAMs and polymer films, i.e. 2-D and quasi-3-D reactive surfaces, respectively, we compared the coupling of PEG_{500}-NH_2 to NHS-C10 SAMs and to PNHSMA surfaces for the same coupling condition (0.1 mM PEG_{500}-NH_2 and 25ºC). The increase in film thicknesses following PEG_{500}-NH_2 coupling and drying, as a measure for grafted layer thickness of PEG, was determined by ellipsometry (Figure 4.5).

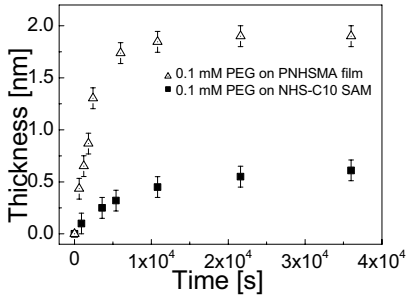

Figure 4.5. Thickness of grafted PEG_{500}-NH_2 on NHS-C10 SAMs and PNHSMA polymer films vs. reaction time.

The coupling reaction on the NHS-C10 SAMs proceeds qualitatively similar to the polymer film, however, the finally reached thickness is significantly lower. The maximum grafted thickness for PEG_{500}-NH_2 on PNHSMA is ~ 1.9 nm, compared to ~ 0.6 nm on NHS-C10 SAMs. This difference in PEG_{500}-NH_2 loading of a factor of > 3 using identical reaction conditions clearly shows that the polymer films offer an advantage in terms of increased number of reactive groups per unit surface area. These reactive groups are expected to reside on top of and inside the polymer film in the surface-near region (see Chapter 3).

Similar to the PNHSMA polymer system, the early stages of PEG_{500}-NH_2 coupling on NHS-C10 SAMs can also be described as a pseudo-first-order reaction. The apparent rate constants determined under the same conditions (0.1 mM PEG_{500}-NH_2) were $k' = 4.1 \times 10^{-4} \pm 6.6 \times 10^{-5}$ s^{-1} and $k' = 1.1 \times 10^{-4} \pm 1.0 \times 10^{-5}$ s^{-1} for the PNHSMA polymer films and the NHS-C10 SAMs, respectively. Hence the reactivity is reduced on the NHS-C10 compared to the PNHSMA film. Similar to the surface hydrolysis (see Chapter 3), this higher rate constant is attributed to a higher reactivity of the NHS ester groups at and near the surface of the polymer film owing to the absence of a near-closed packing of the ester groups and an increase in free volume of PNHSMA films.

Based on the grafted thickness of PEG_{500}-NH_2 molecules determined above, the average grafting density (σ in molecules / nm^2) of the adsorbed PEG_{500}-NH_2 molecules on the SAMs can then be estimated according to equation 1.[31]

$$\sigma = N_A \, d \, \rho_{dry} / M_w \qquad (1)$$

where d is the layer thickness, ρ_{dry} is the density of the dry polymer (1.06 g/ml), M_w is the molar mass (500 g/mol), and N_A (6.022×10^{23} mol^{-1}) is Avogadro's number.

According to this calculation, the grafting density of PEG_{500}-NH_2 on NHS-C10 SAMs is ~ 0.86 nm^{-2}, which agrees favorably with the maximum PEG grafting density of ~ 0.87 nm^{-2} on monolayers reported in the literature for complete coverage. The grafting density of the reactive NHS ester groups on the gold substrate is approximately 4 nm^{-2}, [32] which indicates that only a fraction of the active ester groups have been involved in the coupling reaction. Based on the FTIR data in Figure 4.6, the remaining NHS ester groups in the SAMs appear to be hydrolyzed. An analogous calculation yields a grafting density of ~ 2.6 PEG nm^{-2} for PNHSMA, which is ~ 3 times higher compared to SAMs. Hence it can be concluded at this point that PNHSMA films allow one to couple significantly more amino-functionalized molecules per unit area compared to related SAMs on gold.

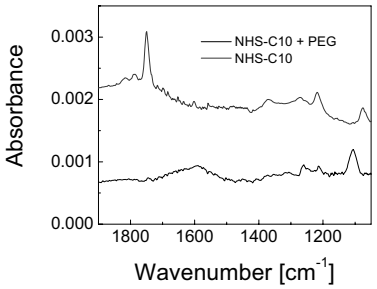

Figure 4.6. IR spectra of NHS-C10 monolayer vs. PEG_{500}-NH_2 grafted NHS-C10 SAM on gold.

An independent confirmation for the increased grafting density of PEG_{500}-NH_2 molecules on PNHSMA films compared to the corresponding SAMs was sought in XPS experiments. The coupling of PEG_{500}-NH_2 to PNHSMA films was studied using XPS with a fixed take-off angle of 45º, which yields information from the top of the film to ~ 7 nm depth inside the film.[33] Figure 4.7 shows the element scan of PNHSMA films before and after 10 h reaction with PEG_{500}-NH_2.

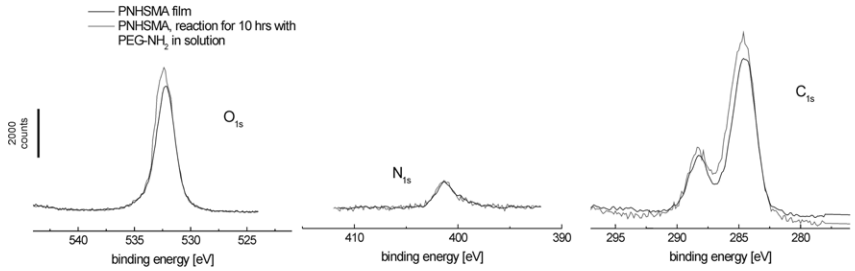

Figure 4.7. Detailed XPS element scans of PNHSMA film before and after grafting of PEG_{500}-NH_2.

For both samples, the integrated area under the N_{1s} peak, observed at 401.5 eV, remained constant. By contrast, the integrated area under the C_{1s} peaks at 284.0 eV (neutral carbons) and at 287.8 eV (carbonyl carbon)[34] increased after PEG_{500}-NH_2 grafting compared to the bare PNHSMA film. Similar trends were observed for the O_{1s} peaks at 532.0 eV.

As expected, the value of the *C/N* ratio increased (from 8.0 ± 0.4 to 9.5 ± 0.8) as the coupling reaction leads to no change in nitrogen and an increase in carbon (and oxygen).[35] Based on a simple calculation, it is found that the surface composition in the sampled depth corresponds to PNHSMA in which ~ 10% of all NHS ester groups have been reacted with PEG_{500}-NH_2 (the same result is obtained if the *O/N* ratio was analyzed; the *O/N* ratio changes from 4.0 ± 0.3 to 4.75 ± 0.2). Assuming a density of PNHSMA of 1 g/cm^3 and using a molar mass of monomeric NHSMA of 183 g/mol, a formal grafting density of PEG of ~ 2.4 PEG molecules per nm^2 can be calculated.[36] This value is in very good agreement with the grafting density calculated based on ellipsometry / FTIR data (see above) and confirms that PNHSMA films possess a quasi-3D reactive structure with more accessible NHS ester groups per unit area compared to corresponding SAMs on gold.

4.3 Swelling Behavior and Stability of PNHSMA Films

For possible applications the swelling behavior and stability of the PNHSMA films in contact with buffer are important factors. Figure 4.8 shows AFM images of PNHSMA films, in which the film has been partially removed, prior to and after treatment for 100 minutes in aqueous buffer (pH = 7.4, ionic strength = 0.15 M).

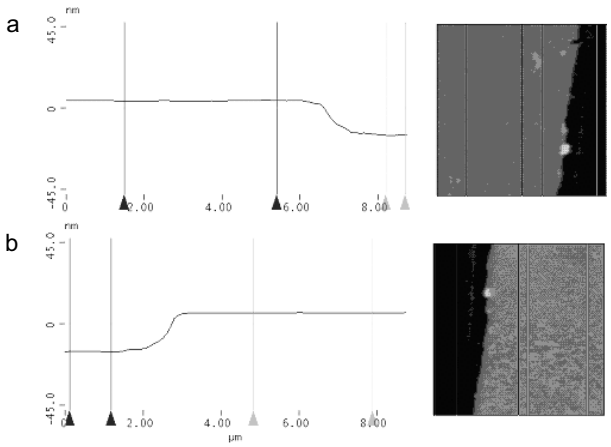

Figure 4.8. (a) AFM height image of PNHSMA film and corresponding step height analysis before treatment in buffer (the step height indicated by the markers is 19.0 nm). (b) AFM height image of PNHSMA film after swelling in buffer solution for 100 minutes and corresponding step height analysis (the step height indicated by the markers is 21.3 nm). All AFM data were acquired in air.

Table 4.2. Film thickness before and after swelling estimated by AFM.

PNHSMA film thickness after drying in vacuum for 10 h	PNHSMA film thickness after immersion in PB buffer (pH=7.4) for 60 minutes	Δd_{film}
13.1 nm	15.2 nm	2.1 nm
12.5 nm	14.7 nm	2.2 nm
19.0 nm	21.3 nm	2.3 nm
18.5 nm	20.7 nm	2.2 nm
38.3 nm	40.3 nm	2.0 nm
39.1 nm	41.2 nm	2.1 nm

It can be seen from the corresponding cross section data in Figure 4.8 that the film thickness increases by 2.3 nm, when the film was in contact with buffer over a period of 100 minutes. Using AFM, we observed a mean increase in film thickness due to swelling of 2.1 ± 0.1 nm for all films independent of the original film thickness (between 12 nm and 40 nm) as shown in Table 4.2. These data are indicative for solvent penetration in the topmost region of the films and hence water uptake and likely swelling.[37] Independent surface plasmon resonance (SPR) measurements for samples supported on gold show changes in optical thickness during the first 60 minutes of treatment. The results above suggest that PNHSMA films can provide an increased number of binding sites compared to NHS-C10 monolayers and show only some limited swelling of the topmost film surface and surface-near region. These features are interesting for applications in which (bio)molecules are immobilized by covalent coupling to solid supports at well-controlled substrate - molecule distances.

4.4 Immobilization of DNA and Surface-Based Hybridization

For the array-based genomics applications mentioned in Chapter 2, among other formats, thin coatings are utilized, which are reactive towards off-chip synthesized oligomeric DNA (or PNA). Essential for the success of the reactive layers is the robust attachment of probe DNA in high coverages in order to maximize the corresponding signals of the utilized label. The coverage should be high, yet it should not result in steric crowding which reduces the hybridization efficiency.[38] In the following sections the investigation of PNHSMA as reactive platform for DNA immobilization and hybridization is discussed (Scheme 4.2).

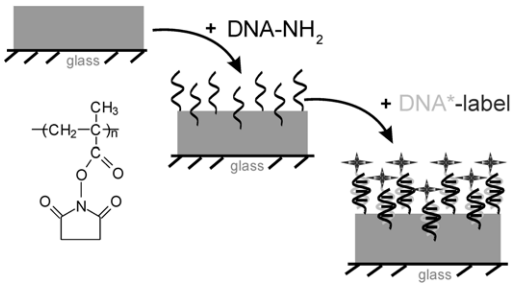

Scheme 4.2. PNHSMA platform for DNA hybridization.

4.4.1 DNA Immobilization Studied by SPR

To test the applicability of PNHSMA as reactive layer for DNA chips, we explored the possibilities to immobilize amino-functionalized DNA on these films. Probe DNA adsorption was followed in real-time by SPR measurements in the kinetic mode by measuring the reflected light at a constant angle just below the resonance angle. Figure 4.9a shows that the immobilization of amino-functionalized probe DNA (25mer) and PNHSMA is initially very rapid and that the DNA adsorption reaches equilibrium in PB buffer after 10 minutes. To calculate the thickness of the immobilized DNA layer from an angular scan (Figure 4.9b), a refractive index of n = 1.464 was used for the polymer film and n = 1.375 for the DNA adlayer.[39] Independent of PNHSMA film thickness, 4.2 ± 0.2 nm of DNA was grafted. Average thicknesses of 2.2 nm for thiolated 25 mer DNA immobilized directly onto bare gold have been reported in the literature.[40] A comparison with the values obtained in our studies indicates that the polymer films indeed yield increased DNA coverages.

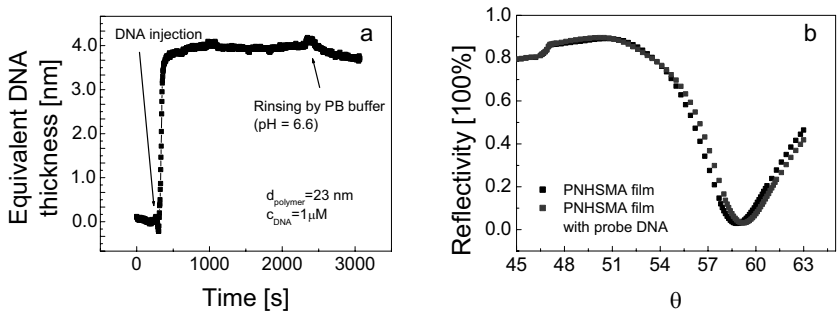

Figure 4.9. (a) SPR angular scans prior to and after DNA immobilization on PNHSMA films. (b) DNA immobilization on PNHSMA film (dry thickness 23 nm) investigated in situ by SPR (kinetic scan).

4.4.2 Investigation of DNA Hybridization by SPFS and Fluorescence Microscopy

After successful immobilization of DNA probe on the PNHSMA surface, as shown by SPR, hybridization of complementary DNA was studied. For this purpose, PNHSMA films were prepared on glass and gold substrates, respectively, and the DNA immobilization on these films was carried out as described above.

We employed SPFS as a very sensitive technique to detect the hybridization of target DNA on probe DNA modified PNHSMA films (Figure 4.10).[41] Upon the addition of the target DNA solution the fluorescence intensity rises very rapidly and reaches a stable, constant value. Rinsing with pure buffer affects the intensity only little, leading to a very slow decrease with time, which can be attributed to desorption of unbound excess target DNA and dehybridization of target DNA.

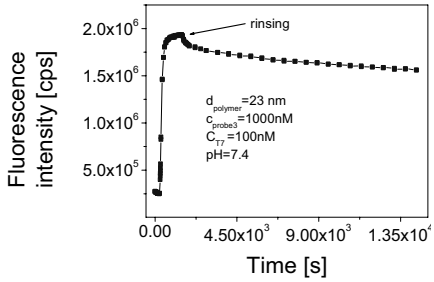

Figure 4.10. Hybridization of complementary target DNA on probe DNA (4.2 nm) modified PNHSMA film (dry thickness 14 nm) investigated by SPFS (PB buffer; pH = 7.4).

To assess the extent of non-specific adsorption during hybridization, total mismatch and complementary DNA were used for SPFS experiment as shown in Figure 4.11a. A weak, yet significant signal for the adsorption of total mismatch DNA was observed. To reduce this apparent non-specific adsorption, different primary amines were used to mask the unreacted NHS groups. The experiments shown here were carried out on samples patched with glycine (Figure 4.11b). The discrimination of different target DNA can be substantially improved using this procedure. Without patching a discrimination ratio of complementary to mismatch of 12 was observed, which improved to 30 after patching with glycine.

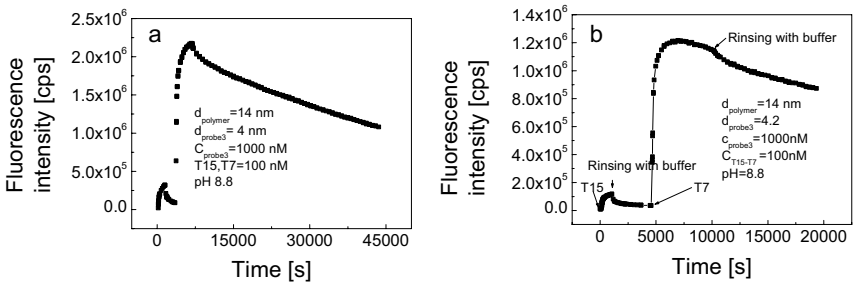

Figure 4.11. (a) SPFS kinetic data for interaction of mismatch target and complementary target DNA with probe DNA modified at pH = 8.8. (b) SPFS kinetic data for interaction of mismatch target and complementary target DNA with probe DNA / glycine modified PNHSMA at pH = 8.8. T7 denotes the complementary target DNA and T15 is the total mismatch DNA.

The hybridization of target DNA was also investigated using fluorescence microscopy. The corresponding micrographs are shown in Figure 4.12. No fluorescence emission was detected for

PNHSMA films modified only with (unlabeled) probe DNA, as well as neat PNHSMA films treated with the dye-labeled target DNA, which is unreactive towards NHS ester groups (Figures 4.12a, 4.12b). By contrast, if the complementary target DNA reacts with PNHSMA films modified with covalently attached probe DNA, strong fluorescence emission was detected (Figure 12c). For the corresponding blank experiment with fluorescently labeled *mismatch* DNA (Figure 12d), no fluorescence emission was detected, which suggests that the hybridization of complementary target DNA was indeed successful. Discrimination ratio of complementary to mismatch of 25 was observed, which is comparable value comparing to SPFS experiment to glycine patched films surface.

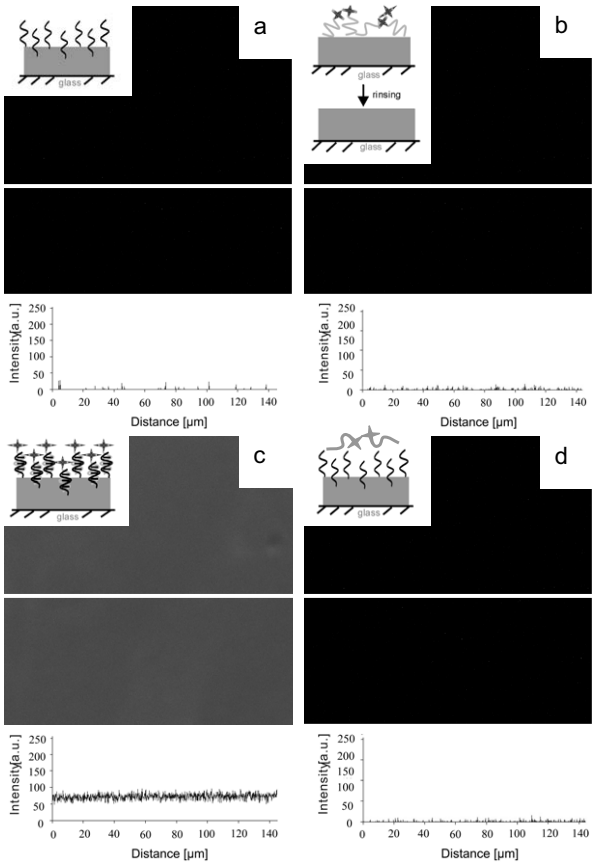

Figure 4.12. Fluorescence microscopy images (top) and corresponding cross sectional intensity plots (bottom) of (a) probe DNA modified PNHSMA films on glass; (b) neat PNHSMA films treated with dye-labeled target DNA after rinsing; (c) probe DNA modified PNHSMA films after hybridization with dye-labeled complementary target DNA after rinsing; (d) probe DNA modified PNHSMA after treatment with dye labeled total mismatch DNA. (Image sizes: 146 × 146 µm^2; the insets show schematically the layer structure; λ_{exc} = 632 nm).

Owing to the effects of fluorescence quenching and decaying coupling efficiency between surface plasmons and surface-immobilized fluorophores, there is an optimized film thickness of ~ 30-50 nm for this particular detection method. Since the film thicknesses of spin-coated films can be easily controlled through variations of polymer solution concentration or spinning speed, reactive thin film systems that show only limited swelling, such as PNHSMA, can be advantageous in this respect.

4.5 Towards the Detection of Pathogenic Bacteria on PNHSMA Films

Recently there has been an increased interest in methods for the detection of bacteria, especially those species that are involved in food poisoning, water contamination, clinical cases, and biological warfare.[42] This interest is the largely a result of increased incidences of *Escherichia coli* O157:H7*, Salmonella, Clostridium and Campylobacter* being found in food and water.[43] Hence there is interest to monitor food and water using suitable biosensors. As introduced also in Chapter 2, a chemical biosensor is a device, which responds to an analyte selectively through a reversible chemical interaction[44] and it can be used for quantitative or qualitative determinations. All sensors are composed of two main regions: one where the selective chemistry occurs and the second being the transducer. The detection of bacteria using sensors is typically assessed via enzyme-tagged immuno-electrochemical assays.[45]

To demonstrate the possibility to apply PNHSMA films in more complex biosensors, the detection of pathogenic bacteria (listeria) was investigated. Listeria is a pathogenic (disease-causing) bacterium that is food-borne and causes an illness called listeriosis.[46] It is frequently overlooked as a possible cause of illness due to its unique growth capabilities. For instance, listeria can grow, albeit slowly, at temperatures as low as 0^{o}C, i.e. inside a fridge.[47]

The requirements for the biosensor architecture and design are shown in Scheme 4.3. Protein G is a globular protein extracted from bacteria. It is mostly used for affinity column to purify antibodies. It can be used to control the orientation of an antibody because it has loci or receptors that bind on the Fc region of the IgG antibody. An antigen is the molecule that an antibody specifically binds. Here, listeria bacteria cells are the antigen. By using surfaces to which protein G was coupled, the antibody binding sites will be exposed to the solution phase environment.

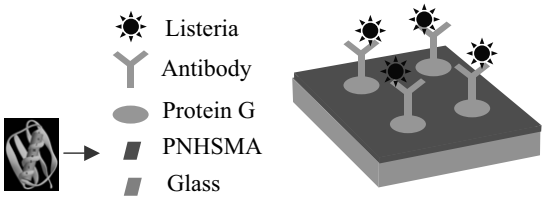

Scheme 4.3. Spin-coated PNHSMA films were firstly derivatized with protein G. The anti-listeria antibody was coupled to the protein. Finally, listeria bacteria were applied on the surface and were captured by the surface-bound antibodies.

First we addressed the possible non-specific adsorption of proteins and antibodies on PNHSMA and PEG_{500}-derivatized PNHSMA on glass. As shown in Figure 4.13, avidin (66 kDa)[48] and a monoclonal antibody against *E. coli* both labeled with fluorescein isothiocyanate (FITC) were incubated on both surfaces. Fluorescence microscopy showed that the protein and antibody were immobilized on PNHSMA films (Figure 4.13a and 4.13c, respectively), while they did not adsorb to a significant extent on the PEG-coated surfaces (Figure 4.13b, d).

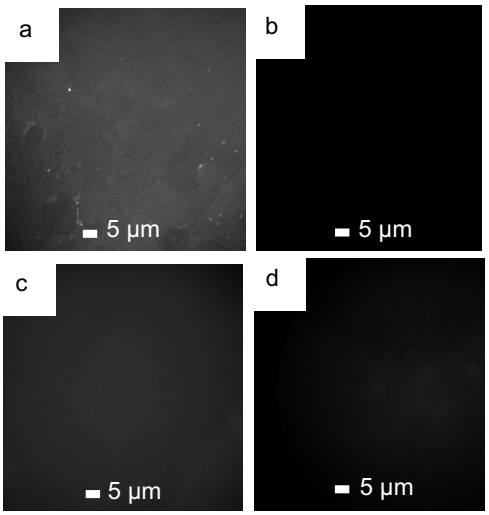

Figure 4.13. Fluorescence microscopy images of avidin-FITC on (a) PNHSMA and on (b) PNHSMA-PEG_{500}, and anti- E. coli-FITC on (c) PNHSMA and on (d) PNHSMA- PEG_{500}.

These measurements show that relevant proteins and antibodies can be firmly immobilized on PNHSMA and do not interact with PEG_{500}-derivatized PNHSMA.

To realize an architecture that could be applied in a biosensor for pathogen detection, protein G was first covalently immobilized on PNHSMA films on glass (compare Scheme 4.3). Anti-Listeria antibodies, spotted on the top of protein layer from a dilution buffer, were immobilized through hydrogen bond formation. Subsequently, the fluorescently-labeled heat-killed Listeria monocytogenes cells were applied on the films. After an incubation time of 5 minutes, the films were rinsed carefully and analyzed by fluorescence microscopy. In Figure 4.14a, very small objects (size ~ 900 nm) with pronounced fluorescence emission can be observed in the anti-listeria functionalized area. Near the periphery of the spot (of anti-listeria), an enrichment of the fluorescent objects can be recognized (likely due to an evaporation phenomenon). Strikingly, outside the spotted area no fluorescence emission is seen. These observations suggest that listeria bacteria have been immobilized on the polymer surface via the corresponding antibody.

Figure 4.14. Optical micrographs of: (a) sensor layer (a PNHSMA film was first derivatized with protein G, followed by immobilization of the anti-Listeria antibody) after reaction with Listeria; (b) PEG_{500}-NH_2 covered PNHSMA film that was exposed to Listeria; (c) sensor layer (a PNHSMA film was first derivatized with protein G, followed by immobilization of the anti-Listeria antibody) after reaction with Escherichia coli.

In a reference experiment, listeria was directly applied onto PEG_{500} covered PNHSMA films. No fluorescence emission was observed on these films, as shown in Figure 4.14b. Using *Escherichia coli* instead of listeria bacteria, also no fluorescence emission was detected on the surface (Figure 4.14c). Since *Escherichia coli* bacteria do not bind, presumably due to the absence of strong interactions with the anti-Listeria antibody, this result shows that the PNHSMA-based platform exhibits some selectivity. In addition, these results suggest that protein G (or at least a large fraction of protein G) has been coupled in an active state, i.e. in the correct orientation and that the antibody attachment was also successful. Thus, PNHSMA films appear as a suitable polymer substrate to be used in the biosensor field for detecting bacteria and likely other species.

In summary, we have shown that spin-coated thin films of poly(*N*-hydroxysuccinimidyl methacrylate) on oxidized silicon, glass and gold substrates are interesting coatings for obtaining robust reactive platforms for biomolecule immobilization with tunable film thickness and high molecular loading capabilities. Compared to SAMs, an increased loading was observed for the covalent coupling of various low molar mass and polymeric primary amines, including 25-mer probe

DNA, PEG, and proteins. This increased loading is attributed to reactions that take place at the surface, as well as in the surface-near region, of the polymer films. The results presented here also suggest that PNHSMA films possess the potential to be applied in sensors that monitor biomolecular interactions, such as hybridization reactions between surface-attached probe oligonucleotides and complementary DNA in solution using, e.g., SPFS measurements, and the detection of pathogens, such as bacteria. In addition, these polymer films are amenable to chemical (and topographical)[49] patterning via soft lithographic approaches to sub-micrometer length scales, as will be discussed in Chapter 6, which increases the scope of the system to include also array-based formats.

4.6 Experimental Section

Materials. The synthesis of *poly(N-hydroxysuccinimidyl methacrylate)* (PNHSMA) (Scheme 1) (M_n of 3650 g/mol; M_w/M_n of 1.3; T_g of 140ºC) is described in Chapter 3. Amino end-labeled PEG (denoted as PEG_{500}-NH_2), purchased from Nektar UK Company (M_n = 500 g/mol, PDI = 1.1), fluoresceinamine (Molecular Probes, Inc. The Netherlands) and the DNA samples (biotin-coupling group at 5' end): P: 25 mer 5'- GGA ATG TGC CAT ACC GAA TCC GTG T –3'; Cy5-labeled target DNA: 5'- CAC GGA TTC GGC ATG – 3'- Cy5, Cy5-labeled mismatch DNA: 5'- TGT GCC TAA GCC ATA - 3'- Cy5, MWG BIOTEC AG, Ebersberg, Germany) were used as received (HPLC-purified > 98%). The DNA samples were stored at -4ºC until use. Glycine was from Sigma with 99% purity. Bovine serum albumin (BSA) labeled with Alexa Fluor®594 was bought from Molecular Probes Inc. and was used as received.

Preparation of Thin Films. Polymer thin films were prepared by spin-coating polymer solutions in DMSO (typical concentration between 10 and 20 mg/ml) onto silicon wafers (111), Au or glass cover slides (Menzel-Glaser), which were previously cleaned by oxygen plasma treatment using an Elektrotech PF 340 apparatus (Pressure of O_2: 0.5 Bar; Current: 30 mA). The samples were spun at 3000 rpm for 30 s using a P6700 spin-coater (Specialty Coating Systems Inc). All spin-coated samples were dried at room temperature for 24 hours in vacuum before analysis. The absence of residual solvent was verified by IR spectroscopy. NHS-C10 monolayers on gold were prepared as reported previously.[17] Mean film thicknesses were determined using a custom-built spectroscopic ellipsometer using a He-Ne laser (λ = 632.8 nm). The refractive index of the PEG films was approximated as 1.4638,[50] while for PNHSMA and NHS-C_{10} 1.50 and 1.45, respectively, were utilized.[51]

PEG_{500}-NH_2 Coupling and Studies of Kinetics. PEG_{500}-NH_2 solutions in PB buffer (pH = 7.4; ionic strength: 0.078 M) were prepared in freshly cleaned glassware with concentrations between 1.0×10^{-4} and 4.0×10^{-4} M. The polymer films and freshly rinsed SAMs were immersed into the corresponding PEG_{500}-NH_2 solution. After a reaction time between 5 min to 10 h the samples were taken out of the corresponding solution and were thoroughly rinsed with Milli Q water. All experiments were carried out at T = 25 ± 2ºC.

Fluoresceinamine Coupling. The polymer films on glass or Si wafer were immersed into a fluoresceinamine solution in PB buffer (pH = 7.4) (2.0×10^{-4}M). After a reaction time between 5 min to 1 h the samples were taken out of solution and were thoroughly rinsed with PB buffer, then Milli-Q water. All experiments were carried out at T = 25 ± 2ºC.

DNA Immobilization and Hybridization. DNA solutions in phosphate buffer (PB) were prepared with a concentration of 1.0×10^{-7} M (pH = 7.4). For covalent coupling to surface-bound reactive ester groups, the polymer films were immersed into the probe DNA solution. After a reaction time of 60 minutes, the samples were taken out and rinsed with PB buffer (pH = 7.4). For hybridization, the films were placed in the target DNA solution in PB (T = 25ºC, pH = 7.4), and after 30 minutes the films were taken out followed by a thorough rinse with PB buffer, and then Milli-Q water.

Fourier Transform Infrared (FTIR) Spectroscopy. Transmission mode FTIR spectra (spectral resolution of 4 cm^{-1}, 1024 scans) were obtained using a BIO-RAD model FTS575C FTIR spectrometer equipped with a liquid nitrogen-cooled cryogenic mercury cadmium telluride (MCT) detector. Background spectra were obtained using oxygen plasma-cleaned silicon wafers. The grazing incidence reflection FTIR spectra of SAMs on gold were collected using a GIR accessory (BIO-RAD) at an angle of incidence of 87º relative to the surface normal.

Atomic Force Microscopy (AFM). The AFM measurements were carried out in intermittent contact (tapping) mode using a NanoScope III multimode AFM (Digital Instruments / Veeco, Santa Barbara, CA) equipped with a 100 µm scanner. Microfabricated silicon tips / cantilevers (Nanosensors, Wetzlar, Germany) were used in ambient atmosphere (ca. 30 % relative humidity, 24ºC temperature) as described in Chapter 4. For the determination of the film thicknesses by profilometry, the film was removed by scratching the samples using sharp tweezers (width of scratch between 15 and 30 μm). Surfaces of films that were immersed in buffer for swelling (60 minutes) were quickly dried in a stream of nitrogen before scratching and subsequent AFM analysis. The captured AFM height images were subjected to a first-order plane fit followed by a cross-section analysis. An accurate calibration of the AFM scanner in the *z*-direction was ensured by using a set of three vertical calibration standards (TGZ 01-03, Silicon-MDT, Moscow, Russia).

X-ray Photoelectron Spectroscopy (XPS). XPS spectra were recorded on a PHI Quantum 2000 Scanning ESCA microprobe using a monochromated X-ray beam (Al-anode; 100 µm diameter / 25 Watt X-ray beam) scanned over 700 µm × 300 µm area at a fixed take-off angle of 45º. Atomic concentrations were determined by numerical integration of the relative peak areas using the Multipak software with supplied sensitivity factors (C1s: 0.314; O1s: 0.733; N1s: 0.499).[52]

Fluorescence Microscopy. Fluorescence micrographs were taken using a Zeiss LSM 510 confocal fluorescence microscope with a BP 500-550 IR filter for fluoresceinamine, a LP 650 filter for Cy5-labeled target DNA and BSA conjugated with Alexa Fluor® 594 with a 633 nm HeNe laser. For excitation an Ar laser (30 mW) was used. A 500-550 nm bandpass filter was selected for experiments with fluoresceinamine and a 650 nm longpass filter was selected for the labeled target Cy5-labeled DNA and BSA-Alexa Fluor® 594, respectively.

SPR and SPFS Set-Ups. The SPR experiments were carried out in the group of Prof. Dr. W. Knoll at the Max-Planck-Institute for Polymer Reserach (Mainz, Germany) on a custom-built SPR setup,[53a] which is based on the configuration introduced by Kretschmann and Raether.[53b] A refractive index of n = 1.464 was used for the polymer film and n = 1.375 for the DNA adlayers. The SPFS set up used has been recently described in detail by Knoll et al.[54]

Experimental Procedure for Non-Specific Adsorption of Listeria. The measurements were carried out by C. Ruengruglikit and Prof. Dr. Q. Huang (Department of Food Science, Rutgers University, New Brunswick, NJ). At room temperature, 0.4 µl of 0.025 mg/ml protein G in 1:1 Glycerol: PBS solution were pipetted on a PNHSMA film or PEG_{500}-NH_2-coated PNHSMA film followed by rinsing with PBS buffer. 0.2 µl of 500 µg/ml Anti-Listeria antibody was spotted on top of protein G in a dilution buffer (1:1 Glycerol/PBS buffer) and was incubated for at least 24 hours at 4°C. Then the surfaces were blocked with 1% w/v BSA and were incubated at room temperature for 2 hours. Fluorescently-labeled heat-killed *Listeria monocytogenes* cells were prepared with 1 mg/ml EtBr in saline by mixing serially diluted cell solution in saline (10, 100, 1000, 10000 dilution factors from stock solution). The solution was mixed and set aside for 5 minutes. The cells were incubated for 40 minutes and unbound cells were rinsed off with washing solution, then PBS buffer and deionized water, respectively. Cells were detected by inverted fluorescent microscopy using a 40x objective lens.

4.7 References

1 Yang, M.; McGovern, M. E.; Thompson, M. *Aanlytica Chimica Acta* **1997**, *346*, 259.

2 Knoll, W.; Yu, F.; Neumann, T.; Schiller, S.; Naumann, R. *Phys. Chem. Chem. Phys*. **2003**, *5*, 5169.

3 Spinke, J.; Liley, M.; Guder, H. J.; Angermaier, L.; Knoll, W. *Langmuir* **1993**, *9*, 1821.

4 Schena, M.; Shalon, D.; Davis, R. W.; Brown, P. O. *Science* **1995**, *270*, 467.

5 Gong, P.; Grainger, D. W. *Surf. Sci* **2004**, *570*, 67 and references herein.

6 MacBeath, G.; Schreiber, S. L. *Science* **2000**, *289*, 1760.

7 Ulman, A. *An Introduction to Ultrathin Organic Films*; Academic Press: Boston, 1991.

8 Ferretti, S.; Paynter, S.; Russell, D. A.; Sapsford, K. E.; Richardson, D. J. *Trac-Trends Anal. Chem*. **2000**, *19*, 530.

9 (a) Chechik, V.; Crooks, R. M.; Stirling, C. J. *Adv. Mater*. **2000**, *12*, 1161. (b) Dordi, B.; Schönherr, H.; Vancso, G. J. *Langmuir* **2003**, *19*, 5780.

10 Spinke, J.; Liley, M.; Schmitt, F. J.; Guder, H. J.; Angermaier, L.; Knoll, W. *J. Chem. Phys*. **1993**, *99*, 7012.

11 Su, X.; Wu, Y.-J.; Robelek, R.; Knoll, W. *Langmuir* **2005,** *21,* 348.

12 (a) Delamarche, E.; Michel, B.; Biebuyck, H. A.; Gerber, C. *Adv. Mater*. **1996**, *8*, 719. (b) Lang, P.; Mekhalif, Z.; Rat, B.; Garnier, F. *J. Electroanal. Chem*. **1998**, *441*, 83. (c) Huseman, M.; Morrisson, M.; Benoit, D.; Frommer, J.; Mate, C. M.; Hinsberg, W. D.; Hedrick, J. L.; Hawker, C. L. *J. Am. Chem. Soc*. **2000**, *122*, 1844.

13 Jérôme, J.; Gabriel, S.; Voccia, S.; Detrembleur, C.; Ignatova, M.; Gouttebaron, R.; Jérôme, R. *Chem. Comm*. **2003**, 2500.

14 Falconnet, D.; Koenig, A.; Assi, F.; Textor, M. *Adv. Funct. Mater*. **2004**, *14*, 749.

15 Malmqvist, M.; Karlsson, R. *Curr. Opin. Chem. Bio*. **1997**, *1*, 378.

16 Dextran gel, a hydrogel system that can provide high affinity binding sites, has been widely investigated as well. It has been shown that the amount of immobilization of proteins on dextran hydrogel is much higher (~ factor of 12) than on typical monolayers due to the higher immobilization capacity of dextran gel.((a) Sigal, G. B.; Bamdad, C.; Barberis, A.; Strominger, J.; Whitesides, G. M. *Anal. Chem*. **1996**, *68*, 490, (b) Gehrke, S. H.; Vaid, N. R.; McBride, J. F. *Biotechnol. Bioeng*. **1998**, *58*, 417. (c) Putka, C. S.; Gehrke, S. H.; Willis, M.; Stafford, D.; Bryant, J. *Biotechnol. Bioeng*. **2002**, *80*, 139) However, the potential drawbacks for dextran gels are that it can increase diffusion lengths (Toomey, R.; Freidank, D.; Rühe, J. *Macromolecules* **2004**, *37*, 882). For selected biosensor detection schemes the pronounced swelling may be disadvantageous.

17 (a) Niemeyer, C. M.; Blohm, D. *Angew, Chem., Int. Ed, Engl*. **1999**, *38*, 2865. (b) Schulze, A.; Downward, J. *Nat. Cell Biol*. **2001**, *3*, E190.

18 (a) Benters, R.; Niemeyer, C. M.; Drutschmann, D.; Blohm, D.; Wöhrle, D. *Nul. Acid Res*. **2002**, *30(e10)*, 1. (b) Pathak, S.; Singh, A. K.; McElhanon, J. R.; Dentinger, P. M. *Langmuir* **2004**, *20*, 6076.

19 Degenhart, G. H.; Dordi, B.; Schönherr, H.; Vancso, G. J. *Langmuir* **2004**, *20*, 6216.

20 Rowan, B.; Wheeler, M. A.; Crooks, R. M. *Langmuir* **2002**, *18*, 9914.

21 Lahann, J.; Balcells, M.; Rodon, T.; Lee, J.; Choi, I. S.; Jensen, K. F.; Langer, R. *Langmuir* **2002**, *18*, 3632.

22 Zhou, X.; Wu, L.; Zhou, J. *Langmuir* **2004**, *20*, 8877.

23 (a) Zhang, Z.; Chen, Q.; Knoll, W.; Foerch, R.; Holcomb, R.; Roitman, D. *Macromolecules* **2003**, *36*, 7689. (b) Zhang, Z.; Knoll, W.; Foerch, R.; Holcomb, R.; Roitman, D. *Macromolecules* **2005**, *38*, 1271.

24 Golze, S. Ph. D. thesis; 2001; University of Mainz.

25 Yu, F.; Persson, B.; Löfås, S.; Knoll, W. *J. Am. Chem. Soc*. **2004**, *126*. 8902.

26 (a) Liebermann, T.; Knoll, W. *Colloids. Surf. A* **2000**, *171*, 115. (b) Liebermann, T.; Knoll, W.; Sluka, P.; Herrmann, R. *Colloids. Surf. A* **2000**, *169*, 337. (c) Yu, F.; Yao, D.; Knoll, W. *Anal. Chem.* **2003**, *75*, 2610.

27 Harder, P.; Grunze, M.; Dahint, R.; Whitesides, G. M.; Laibinis, P. E. *J. Phys. Chem. B* **1998**, *102*, 426.

28 Frutos, A. G.; Brocknam, J. M.; Corn, R. M. *Langmuir* **2000**, *16*, 2192.

29 The absorbance at 1344 cm^{-1} (EG CH_2 wagging band), which can be exclusively attributed to the crystallized fraction of PEG, is negligible for the film after PEG coupling (Schönherr, H.; Frank, C. W. *Macromolecules* **2003**, *36*, 1188).

30 For this analysis we excluded data with PEG coverage > 90% as these introduce considerable error in the analysis owing to the large uncertainties of the corresponding values.

31 Mougin, K.; Lawrence, M. B.; Fernandez, E. J.; Hillier, A. C. *Langmuir* **2004**, *20*, 4302.

32 Dordi, B.; Schönherr, H.; Vancso, G. J. *Langmuir* **2003**, *19*, 5780.

33 Liu, Z.; Pappacena, K.; Cerise, J.; Kim, J.; Durning, C. J.; O´Shaughnessy, B.; Levicky, R. *Nanoletters* **2002**, *2*, 219.

34 Tanaka, K.; Takahara, A.; Kajiyama, T. *Macromolecules* **1996**, *29*, 3232.

35 The theoretical C/N ratio of PNHSMA is 8, while for a 100% converted PNHSMA one can calculate a C/N ratio of 22.

36 The grafting density σ_{PEG} can be calculated as:

$$\sigma_{PEG} \approx 10\ \%\ d_{XPS}\ \rho_{PNHSMA}\ N_A\ M^{-1}$$

where d_{XPS} is information depth of the XPS experiment, ρ_{PNHSMA} is the density of PNHSMA (~ 1 g/cm^3), N_A (6.022 $\times 10^{23}$ mol^{-1}) is Avogadro's number, and M is the molar mass (183 g/mol) of monomeric PNHSMA.

37 During this time some hydrolysis of NHS ester groups at the film surface will occur to a negligible extent, if we extrapolate from the data reported in Chapter 3 to pH 7.7.

38 Podyminogin, M. A.; Lukhtanov, E. A.; and Reed M. W. Nucleic Acids Research 2001, 29, 5090.

39 Zizlsperger, M. PhD. Thesis, Johannes-Gutenberg-Universität Mainz, Germany, 1998.

40 Aqua, T.; Naaman, R.; Daube, S. S. *Langmuir* **2003**, *19*, 10573.

41 Chen, Q.; Förch, R.; Knoll, W. *Chem. Mater*. **2004**, *16*, 614.

42 Deisingh, A. K.; Thompson, M. *Anal*. **2002**, *127*, 567.

43 Bacteria are microscopic organisms with each bacterium being a single autonomous cell. A cell contains a double layer of phospholipid molecules interspersed with cholesterol and proteins (many of which are receptors for chemical signals). The diversity of chemical signals act through G-protein-linked receptors. Several human diseases have been linked to alterations in cell-surface receptors. These surface receptors activate intracellular signaling cascades. These signaling cascades regulate numerous cellular functions from cell division to cell growth and development. Defects in these proteins (usually stemming from defects in the genes that encode them) can result in disease. Biosensors are needed for determining the interactions between the proteins and cells.

44 Cattrall, R. W. *Chemical Sensor*, Oxford University Press, Oxford, **1997**.

45 Rishpon, J.; Gezundhajt, Y.; Soussan, L.; Rosenmargalit, I.; Hadas, E. *ACS Symp. Ser*., **1992**, *511*, 59.

46 Listeria monocytogenes can cause a variety of diseases, including infections in pregnancy ranging from a mild chill to a severe illness, which may precipitate premature birth or miscarriage, and meningitis in newborn children. Septicaemia and meningitis occurs in adults whose immunity to infection is impaired, such as those suffering from

cancer or leukaemia or transplant patients. Infection does occur in otherwise healthy adults and children although this is extremely rare.

47 Lappi, V. R.; Ho, A.; Gall, K.; Wiedmann, M. *J. Food. Proteci.* **2004**, *65*, 1022.

48 Avidin is a highly cationic 66,000-dalton glycoprotein with an isoelectric point of about 10.5. It is thought that avidin's positively charged residues and its oligosaccharide component can interact nonspecifically with negatively charged cell surface and nucleic acids, sometimes causing background problems in some histochemical applications and flow cytometry. Avidin has a high affinity with biotin. Avidin binds four biotins per molecules with high affinity and selectivity.

49 Topographically structure surfaces via capillary force lithography and hot embossing / nanoimprint lithography have been successfully prepared. The data is, however, not reported in this thesis.

50 *Polymer Handbook*, 3rd ed. Brandrup, J.; Immergut, E. H. John Wiley & Sons: New York, **1989**.

51 Prime, K. L.; Whitesides, G. M. *J. Am. Chem. Soc.* **1993**, *115*, 10714.

52 Reilman, R. F.; Msezane, A.; Manson, S. T. *J. Electron Spectroscopy* **1976**, *8*, 389.

53 (a) Rothenhäusler, B.; Knoll, W. *Nature* **1988**, *332*, 615-617. (b) Kretschmann, E.; Raether, H. *Z. Naturforsch*. **1968**, *23A*, 2135-2136.

54 Surface Plasmon Resonance Fluorescence Spectroscopy (SPFS) and its applicability in surface and interface analysis have been reviewed recently (Knoll, W.; Park, H.; Sinner, E. K.; Yao, D. F.; Yu, F. *Surf. Sci.* **2004**, *570*, 30-42.). The evanescent field of surface plasmons, excited at a metal/dielectric interface by a monochromatic light beam (He-Ne laser), is used to excite surface-immobilized fluorophores. The fluorescence emission of the surface bound dye molecules excited by the amplified electromagnetic field leads to an intensity enhancement. Compared to conventional (label-free) SPR the sensitivity and specificity of the binding assays are thus increased.

Chapter 5

Tailored Biointerfaces via Derivatization of Polystyrene-b-Poly(*tert*-butyl acrylate) Thin Films

The investigation of polystyrene-b-poly(tert-butyl acrylate) (PS_{690}-b-$PtBA_{1210}$) films and their derivatization to obtain tailored biointerfaces is presented in this Chapter. Derivatized PS_{690}-b-$PtBA_{1210}$ polymer films show good stability under a broad range of conditions. Hydrolysis of the reactive t-butyl acrylate ester groups was performed in trifluoracetic acid, hydrochloric acid solution, and in HCl gas phase. After the subsequent activation by N-hydroxysuccinimide (NHS) ester groups a variety of amino-functionalized (bio)molecules can be covalently immobilized on the hydrolyzed surfaces. The reactivity of the PS_{690}-b-$PtBA_{1210}$ films and in particular the controllable loading with amino functionalized poly(ethylene glycol) were studied by infrared and X-ray photoelectron spectroscopy (XPS). Subsequently, the immobilization of biologically relevant molecules, such as bovine serum albumin (BSA) and poly(L)lysine (PLL), on PS_{690}-b-$PtBA_{1210}$ films were studied by fluorescence microscopy. To demonstrate possible applications of the PS_{690}-b-$PtBA_{1210}$ based platform as biointerfaces, hybridization of target DNA with immobilized probe DNA, as well as the interaction of two different types of cells, i.e. K562 and pancreatic cancer cells, on functionalized PS-b-PtBA films were investigated.

5.1 Introduction

The design of interfaces between the biological environment and various (bio)materials is often an important determinant of the ultimate biomaterial performance.[1] Biointerfaces are central to biology and medicine and are crucial for implants, biosensors, drug delivery, proteomics, and many other fields.[2] In particular, biointerfaces play an important role in cell engineering in the field of microfabrication.[3]

In general, cells can be divided into two types: prokaryotic cells, which lack a defined nucleus and have a simplified internal organization; and eukaryotic cells, which have a more complicated internal structure, including a defined, membrane limited nucleus. Cells interact with the external environment via transmembrane proteins and many of these proteins are receptors, which are characterized by an extracellular ligand-binding domain and an intracellular signaling domain. Many of the proteins associated with the plasma membrane are tightly bound to it, as shown in Scheme 5.1. Some transmembrane proteins that span the bilayer several times form a hydrophilic channel through which certain ions and molecules can enter (or leave) the cell. Defects in these proteins (usually stemming from defects in the genes that encode them) can result in disease, for example, in humans. It is by now well established that the control of the interaction between cells and proteins on surface becomes very

important not only for the design of cell-based assays,[4] but also for fundamental studies of cellular processes and cell behavior.[5]

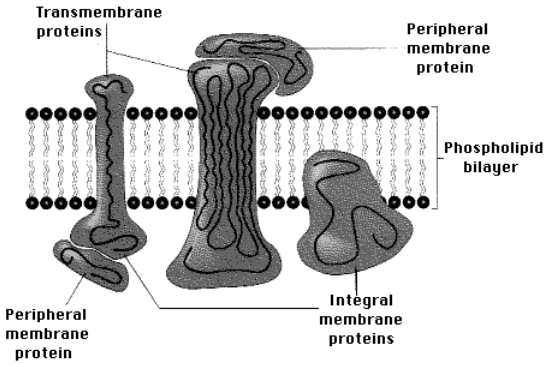

Scheme 5.1. Schematic of the plasma membrane with transmembrane, peripheral and integral membrane proteins (adapted from http://users.rcn.com/jkimball.ma.ultranet/BiologyPages).

Artificial or biomimetic biointerfaces can be fabricated (or surface engineered) starting from suitable platforms. These platforms are in many cases functionalized via selective surface chemical reactions, e.g., with appropriate proteins. In addition to the desired control of the interaction between cells and proteins, one important property of biointerfaces in general is the need of antifouling layers, such as for example, poly(ethylene glycol) (PEG) layers, that prevent non-specific adsorption of biomolecules (proteins etc.). In this context, active organic and polymeric films show very attractive features, which make them suitable platforms to obtain biointerfaces. During the last decade, self-assembled monolayers (SAMs) have been studied in a broad range of biochemical reactions, such as protein immobilization, diagnostic assays, high throughput drug screening, and cultures of attached cells,[6] because of their defined and flexible surface chemistry and design.

In the previous Chapter, spin-coated thin films of reactive poly(*N*-hydroxysuccinimidyl-methacrylate) (PNHSMA) films were introduced as new (bio)reactive thin film platforms.[7] A broad range of moleucles can be directedly deposited on these films in a simple way through covalent bond formation. Several advantages were found for this active homopolymer, such as high reactivity, high loading and tunable film thickness. However, one drawback of this polymer was found, that is, short shelf life due to the high sensitivity the NHS ester groups to humidity.[8]

As shown in this Chapter, PS_{690}-b-$PtBA_{1210}$ diblock copolymer thin films with reactive t-butyl acrylate (tBA) ester groups were developed to be used as an alternative polymer-based potential bioplatform. Such polymer films show increased stability under typical processing condition due to the presence of a water insoluble PS block. The tunable film thickness, the reactive PtBA skin layer (see Chapter 3), and the stability under a wide range condition render PS_{690}-b-$PtBA_{1210}$ diblock copolymer a promising biointerface platform for studying protein immobilization and cell adhesion.

5.2 Investigation of the Surface Chemistry of PS_{690}-b-$PtBA_{1210}$ Films

The hydrolysis of reactive tBA groups in the PtBA skin layer in 3M aqueous HCl and its kinetics have already been discussed in Chapter 3. In this current Chapter, the surface hydrolysis of PS_{690}-b-$PtBA_{1210}$ films is investigated under different conditions in order to maximize the degree of hydrolysis and thereby degree of functionalization of PS_{690}-b-$PtBA_{1210}$ block copolymer films. Functionalization of the polymer films with BSA, PLL, as well as 25-mer probe DNA will be then treated. Finally, the interaction of K562 and pancreatic cancer cells with derivatized PS_{690}-b-$PtBA_{1210}$ is discussed.

5.2.1 Surface Hydrolysis of PS_{690}-b-$PtBA_{1210}$ Films

The hydrolysis reaction under different conditions, the functionalization of the PtBA skin layer, and the subsequent immobilization of amino functionalized molecules are shown in Scheme 5.2.

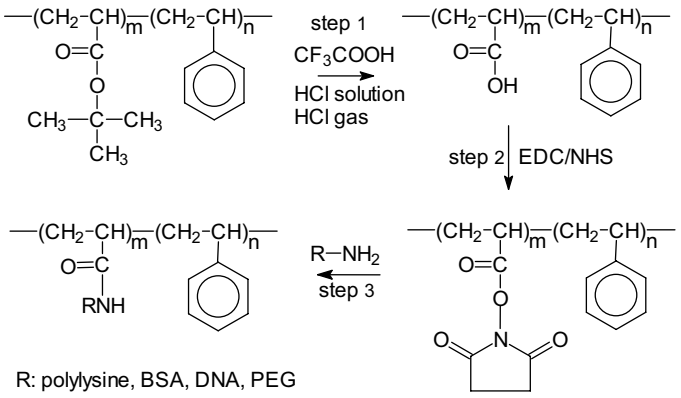

Scheme 5.2. Schematic of hydrolysis, functionalization and immobilization on a PtBA skin layer of PS_n-b-$PtBA_m$ diblock copolymer.

As extension of the work reported in Chapter 3, the possibly different hydrolysis behavior of PS_{690}-b-$PtBA_{1210}$ films in HCl gas and in neat trifluoroacetic acid was investigated. The FTIR transmission spectra of the films on oxidized silicon under different acid conditions are shown in Figure 5.1. For comparison, we show data for the maximum possible degree of hydrolysis for all three different conditions. The spectrum of the unreacted films (0 min) shows some characteristic and intense adsorptions of the PtBA block, i.e. ν(C=O) at 1732 cm^{-1} and ν(C-O) at 1254/1159 cm^{-1}, the *tert*-butyl group ($\nu_{as}(CH_3)$ at 2978 cm^{-1} and a doublet at 1393/1368 cm^{-1} assigned to the symmetric methyl deformation mode.[9]

The hydrolysis of the PtBA phase results in the formation of carboxylic acid functionalized polymer chains. From Figure 5.1 it can be seen that the integrated absorption of the tert-butyl group at 2978 cm^{-1} and 1393/1368 cm^{-1} decreased for practically infinite reaction time in 3 M HCl aqueous solution, while the peak assigned to the *tert*-butyl groups disappeared after hydrolysis in gaseous HCl and trifluoroacetic acid. These data demonstrate that the hydrolysis of the entire film was already

complete in trifluoroacetic acid and HCl gas. In addition, the reaction did not go to completion in 3 M HCl solution, which suggests that hydrolysis occurs only at and near the surface of the polymer films.

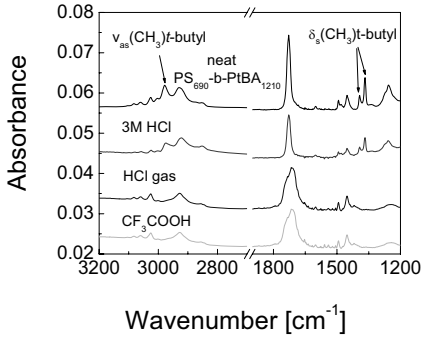

Figure 5.1. Transmission FTIR spectra of films of PS-b-PtBA on oxidized silicon in comparison with films showing the maximum possible degree of hydrolysis (hydrolysis for 5 days under 3M HCl solution, t = 2 hrs in HCl gas phase, and t = 15 min for the reaction in trifluoroacetic acid, respectively.

Static water contact angles (CA) measured on the films after hydrolysis under different conditions are plotted in Figure 5.2a as a function of hydrolysis time. It can be seen that the CA decrease is very fast in trifluoroacetic acid with progressing hydrolysis, while the CA decrease is the slowest for the hydrolysis in 3 M HCl. In addition, it was found that the hydrolysis of the polymer surface cannot reach completion in 3 M HCl condition compared to the other two conditions even with much longer reaction time as shown in Figure 5.2b. This result suggests that the hydrolysis of PS_{690}-b-$PtBA_{1210}$ films in 3 M HCl may lead to a lower degree of carboxylic acid functionalities at the surface compared to samples hydrolyzed in HCl gas or in trifluoroacetic acid.

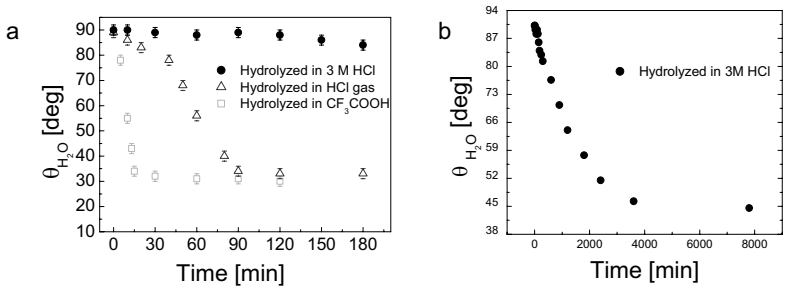

Figure 5.2. (a) Static contact angles measured for films of PS-b-PtBA on SiO_2 under different reaction conditions at different reaction time. (b) Static contact angles measured for films of PS-b-PtBA on SiO_2 in 3M HCl for long reaction time.

To further compare the hydrolysis of the films under different conditions and to study the topographic and phase changes after hydrolysis for different cases, tapping mode atomic force microscopy (TMAFM) was used to image the film surface. Figure 5.3 a and b show AFM topographic

and phase images of PS_{690}-b-$PtBA_{1210}$ films before hydrolysis. Here, the film thickness was around 90 nm with a domain spacing of ca. 83 nm according to AFM measurements. The mean roughness (R_a)[10] assessed from 1.0 μm^2 topographical images was 0.9 nm. Phase contrast was not so clearly observed, which may be attributed to the glassy character of both blocks of the block copolymer and hence similar energy dissipation.

Figure 5.3c and d show the height and phase images of the polymer films after reaction for 2 hrs in 3 M HCl aqueous solution. Compared to untreated films, many short worm-like features appeared and fully covered the whole surface. Typical dimensions of these features were ~13 nm. These features were identified as swollen PAA-rich globules on the film surface due to uptake water from the solution. The mean roughness (R_a) measured increased up to 1.4 nm. The features observed in the height images were also clearly recognized in the phase images.

If the films were hydrolyzed in HCl gas phase for 2 hrs (hydrolysis goes to completion as proved by IR), different topographical and phase images were observed by AFM as shown in Figure 5.3 e and f. Longer worm-like feature surface were observed, but also block copolymer microphase separation was more pronounced. These observations may be attributed to the fact that all PtBA groups have been reacted to PAA. The thus altered intermolecular interactions lead to an increase the corresponding Flory-Huggins parameter.[11] The measured R_a assessed from 1.0 μm^2 was increased to 5.1 nm.

Similar results have been obtained for the films hydrolyzed in trifluoroacetic acid about 15 min in Figure 5.3 g and h (hydrolysis reached completion as proved by IR above). The measured R_a assessed from 1 μm^2 was about 5.3 nm.

From a comparison of the surface roughness values, we can conclude that the surface area of the films after hydrolysis in HCl gas and trifluoroacetic acid will be larger compared to films hydrolyzed in 3 M HCl solution.[12] In addition, the PAA groups resulting from the hydrolysis of PtBA functional groups can be swollen by uptake of water from the solution. These properties may yield advantages for such hydrolyzed films, that is, providing high densities of active functional groups at the surface in a water-swollen gel-like state. However, to obtain such reactive films takes 2 hours in HCl gas, whereas 15 minutes are sufficient if the hydrolysis is performed in trifluoroacetic acid.

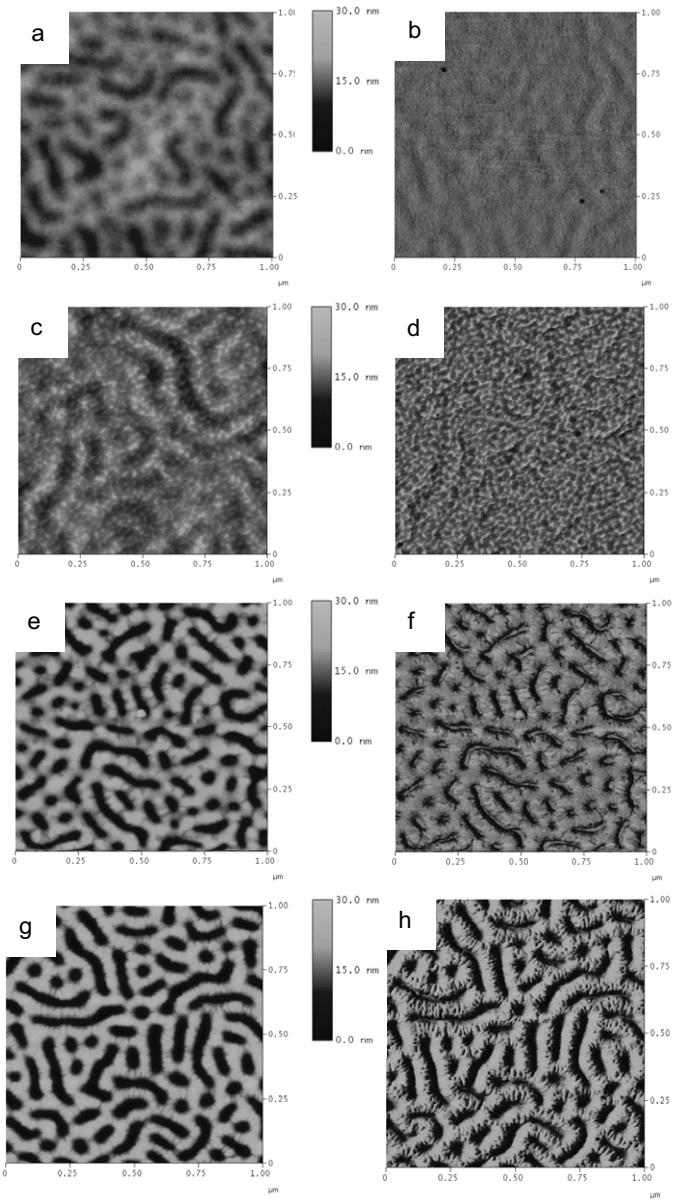

Figure 5.3. TMAFM (a) height and (b) phase image of PS-b-PtBA copolymer film after annealing in vacuum oven. TMAFM (c) height and (d) phase images of PS-b-PtBA after hydrolysis in 3 M HCl aqueous solution. TMAFM images (e) height and (f) phase of PS-b-PtBA after hydrolysis in HCl gas for 24 hrs. TMAFM images (g) height and (h) phase of PS-b-PtBA after hydrolysis in trifluoroacetic acid for 15 min.

5.2.2 Covalent Coupling of PEG to Activated PS_{690}-b-$PtBA_{1210}$ Films

The carboxylic acid generated in the hydrolysis reaction of the PS_{690}-b-$PtBA_{1210}$ films can be activated with NHS ester moieties using a standard recipe as described in Chapter 4. The subsequent covalent coupling reaction of the activated NHS ester groups at and near the surface of PS_{690}-b-$PtBA_{1210}$ films with amino groups terminated PEG_{500}-NH_2 from aqueous solution was investigated by FTIR spectroscopy as shown in Figure 5.4a. Two new additional absorption bands at 1645 cm^{-1} (amide I) and 1544 cm^{-1} (amide II) were observed in the spectra. This result showed that the PEG molecules were covalently grafted on the polymer film through amide linkage formation (see also Chapter 4). The kinetics of immobilization of PEG-NH_2 molecules was followed by ellipsometry. Figure 5.4b shows the grafting thickness of the grafted PEG layer determined by ellipsometry for different reaction times. The maximium thickness of PEG_{500}-NH_2 was ~1.9 nm. A grafting density of PEG of ~ 2.9 PEG molecules per nm^2 was thus calculated.[13] This density is about 3 times higher than the maximum grafting density of PEG molecules on SAMs (~ 0.87 nm^{-2}, see Chapter 4).

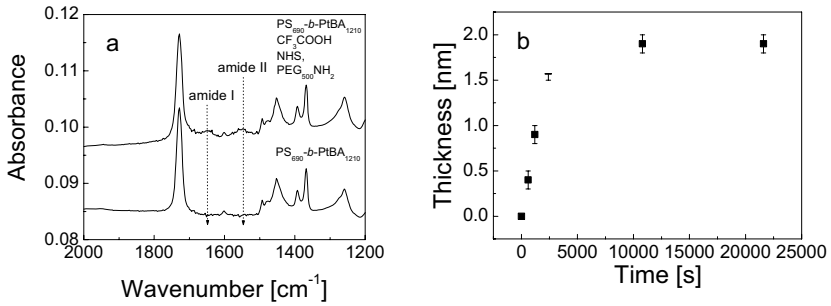

Figure 5.4 (a) Transmission mode FTIR data of neat PS_{690}-b-$PtBA_{1210}$ film and PS_{690}-b-$PtBA_{1210}$ film after hydrolysis, activation, and reaction with PEG_{500}-NH_2. The presence of the amide I (1645 cm^{-1}) and amide II (1544 cm^{-1}) bands suggest that the PEG_{500}-NH_2 molecules were covalently bound to the polymer surface. (b) Thickness changes of the grafted PEG_{500}-NH_2 layer on PS-b-PtBA film. The thickness was determined by ellipsometry.

To confirm the successful surface derivatization, XPS experiments were performed with a take-off angle of 45º (Figure 5.5). For neat PS_{690}-b-$PtBA_{1210}$ films, only the C_{1s} peaks at 284.07 eV and O_{1s} at 532.0 eV[14] were observed. After coupling of PEG molecules on the polymer film surface, not only the C_{1s} peaks at 284.3 eV and the O_{1s} peak at 532.0 eV, but also an N_{1s} peak at 401.5 eV, were observed. The *C/N* ratio of PEG_{500}-NH_2 functionalized films was about 7. The surface composition in the sampled depth hence corresponds to a polymer film in which ~ 11.5% has been reacted with PEG-NH_2. A grafting density of PEG of ~ 2.9 PEG molecules per nm^2 was thus calculated, which is in excellent agreement with the ellipsometry results shown above.

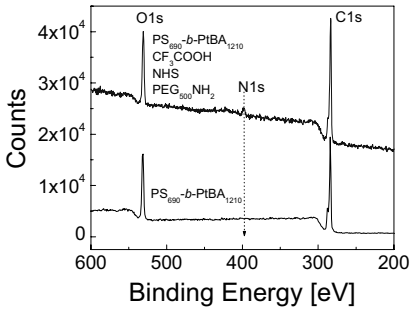

Figure 5.5. XPS element scans of a neat PS_{690}-b-$PtBA_{1210}$ film and a PS_{690}-b-$PtBA_{1210}$ film after hydrolysis, activation, and reaction with PEG_{500}-NH_2.

Similar to the PNHSMA polymer system shown in Chapter 4, high molecular loading of the activated PS_{690}-b-$PtBA_{1210}$ films can be achieved in coupling reactions with PEG_{500}-NH_2. As mentioned before, PEG is a very important biomaterial coating due to the fact that it inhibits non-specific protein adsorption.[15] It is thought that the PEG grafting density, the chain length, and the conformation are important factors for the inhibition of non-specific adsorption of various types of biomolecules.[16]

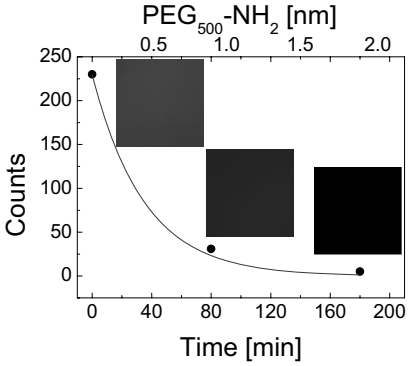

Figure 5.6. Plots of integrated fluorescence emission intensity (the PEG thickness was determined by ellipsometry for each coupling time) of PEG-functionalized PNHSMA films treated with BSA for 30 min followed by rinsing with PB (pH 7.4) and drying vs reaction time / PEG thickness. The insets show representative fluorescence microscopy images acquired for the corresponding samples (image size : 145 × 145 μm^2).

The effectiveness of blocking the polymer layer against adsorption of proteins was consequently tested as a function of PEG_{500}-NH_2 grafting thickness. Covalently attached or physisorbed dye-labeled bovine serum albumin (BSA) was detected by fluorescence microscopy. Figure 5.6 shows the decrease of the fluorescence emission intensity of BSA for different PEG_{500}-NH_2 grafting thicknesses. Without any PEG coating, strong fluorescence emission was observed, which indicates a significant coverage

of the corresponding fluorescent adsorbate. With increasing thickness of the grafted PEG_{500}-NH_2 layers, a significant reduction of adsorbate coverage was observed (the ratio of the fluorescence emission intensity on the films with 3 hrs PEG blocking vs. the background fluorescence of neat PS_{690}-b-$PtBA_{1210}$ is about 2). Therefore, it can be concluded at this point that the grafted PEG layers with 1.9 nm thickness effectively inhibit the immobilization of BSA.

5.3 Covalent Coupling of Biomolecules to Activated PS_{690}-b-$PtBA_{1210}$ Films

The covalent grafting of amino functionalized PEG molecules with NHS activated PS_{690}-b-$PtBA_{1210}$ films have been earlier demonstrated by IR spectroscopy. To prove that other amino functionalized biomolecules can also be covalently immobilized on the PS_{690}-b-$PtBA_{1210}$ films, fluorescence microscopy was used. These studies were focussed on the immobilization of amino end functionalized 25-mer DNA, BSA, and PLL.

The grafting of probe DNA (25 mer) on activated PS_{690}-b-$PtBA_{1210}$ films[17] from buffer solution (100 nM) was studied by ellipsometry, as shown in Figure 5.7. A maximum coupling thickness (4 nm) of probe DNA after 2 hrs can be achieved, which is similar to the data obtained for PNHSMA films (compare with Chapter 4). The maximum grafting thickness of DNA with 25 mer on SAMs was reported to be about 2.2 nm,[18] which is about 2 times lower than the value obtained on PS_{690}-b-$PtBA_{1210}$ films. This grafting thickness for DNA suggests that high loading was obtained on activated polymer films.

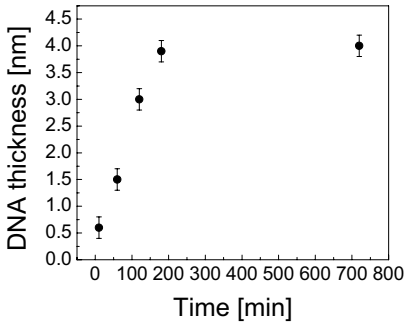

Figure 5.7. Thickness changes of the grafted DNA layer on PS_{690}-b-$PtBA_{1210}$ film. The thickness was determined by ellipsometry.

Further, the reactivity of activated PS_{690}-b-$PtBA_{1210}$ films to biomolecules was followed by fluorescence microscopy. We studied dye-labeled BSA, as well as PLL, which was subsequently labeled by reaction with Alexa Fluor®594 labeled isothiocyanate. The films obtained were then analyzed by fluorescence microscopy, as shown in Figure 5.8b. As a reference experiment, a neat PS_{690}-b-$PtBA_{1210}$ film was measured. No fluorescence emission was detected for the neat film (Figure 5.8a), while the fluorescence emission from the PLL-covered polymer film demonstrated that the PLL was successfully immobilized on the PS_{690}-b-$PtBA_{1210}$ film. BSA was coupled to activated PS_{690}-b-

$PtBA_{1210}$ films from solution and detected via the fluorescence emission of the attached dye (Figure 5.8c).

These data show that proteins and polypeptides can be successfully immobilized. The demonstration of the working principle and architecture of a biosensor for the detection of cells will be discussed in section 5.4 in this Chapter.

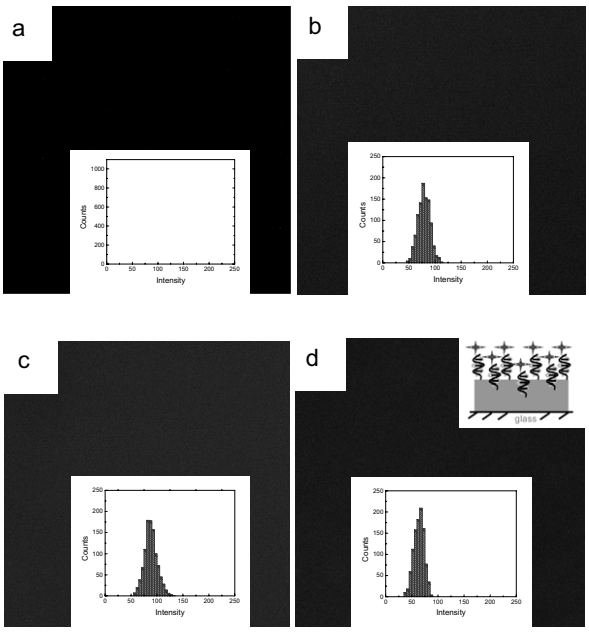

Figure 5.8. Fluorescence microscopy images and fluorescence emission histograms of (a) PS-b-PtBA film (b) PS-b-PtBA film, hydrolysis 20 min in solution, reactivation 30 min by EDC/NHS from PB solution (1 M, pH: 7.4), coupling 60 min with PLL from PB solution (0.1 mM, pH: 7.4). Finally Alexa Fluor®594 labeled isothiocyanate was applied on the surface for labeling. (c) PS-b-PtBA film, hydrolysis 20 min in solution, reactivation 60 min by EDC/NHS from PB solution (1 M, pH: 7.4), coupling 60 min with BSA from PB solution (0.1 mM, pH: 7.4). (d) PS-b-PtBA film, hydrolysis 20 min in solution, reactivation 30 min by EDC/NHS from PB solution (1 M, pH: 7.4), coupling 60 min with probe DNA from PB solution (100 nM, pH: 7.4), hybridization 60 min with complementary DNA from PB solution (100 nM, pH: 7.4). All image sizes were 146×146 μm^2.

Finally, the hybridization of target DNA was investigated using fluorescence microscopy. The corresponding micrographs are shown in Figure 5.8d. Similar to immobilization of proteins on PS_{690}-b-$PtBA_{1210}$ films, amino group-functionalized probe DNA with 25 mer was first immobilized on the NHS ester activated PS_{690}-b-$PtBA_{1210}$ films from solution. Then the dye labeled complementary target DNA reacted with polymer films modified with covalently attached probe DNA in solution. Strong fluorescence emission was detected, as shown in Figure 5.8d. The observed fluorescence emission

demonstrates that the probe DNA is accessible to solution-borne complementary target DNA, hence activated PS_{690}-b-$PtBA_{1210}$ films can be used in principle as a platform to detect the DNA as PNHSMA system described in Chapter 4. As reference experiment, the total mismatch target DNA was also tested and no fluorescence emission could be detected (data is not shown here).

The successful immobilization of biomolecules on PS_{690}-b-$PtBA_{1210}$ films suggests that this polymer system may be very useful in applications where tailored biointerfaces are required. This platform may be of use to prepare robust biosensors, to control, for example, the interaction between cells and substrates, or to facilitate the fabrication of rapid, high-throughput genetic analysis screening biosensors, for example DNA assays.

5.4 Cell Adhesion Studies on PS_{690}-b-$PtBA_{1210}$ Films

To demonstrate that PS_{690}-b-$PtBA_{1210}$ films can be used as biointerface to address important aspects of cell membrane organization, the interaction of K562 cells[19] with PLL and PEG_{500}-NH_2 immobilized on polymer films was investigated in collaboration with Prof. M. García-Parajó (Applied Optics Group, University of Twente) by wide field optical microscopy. Figure 5.9a shows the surface coverage of K562 cells on different kinds of films after applying different surface chemistry. PLL-covered surfaces were studied first. After the film was incubated in the cell solution, cells were imaged by wide field optical microscopy (Figure 5.9b). Cell surface coverages on PLL functionalized films are very high and cells can be found almost everywhere. Cell - surface interaction with the neat PS_{690}-b-$PtBA_{1210}$ films was also studied. For both cases, it was found that cell morphology was not affected by the presence of the PS_{690}-b-$PtBA_{1210}$ substrate.

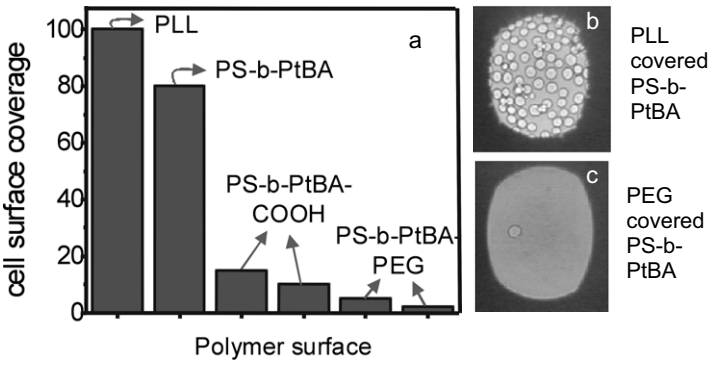

Figure 5.9. (a) Histogram of cell surface coverage vs polymer surface with different composition is obtained from wide field optical microscope images. (b) Wide field optical micrograph of PLL covered PS_{690}-b-$PtBA_{1210}$ films (scale: 150 μm × 150 μm). (c) Wide field optical micrograph of PEG_{500}-NH_2 covered PS_{690}-b-$PtBA_{1210}$ film (scale: 150 μm × 150 μm).

To prevent K562 cell adhesion via non-specific interactions, hydrolyzed PS_{690}-b-$PtBA_{1210}$ films and PEG_{500}-NH_2 functionalized PS_{690}-b-$PtBA_{1210}$ films were incubated in the cell solution. For both cases, cell surface coverage has decreased largely. Especially, the cell surface coverage was found to decrease very much and only very few isolated cells were found on the PEG_{500}-NH_2 functionalized surface as seen in Figure 5.9c. The result demonstrates that PEG_{500}-NH_2 functionalized surfaces can be used as antifouling layer for preventing the cell interaction with the substrate.

Subsequently, the interactions of pancreatic cancer cells with PEG functionalized PS_{690}-b-$PtBA_{1210}$ films were investigated in collaboration with Dr. J. Schnekenburger from the University of Münster in Germany. In the attempt to optimize the blocking ability of PEG layers to prevent adhesion of the pancreatic cancer cells, two different types of PEG molecules with different weight average molar mass M_n were used, that is, PEG_{500}-NH_2 and PEG_{5000}-NH_2. The rational behind this experiment is that it is known that the chain length and grafting density of PEG molecules exert a large influence on the antifouling properties.[20] The maximum grafting thickness of PEG on PS_{690}-b-$PtBA_{1210}$ was studied by ellipsometry after covalent coupling on NHS activated polymer films, as shown in Figure 5.10. To achieve maximum grafting thickness, 6 hours reaction time was needed. A maximum grafting thickness of PEG_{5000}-NH_2 layers of 4 nm was obtained, which is about two times larger than the maximum grafting thickness of PEG_{500}-NH_2 layers. This difference can be expected to result in different efficiencies as blocking layer for non-specific adsorption.

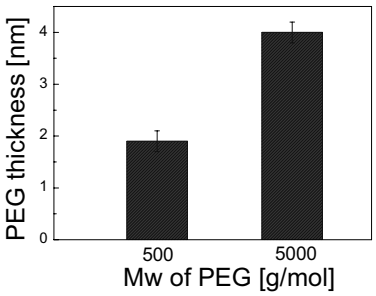

Figure 5.10: Ellipsometric thickness PEG-NH_2 on PS_{690}-b-$PtBA_{1210}$ polymer surface for PEG_{500}-NH_2 and PEG_{5000}-NH_2. PS_{690}-b-$PtBA_{1210}$ films were hydrolyzed in CF_3COOH for 20 min, activated for 30 min by EDC/NHS in PB solution (1 M, pH: 7.4), followed by coupling of PEG from PB solution for 6 hrs (pH: 7.4).

Pancreatic cancer cells were first applied to PLL covered PS_{690}-b-$PtBA_{1210}$ films. The wide field optical microscopy image shown in Figure 5.11a gives evidence that the cancer cells not only can adhere, but also stretched on the film.

For preventing the adhesion of pancreatic cancer cells, the interaction of pancreatic cancer cells on PEG_{500}-NH_2 covered surface was studied (Figure 5.11b). It is found that although some pancreatic cells still adhere to the substrate THEY DO NOT STRETCH and eventually die on the PEG_{500}-NH_2

covered surface, as can be judged from their round shape. If PS_{690}-b-$PtBA_{1210}$ films were modified with PEG_{5000}-NH_2 (4 nm thickness), only isolated round cancer cells were observed, as shown in Figure 5.11c. Under these conditions cells adhered in areas that appeared to exhibit defects in the form of cracks.

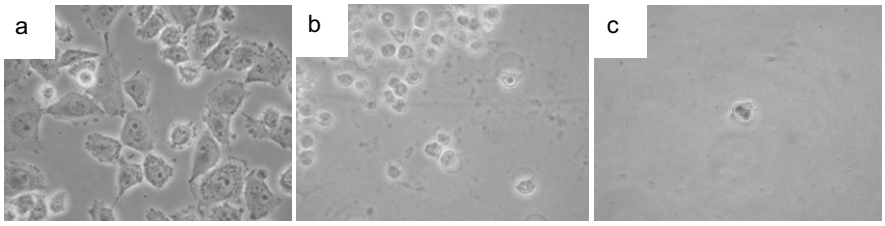

Figure 5.11 Optical microscopy images of cancer cells on (a) PLL covered; (b) PEG_{500}-NH_2 covered (layer thickness = 1.8 nm); (c) PEG_{5000}-NH_2 covered PS-b-PtBA films (layer thickness = 4.0 nm).

Hence, in agreement with the literature, PEG with high M_w was found to be much more efficient for blocking the surface compared to low M_w PEG molecules. These results also show that the PtBA-b-PS films are a promising platform to study the cell-substrate interaction for biological applications in the future.

In summary, spin-coated ultrathin PS_{690}-b-$PtBA_{1210}$ films can be hydrolyzed under different conditions. Following a standard activation with NHS ester groups, a variety of (bio)molecules can be covalently immobilized. The function of antifouling layers based on grafted PEG, DNA hybridization, as well as protein immobilization were demonstrated. Using this polymer as a platform to engineer designed biointerfaces provides, also in conjunction with the patterning approaches introduced in the later Chapters 6, 7, and 8, new possibilities for fundamental biological research involving cell biology (as shown by the studies on cell-surface interactions). In addition, PS_{690}-b-$PtBA_{1210}$ films and related systems may comprise attractive platforms for the preparation of high throughput screening arrays and (bio)affinity assays.

5.5 Experimental Section

Materials: The PS_{690}-b-$PtBA_{1210}$ diblock copolymers were purchased from Polymer Source Company (Dorval, Canada) and were used as received. Amino functionalized-labeled PEG (denoted as PEG-NH_2) was purchased from Nektar UK Company (M_n = 500 or 5000 g/mol, PDI = 1.1). Fluoresceinamine was acquired from Molecular Probes, Inc. The Netherlands; for the DNA samples, see Chapter 4. Alexa Fluor®594 labeled isothiocyanate and bovine serum albumin (BSA) with Alexa Fluor®594 conjugate were bought from Molecular Probes and used as received. Poly(L)lysine was bought from Sigma and stored at –20°C.

K 562 cell adhesion experiments were performed by Dr. M. F. Garcia-Parajo and Ir. A. Bouma (Applied Optics Group, MESA+, University of Twente). Cancer cell adhesion experiments were carried out in the lab of Dr. I. Bredebusch and Dr. J. Schnekenburger (Gastroenterologische

Molekulare Zellbiologie; Medizinische Klinik und Poliklinik B; Westfälische Wilhelms-Universität, Münster, Germany).

Film preparation: Polymer films were prepared by spin coating polymer solutions in toluene (conc. 10mg/ml) onto oxygen plasma cleaned silicon wafers. The samples were spun at 3000 rpm for 30 s using a P6700 spin coater (Specialty Coating Systems Inc). All spin-coated samples were annealed at 135°C for 24 hours in vacuum before analysis. Mean film thickness were determined by a custom-built spectroscopic ellipsometer using a He-Ne (λ = 632.8 nm) laser. The refractive index of the polymer film was approximated as 1.48.

Hydrolysis: In solution: The polymer films were hydrolyzed in neat trifuoroacetic acid for 20 min. For gas phase hydrolysis, the samples were exposed to acid vapors of 6M HCl by placing them 10 millimeters above the liquid surface in a closed beaker. All experiments were performed at room temperature. At specified time intervals, samples were removed from the beaker. All hydrolyzed films were rinsed three times using Milli-Q water, and finally dried in a stream of nitrogen.

Activation of Hydrolyzed Polymer Films. The COOH groups on polymer films after hydrolysis were activated by immersion in an aqueous solution of 1-ethyl-3-(dimethylamino)-propylcarbodiimide (EDC, 1 M) and N-hydroxysuccinimide (NHS, 0.2 M) for 30 min. The samples were then rinsed with Milli-Q water, dried in a stream of nitrogen, and used immediately thereafter.

Immobilization of (Bio)Molecules on Polymer Films. For PEG coupling from solution, the polymer films were immersed into the corresponding PEG-NH_2 solution (100 μM PEG solution, PB, pH = 7.4). After a reaction time between 5 min to 10 h, the samples were taken out of the corresponding solution and thoroughly rinsed with Milli-Q water. BSA and PLL were immersed into the corresponding solution (100 μM, PB, pH = 7.4). DNA immobilization (100nM) in phosphate buffer was carried out the same procedure as for PEG coupling. Afterwards, the hybridization of target DNA with dye (100 nM) was followed in phosphate buffer. Then the films were rinsed with PB (pH = 7.4) and Milli-Q water, and dried in a nitrogen stream. All experiments were carried out at T = 25 ± 2º.

X-ray Photoelectron Spectroscopy (XPS). XPS spectra were recorded on a PHI Quantum 2000 Scanning ESCA microprobe using a monochromated X-ray beam (Al-anode); 100 μm diameter / 25 Watt X-ray beam scanned over 700 μm × 300 μm area take-off angle of 45º. Atomic concentrations were determined by numerical integration of the relative peak areas using the Multipak software with supplied sensitivity factors (C1s: 0.314; O1s: 0.733; N1s: 0.499).[21]

AFM Experiment: The AFM measurements were carried out with a NanoScope Ш multimode AFM (Digital Instruments, Santa Barbara, CA) using a 10 μm scanner. Tapping mode AFM scans were performed with silicon cantilevers/tips (Nanosensors, Wetzlar, Germany) in air. The instrument was operated at frequencies slightly lower than the natural resonance frequency of the cantilever in air, the free amplitude was kept constant. The amplitude-damping (setpoint) ratio was adjusted to ≈0.9.

Contact Angles Measurement: The contact angles were measured on a contact angle microscope (Data Physis, OCA 15Plus) with Millipore water as the probe liquid. Advancing and receding contact angles were measured at room temperature.

Infrared Spectroscopy: The FTIR spectra were obtained using a BIO-RAD model FTS575C FTIR spectrometer equipped with a liquid nitrogen-cooled cryogenic mercury cadmium telluride (MCT)

detector. Spectral resolution was maintained at 4 cm^{-1} with 1024 scans. Transmission mode FTIR spectra were used for the ultrathin polymer films on silicon wafers.

Fluorescence Experiment. Fluorescence micrographs were taken using a Zeiss LSM 510 confocal fluorescence microscope with a LP 650 filter for isothiocyanates, Cy5-labeled target DNA, and BSA conjugated with Alexa Fluor® 594 with a 633 nm HeNe laser. For excitation an Ar laser (30 mW) was used. A 650 nm longpass filter was selected for isothiocyanates, Cy5-labeled target DNA, and BSA conjugated with Alexa Fluor® 594, respectively.

5.6 References

1 Cheng, X.; Wang, Y.; Hanein, Y.; Bohringer, K. F.; Ratner, B. D. *J. Biomed. Mater. Res*. **2004**, *70A*, 159.

2 Kasemo, B. *Surf. Sci*. **2002**, *500*, 656.

3 Biran, I.; Walt, D. R. *Anal. Chem*. **2002**, *74*, 3046.

4 HOcvirk, GH.; HSalimi-Moosavi, HH; HSzarka, R. JH.; HArriaga, E. AH.; HAndersson, P. EH.; HSmith, RH.; HDovichi, N. JH.; HHarrison, D. JH. *Proceedings of the IEEE* **2004**, *92*, 115.

5 (a) HHChen, C. S.; HMrksich, MH.; HHuang, SH.; HWhitesides, G. MH.; HIngber, D. EH. *Science* **1997**, *276*, 1425. (b) Kemkemer, R.; HCsete, MH.; HSchrank, SH.; HKaufmann, DH.; HSpatz, JH. *Mater. Sci. Engin. C*. **2003**, *23*, 437.

6 (a) Ferretti, S.; Paynter, S.; Russell, D. A.; Sapsford, K. E.; Richardson, D. J. *TrAC* **2000**, *19*, 530. (b) Mrksich, M. *Chem. Soc. Rev*. **2000**, *29*, 267. (c) Ostuni, E.; Yan, L.; Whitesides, G. M. *Coll. Surf. B*. **1999**, *15*, 3. (d) Patel, N.; Davies, M. C.; Hartshorne, M.; Heaton, R. J.; Roberts, C. J.; Tendler, S. J. B.; Williams, P. M. *Langmuir* **1997**, *13*, 6485.

7 Feng, C. L.; Zhang, Z.; Förch, R.; Knoll, W.; Vancso, G. J.; Schönherr, H. *Biomacromolecules* **2005**, in press.

8 Gong P.; Grainger, D. W. *Surface Science* **2004**, *570*, 67.

9 Bellamy, L. J. *The Infrared Spectra of Complex Molecules*; Wiley: New York, **1975**.

10 Schönherr, H.; Vancso, G. J. *J. Polym. Sci. B, Polym. Phys*. **1998**, *36,* 2483.

11 Bates, F. S.; Fredrickson, G. H. *Annu. Rev. Phys. Chem*. **1990**, *41*, 525.

12 An increase in exposed surface area of 15% was estimated based on the analysis of the AFM height images.

13 The grafting density σPEG can be calculated as:

$$\sigma PEG \approx 10\ \%\ dXPS\ \rho PtBA\ NA\ M\text{-}1$$

where dXPS is information depth of the XPS experiment, ρPtBA is the density of PtBA (~ 1 g/cm3), NA (6.022 × 1023 mol-1) is Avogadro's number, and M is the molar mass (183 g/mol) of monomeric PtBA.

14 Tanaka, K.; Takahara, A.; Kajiyama, T. *Macromolecules* **1996**, *29*, 3232.

15 Harris, J. M. *Introduction to Biotechnical and Biomedical Applications of Poly(ethylene glycol)*. Plenum Press: New York, **1992**, p1.

16 Groll, J.; Ameringer, T.; Spatz, J.; Möller, M. *Langmuir* **2005**, *21*, 1991.

17 A PS_{690}-b-$PtBA_{1210}$ film was first hydrolyzed by trifluoroacetic acid for 15 min and subsequently activated with NHS ester groups for about 30 min.

18 Aqua, T.; Naaman, R.; Daube, S. S. *Langmuir* **2003**, *19*, 10573.

19 K562 cells are probably the most widely used experimental model of chronic phase of chronic myelogenous leukemia (CML) (Kuželová, K.; Grebeńová, D.; Marinov, I.; Hrkal, Z. *J. Cellular Biochem*. **2005**, *95*, 268).

20 Deible, C. R.; Petrosko, P.; Johnson, P. C.; Beckman, E. J.; Russell, A. J.; Wagner, W. R. *Biomaterials* **1998**, *19*, 1885.

21 Reilman, R. F.; Msezane, A.; Manson, S. T. *J. Electron Spectroscopy* **1976**, *8*, 389.

Chapter 6

Fabrication of Robust Biomolecular Patterns by Reactive Microcontact Printing on NHS Ester Containing Polymer Films*

In this Chapter, the fabrication of robust biomolecule microarrays by reactive microcontact printing (μCP) on spin-coated thin films of poly(N-hydroxysuccinimidyl methacrylate) (PNHSMA) on oxidized silicon and glass is described. The approach combines the advantages of activated polymer thin films as coupling layers, characterized by high reactivity and high molecular loading (see Chapter 3 and 4), with the versatility and flexibility of soft lithography. The transfer of amino end functionalized poly(ethylene glycol) (PEG_{500}-NH_2) from oxidized poly(dimethyl siloxane) (PDMS) elastomer stamps to PNHSMA films was shown by FTIR spectroscopy, X-ray photoelectron spectroscopy (XPS), fluorescence microscopy and ellipsometry measurements to result in covalent coupling and identical grafting densities as reported in Chapter 4 for coupling from solution. The PEG-protected areas effectively inhibited the adsorption of fluoresceinamine, bovine serum albumin (BSA), as well as 25-mer DNA, while the unreacted NHS ester groups retained their reactivity towards primary amino groups. Biomolecule microarrays were thus conveniently fabricated in a 2-step procedure. The hybridization of target DNA to immobilized probe DNA in micropatterns proved the concept of reactive μCP on activated polymer films for obtaining robust platforms for biomolecule immobilization and screening.

6.1 Introduction

Controlling the selective immobilization of (bio)molecules in defined positions of a surface is very important for the development of biosensors and high-throughput biomolecule screening assays.[1] In the development of rapid, robust screening microarrays several strategies have been successfully applied. These comprise, among others, robot-based high-precision contact-printing,[2] multistep photolithography,[3] selective molecular assembly patterning,[4] and soft lithographic approaches, such as the microcontact printing (μCP) method.[5] As discussed in Chapter 2, the μCP technique developed by Whitesides et al.[6] is widely used for the fabrication of monolayer-based micrometer and sub-micrometer scale patterns. In applications, such as the development of certain biosensors,[7] the simplicity of the method, as well as the low cost, the flexibility, and the possibility to pattern curved substrates make μCP very attractive.

Using μCP one can transfer a variety of molecules with sub-micrometer resolution to reactive substrates without the need for dust-free environments or harsh chemical treatments.[8] Molecules can be patterned normally through physical interaction (including electrostatic and hydrophobic interactions),[9] or covalently coupling[10] with the substrate. However, the coverage or activity

* Part of the work described in this chapter has been published in: Schönherr H.; Feng C. L.; Shovsky A.; Degenhart G.; Dordi B.; Zhang Z.; Förch R.; Knoll W.; Vancso G. J. *PMSE Prepr*. **2004**, *90*, 689-690. Feng, C. L.; Vancso, G. J.; Schönherr, H. *Adv. Funct. Mater.* **2006**, *in press*.

quantitation of molecules immobilized in patterns through mere physical interactions are often difficult to achieve because the molecules can be washed away during the processing conditions.[11] Covalent linkages, on the other hand, are thought to provide more specific and stronger attachment.[12,13] In general, covalent attachment utilizes bifunctional linker chemistry that involves, e.g, amide or imine bond formation, gold-thiol interactions, or silane chemistry.[14] These approaches afford efficient and secure immobilization of (bio)molecules on suitable substrates.

Although μCP is a simple and flexible method for covalent coupling of biomolecules onto monolayers,[15] these reactions require highly activated species, because no or little solvent is involved in this procedure.[16] Recently, it has been shown that the methodology can be extended to perform local chemical reactions, including catalytic reactions,[17] coupling and protection/deprotection reactions.[13,18]

For the mentioned screening-type applications, polymeric thin films have been shown to possess a number of important advantages compared to SAM-based systems. These advantages comprise robustness and stability, high molecular loading, high reactivity, and the inherent possibility to introduce simultaneously chemical (compositional), as well as topographical patterns and structures. Hence it is not surprising that patterned thin films of polymers have a wide range of applications, for example, as etch resists,[19] in biological[20] and chemical sensors,[21] and in tissue engineering.[22] Thin films of patterned polymers that incorporate reactive functional groups provide a surface that can be further modified by chemical reactions.[23] To increase the molecular loading, hydrogels,[24,25] dendrimers,[11,26,27,13] hyperbranched polymers,[28] chemical vapor deposition approaches,[29] self-assembled polyelectrolyte mutilayers,[30] plasma polymers,[31] and polymer brushes obtained by grafting-from approaches[32] have been investigated.

We have introduced reactive homopolymer ultrathin films based on poly(*N*-succinimidyl methacrylate) (PNHSMA) as platforms for biomolecule immobilization with high molecular loading (see Chapter 4). These and related polymer systems (Chapter 5) possess several advantages compared with other polymer films and in particular compared with monolayers. Firstly, a large fraction of activated ester side groups of PNHSMA are exposed, which are very reactive towards nucleophiles.[33] Secondly, the coupling reactions are not limited to the very surface of the films. Thus, these films are appropriate to anchor a large variety of molecules, including amino-terminated DNA, proteins and synthetic polymers, in high coverages (reactive quasi-3D film structure) (see Chapter 4). Thirdly, ultrathin films of PNHSMA can be easily prepared by spin-coating and the film thickness is tunable. This may help to contribute to solve the problem of fluorescence quenching due to energy transfer to the underlying metal substrate in optical detection schemes, such as fluorescence enhanced SPR.[34] Finally, the very good stability of PNHSMA compared with other functionalized polymers (e.g. poly(ethylene imine) is water soluble[13]) can expand the application of the polymer in preparing new platforms.

In this chapter, the PNHSMA-based platforms are expanded to patterned biomolecular films. These patterned platforms can be conveniently fabricated using a simple 2-step procedure exploiting

reactive microcontact printing followed by wet chemical derivatization. The robustness of the PHNSMA platform, the quasi-3D loading and the versatility of reactive microcontact printing together with predictable coupling of biomolecules from buffered solution render this approach attractive for the fabrication of bioreactive screening platforms.[35]

6.2 Approaches for Micro-Patterning of PNHSMA Films

For the fabrication of bioreactive micropatterns using reactive polymer thin films, a simple, yet robust procedure was developed. Surface patterns were obtained by reactive microcontact printing of PEG_{500}-NH_2 on spin-coated films of PNHSMA on oxidized silicon, followed by backfilling with the corresponding amino-functionalized compounds in solution. This coupling reaction leads to a robust, irreversible immobilization via the formation of covalent amide bonds.

The approach is depicted schematically in Scheme 6.1. Essential for the successful realization of the approach is the controlled covalent coupling of a densely grafted layer of PEG, a sufficiently effective function of this blocking layer, the retention of reactivity of NHS esters in the unreacted areas, as well as the absence of restructuring / reorientations of the polymer - solution interface.

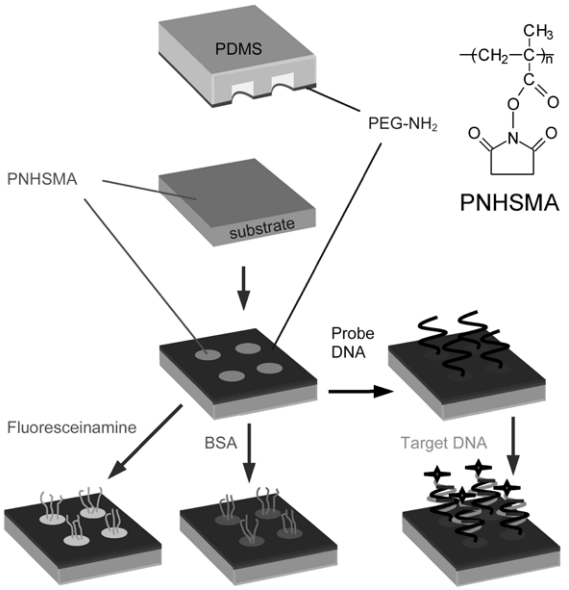

Scheme 6.1. Scheme of the patterning of PNHSMA by reactive µCP of PEG_{500}-NH_2 and area-selective immobilization of molecules from solution to the remaining reactive areas of the PNHSMA film. The layer of PEG serves as a blocking layer and prevents non-specific adsorption (NSA) of fluoresceinamine, BSA or probe DNA. Finally, the hybridization of dye-labeled target DNA the surface presenting complementary probe DNA was investigated.

6.3 Functionalization of PNHSMA Films by Reactive µCP

Using a featureless PDMS stamp PEG_{500}-NH_2 was transferred and coupled covalently to NHS ester groups exposed at the surface of PNHSMA films. In FTIR spectra several bands attributed to the

grafted PEG were observed after the grafting reaction (Figure 6.1a). Among these are the band at 1107 cm^{-1}, assigned to the C-O-C vibration, as well as the bands at 1262 cm^{-1} and 1460 cm^{-1} attributed to the EG CH_2 twist vibration, and the EG CH_2 scissor vibration, respectively.[32,36] More importantly, two new bands at 1645 cm^{-1} (amide I) and 1543 cm^{-1} (amide II) were observed after the coupling reaction with PEG_{500}-NH_2. This observation demonstrates that the PEG molecules have been *covalently* grafted to the PNHSMA film by amide linkage formation.[37]

A maximum thickness of the grafted PEG_{500} layer of ~ 1.8 nm was observed by ellipsometry on PNHSMA films (Figure 6.1b), which is to within the error identical to the value observed for PEG_{500} coupled from solution.[25] This surface coverage (~ 2.7 PEG molecules per nm^2) is ~ 3 times higher than the maximum grafting density of PEG molecules on SAMs (~ 0.87 nm^{-2}).[25] The data suggest that reactive μCP leads to identical coverages as the solution phase reaction, thus the quasi-3D loading capability is restored also under these solvent-free conditions.

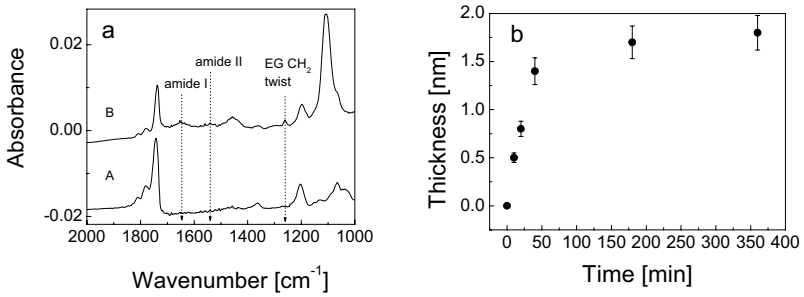

Figure 6.1. (a) FTIR spectra of PNHSMA (A) before and (B) after grafting of PEG_{500}-NH_2 using a featureless stamp. (b) Grafted thickness of PEG vs stamp - film contact time (during reactive μCP) measured by ellipsometry.

Very similar to the coupling of PEG_{500}-NH_2 from solution, the coupling kinetics (estimated in an analysis of the integrated absorbance under the band attributed to the EG CH_2 twist vibration) are consistent with an exponential (pseudo-first order) reaction kinetics (see Chapter 4). An apparent rate constant of $k'_{app} = 4.1 \times 10^{-4} \pm 4.9 \times 10^{-5}$ s^{-1} was determined based on the data shown in Figure 6.1b. This rate is comparable to the rate of the solution phase coupling reaction using a concentration of 0.1 mM of PEG_{500}-NH_2.[25]

Thus, in addition to the successful covalent coupling and increased molecular loading compared to SAM-based platforms, the coverage of grafted PEG on PNHSMA films appears to be controllable by changing the μCP contact time.

To further investigate the loading of the PNHSMA films, when long stamp-film contact times are used, XPS experiments were performed (take-off angle of 45º). Figure 6.2 shows the elements scans of a PNHSMA film and PEG_{500}-NH_2-grafted PNHSMA film, respectively. The O_{1s}, N_{1s}, and C_{1s} peaks

were observed at 532.2 eV, 401.5 eV and 284.0 eV (neutral carbons) and at 287.8 eV (carbonyl carbon), respectively.

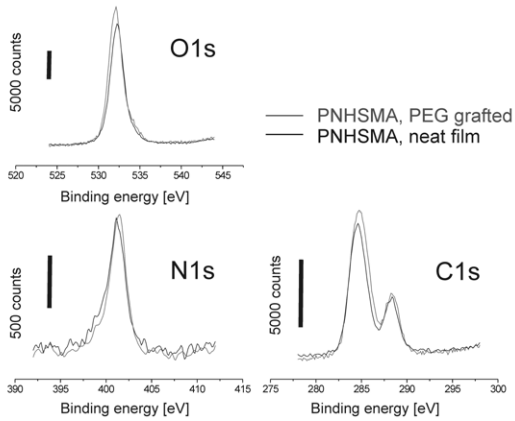

Figure 6.2. XPS element scans of neat PNHSMA film on oxidized silicon and PNHSMA film after grafting with PEG_{500}-NH_2 by reactive μCP.

The area of the nitrogen peak was observed to be constant for both samples, as expected, while the areas of the oxygen and the carbon peaks both increased after coupling of PEG_{500}-NH_2 on the PNHSMA films. The *C/N* ratios were calculated from the peak areas as shown in Table 6.1. Using a simple calculation, it is found that the surface composition in the sampled depth corresponds to PNHSMA in which ~ 11% of all NHS ester groups have been reacted with PEG_{500}-NH_2. A formal grafting density of PEG of ~ 2.8 PEG molecules per nm^2 was thus estimated.[38] This value is in excellent agreement with the ellipsometry data discussed above and confirms that PNHSMA films are loaded very efficiently with PEG by reactive μCP. Similar to the coupling reaction in solution, the coupling reactions during reactive μCP are very likely not limited to the very surface of the polymer films, but proceed into the surface-near regions of the films.

Table 6.1. XPS data of PNHSMA films before and after grafting of PEG_{500}-NH_2.

Sample	Theoretical *C/N* ratio	Experimental *C/N* ratio (μCP)
PNHSMA film	8	8.0 ± 0.4
PNHSMA fully PEG-covered	22	9.8 ± 1.0

6.4 Non-Specific Adsorption (NSA)

It is established that the PEG grafting density, in addition to the molar mass, is an important factor for the inhibition of NSA of various types of biomolecules.[39] As shown above, the grafting density of PEG_{500}-NH_2 on PNHSMA films can be conveniently controlled by changing the reaction (stamp-film contact) time. The effectiveness of the blocking the polymer layer against covalent coupling (and / or NSA) of solution-borne nucleophiles was consequently tested as a function of PEG_{500}-NH_2 grafting

thickness with fluoresceinamine and with dye-labeled BSA by fluorescence microscopy. Figure 6.3 shows the decrease of the fluorescence emission intensity of fluoresceinamine and BSA, respectively, on PNHSMA films for different PEG_{500}-NH_2 grafting thicknesses. Without any PEG coating, strong fluorescence emission was observed in both cases indicating a significant coverage of the corresponding fluorescent adsorbate. Increasing reaction times in the reactive μCP step using a featureless stamp (i.e. increasing thickness of the grafted PEG_{500}-NH_2 layers) were found to lead to a significant reduction of adsorbate coverage. For the maximum PEG_{500}-NH_2 grafting thickness of 1.8 nm, the ratio of the observed fluorescence emission intensity vs. the background fluorescence of neat PNHSMA was found to be only 1.5. Hence it can be concluded at this point that the grafted PEG layers with 1.8 nm thickness inhibit the immobilization of fluoresceinamine and BSA effectively.

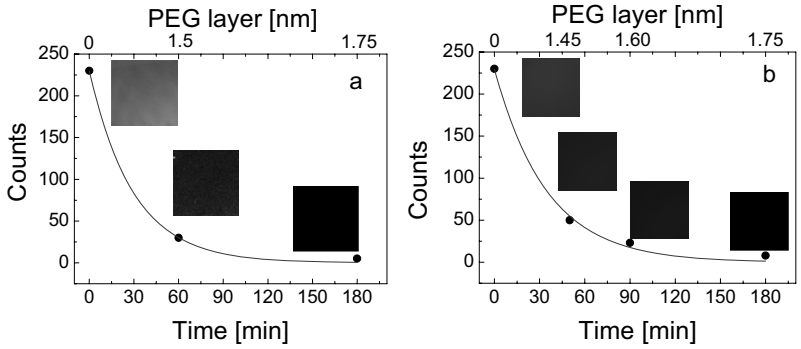

Figure 6.3. Plots of integrated fluorescence emission intensity (the PEG thickness was determined by ellipsometry for each coupling time) of PEG-functionalized PNHSMA films treated with (a) fluoresceinamine; (b) BSA for 30 min followed by rinsing with PB buffer (pH 7.4) and drying vs reaction (stamp-film contact) time / PEG thickness. The insets show representative fluorescence microscopy images acquired for the corresponding samples (image size: 145 × 145 μm^2).

6.5 Patterning of PNHSMA and Coupling of (Bio)molecules to Patterned Films

The PEG layers described above can be used as blocking layer to guide the immobilization (via covalent coupling) of other active molecules to the unpassivated areas on patterned PNHSMA surface (prepared according to Scheme 6.1). To test the retention of reactivity of NHS esters in the unreacted areas of the patterns, PEG_{500}-NH_2 was grafted to the surface of PNHSMA films using PDMS stamps with circular depressions (diameter: 15 μm; depth 2 μm), followed by reaction with solution-borne primary amines (Scheme 6.2).

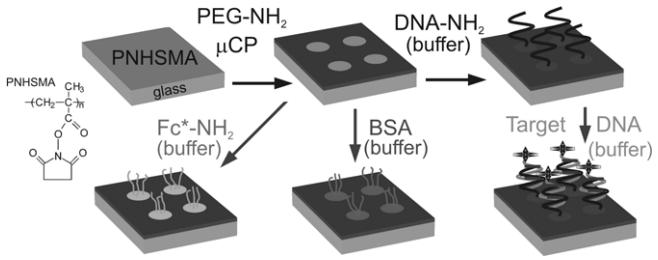

Scheme 6.2. Scheme of the patterning of PNHSMA by reactive μCP of PEG_{500}-NH_2 and area-selective immobilization of fluoresceinamine, BSA or probe DNA molecules from solution to the remaining reactive areas of the PNHSMA film. Finally, the hybridization of dye-labeled target DNA the surface presenting complementary probe DNA was investigated.

The patterned PEG-PNHSMA surfaces were analyzed by contact mode AFM. Figure 6.4a shows a corresponding height image. No obvious changes can be observed compared to the unpatterned film surface (shown to scale in the inset). By contrast, in the corresponding AFM friction image a regular pattern of locally different friction forces on the PEG-patterned PNHSMA film is clearly observed (Figure 6.4b). The inset represents the (featureless) friction image of a neat PNHSMA film. We assign the bright areas (high friction force) to the PEG-covered areas and the dark areas (low friction force) to the underivatized PNHSMA surface. The contrast is likely related to differences in surface energies,[39] as well as differences in capillary forces that reflect the different hydrophilicities of the surface functional groups.[40]

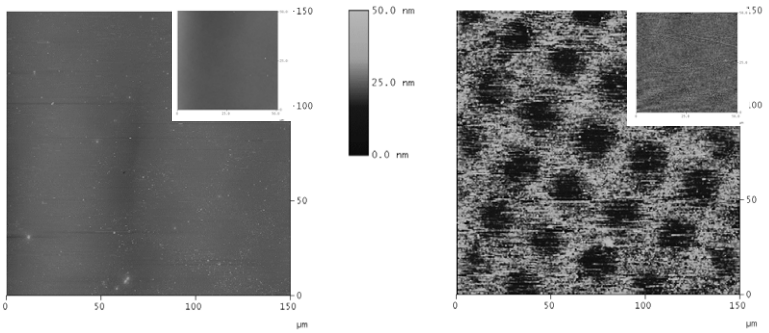

Figure 6.4. (a) Height and (b) friction mode AFM images of PNHSMA films after reactive μCP with PEG_{500}-NH_2: (inset: corresponding height and friction images of neat PNHSMA film shown to scale).

After treating the patterned sample with NH_2-end labeled 25-mer probe DNA in buffer, elevated circular areas with 15 μm diameter were observed in AFM contact mode height and friction images (Figure 6.5). Compared to the surrounding PEG matrix layer, the elevated circular areas showed a step height of ~1.2 nm. These data indicate that the attachment of probe DNA occurs selectively in the circular areas that were not reacted with PEG in the reactive μCP step.

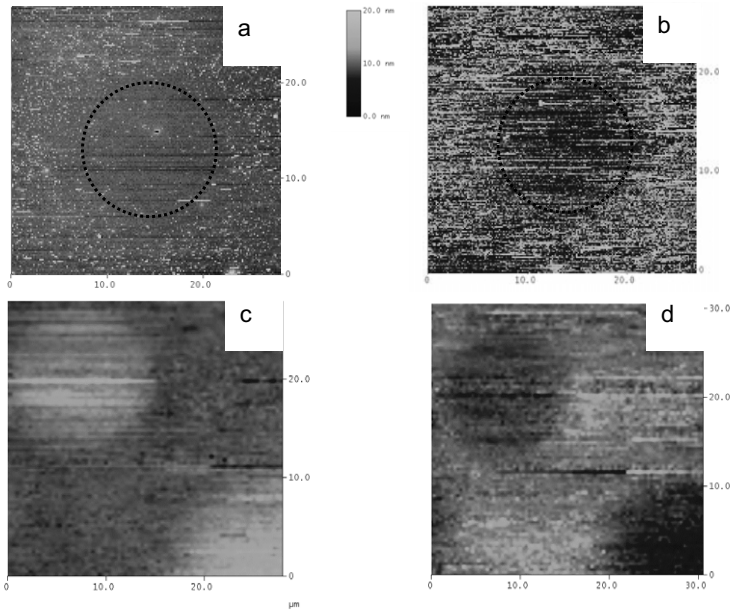

Figure 6.5. Local immobilization of probe DNA on PEG_{500} patterned films investigated by contact mode AFM: (a) Height and (b) friction image of PEG-patterned PNHSMA film; (c) Height and (d) friction image of probe DNA modified PEG-patterned PNHSMA film. The circles in panels (a) and (b) show the position of the dot.

The retention of reactivity of NHS esters in the unreacted areas of the patterns was then tested with dye-labeled adsorbates using fluorescence microscopy. As shown in Figure 6.6, the coupling of fluoresceinamine, as well as BSA, yielded well-defined patterns with very uniform spot shape and size, as well as homogeneous fluorescence intensity. The fluorescence in PEG-covered areas is negligible indicating low residual coupling or NSA.

These experiments show that the directed deposition of fluoresceinamine and BSA on PEG patterned PNHSMA film with high PEG coverage is possible. The reactivity of NHS esters in the previously unreacted areas is retained and the fluorescently labeled molecules are coupled through the formation of robust covalent bonds to form the observed regular fluorescence emission pattern. The coverage of the immobilized molecules is similar compared to the results reported in Chapter 4 for coupling from solution on neat PNHSMA films. It demonstrates that the retention of NHS esters can be achieved after PEG transfer by reactive µCP. Thus, biomolecule micropatterns can be prepared by the combination of reactive µCP of PEG_{500}-NH_2 on PNHSMA followed by covalent coupling of amino functionalized biomolecules from solution.

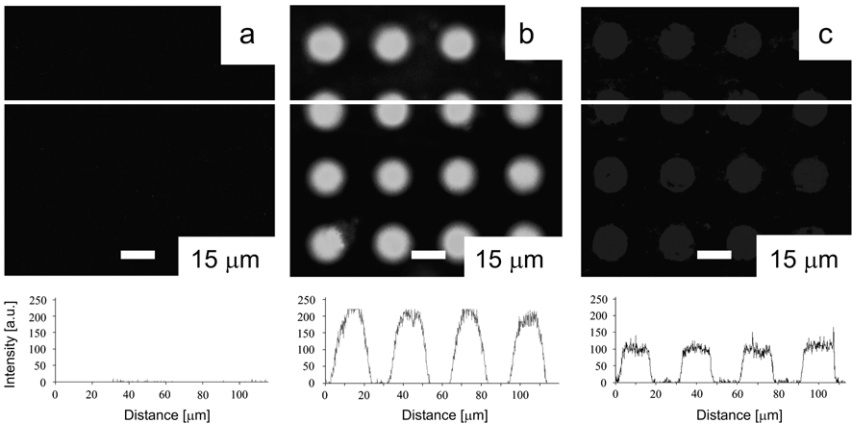

Figure 6.6. Fluorescence microscopy images (top) and corresponding cross sectional intensity plots (bottom) (125 × 125μm^2) of (a) PNHSMA film with patterned PEG layer (thickness ~ 1.8 nm), (b) patterned PEG layer following coupling of fluoresceinamine, and (c) patterned PEG layer following BSA coupling.

6.6 DNA Hybridization

For the demonstration of the applicability of the approach described to screening assays, the hydridization of target DNA to immobilized probe DNA patterns (see above) was investigated. Amino end-labeled 25-mer probe DNA was covalently coupled to PEG patterned PNHSMA, followed by a treatment with dye-labeled complete mismatch target DNA or matching target DNA, respectively. Following careful rinsing with PB buffer (pH: 7.4), the samples were investigated by fluorescence microscopy (Figure 6.7). While no fluorescence was observed for the probe DNA - mismatch target DNA combination, the matching DNA strands yielded a well defined pattern in the microscopy images. Hence the dye-labeled complete mismatch DNA was completely rinsed off from the patterned film, while the matching strand of target DNA hybridized with probe DNA in the corresponding areas.

The homogeneity of the patterned spots in terms of shape and size is adequate, while the fluorescence emission is not entirely homogeneous. This may be related to local heterogeneities in hybridization efficiency. The immobilization and hybridization of DNA on PNHSMA films has been previously studied in detail by using of surface plasmon resonance (SPR), surface plasmon resonance enhanced fluorescence spectroscopy (SPFS) (see Chapter 4). As we show here, the loading of various molecules in micropatterns is sufficiently high to analyze the coverage conveniently by fluorescence microscopy approaches. The discrimination between total mismatch DNA and fully complementary target DNA was ~ 50. Comparing to glycine blocking layer for non-specific adsorption of DNA described in Chapter 4, it is efficient for preventing the non-specific adsorption of DNA using PEG as blocking layer.

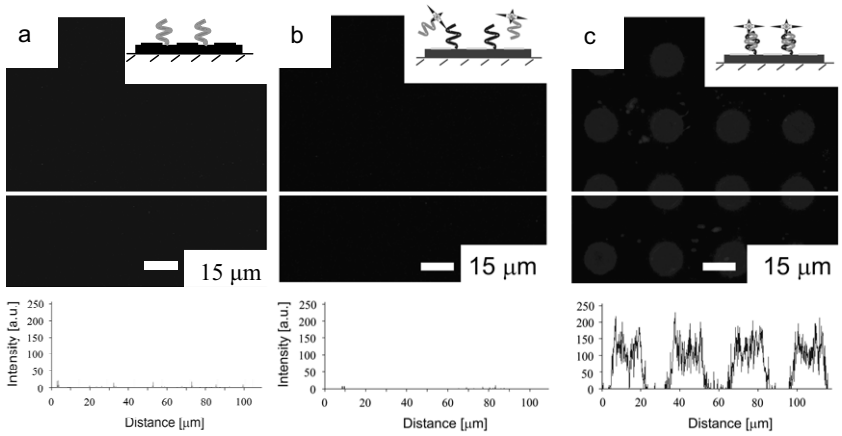

Figure 6.7. Fluorescence microscopy images (top) and corresponding cross sectional intensity plots (bottom) (125 × 125 µm²) of PEG patterned PNHSMA (a) after immobilization of probe DNA, (b) after hybridization with total mismatch target DNA and rinsing, (c) after hybridization with complementary target DNA.

One possible disadvantage of PNHSMA films is that the NHS ester functional groups are sensitive to humidity and UV light. Concomitantly the shelf life of such activated films is limited.[41] However, even previously partially hydrolyzed films can be reactivated using appropriate reactions. This reactivation has been performed successfully, as judged by FTIR spectroscopy (no data shown). Hence this methodology can be extended to activate chemically more stable protected carboxyl functionalities. Thereby the concept of using thin activated polymer films to fabricate quasi-3D bioreactive and bioactive matrices in a micropatterned format, using the reactive microcontact printing approach described above, can be further expanded (Chapter 7). Together with the flexibility of thin polymer films in topographic patterning, using embossing or micromolding techniques (see also Chapter 5), applications of these platforms not only for biosensor and microarray applications, but also for the study of cellular and sub-cellar behavior can be anticipated.[42]

In summary, the development of a novel micropatterning strategy that relies on reactive microcontact printing for the local passivation of thin substrate-supported reactive polymer films to fabricate robust biomolecule microarrays has been presented. The localized deposition and covalent coupling of amino end functionalized poly(ethylene glycol) was shown to the desired yield blocking layers, while the high reactivity and high molecular loading of poly(*N*-hydroxysuccinimidyl methacrylate) films was retained in the unfunctionalized areas. Using this methodology biomolecule microarrays can thus be conveniently fabricated in a 2-step procedure. As demonstrated by the immobilization of organic dyes, proteins and the hybridization of target DNA to immobilized probe DNA in micropatterns, the concept of reactive µCP on activated polymer films appears to be very

flexible for obtaining robust platforms for biomolecule immobilization and screening. The extension of the pathogen detection work, discussed briefly in Chapter 4, to patterned sensor formats is currently underway.

6.7 Experimental Section

Materials. The synthesis of *poly(N-hydroxysuccinimidyl methacrylate)* (PNHSMA) (M_n of 3650 g/mol; M_w/M_n of 1.3; T_g of 140ºC) is described in Chapter 3.[25] Amino end-labeled PEG (denoted as PEG_{500}-NH_2), purchased from Nektar UK Company (M_n = 500 g/mol, PDI = 1.1), fluoresceinamine (Molecular Probes Inc., The Netherlands) and the DNA samples (amino end functionalized probe DNA (5' end): 25 mer 5'- GGA ATG TGC CAT ACC GAA TCC GTG T –3'; Cy5-labeled target DNA: 5'- CAC GGA TTC GGC ATG – 3', Cy5-labeled mismatch DNA: 5'- TGT GCC TAA GCC ATA - 3', MWG BIOTEC AG, Ebersberg, Germany) were used as received. The DNA samples were stored at -4ºC until use. Bovine serum albumin (BSA) labeled with Alexa Fluor®594 was bought from Molecular Probes Inc. and was used as received.

Preparation of Thin Films. PNHSMA thin films were prepared by spin-coating solutions of PNHSMA in DMSO (typical concentration between 10 and 20 mg/ml) onto silicon wafers (111) or glass cover slides (Menzel-Glaser), which were previously cleaned by an oxygen plasma treatment using an Elektrotech PF 340 apparatus (pressure of O_2: 0.5 bar; current: 30 mA). All spin-coated samples were dried at room temperature for 24 hours in vacuum before analysis. Mean film thicknesses were determined using a custom-built spectroscopic ellipsometer using a He-Ne laser (λ = 632.8 nm). The refractive index of PEG was approximated as 1.4638,[43] while for PNHSMA 1.50 was used.[44] The film thickness was 20 - 40 nm.

Patterning of Films. Microcontact printing stamps were prepared according to literature procedures.[45] The stamps were mildly oxidized in an ozone plasma reactor for 50 min[46] and were inked by soaking them in a 200 μM solution of PEG_{500}-NH_2 in PB buffer (pH = 7.4) for 60 min. Before reactive microcontact printing, the stamps were blown dry in a stream of nitrogen. Then the PEG_{500}-NH_2 loaded stamps were applied for different time on the PNHSMA films (the stamp, surface area 1 cm^2, was loaded with a mass of 30 g). After careful removal of the stamp, the film surface was rinsed with Milli-Q water.

Coupling of fluoresceinamine. The pre-formed PEG pattern was backfilled with fluoresceinamine by immersing the patterned film inside a fluoresceinamine solution (100 μM, PB buffer: pH = 7.4) for 30 minutes. Then the samples were taken out, rinsed with PB buffer (pH = 7.4) and Milli-Q water, and dried in a stream of nitrogen. Finally, the samples were dried in vacuum for 1 day before the fluorescence experiment.

Coupling of BSA. BSA was coupled from solution (100 μM, PB buffer: pH = 7.4; 30 minutes) using the same procedure as described above for fluoresceinamine.

Coupling of DNA and hybridization. DNA immobilization was carried out in buffer (100 nM in PB buffer: pH = 7.4) on patterned PNHSMA film following the same procedure as for fluoresceinamine. Afterwards, the hybridization of dye-labeled target DNA (100 nM) was carried out in phosphate buffer as described previously.[25]

Fourier Transform Infrared (FTIR) Spectroscopy. Transmission mode FTIR spectra (spectral resolution of 4 cm^{-1}, 1024 scans) were obtained using a BIO-RAD model FTS575C FTIR spectrometer equipped with a liquid nitrogen-cooled cryogenic mercury cadmium telluride (MCT) detector. Background spectra were obtained using oxygen plasma-cleaned silicon wafers.

X-ray Photoelectron Spectroscopy (XPS). **X-ray Photoelectron Spectroscopy (XPS)**. XPS spectra were recorded on a PHI Quantum 2000 Scanning ESCA microprobe using a monochromated X-ray beam (Al-anode; 100 μm diameter / 25 Watt X-ray beam) scanned over 700 μm × 300 μm area at a fixed take-off angle of 45º. Atomic concentrations were determined by numerical integration of the relative peak areas using the Multipak software with supplied sensitivity factors (C1s: 0.314; O1s: 0.733; N1s: 0.499).[47]

Fluorescence Microscopy. Fluorescence microscopy images of dry samples on glass cover slips were recorded at room temperature on a Zeiss LSM 510 confocal laser scanning microscope using a Plan-Apochromat® 63×/1.4 NA oil-immersion objective. Fluoresceinamine was excited with the 488 nm line of an Ar^+ laser, and Cy5-labeled DNA and BSA conjugated with Alexa Fluor® 594 with a 633 nm HeNe laser. The fluorescence emission of these dyes was recorded with photomultiplier tubes (Hamamatsu R6357) after spectral filtering with a 500-550 nm bandpass filter and a 650 nm longpass filter for fluoresceinamine and Cy5-labeled DNA and BSA-Alexa Fluor® 594, respectively. Images were acquired with maximum pinhole diameters.

Atomic Force Microscopy (AFM). The contact mode AFM measurements were carried out with a NanoScope Ш multimode AFM (Digital Instruments / Veeco, Santa Barbara, CA) using a 100 μm scanner and microfabricated silicon nitride tips / cantilevers (Model NP, Veeco Nano Probe, Veeco, Santa Barbara, CA) in ambient atmosphere (ca. 30 % relative humidity, 24ºC temperature).

6.8 References

1 (a) Singhvi, R.; Kumar, A.; Lopez, G. P.; Stephanopoulos, G. N.; Wang, D. I.; Whitesides, G. M. *Science* **1994**, *264*, 696. (b) Lopez, G. P.; Biebuyck, H. A.; Harter, A. R.; Kumar, A.; Whitesides, G. M. *J. Am. Chem. Soc*. **1993**, *115*, 10774. (d) Patel, N.; Padera, R.; Sanders, G. H. W.; Cannizzaro, S. M.; Davies, M. C.; Langer, R.; Roberts, C. J.; Tendler, S. J. B.; Williams, P. M.; Shakesheff, K. M. *FASEB J*. **1998**, *12*, 1447. (e) Ostuni, E.; Kane, R.; Chen, C. S.; Ingber, D. E.; Whitesides, G. M. *Langmuir* **2000**, *16*, 7811. (f) Yousaf, M. N.; Houseman, B. T.; Mrksich, M.; *Proc. Natl. Acad. Sci. U.S.A*. **2001**, *98*, 5992.

2 MacBeath, G.; Schreiber, S. L. *Science* **2000**, *289*, 1760.

3 Brack, H. P.; Padeste, C.; Slaski, M.; Alkan, S.; Solak, H. H. *J. Am. Chem. Soc*. **2004**, *126*, 1004.

4 Lussi, J. W.; Michel, R.; Reviakine, I.; Falconnet, D.; Goessl, A.; Csucs, G.; Hubbell, J. A.; Textor, M. *Progress in Surface Science* **2004**, *76*, 55.

5 (a) Kumar, A.; Abbott, N. A.; Kim, E.; Biebuyck, H. A.; Whitesides, G. M. *Langmuir* **1995**, *28*, 219. (b) Wang, C.; Zhang, Y. *Adv. Mater*. **2005**, *17*, 150.

6 Kumar, A.; Whitesides, G. M. *Appl. Phys. Lett*. **1993**, *63*, 2002.

7 Crooks, R. M.; Ricco, A. J. *Acc. Chem. Res*. **1998**, *31*, 219.

8 (a) Xia, Y. N.; Whitesides, G. M. *Angew. Chem., Int. Ed*. **1998**, *37*, 551. (b) Quake, S. R.; Scherer, A. *Science* **2000**, *290*, 1536.

9 (a) Renault, J. P.; Bernard, A.; Juncker, D.; Michel, B.; Bosshare, H. R.; Delamarche, E. *Angew. Chem.; Int. Ed.* **2002**, *41*, 2320. (b) Bruckbauer, A.; Zhou, D. J.; Ying, L. M.; Korchev, Y. E.; Abell, C.; Klenerman, D. *J. Am. Chem. Soc*. **2003**, *125*, 9834.

10 Anzai, J.; Kobayashi, Y.; Nakamura, N.; Nishimura, M.; Hoshi, T. *Langmuir* **1999**, *15*, 221.

11 Pathak, S.; Singh, A. K.; McElhanon, J. R.; Dentinger, P. M. *Langmuir* **2004**, *20*, 6075.

12 Williams, R. A.; Blanch, H. W. *Biosens. Bioelectron*. **1994**, *9*, 159.

13 Degenhart, G. H.; Dordi, B.; Schönherr, H.; Vancso, G. J. *Langmuir* **2004**, *20*, 6216.

14 (a) Wadu-Mesthrige, K.; Amro, N. A.; Garno, J. C.; Xu, S.; Liu, G. Y. *Biophys. J*. **2001**, *80*, 1891. (b) Kenseth, J. R.; Harnisch, J. A.; Jones, V. W.; Porter, M. D. *Langmuir* **2001**, *17*, 4105. (c) Zhou, D.; Wang, X.; Birch, L.; Rayment, T.; Abell, C. *Langmuir* **2003**, *19*, 10557.

15 Lahiri, J.; Ostuni, E.; Whitesides, G. W. *Langmuir* **1999**, *15*, 2055.

16 Yang, Z.; Chilkoti, A. *Adv. Mater*. **2000**, *12*, 413.

17 Li, X. M.; Péter, M.; Huskens, J.; Reinhoudt, D. N. *Nano Lett*. **2003**, *3*, 1449.

18 Sullivan, T. P.; van Poll, M. L.; Dankers, P. Y. W.; Huck, W. T. S. *Angew, Chem., Int. Ed, Engl*. **2004**, *43*, 4190.

19 Xia, Y.; Mrksich, M.; Kim, E.; Whitesides, G. M. *J. Am. Chem. Soc*. **1995**, *117*, 9576.

20 Knoll, W.; Matsuzawa, M.; Offenhäusser, A.; Rühe, J. *Isr. J. Chem*. **1996**, *36*, 357.

21 Wells, M.; Crooks, R. M. *J. Am. Chem. Soc*. **1996**, *118*, 3988.

22 Langer, R.; Vacanti, J. P. *Science* **1993**, *260*, 920.

23 (a) Bruening, M. L.; Zhou, Y.; Aguilar, G.; Agee, R.; Bergbreiter, D. E.; Crooks, R. M. *Langmuir* **1997**, *13*, 770. (b) Chance, J. J.; Purdy, W. C. *Langmuir* **1997**, *13*, 4487.

24 Malmqvist, M.; Karlsson, R. *Curr. Opin. Chem. Bio*. **1997**, *1*, 378.

25 (a) Sigal, G. B.; Bamdad, C.; Barberis, A.; Strominger, J.; Whitesides, G. M. *Anal. Chem*. **1996**, *68*, 490, (b) Gehrke, S. H.; Vaid, N. R.; McBride, J. F. *Biotechnol. Bioeng*. **1998**, *58*, 417. (c) Putka, C. S.; Gehrke, S. H.; Willis, M.; Stafford, D.; Bryant, J. *Biotechnol. Bioeng*. **2002**, *80*, 139.

26 (a) Niemeyer, C. M.; Blohm, D. *Angew, Chem., Int. Ed, Engl*. **1999**, *38*, 2865. (b) Schulze, A.; Downward, J. *Nat. Cell Biol*. **2001**, *3*, E190.

27 Benters, R.; Niemeyer, C. M.; Drutschmann, D.; Blohm, D.; Wöhrle, D. *Nul. Acid Res*. **2002**, *30(e10)*, 1.

28 Rowan, B.; Wheeler, M. A.; Crooks, R. M. *Langmuir* **2002**, *18*, 9914.

29 Lahann, J.; Balcells, M.; Rodon, T.; Lee, J.; Choi, I. S.; Jensen, K. F.; Langer, R. *Langmuir* **2002**, *18*, 3632.

30 Zhou, X.; Wu, L.; Zhou, J. *Langmuir* **2004**, *20*, 8877.

31 (a) Zhang, Z.; Chen, Q.; Knoll, W.; Foerch, R.; Holcomb, R.; Roitman, D. *Macromolecules* **2003**, *36*, 7689. (b) Zhang, Z.; Knoll, W.; Foerch, R.; Holcomb, R.; Roitman, D. *Macromolecules* **2005**, *38*, 1271.

32 Rühe, J.; Golze, J.; Freidank, D. *Abstracts of Papers of the American Chemical Society* **2001**, *221*, 321.

33 Jérôme, C.; Gabriel, S.; Voccia, S.; Detrembleur, C.; Ignatova, M.; Gouttebaron, R.; Jérôme, R. *Chem. Commun*. **2003**, 2500.

34 Yu, F.; Persson, B.; Löfås, S.; Knoll, W. *J. Am. Chem. Soc*. **2004**, *126*. 8902.

35 The patterns are, for instance, fully compatible with the work on pathogen screening (e.g. listeria), as demonstrated in Chapter 4.

36 The succinimide carbonyl band at 1745 cm^{-1} was observed before and after PEG coupling (there is a contribution from the bulk of the film to the measured signal).

37 Frutos, A. G.; Brocknam, J. M.; Corn, R. M. *Langmuir* **2000**, *16*, 2192.

38 The grafting density σ_{PEG} can be calculated as:

$$\sigma_{PEG} \approx 10\ \%\ d_{XPS}\ \rho_{PNHSMA}\ N_A\ M^{-1}$$

where d_{XPS} is information depth of the XPS experiment, ρ_{PNHSMA} is the density of PNHSMA (~ 1 g/cm^3), N_A (6.022 $\times 10^{23}$ mol^{-1}) is Avogadro's number, and M is the molecular mass (183 g/mol) of monomeric PNHSMA.

39 Groll, J.; Ameringer, T.; Spatz, J.; Möller, M. *Langmuir* **2005**, *21*, 1991.

40 Yu, J. C.; Yu, J.; Tang, H. Y.; Zhang, L. *J. Mater. Chem*. **2002**, *12*, 81.

41 Gong, P.; Grainger, D. W. *Surface Science* **2004**, *570*, 67.

42 Chen, C. S.; Mrksich, M.; Huang, S.; Whitesides, G. M.; Ingber, D. E. *Science* **1997**, *276*, 1425.

43 Brandrup, J.; Immergut, E. H. *Polymer Handbook*, 3rd ed. John Wiley & Sons: New York, **1989**.

44 Prime, K. L.; Whitesides, G. M. *J. Am. Chem. Soc*. **1993**, *115*, 10714.
45 Kumar, A.; Whitesides, G. M. *Appl. Phys. Lett*. **1993**, *63*, 2002.
46 Hillborg, H.; Tomczak, N.; Oláh, A.; Schönherr, H.; Vancso, G. J. *Langmuir* **2004**, *20*, 785.
47 Reilman, R. F.; Msezane, A.; Manson, S. T. *J. Electron Spectroscopy* **1976**, *8*, 389.

Chapter 7

Reactive μCP on Ultrathin Block Copolymer Films: Investigation of the μCP Mechanism and Applications to Sub-μm (Bio)molecular Patterning*

In this chapter, three different, complementary lithographic approaches to produce chemical patterns on ultrathin polystyrene-b-poly(t-butyl acrylate) (PS_{690}-b-$PtBA_{1210}$) films are introduced, which can be expanded to obtain patterns of biomolecules with (sub)micrometer feature sizes. In approach (A), PS_{690}-b-$PtBA_{1210}$ films were homogeneously hydrolyzed and subsequently functionalized with (N-hydroxysuccinimide) (NHS). Two types of molecules, fluoresceinamine and BSA, were patterned and covalently bound on the activated polymer films in sequential direct molecular transfer steps using reactive μCP. NHS functionalized polymer films were also patterned with $PEG_{500}NH_2$ by reactive μCP in approach (B). The PEG layer was used as antifouling layer to prevent the non-specific adsorption of (bio)molecules in the subsequent covalent coupling step of fluoresceinamine and bovine serum albumin (BSA) carried out in solution. The area selective immobilization was also successfully demonstrated for 25-mer probe DNA, as shown by the fluorescence microscopic detection of the hybridization of dye-labeled target DNA. In approach (C), the polymer films were locally hydrolyzed with trifluoroacetic acid that was locally applied on the films using acid soaked poly(dimethyl siloxane) (PDMS) stamps. A detailed study of the reactive μCP mechanism led to the conclusion that ink spreading and diffusion must be controlled for faithful pattern transfer, in particular on the sub-μm level. In addition, it was found that patterns with micrometer scale dimensions could be fabricated by using stamps with > 10 μm dimensions by controlling the spreading of trifluoroacetic acid. Thus, ultrahigh density patterns can be conveniently fabricated.

7.1 Introduction

The fabrication of biomolecular patterns with dimensions ranging from the mm to 10 micrometer scale has become important for the development of biosensors, biomaterials, genomic arrays, as well as tissue engineering.[1] For fundamental studies of cell biology and future miniaturized applications in the named areas even smaller patterns are required. Cells and proteins have been previously patterned on various substrates using self-assembled monolayers (SAMs),[2] metal templates,[3] stamped proteins and peptides,[4] bio and comb polymers,[5] microfluidic channels,[6] and membranes.[7] As an attractive method to pattern biological molecules, microcontact printing (μCP) techniques became very popular due to their simplicity, flexibility, and low cost compared to other techniques.[8] Using μCP, Khademhosseini et al.[9] have demonstrated a simple process that can be used to pattern oxide-based

* Part of the work described in this Chapter has been published in: Schönherr, H.; Feng, C. L.; Vancso, G. J. *Polymer Prepr.* **2006**, *in press*.

substrates with biofouling-resistant polymers (poly(ethylene glycol)-based random copolymer) with precise control over surface topography. Such controlled patterns can be used further for patterning proteins and cells. Control of biopolymer binding and release, or cell attachment on micropatterned materials with appropriate features fabricated by μCP have been studied in detail.[10] Microarrays containing up to sixteen different proteins were fabricated on polystyrene through physical adsorption by simple μCP molecular transfer techniques combined with microfluidic networks.[11] In addition, the preparation of multi-protein arrays on polymer films by μCP was also studied and tested as a detection system for specific antibodies.[12] After fabrication, immunoassays were successfully carried out using the patterned protein microarrays. The characterization revealed the high quality of the protein deposition and indicated a high degree of selectivity for the targeted antigen-antibody interactions.

It has been pointed out throughout this thesis that an important part of the biosensor design is the (bio)chemical nature of the interfacial layer at the sensor surface. Compared to SAMs, polymers have several distinct advantages, including low cost, ease of film preparation, stability, and three dimensional structure and functionalities.[13] As an alternative to the PNHSMA system discussed in the previous chapters, the biomolecular patterning of the PtBA skin layer in PS-b-PtBA polymer thin films will be treated in this chapter. One additional advantage of the PS_{690}-*b*-$PtBA_{1210}$ diblock copolymer system is the high stability for a broad range of processing conditions because this diblock copolymer contains a water insoluble polystyrene block (see Chapter 5). In addition, the microphase separation observed for this block copolymer offers the possibility to fabricate nanometer scale patterned surfaces, as described in Chapter 8.

In this Chapter, three patterning approaches are discussed to direct the deposition of biomolecules on PS_{690}-*b*-$PtBA_{1210}$ diblock copolymer films, as shown in Figure 7.1. In approach (A), two different types of molecules, bovine serum albumin (BSA) and fluoresceinamine, were directly stamped onto the polymer films in two sequential reactive μCP steps for covalent binding in micrometer scale patterns. In approach (B), a passivation layer of $PEG_{500}NH_2$ was locally transferred onto NHS activated PS_{690}-*b*-$PtBA_{1210}$ films. The covalent coupling of fluoresceinamine and BSA, confined to the remaining activated NHS functionalized areas, was then carried out from solution. In approach (C), reactive μCP was used to locally hydrolyze PS_{690}-*b*-$PtBA_{1210}$ films followed by activation and bioconjugation from buffer. This approach represents an interesting tool to produce (bio)reactive patterns based on polymeric film platforms down to sub-micrometer length scales, and thus lays the foundations for the fabrication of ultrahigh density biomolecular arrays.

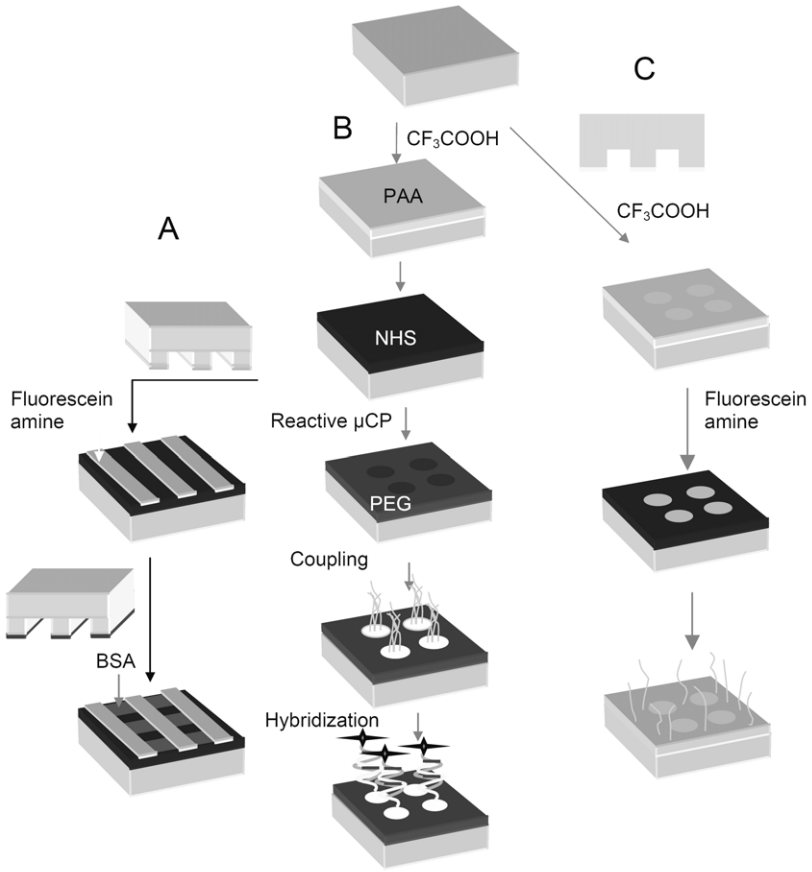

Figure 7.1. Scheme of the three investigated patterning approaches of PS_{690}-b-$PtBA_{1210}$ platforms via soft lithography and the subsequent directed deposition of (bio)molecules from solution. Approach (A): PS_{690}-b-$PtBA_{1210}$ films are homogeneously hydrolyzed with trifluoroacetic acid and activated with NHS/EDC. Fluoresceinamine and BSA were patterned by direct µCP molecular transfer. Approach (B) comprises the local passivation of NHS activated PS_{690}-b-$PtBA_{1210}$ films with $PEG_{500}NH_2$ via reactive µCP. This covalently bound PEG layer prevents the non-specific adsorption of (bio) molecules and allows one to couple amino functionalized fluoresceinamine, BSA, and probe DNA directly to the remaining NHS areas on the polymer films from buffer solution. Approach (C) includes the local hydrolysis of PtBA by reactive µCP, followed by activation with NHS/EDC and finally the directed deposition of amino functionalized (bio)molecules through covalent binding on the patterned surface.

7.2 Strategy A: Fabrication of Multimolecular Arrays by Direct Molecular Transfer

The direct transfer of biomolecules using µCP approaches is an established micropatterning strategy.[14] We first demonstrate that the PS-b-PtBA platform is fully compatible with this approach

and yields robust assemblies owing to the covalent attachment. For this purpose two different kinds of molecules were transferred and coupled to the same PS_{690}-b-$PtBA_{1210}$ film. The films were initially homogeneously hydrolyzed with trifluoroacetic acid solution and then activated with NHS / EDC. Subsequently, a fluoresceinamine covered PDMS stamp (lines: 10 × 5 μm^2) was brought to contact with the film. After a contact time of 30 min, the stamp was peeled off and Alexa Fluor®594 labeled BSA molecules were deposited by a second printing step on the pre-patterned film (the stamping direction was perpendicular to the original fluoresceinamine pattern). Using fluorescence microscopy, the patterned films were investigated (Figure 7.2).

Figure 7.2a shows the fluorescence emission of the fluoresceinamine, while Figure 7.2b is the corresponding image for dye-labeled BSA. These images suggest that the corresponding molecular ink has been faithfully transferred in the stamp - film contact region (width 10 mm). Cross contamination appears to be not pronounced. In order to assess possible cross contamination effects and ink spreading, several cross sectional plots were analyzed.

From profiles 1 and 2 in Figure 7.2a, fluorescent emission with regular patterns (corresponding to the extensions of the stamp-film contact areas, width 10 μm) was observed, which demonstrates that successful transfer of fluoresceinamine molecules was obtained during reactive μCP. Profile 3 displays the fluorescence emission along a printed line. In addition, no fluorescence emission can be observed on the areas that were not in contact with the fluoresceinamine inked stamp (profile 4). These data suggests that pattern transfer on PS_{690}-b-$PtBA_{1210}$ films can be controlled well by reactive μCP.

At the same position as shown in Figure 7.2a four profiles were also drawn in the fluorescence micrograph of the emission of the labeled BSA. Profile 1 was plotted along the direction of BSA pattern in Figure 7.2b. Fluorescence emission with a regular pattern was observed here as well (width 5 μm). Because fluoresceinamine was covalently coupled onto the surface in the first step, most of the NHS groups on the overlapped area were already occupied by fluoresceinamine molecules. Thus only few, if any, NHS groups were available for covalent coupling of BSA on the overlapped area during the second coupling step. So more BSA molecules were coupled on the area without fluoresceinamine molecules. Profile 2 in Figure 7.2b demonstrates that no fluorescence emission could be detected for areas in which no stamp - sample contact took place in the second printing step. By contrast, weak fluorescence emission originating from the dye-labeled BSA was still detected, as shown by profile 3. For further proving that BSA was transferred onto polymer film by reactive μCP, profile 4 was analyzed. It was found that the width of patterned BSA is 10 μm, which corresponds to the line width of the PDMS stamp in the particular direction.

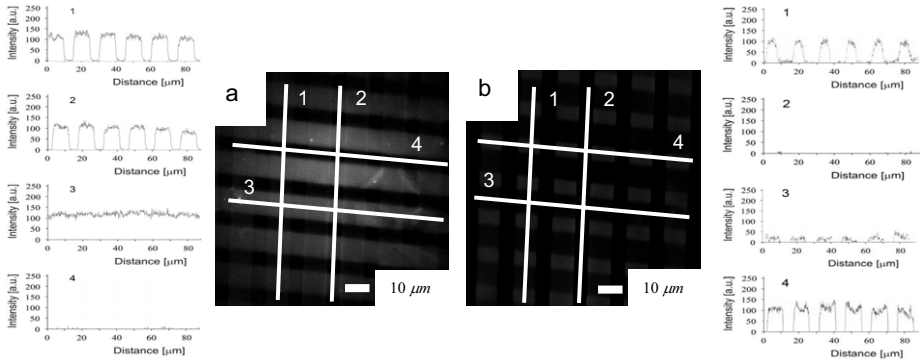

Figure 7.2. Fluorescence microscopic analysis of sequential 2-step μCP: (a) Fluoresceinamine was firstly transferred to the film by PDMS stamp (1 hr reaction time). (b) Then BSA was transferred as well in perpendicular direction (1 hr reaction time).

In addition, it was observed that similar patterns with two different types of molecules could be conveniently fabricated over large areas up to 1 cm^2. As revealed by fluorescence microscopy, the patterns were very homogeneous, thus indicating good conformal stamp - polymer film contact and good molecular transfer. Using this simple approach, it is hence also possible to prepare multimolecular biomolecular patterns on the polymer platforms introduced in this thesis.

7.3 Strategy B: Local Passivation of PS_{690}-b-$PtBA_{1210}$ Films

One possible disadvantage of the direct molecular transfer (strategy A) is that biomolecules are brought into contact with air, which may lead to denaturation. To overcome this limitation, the area selective deposition of (bio)molecules *from solution* has been studied, as described in approach (B), via the local passivation of NHS activated PS_{690}-b-$PtBA_{1210}$ films with PEG. The surface of PS_{690}-b-$PtBA_{1210}$ films was firstly homogeneously hydrolyzed using trifluoroacetic acid, followed by activation with NHS/EDC. By reactive μCP using a $PEG_{500}NH_2$ covered PDMS stamp (depressions with 15 μm and 30 μm spacing, square geometry), a $PEG_{500}NH_2$ layer was successfully transferred on the activated films. This antifouling PEG layer prevents locally the immobilization of solution-borne amino-functionalized (bio)molecules, such as fluoresceinamine, dye labeled BSA, and probe DNA, while the coupling proceeds efficiently in the remaining NHS activated areas. The thus obtained patterned films were analyzed by fluorescence microscopy.

Figure 7.3 shows the results of fluorescence microscopy experiments after fluoresceinamine and BSA were covalently coupled on $PEG_{500}NH_2$ prepatterned films. For comparison, the data of $PEG_{500}NH_2$ prepatterned PS_{690}-b-$PtBA_{1210}$ films are also shown. For the PEG patterns, negligible background fluorescence emission was observed (Figure 7.3a). After coupling fluoresceinamine to the patterned films from solution, highly fluorescent circular features were observed (Figure 7.3b). The coupling of proteins to the circular NHS activated areas proceeded also area-selectively as shown in Figure 7.3c for BSA.

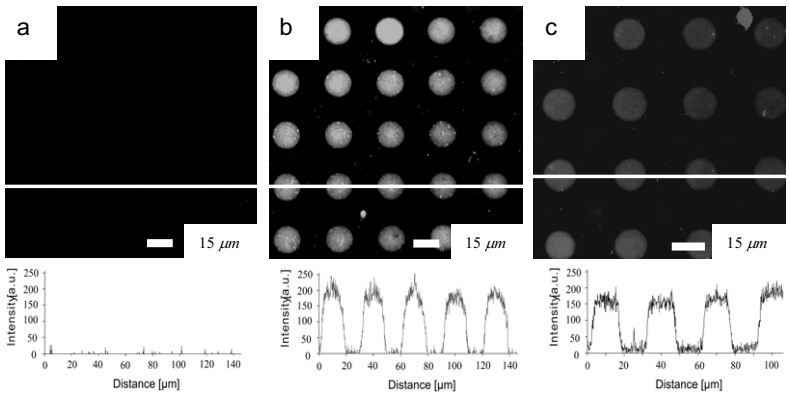

Figure 7.3. Fluorescence microscopy images of PS_{690}-b-$PtBA_{1210}$ (a) after patterning $PEG_{500}NH_2$ (stamp - sample contact time: 180 minutes); (b) following reaction with fluoresceinamine from solution (stamp - sample contact time: 180 minutes; reaction time: 30 minutes; (c) following BSA binding on patterned surface from solution (stamp - sample contact time: 180 minutes; reaction time: 30 minutes).

Subsequently, the hybridization of target DNA on probe DNA prepatterned PS_{690}-b-$PtBA_{1210}$ films was investigated. Probe DNA (25 mer) was firstly applied on $PEG_{500}NH_2$ prepatterned films from buffer solution. The film was then put inside a solution containing complementary target DNA. PS_{690}-b-$PtBA_{1210}$ films functionalized with probe DNA showed negligible fluorescence emission (Figure 7.4a). After hybridization with dye-labeled complementary target DNA, a regular fluorescent pattern (diameter of circular dots: 15 μm) was detected (Figure 7.4b). This experiment suggests that the directed deposition of probe DNA can be achieved similar to the directed deposition of fluoresceinamine and BSA, and that it is possible to use such polymer films as substrates for biosensors to detect DNA hybridization also in patterned array-based formats.

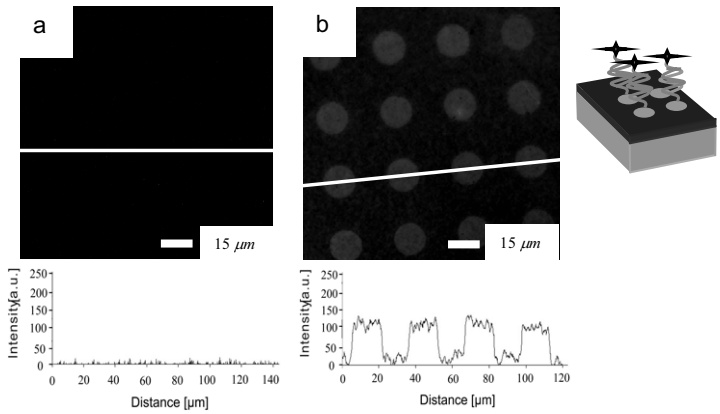

Figure 7.4. Fluorescence microscopy images of (a) PS_{690}-b-$PtBA_{1210}$ surface that was patterned with $PEG_{500}NH_2$, activated and functionalized with probe DNA from solution; (b) probe DNA modified PS_{690}-b-$PtBA_{1210}$ surface following hybridization with complementary target DNA.

7.4 Strategy C: Local Deprotection of PS_{690}-b-$PtBA_{1210}$ Films

Local deprotection (local hydrolysis) was performed by transferring trifluoroacetic acid onto PS_{690}-b-$PtBA_{1210}$ films via a PDMS stamp (circular features with diameter 15 μm). Since the wettability of the stamp is a crucial parameter for obtaining controlled and faithful replication of the pattern of the stamp in many μCP approaches, as-prepared and UV ozone-treated PDMS stamps were tested. The stamps were first covered with one drop of trifluoroacetic and after a certain drying time, they were brought into conformal contact with the polymer films. The locally reacted films were then activated with NHS/EDC, followed by labeling via covalent coupling with fluoresceinamine. Finally, the films were analyzed by fluorescence microscopy.

As shown in Figure 7.5, a matrix with pronounced fluorescence emission and diffuse (untreated PDMS, Figure 7.5a) or ring-like (oxidized PDMS, Figure 7.5b) circular features in a matrix with lower fluorescence emission were observed. While the periodicity and symmetry of the pattern (Figure 7.5a) were consistent with those of the stamp, the diameter of the circular non-fluorescent features, i.e. those areas that were not in conformal contact with the stamp, did not correspond to the size of the depressions in the stamp.

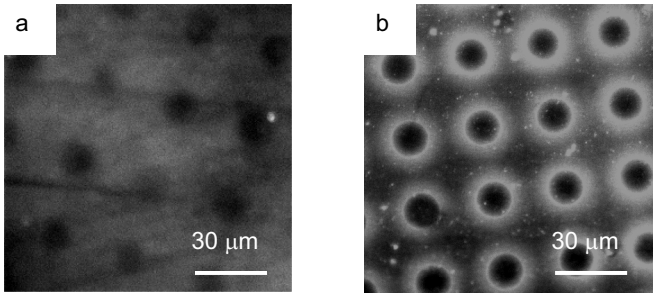

Figure 7.5. Fluorescence microscopy images of PS_{690}-b-$PtBA_{1210}$ after local hydrolysis, activation with NHS/EDC (30 minutes), and following coupling with fluoresceinamine from solution (30 minutes). (a) PDMS stamp was cleaned with ethanol. (b) PDMS was oxidized using a UV ozone treatment. For both experiments identical conditions were used (evaporation time of trifluoroacetic: 2 minutes; stamp - film contact time 10 minutes).

Apparently, local deprotection has been hampered by inadequate printing conditions. Furthermore, the surface properties of the PDMS stamp showed a noticeable effect of the chemical patterns obtained under identical conditions. The untreated stamps were visibly not wetted completely, which led to irreproducible results.[15] By contrast, the oxidized stamps were wetted completely and showed reproducible printing behavior. Hence in the following sections, the results obtained using oxidized PDMS will be discussed exclusively.

Based on the above observations, ink spreading, ink diffusion or a film reorientation can be identified as possible origin for the poor pattern quality. In order to optimize the pattern quality and in order to obtain a better insight into the underlying processes, the mechanism of reactive μCP was investigated in more detail. In particular the effect of printing time and ink loading on the stamp were systematically investigated using fluorescence microscopy and AFM on NHS ester activated and subsequently fluoresceinamine labeled samples.

7.4.1 Analysis by Fluorescence Microscopy

To better understand the reactive microcontact printing process, fluorescence microscopy on locally hydrolyzed, subsequently NHS activated and fluorescently labeled PS_{690}-b-$PtBA_{1210}$ films were used (Figure 7.6). For identical ink loading on the stamp, realized by applying a drop of constant volume (V = 50 μL) onto oxidized PDMS stamps and using a constant evaporation time of 3 min evaporating, the stamp - film contact time had only a limited effect on the patterns fabricated. As shown in Figure 7.6, ring-like features with high fluorescence emission intensity were observed for all printing times. The interior of the circles showed very low fluorescence emission, while the surrounding matrix showed increasingly homogeneous emission intensities for printing times up to 10 minutes.

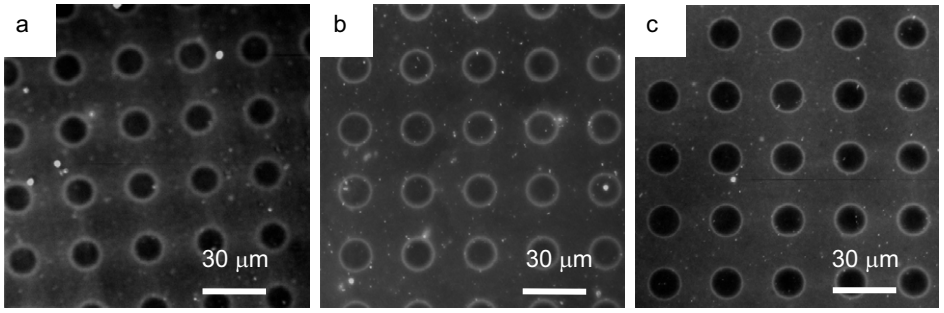

Figure 7.6. Fluorescence microscopy images of films after reactive μCP with CF_3COOH for (a) 5 minutes, (b) 10 minutes and (c) 20 minutes. The ink loading, as well as the labeling conditions were identical (evaporating time of trifluoroacetic acid on PDMS: 3 min, 30 minutes EDC/NHS, 30 minutes fluoresceinamine).

Subsequently, the effect of ink loading on the stamp was systematically investigated. Figure 7.7a shows a fluorescence microscopy image of a film after local hydrolysis by reactive μCP (evaporation time 30 seconds). First, fluorescence emission was observed across the entire surface. Particularly strong fluorescence emission was observed *inside* the circular features. These features correspond to regions of depressions in the stamp, as judged from their size and geometry; i.e. these areas are regions of the stamp - film contact, where no direct contact between the PDMS and the polymer film was possible.

After local hydrolysis for 1 minute evaporation time a completely different pattern was observed (Figure 7.7b). First, it was found that the fluorescence emission is not detected over the entire surface. No fluorescence emission was observed in the center (diameter ~ 4 μm) of circular features that were arranged in a square geometry with a periodicity of 30 μm. Very strong fluorescence emission was observed for ring-like features (diameter ~ 15 μm), which correspond to the diameter of the circles of the stamp. In addition, halos around these rings were also observed.

Increasing evaporation times led to systematic changes in the dimensions, as well as the relative fluorescence emission intensities of all described features, i.e. center areas, rings and halos (Figures 7.7c-d). For the longest evaporation time a clear pattern of non-fluorescent circular areas in a highly fluorescent matrix was observed (Figures 7.7e). The halo was absent.

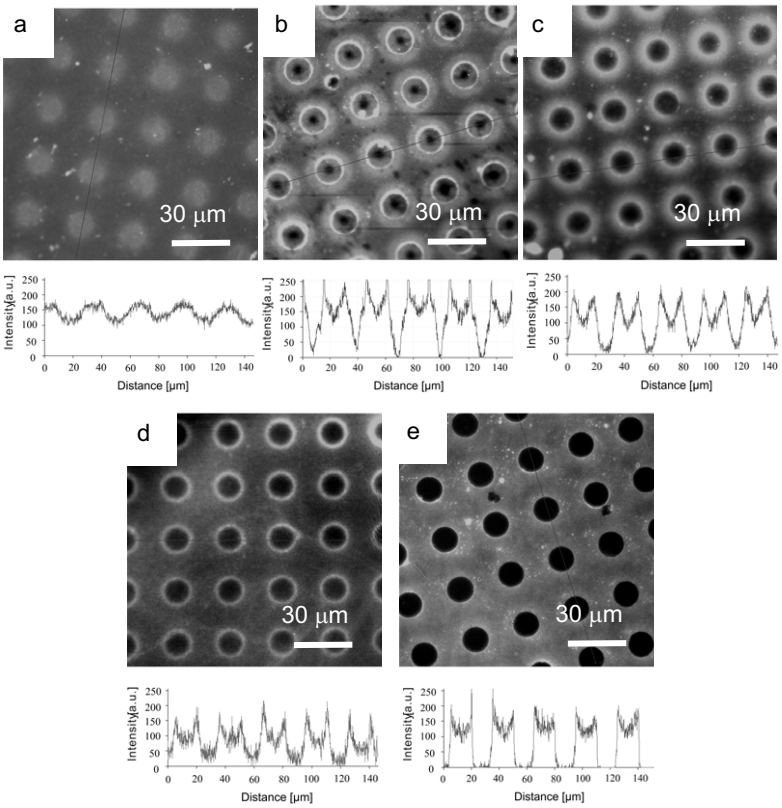

Figure 7.7. Fluorescence microscopy images and corresponding intensity profiles of films following local hydrolysis by reactive μCP, activation and labeling. All data are obtained under the same reaction conditions (Local hydrolysis 10 min, 30 min EDC/NHS, 30 min fluoresceinamine for all the cases) except for CF_3COOH evaporation time that was varied systematically: (a) 30 sec (b)1 min (c) 2 min (d) 3 min (e) 4 min.

For the analysis, we define three parameters D_{ring}, D_{halo} and D_{center}, which correspond to the diameters of the rings, the halo and the central low fluorescence part of the circles.[16] All the values of D_{halo} and D_{center}, as measured from the fluorescence microscopy images (Figure 7.8), are plotted in Figure 7.8b. It was found that D_{halo} decreased and D_{center} increased with increasing evaporation times. Both D_{halo} and D_{center} leveled off at 15 μm, which corresponds the size of circles of the stamp, for long evaporation times. Empirically it was found that D_{halo} is proportional to $t^{-v_{halo}}$, while D_{center} is proportional to $t^{v_{center}}$. t denotes the evaporation time of trifluoroacetic acid on the PDMS stamp before local hydrolysis. v_{halo} represent the rate with which the diameter D_{halo} decreases and v_{center} represents the rate with which the diameter D_{center} increases. The parameters v_{halo} and v_{center} were obtained by double logarithmic fitting (shown in Figure 7.8c and d).

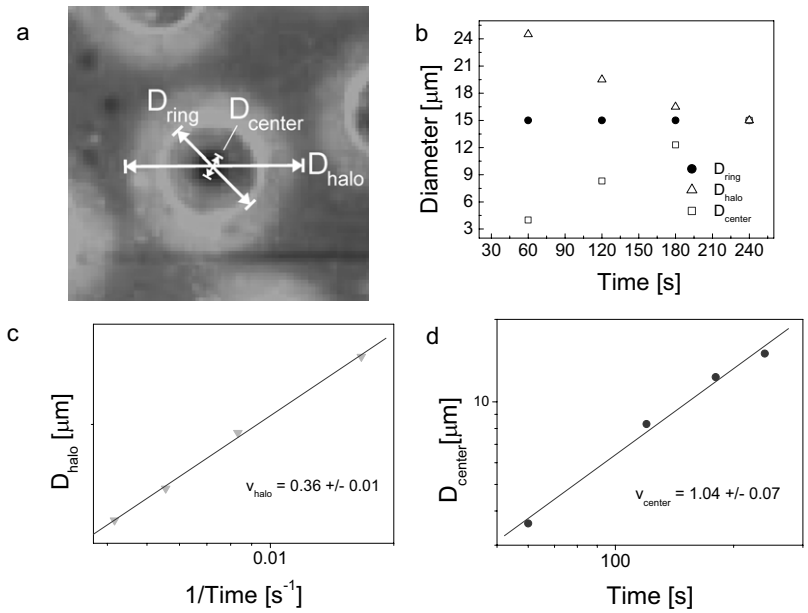

Figure 7.8. (a) Schematic the diameter of the D_{halo} and D_{center} (b) Plot of the diameter changes of unmodified area and the halo. (c) Scaling analysis of D_{halo} vs t^{-1} (d) Scaling analysis of D_{center} vs t.

The in-plane motion of the acid, as seen indirectly from the fluorescence microscopy data, is a superposition of (liquid) acid flow, as well as acid diffusion on the surface. In addition one must consider acid diffusion from the PDMS stamp into the polymer film. For low ink coverages surface diffusion can be assumed to largely govern the flux of the trifluoroacetic acid. Although the diffusion constant of organic acids is small, typically $D \approx 10^{-5}$ cm^2 s^{-1}, its effects are dramatic at the microscale.[17] Simulations by Delamarche et al.[18] show that traveling distance of molecules on a surface by diffusion is about 100 μm within ~ 15 ms. From the above analysis, pronounced diffusion must have occurred, when $D_{halo} > D_{center}$. In this case, the resolution of the pattern will be limited. By contrast, if $D_{halo} = D_{center}$, negligible diffusion has occurred during local hydrolysis and the pattern of the stamp is faithfully transferred (see also below).

7.4.2 Analysis by AFM

Using AFM, possible changes of the morphology of PS_{690}-b-$PtBA_{1210}$ films as a result of the local hydrolysis were studied systematically. Here only the effect of ink loading on the local hydrolysis was investigated in detail. Figure 7.9 shows the morphological changes of the hydrolyzed films together with the corresponding cross-sectional thickness profiles. After 1 minute evaporation time ring-like features with a height (*h*) of 388 ± 25 nm were observed (Figure 7.9a). The diameter (*d*) of the circles of 15 ± 1 μm corresponded to the diameter of the features in the stamp. In addition, it was found that the area inside the circles was elevated with respect to the remainder of the film with an average height (*l*) of 70 ± 10 nm.

For longer evaporation times, *h* and *l* were found to decrease, while *d* stayed constant (Figure 7.9 e, f). The observed profiles are reminiscent of the profiles obtained by capillary force lithographic approaches.[19] In these experiments, polymer films (partially) wet a contacting stamp, when the temperature is raised above the glass transition temperature (T_g) of the polymer, or if the polymer is plasticized by low molar mass molecules coated on the stamp.[20] The changes observed here can be tentatively ascribed to a similar effect as a consequence of the occurring reaction of PtBA to PAA (see below) or the plasticizing effect of trifluoroacetic acid (see below).

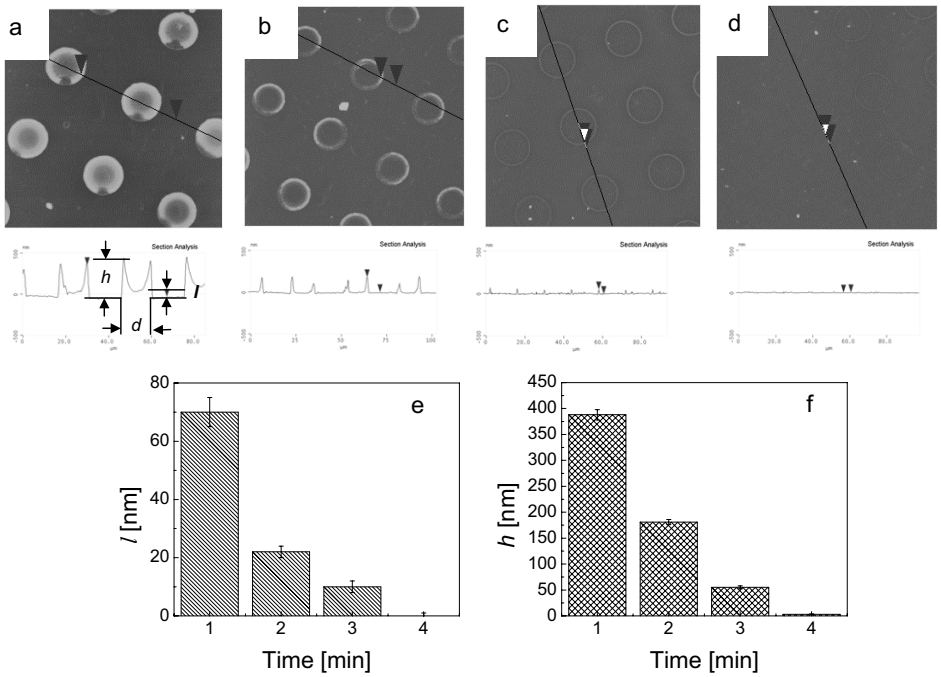

Figure 7.9. AFM height images incl. cross-sectional analyses reveal the changes of the morphology of the polymer films vs the loading of trifluoroacetic acid during local hydrolysis. The trifluoroacetic acid on stamp evaporated (a) 1 min; (b) 2 min; (c) 3 min; (d) 4 min, respectively. (e) Plot of average of film inside circles vs evaporating time of trifluoroacetic acid. (f) Plot of height of the rings vs evaporating time of trifluoroacetic acid.

7.4.3 Mechanism of Local Hydrolysis

The fluorescence microscopic images represent the local chemical composition and thus indicate to which extent the hydrolysis proceeded during the μCP step. From the analysis of the observed features and fluorescence emission intensities, as shown above, the presence and local concentration of the organic acid, which induces the hydrolysis, can be qualitatively estimated.

Initially the oxidized PDMS stamp was covered with a liquid layer of trifluoroacetic acid. The acid spread over the stamp indicating a contact angle close to 0°. The acid filled the circular depressions in the stamp and may have also formed a liquid film of not well-known thickness on the stamp. From the volume of the drop and the stamp design an initial layer thickness of ~ 200 μm was calculated. Since trifluoroacetic acid is volatile,[21] it thus evaporated rapidly in these experiments.

For the discussion of the observations and the formulation of a mechanism of the local hydrolysis, there are three different cases that need to be taken into account. These cases can be identified based on the following observations and arguments:

(1) The observation of the strong fluorescence emission from circular areas that were not in conformal contact with the stamp (Figure 7.7a) leads to the conclusion that the depressions are still acid-filled after evaporation times of 30 seconds. The observed circular areas of high fluorescence emission intensity are consistent with a hydrolysis induced by liquid acid present in the circular pits of the stamp.

(2) Ultimately, for very long evaporation time, no liquid acid will be present on the stamp surface, but the PDMS is likely swollen with acid, at least in the near-surface region.

(3) For intermediate evaporation time, and thus lower acid coverage, a thinner film of acid can be expected to remain on the stamp surface, when the stamp is brought into contact with the polymer film.

To develop the optimum printing conditions, the three cases identified will be discussed in the following section:

1. When the stamp, including the depressions, is covered with liquid trifluoroacetic acid, the ink may spread across the surface upon establishing contact between the stamp and substrate. Acid transport via diffusion can likely be ignored. In this case, hydrolysis occurs not only in the area of conformal contact between the PDMS stamp and the polymer, where a thin acid film may be present (or where acid may diffuse from the stamp into the film), but predominantly in the areas where the voids (depressions) in the stamp are located. As shown schematically in Figure 7.10, these voids may serve as a reservoir of liquid acid. Depending on the amount of acid on the stamp, the depressions may be more or less filled (Figure 7.10a /b). Because of the locally high concentration of acid in both cases, the degree of hydrolysis of the tBA functional groups in the circular area will be high compared to the matrix.

Further, in the case of partially filled depressions, the wetting of trifluoroacetic acid can be expected to lead to the formation of a meniscus (Figure 7.10b), which will provide an increased ink supply when the acid starts to evaporate and to diffuse into the PDMS stamp and the film.[22] Hence the meniscus can be regarded as reservoir of acid near the stamp walls. This reservoir may explain the

observation of a pronounced highly fluorescent ring for high to intermediate ink loading (Figure 7.7b-d).

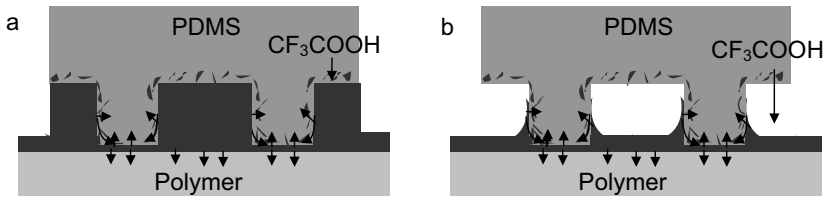

Figure 7.10. Scheme of local hydrolysis in the presence of liquid trifluoroacetic acid.

2. For the case that the stamp material is swollen with trifluoroacetic acid and no liquid acid is present on the surface, the reactive ink can exclusively be supplied by diffusion from the PDMS stamp into the film. Similar to SAMs (Chapter 2), there are several possible pathways that comprise diffusion through the gas phase, diffusion from the stamp into the film in the corresponding contact area and diffusion of ink along the surface of the polymer film. The fluorescence microscopic observations of non-fluorescent circles and the halo (Figure 7.7e) suggest that diffusion through the gas phase and surface diffusion can be neglected. The mechanism, as depicted schematically in Figure 7.11, would also account for the absence of the fluorescent as well as topographic ring-like features, since no liquid is present that could serve as acid reservoir and cause for capillary forces, respectively. Hence under these conditions an optimized pattern fabrication on PS_{690}-*b*-$PtBA_{1210}$ films can be achieved in which the size of the chemical patterns obtained correspond to those present on the PDMS stamp (see also section 7.4.4 below).

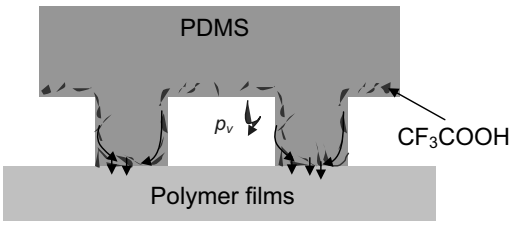

Figure 7.11. Scheme of local hydrolysis in the absence of liquid trifluoroacetic acid. The stamp is swollen with the acid (p_v denotes the vapor pressure of the trifluoroacetic acid).[23]

3. If the stamp surface is partially covered with liquid acid, a complex situation is expected. During stamping under these conditions, the trifluoroacetic acid will spread initially towards the depressions of the stamps, as shown in Figure 7.12. Since there is only limited amount of acid present, there may be only in the initial stage (if at all) a complete liquid acid layer that spans the entire area of the depression. As a result of the previously mentioned capillary forces, “macroscopic” liquid reservoirs will be formed along the wall of the stamp in the void space stamp. This may result in several effects:

a). Depending on the amount of the acid in the void along the wall, there will be unhydrolyzed areas located inside the void areas.

b). The acid molecules may diffuse over the surface either from the liquid (meniscus) reservoir or the PDMS stamp, which leads to the formation of the halos, as detected by fluorescence microscopy (Figure 7.7b, c and d).

c). The high concentration reservoir near the wall will lead to locally very rapid hydrolysis and also for the longest availability, in the case that the liquid acid evaporates or partitions into the stamp or the film. This will result in the highest local conversion, as confirmed by the presence of the highly fluorescent rings. In addition, the hydrolysis product PAA, as well as possibly plasticized PtBA are mobile enough to be forced by capillary forces to wet the wall of the stamp and hence lead to the observed topographic changes (Figure 7.9 a - c).[24]

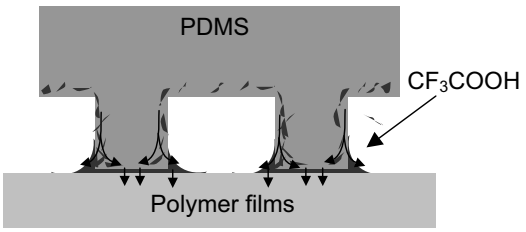

Figure 7.12. Scheme of local hydrolysis in the presence of a limited amount of liquid trifluoroacetic acid.

7.4.4 Local Deprotection on the Sub-μm Scale

The mechanism sketched in the previous section is consistent with the observation made by fluorescence microscopy and AFM. For faithful pattern transfer, the presence of liquid acid on the stamp must be avoided. On the other hand, the phenomena of ink spreading and surface diffusion may be exploited for reducing the pattern size below the size of the features on the stamp, as will be discussed below.

As shown above, it is possible to replicate the patterns present on the stamps faithfully by reactive μCP on the micrometer scale, when the loading of trifluoroacetic acid on the oxidized PDMS stamps is well controlled. To validate the analysis for sub-wavelength scale patterns using an alternative viable method, micrometer scale patterned films were first investigated using contact mode AFM. Figure 7.13 shows height and friction images obtained simultaneously on such patterned films. No morphology is observed here. However, a clear friction force contrast is observed in Figure 7.13b, that is, low friction force circles in a high friction force matrix. Here, the dark area is ascribed to more hydrophobic area (PtBA) and the bright area to more hydrophilic part (PAA).[25] The data suggest that the reaction occurred selectively in the area where the acid-soaked stamp contacted the polymer surface.

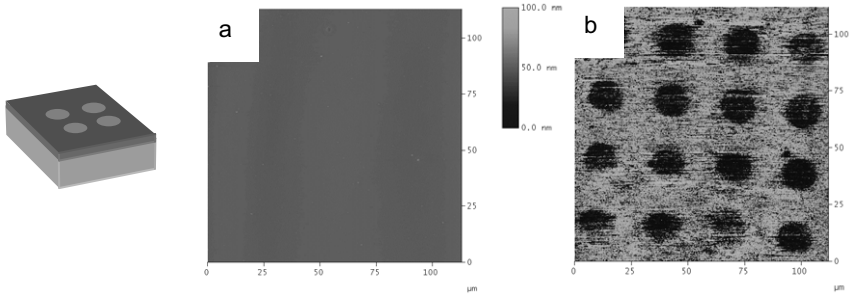

Figure 7.13. AFM height and friction images acquired after local hydrolysis by reactive μCP. The bright area (matrix) is ascribed to hydrophilic part (PAA); the dark area (circles) is ascribed to hydrophobic part (PtBA).

The film shown in Figure 7.13 was activated with NHS/EDC, followed by labeling with fluoresceinamine. Optimized regular patterns with homogeneous fluorescence emission were observed with feature sizes that correspond to the corresponding sizes on the PDMS stamps (diameter of circle: 15 μm), as shown in Figure 7.14.

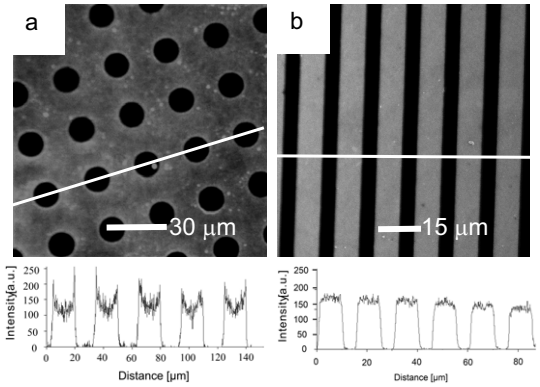

Figure 7.14. Fluorescence microscopy images (a) obtained by 10 × 5μm² PDMS stamp; (b) obtained by 15μm circle PDMS stamp (and corresponding cross-sectional plot) reveal the optimized pattern of fluoresceinamine on PS_{690}-b-$PtBA_{1210}$ films.

The results shown above demonstrate that micrometer-sized features can be replicated faithfully. For reduced pattern dimensions (sub-micrometer length scales), however, surface diffusion and diffusion via the gas phase may become a limiting factor. Using AFM, the patterning by reactive μCP on PS_{690}-*b*-$PtBA_{1210}$ films was tested down to the 300 nm level. Figure 7.15 shows AFM images of PS_{690}-*b*-$PtBA_{1210}$ films chemically patterned by local hydrolysis using a stamp with 500 nm × 300 nm line features. AFM height and friction images were captured simultaneously. The height difference due to capillary force effects was very small (< 7 nm), while the friction image in Figure 7.15b shows a regular pattern of alternating lines with high and low friction forces. The width of the single stripe of the bright area is 500 ± 20 nm and the width of the single stripe of the dark area is 300 ± 20 nm. The

bright area corresponds to high friction forces (attributed to the hydrophilic reaction product PAA); the dark area corresponds to low friction forces (attributed to the more hydrophobic PtBA).

We have also successfully derivatized these sub-micrometer patterned films, as shown by tapping mode AFM phase imaging (no data shown) in conjunction with spectroscopic and fluorescence microscopic techniques. These results suggest that sub-micrometer fabrication can be achieved by this simple process and that the mentioned diffusion is not (yet) a significant problem.

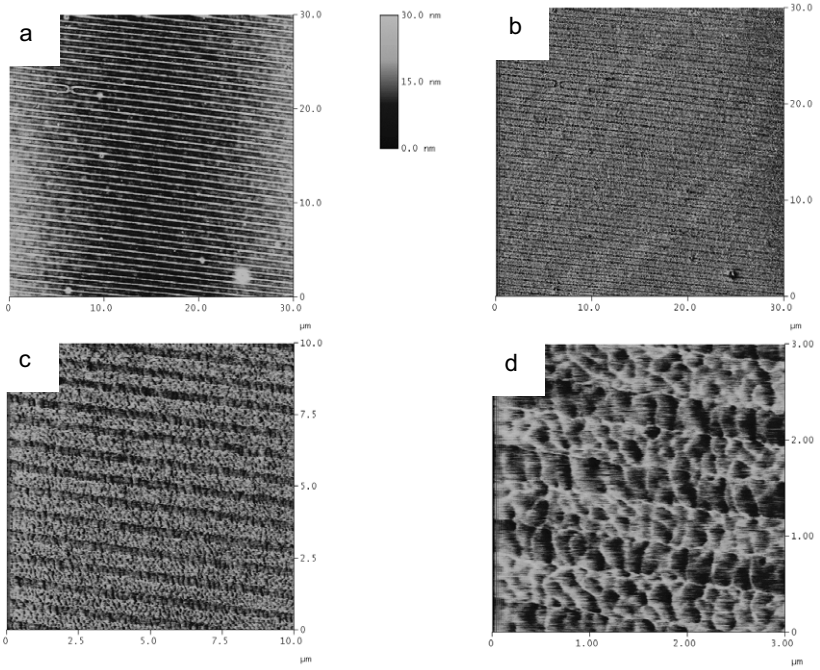

Figure 7.15. AFM height (a) and friction (b, c, d) images after local hydrolysis by reactive μCP. The stripes with high friction force contrast (width ~ 500 nm) are ascribed to the hydrophilic part (PAA); the low friction force stripes (width ~ 300 nm) are ascribed to the hydrophobic part (PtBA). Note in (a) and (b) how a defect in the stamp has been faithfully reproduced.

As alluded above, there is an alternative option to reduce the pattern size *without* changing the feature sizes on the stamp used for reactive μCP. The approach exploits controlled wetting and diffusion of the organic acid. When the PDMS stamp is covered with a very thin homogeneous (liquid) trifluoroacetic acid layer (case 3., section 7.4.3), the probability for each molecule to be captured on the polymer surface at a distance *R* from the edge of PDMS stamp is isotropic during local hydrolysis. This probability should be a decreasing function of *R* due to the vanishing liquid reservoir (at the meniscus) and thus decreasing concentration gradient. In this case, the areas in which hydrolysis has occurred are expected to be circular for the here utilized stamp geometry.[26,27] Considering the already discussed experimental data, it is clear that the degree of hydrolysis is a function of R as well.

However, if the coverage of carboxylic acid groups is above a necessary threshold level, a layer with defined useful properties may be coupled covalently following activation with NHS.

As an example the patterning of PS_{690}-*b*-$PtBA_{1210}$ films with a (fluorescently labeled) protein is discussed. By covering the stamp (15 μm diameter depressions, 30 μm periodicity, as used previously) with 50 μL of trifluoroacetic acid followed by 1 minutes of evaporation, a thin acid layer was achieved on the oxidized stamp. The hydrolysis by reactive μCP was thus carried out in a regime assigned to case 3. (section 7.4.3), where some spreading of the ink occurs. The combination of ink spreading and evaporation defines the area on the polymer films that is being hydrolyzed and thus can be further modified. Following hydrolysis and activation with NHS, $PEG_{500}NH_2$ was firstly coupled to the matrix of locally hydrolyzed PS_{690}-*b*-$PtBA_{1210}$. The layer of PEG is dense enough to function as an antifouling layer against non-specific adsorption of BSA. By contrast, the unhydrolyzed PtBA areas, which, owing to the isotropic spreading and diffusion, are located in positions corresponding exactly to the center location of the circular depressions, exhibit different behavior in contact with BSA. In these areas, pronounced non-specific adsorption was observed, resulting in a well-defined BSA pattern (Figure 7.16).

Negligible fluorescence emission was observed in the PEGylated matrix, while a regular pattern of bright fluorescence attributed to the dye label of BSA dots (average size 4 ± 0.5 μm) showed that a defined biomolecular pattern with *reduced* feature sizes, yet identical spacing was realized. Thus, these experiments demonstrate that it is possible to produce the chemical patterns with controllable size by reactive μCP. In particular it is important to point out that small diameter spots with large spacings can only be prepared to a limited spot / spacing ratio by direct protein transfer[28] due to mechanical instabilities of the pillars of the corresponding stamps.

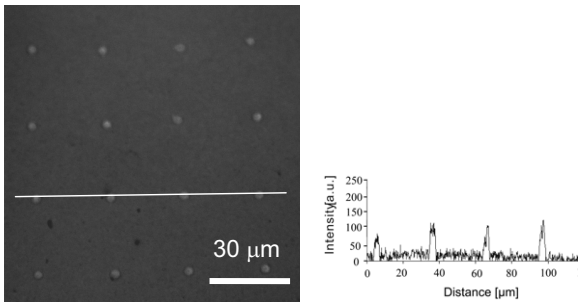

Figure 7.16. Fluorescence microscopy image and intensity profile of BSA pattern on block copolymer film. The trifluoroacetic acid on the PDMS stamp was evaporated for 1 minute before stamping. After local hydrolysis and activation with NHS/EDC on the patterned surface, $PEG_{500}NH_2$ molecules were coupled to the matrix first. Then, BSA was applied from the solution. The size of the dots is significantly smaller than the diameter of the depressions on the stamp (15 μm). However, the pattern periodicity remained 30 μm.

In summary, PS_{690}-b-$PtBA_{1210}$ films, which are stable in a wide range of different environments and processing conditions, were successfully deprotected and subsequent derivatizated *locally* in aqueous media *without* dissolution or removal of the film.[29] The PtBA skin layer present can be easily locally hydrolyzed by reactive microcontact printing, followed by activation with NHS ester groups. Using three different complementary approaches, the selective covalent coupling of fluoresceinamine, BSA and probe DNA, as well as successful hybridization on the polymer films, showed that PS_{690}-b-$PtBA_{1210}$ films can be used as an alternative substrate for developing robust patterned biochips. In particular, the covalent immobilization of (bio)molecules *via* amide linkage formation in *aqueous media, i.e. without the need to expose biomolecules to air,* provides an efficient and secure attachment of molecules on substrate compared to mere physical interactions.[30] Finally, reactive μCP on PS-b-PtBA film-based platforms comprises a simple way to produce reactive patterns even down to sub-micrometer length scales, as shown by using stamps with sub-micrometer features, as well as by exploiting controlled ink spreading and diffusion. Thus, based on these approaches and platforms ultrahigh density patterns can be conveniently fabricated.

7.5 Experimental Section

Materials: PS_{690}-b-$PtBA_{1210}$ diblock copolymer was purchased from Polymer Source Company (Dorval, Canada) and used as received. The molar mass and polydispersity were 202.4 kg/mol and 1.03, respectively. Amino end-labeled PEG (denotes as $PEG_{500}NH_2$), purchased from Nektar UK Company (M_n = 500 g/mol, PDI = 1.1), fluoresceinamine (Molecular Probes, Inc. The Netherlands) and the DNA samples (probe DNA: P: 25 mer 5'- GGA ATG TGC CAT ACC GAA TCC GTG T –3′; Cy5-labeled target DNA: 5'- CAC GGA TTC GGC ATG – 3', Cy5-labeled mismatch DNA: 5'- TGT GCC TAA GCC ATA - 3', MWG BIOTEC AG, Ebersberg, Germany) were used as received. DNA samples were stored at -4ºC until use. Bovine serum albumin (BSA) with Alexa Fluor®594 conjugate was bought from Molecular Probes and used as received.

Preparation of Thin Films. Thin polymer films were prepared by spin-coating polymer solutions in toluene (typical concentration between 10 and 20 mg/ml) onto silicon wafers (111) or glass (cover slide from Menzel-glaser), which were previously cleaned by an oxygen plasma using an Elektrotech PF 340 apparatus (Pressure of O_2: 0.5 Bar; Current: 30 mA). All spin-cast samples were dried at room temperature for 24 hours in vacuum before analysis. Mean film thicknesses were determined using a custom-built spectroscopic ellipsometry using a He-Ne laser (λ = 632.8 nm). The refractive index of the PEG films was approximated as 1.4638,[31] while for polymer as 1.513.[32]

Functionalization of Hydrolyzed Polymer Films. The COOH groups obtained on the polymer films after hydrolysis were activated by immersion into an aqueous solution of 1-ethyl-3-(dimethylamino)-propylcarbodiimide (EDC, 1 M) and *N*-hydroxysuccinimide (NHS, 0.2 M) for 30 min. The samples were then rinsed with Milli-Q water, dried under a stream of nitrogen, and used immediately thereafter.

Local Hydrolysis and Fluoresceinamine Coupling. The PDMS stamps prepared according to the literature[33] were mildly oxidized in an UV ozone plasma reactor for 50 min. A drop of trifluoroacetic

acid (50 μL) was applied on the stamp (1 × 1 cm^2) and the acid was dried in air from 30 second to 4 min. Then the stamp was brought to contact with the surface of polymer films and kept for 20 min. After peeling off the stamp, the films were rinsed three times using Milli-Q water and were subsequently activated with NHS/EDC. The films were immersed in fluoresceinamine solution (100 μM, PB, pH = 7.4). Then the samples were taken out, rinsed by PB and Milli-Q water, and dried in a stream of nitrogen.

Homogeneous Hydrolysis and (Bio)molecule Coupling. The polymer films were hydrolyzed in trifluoroacetic acid liquid phase for 20 min, rinsed three times using Milli-Q water, and functionalized with NHS/EDC. For $PEG_{500}NH_2$ coupling from solution, the polymer films were subsequently immersed into the corresponding $PEG_{500}NH_2$ solution (200 μM $PEG_{500}NH_2$ solution, PB, pH = 7.4). After a reaction time between 5 min to 10 h, the samples were taken out of the solution and were thoroughly rinsed with Milli-Q water. For $PEG_{500}NH_2$ patterning on functionalized polymer film, the oxidized stamps were inked by soaking them into 200 μM PEG solution for 60 min (PB, pH = 7.4). Before printing, the stamps were blown dry in a stream of nitrogen. The stamps were applied on functionalized polymer film, then carefully removed, and rinsed with Milli-Q water. The PEG patterned films were immersed in fluoresceinamine solution (100 μM, PB: pH = 7.4) or BSA solution (200 μM, PB: pH = 7.4). Then the samples were taken out, rinsed with PB and Milli-Q water, and dried in a stream of nitrogen. Finally, the samples were dried inside a vacuum oven for 1 day prior to the fluorescence microscopy experiments. DNA immobilization (100nM) in phosphate buffer on $PEG_{500}NH_2$ patterned films was carried out as described for coupling fluoresceinamine or BSA. Afterwards, the hybridization of target DNA with dye (100 nM) was carried out in phosphate buffer. Then the films were rinsed with PB (pH = 7.4) and Milli-Q water, and dried in a stream of nitrogen. All experiments were carried out at T = 25 ± 2º.

Fluorescence Microscopy. Fluorescence microscopy images of dry samples on glass cover slips were recorded at room temperature on a Zeiss LSM 510 confocal laser scanning microscope using a Plan-Apochromat® 63×/1.4 NA oil-immersion objective. Fluoresceinamine was excited with the 488 nm line of an Ar^+ laser, and Cy5-labeled DNA and BSA conjugated with Alexa Fluor® 594 with a 633 nm HeNe laser. The fluorescence emission of these dyes was recorded with photomultiplier tubes (Hamamatsu R6357) after spectral filtering with a 500-550 nm bandpass filter and a 650 nm longpass filter for fluoresceinamine and Cy5-labeled DNA and BSA-Alexa Fluor® 594, respectively. Images were acquired with maximum pinhole diameters.

Atomic Force Microscopy (AFM). The contact mode AFM measurements were carried out with a NanoScope III multimode AFM (Digital Instruments / Veeco, Santa Barbara, CA) using a 100 μm scanner and microfabricated silicon tips / cantilevers (Nanosensors, Wetzlar, Germany) in ambient atmosphere (ca. 30 % relative humidity, 24ºC temperature) as described in Chapter 4.

7.6 References

1 (a) Blawas, A. S.; Reichert, W. M. *Biomaterials* **1998**, *19*, 959. (b) Mrksich, M.; Whitesides, G. M. *Trends Biotechnol.* **1995**, *13*, 228. (c)Veiseh, M.; Zareie, M. H.; Zhang, M. Q. *Langmuir* **2002**, *2*, 227.

2 (a) Mrksich, M.; Whitesides, G. M. *Annu. Rev. Biophys. Biomol. Struct*. **1996**, *25*, 55. (b) Prime, K. L.; Whitesides, G. M. *Science* **1991**, *252*, 1164.

3 O'Neill, C.; Jordan, P.; Riddle, P.; Ireland, G. *Cell Sci.* **1990**, *95*, 577.

4 Hyun, J.; Zhu, Y. J.; Liebmann-Vinson, A.; Beebe, T. P.; Chilkoti, A. *Langmuir* **2001**, *17*, 6358.

5 (a) Bhatia, S. N.; Yarmush, M. L.; Toner, M. *J. Biomed. Mater. Res.* **1997**, *34*, 189. (b) Hyun, J.; Ma, H.; Zhang, Z.; Beebe, T. P.; Chilkoti, A. *Adv. Mater.* **2003**, *15*, 576.

6 Takayama, S.; McDonald, J. C.; Ostuni, E.; Liang, M. N.; Kenis, P. J. A.; Ismagilov, R. F.; Whitesides, G. M. *Proc. Natl. Acad. Sci. USA* **1999**, *96*, 5545.

7 Ostuni, E.; Kane, R.; Chen, C. S.; Ingber, D. E.; Whitesdes, G. M. *Langmuir* **2000**, *16*, 7811.

8 Jones, V. W.; Kenseth, J. R.; Porter, M. D.; Mosher, C. L.; Henderson, E. *Anal. Chem.* **1998**, *70*, 1233.

9 Khademhosseini, A.; Jon, S.; Suh, K. Y.; Tran, T. T.; Eng, G.; Yeh, J.; Seong, J.; Langer, R. *Adv. Mater.* **2003**, *15*, 1995.

10 de las Heras-Alarcón, C.; Farhan, T.; Osborne, V. L.; Huck W. T. S.; Alexander C. *J. Mater. Chem.* **2005***, 15,* 2089.

11 Bernard, A.; Renault, J. P.; Michel, B.; Bosshard, H. R.; Delamarche, E. *Adv. Mater.* **2000**, *12*, 1067.

12 Inerowicz, H. D.; Howell, S.; Regnier, F. E.; Reifenberger, R. *Langmuir* **2002**, *18*, 5263.

13 Schönherr, H.; Feng, C. L.; Shovsky, A. *Langmuir* **2003**, *19*, 10843.

14 Feng, C. L.; Vancso, G. J.; Schönherr, H. *Adv. Funct. Mater.* **2006**, *in press*.

15 The untreated stamps may have shown irreproducible surface properties as judged from the widely varying printing results for nominally identical conditions.

16 The diameters were estimated as follows: The diameters of rings and circles were determined by measuring the average width of half height of the rings and circles from the corresponding sections of the fluorescent images. The average diameters of halos were measured directly from fluorescent images. As comparison, all the fluorescent images were acquired under the same condition.

17 As comparison with trifluoroacetic acid, for Lactic acid $D \approx 10^{-5}$ cm^2 s^{-1}, see: Nomura, S.; Yang, Y. G.; Inoue, C.; Chida, T. *Anal. Sci.* **2002**, *18*, 1081.

18 Delamarche, E.; Schmid, H.; Bietsch, A.; Larsen, N. B.; Rothuizen, H.; Michel, B.; Biebuyck, H. *J. Phys. Chem. B*. **1998**, *102*, 3324.

19 Xia, Y. N.; Whitesides, G. M. *Angew. Chem., Int. Ed.* **1998**, *37*, 551.

20 Feng, C. L.; Vancso, G. J.; Schönherr, H. *unpublished data*.

21 Gaussier, H.; Morency, H.; Lavoie, M. C.; Subirade, M. *Appl. Environ. Microbiol*. **2000**, *68*, 4803.

22 After printing times of ≥ 5 minutes, no liquid acid was observed on the stamp and the film surface.

23 Bird, R.B.; Stewart, W.E.; Lightfoot, E.N. *Transport Phenomena*. John Wiley & Sons. NY. **1960**, 780.

24 Biebuyck, H. A.; Whitesides, G. M. *Langmuir* **1994**, *10*, 4851.

25 Feng, C. L.; Zhang Y. J.; Jin, J.; Song Y.; Xie, L.; Qu, G.; Jiang, L.; Zhu, D. *Langmuir* **2001**, *19*, 4593.

26 Sheehan, P. E.; Whitman, L. J. *Phys. Rev. Lett*. **2002**, *88*, 156104.

27 Jang, J.; Strat, R. M. *J. Chem. Phys*. **2001**, *115*, 2721.

28 Michel, B.; Bernard, A.; Bietsch, A.; Delamarche, E.; Geissler, M.; Juncker, D.; Kind, H.; Renault, J. P.; Rothuizen, H.; Schmid, H.; Schmidt-Winkel, P.; Stutz, R.; Wolf, H. *IBM J. Res. Dev*. **2001**, *45*, 697.

29 Husemann, M.; Morrison, M.; Benoit, D.; Frommer, J.; Mate, C. M.; Hinsberg, W. D.; Hedrick, J. L.; Hawker, C. J. *J. Am. Chem. Soc*. **2000**, *122*, 1844.

30 (a) Renault, J. P.; Bernard, A.; Juncker, D.; Michel, B.; Bosshare, H. R.; Delamarche, E. *Angew. Chem.; Int. Ed.* **2002**, *41*, 2320. (b) Bruckbauer, A.; Zhou, D. J.; Ying, L. M.; Korchev, Y. E.; Abell, C.; Klenerman, D. *J. Am. Chem. Soc*. **2003**, *125*, 9834.

31 *Polymer Handbook*, 3rd ed. Brandrup, J.; Immergut, E. H. John Wiley & Sons: New York, 1989.

32 Prime, K. L.; Whitesides, G. M. *J. Am. Chem. Soc*. **1993**, *115*, 10714.

33 Kumar, A.; Whitesides, G. M. *Appl. Phys. Lett*. **1993**, *63*, 2002.

Chapter 8

Nanofabrication on Reactive Block Copolymer Film Platforms: Towards Microdomain-Selective Chemical Functionalization*

The surfaces of polystyrene-b-poly(t-butyl acrylate) (PS_{690}-b-$PtBA_{1210}$) ultrathin films were restructured using cyclohexane as selective solvent. As revealed by AFM and spectroscopic techniques, the surface exposed PtBA islands in a matrix of unreactive PS. Covalent attachment of amino functionalized (bio)molecules, following hydrolysis with trifluoroacetic acid and activation with NHS/EDC, confined to the nanodomains was successful as analyzed by fluorescence microscopy. The domain selective immobilization of molecules was also investigated on the nanometer scale by AFM force volume mapping. The combination of solvent treatment and subsequent reactive μCP afforded films patterned on multiple length scales with bovine serum albumin (BSA). Finally, the feasibility of local delivery and covalent coupling of molecules on chemically activated PS-b-PtBA by transferring dendrimers onto block copolymer films by dip-pen nanolithography was demonstrated. Thereby the groundwork for a future extension of these block copolymer platforms for the development of array-based screening formats with ultrahigh information content, as well as tailored biointerfaces for cell-surface studies, has been laid.

8.1 Introduction

Microphase separated block copolymers represent a very versatile class of materials for generating functional nanoscopic structures, as discussed also in Chapter 2. Compared to top-down structuring and patterning methods, such as optical, electron beam or other lithographies, the bottom-up self-assembly route offers a number of advantages, including spontaneous structure formation on programmable length scales down to the nm size regime. However, it has been realized that control of both the orientation and lateral ordering of the nanoscopic domains is essential to fully realize the potential of these materials. This requires the use of external fields, such as electric fields,[1] mechanical shear,[2] temperature gradients,[3] crystallization,[4] or the use of prepatterned substrates (graphoepitaxy).[5] For various possible future applications, block copolymer films should constitute what may be called a nanoperiodic chemically functionalized surface, i.e., a heterogeneous surface exhibiting an ordered array of nanoscopic areas of different chemical composition and thus different chemical reactivity.[4]

Such nanoperiodic chemically functionalized surfaces have been reported primarily for polystyrene-b-poly(methyl methacrylate) (PS-b-PMMA) systems owing to the similarity of the surface tensions of the two blocks.[6] Lopes et al. successfully deposited gold nanoparticles on PS-*b*-PMMA

---

* Part of the work described in this chapter has been published in: Schönherr H.; Feng C. L.; Tomczak, N.; Vancso G. J. *Macromolecular Symposia*. **2005**, *in press*.

diblock copolymer scaffolds.[7] Morkved et al. also discussed the mesoscopic self-assembly of gold nanoparticles on symmetric PS-*b*-PMMA and asymmetric PS-*b*-P2VP.[8] In addition, very recently spin-coated block copolymer films have been used to control the deposition of proteins and other biomolecules on nanometer length scales.[9] Kumar et al. exploited unspecific interactions (physisorption) to immobilize various proteins on microphase-separated domains of PS-*b*-PMMA ultrathin films. However, since the biomolecules are bound only via weak unspecific interactions, these assemblies can be expected to be unstable.

As sketched in the introductory chapters, nanoperiodic chemically functionalized surfaces could also be exploited in conjunction with scanning probe lithography (SPL) approaches[10] to prepare platforms for screening of (bio)molecular interactions,[11] surface reactions,[12] and cell-surface interactions,[13] among other possible applications. Two possible advantages can be considered for these patterned nanoreactive PtBA platforms compared to further miniaturized reactive microcontact printing (following the approaches discussed in Chapter 7 to smaller stamp features), if ultimately nanometer precision is required for such arrays:

a) The immobilization of (bio)molecules is confined to the nanoreactive PtBA islands, thereby the pattern is defined by the template structure of the reactive film;

b) Compared to nanospotting[14] or nanocontact printing[15] on unpatterned films, diffusion may be better controlled because of the inert PS matrix around the reactive islands.

The reactivity of the PtBA block has been treated in detail in various preceding chapters and the combination of these versatile and robust platforms with top-down patterning methodologies (reactive microcontact printing) showed that patterns down to the 300 nm range can be fabricated. However, in these experiments the inherent microphase separation of diblock copolymers has not been utilized. In fact, reactions were carried out on the PtBA skin layer. For the creation of chemically functionalized surfaces with periodicities on the sub-100 nm length scale, the microphase separation of these diblock copolymers will be exploited. Hence in this final experimental chapter, the first steps towards the fabrication of such platforms based on ultrathin films of PS_{690}-b-$PtBA_{1210}$ diblock copolymers will be described and future directions, e.g. via implementation of scanning probe lithographic approaches, will be indicated.

8.2 Solvent Induced Surface Reorientation of PS-b-PtBA Films

The conventional film preparation of spin-coating and annealing results for the PS_{690}-b-$PtBA_{1210}$ diblock copolymer system on glass and oxidized silicon in the formation of a PtBA skin layer (Chapter 3). Due to the balance of interfacial energies symmetric wetting is observed. Thus, in order to expose both blocks at the film - air interface and to obtain the desired nanoperiodic chemically functionalized surface, a solvent treatment procedure was used. By applying a selective solvent for the PS block,

which is not exposed at the surface of the as-prepared films, via a PDMS stamp, as shown in Figure 8.1, a surface can be obtained that exposes both blocks.

For this purpose ultrathin PS_{690}-b-$PtBA_{1210}$ copolymer films (d = 100 ± 5 nm) were first spin-coated onto a flat silicon (or glass) substrate.[16] Cyclohexane, which is a non-solvent for PtBA and a better solvent for PS (even though it is not more than a marginal solvent), was then applied onto a featureless PDMS stamp. This stamp was brought into contact with the block copolymer film surface. Owing to the selectivity of the solvent and the concomitant restructuring of the film, as a consequence of swelling and solvent evaporation, both blocks were exposed.

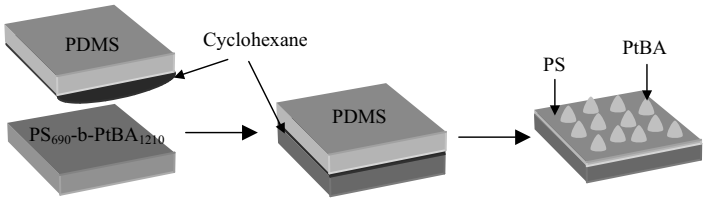

Figure 8.1. Schematic of the selective solvent treatment procedure applied to PS_{690}-b-$PtBA_{1210}$ films.

Since cyclohexane is a better solvent for PS, the film - stamp interface will be enriched in the minority phase of the block copolymer , i.e. PS. Even though cyclohexane is a bad solvent for PtBA, it swells the polymer and depresses T_g to below ambient temperatures.[17] Due to its poor solubility, the majority phase will solidify first upon removal of the stamp and the concomitant solvent evaporation. The PS phase still contains some solvent and will therefore continue to shrink until T_g > 20°C.[18] Consequently, a surface morphology as shown in Figure 8.1 is obtained, in which the PtBA block forms (reactive) islands with a diameter of ~ 50 nm in a non-reactive PS matrix. Similar block copolymers, in which PS was the majority phase, did not show similar defined patterns. Following hydrolysis and NHS activation, the PtBA islands can be used to covalently immobilize amino functionalized molecules.

The changes in the film surface composition induced by the treatment were already reported in Chapter 3. Based on evidence from XPS and contact angle measurements with diiodomethane as a probe liquid, PS and PtBA were concluded to coexist on the film surface.[16]

The morphology of the polymer films was further investigated with intermittent contact mode atomic force microscopy (AFM), as shown in Figure 8.2. After annealing PS_{690}-b-$PtBA_{1210}$ film at 130ºC, a microphase separated film was observed with in plane cylindrical structures (Figure 8.2 a, b). The equilibrium domain spacing calculated based on the AFM data was 80 ± 5 nm. After the cyclohexane solvent treatment, the surface morphology was characterized by an irregular pattern of protrusions (Figure 8.2c, d), which had typical heights of ~ 4 nm, diameters of 50 ± 5 nm, and a mean separation distance of 80 ± 5 nm.

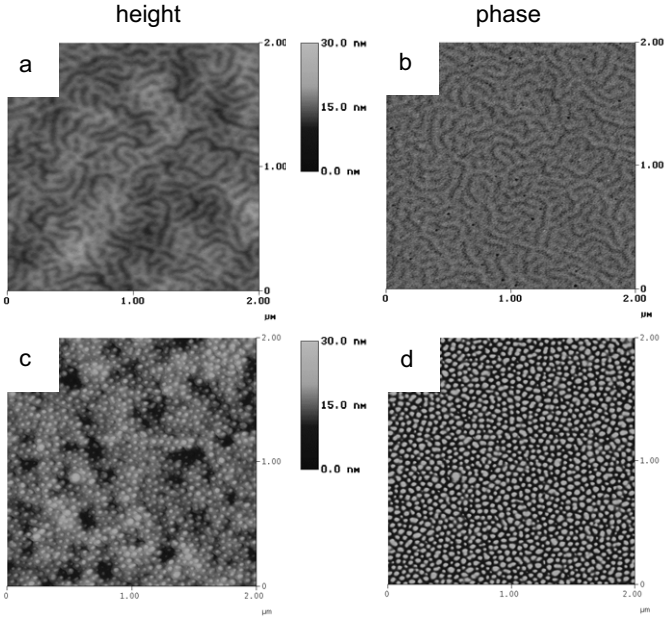

Figure 8.2. Tapping mode AFM images of spin-coated PS_{690}-b-$PtBA_{1210}$ films: (a) Height and (b) phase images acquired for polymer films after annealing in vacuum at 130°C; (c) Height and (d) phase images acquired for polymer films after cyclohexane treatment and drying.

The surface area covered by the phase with bright phase contrast in the AFM images ($\chi \sim 0.55$) showed a clear correspondence with the surface composition by XPS (surface coverage χ(PtBA) ~ 0.60, see Chapter 3). Similarly, the hydrolysis kinetics (see also Chapter 3) were in favorable agreement with the interpretation that in the cyclohexane-treated films *both* blocks are exposed at the surface and that PtBA is located inside the nanodomains seen in Figure 8.2.

8.3 Domain Selective Coupling on Solvent Treated Polymer Films

The results of section 8.2 indicate that PtBA is exposed in the form of isolated islands (nanodomains) in a matrix of chemically inert PS. This film morphology would imply that it is in principle possible to perform surface chemical reactions inside these domains.

8.3.1 Global Characterization of Domain Selective Coupling

Domain-selective hydrolysis reactions of PS_{690}-b-$PtBA_{1210}$ films have been already characterized on a global level by using infrared spectroscopy and contact angle measurements (Chapters 3 and 5). Here we will focus on the domain selective coupling of amino-functionalized molecules to hydrolyzed and subsequently NHS ester activated PS_{690}-b-$PtBA_{1210}$ films.

PS_{690}-b-$PtBA_{1210}$ polymer films were first hydrolyzed using trifluoroacetic acid and then activated with NHS/EDC. After coupling of fluoresceinamine, fluorescence microscopy was used to assess the

coverage of fluorescent adsorbate. As shown in Figure 8.3, the neat film exhibited more intense fluorescence emission compared to the solvent treated film. From the corresponding intensity histograms it can be seen that the fluorescence emission intensity of the solvent treated film is lower by a factor of 3/5 compared to the neat block copolymer films. This result is in good agreement with the surface coverages assessed based on XPS investigations (Chapter 3), as well as the AFM data shown above. The surface coverages do not appear to have changed significantly during the wet chemical derivatization reactions.

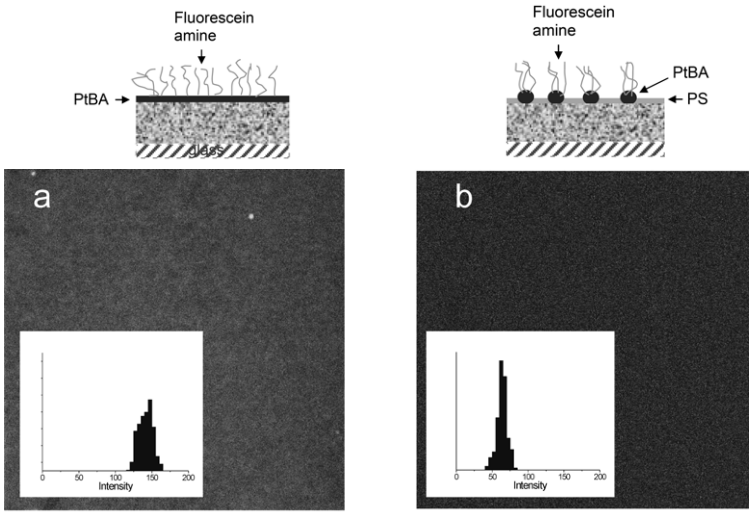

Figure 8.3. Fluorescence microscopy images (146 μm x 146 μm; insets: intensity histograms) of (a) PS_{690}-b-$PtBA_{1210}$ film following hydrolysis, activation with EDC/NHS, and coupling with fluoresceinamine. (b) PtBA film following cyclohexane treatment, hydrolysis, activation by EDC/NHS, coupling with fluoresceinamine.

However, these results should not be over-interpreted as there may be several factors that could cancel each other, such as film restructuring (leading to increased exposed surface areas) vs. incomplete chemical derivatization reactions (activation with NHS and / or fluoresceinamine coupling). In addition, due to lack of spatial resolution of the methods applied, little is known about the homogeneity of the reactions on the length scale defined by the dimensions of the domains.

8.3.2 Characterization of Domain Selective Coupling on the Nanometer Level

The analysis of the extent and homogeneity of surface chemical reactions on the nanometer level is certainly a significant challenge that needs to be resolved in order to successfully fabricate and analyze platforms for screening of (bio)molecular interactions, surface reactions, etc. Chemical force microscopy (CFM)[19] may comprise an approach to address this challenge. Other methods, including small area mass spectrometry (nano SIMS)[20] or more advanced AFM techniques may contribute to solving these and related issues in the future.[21]

As a scanning probe technique, CFM combines chemical discrimination with the high spatial resolution of SFM by exploiting the forces between the tip and the surface.[22] This is realized by the acquisition of pull-off forces as a function of precise lateral displacement. In position-resolved force measurements one can take full advantage of the high-resolution microscopic nature of experiment and thus obtain novel insight into forces and adhesive properties on nanometer scale that can be translated into local (chemical) compositions.

For this purpose, pull-off forces were measured in so-called force volume (FV) images[23] for solvent treated PS_{690}-b-$PtBA_{1210}$ polymer films at various stages of the sequential derivatization. The results are illustrated in Figure 8.4, where representative force volume images are shown. In Figure 8.4 a and b, the microdomain structure of the solvent treated film and the low pull-off forces measured on top of these domains (compared to the PS matrix) are displayed. The domains of low pull-off force observed corresponded systematically to the islands in the height image, as indicated by the circles. After hydrolysis with trifluoroacetic acid, the force images showed a significant increase in pull-off force (Figure 8.4c and d). The islands showed higher pull-off force compared to the PS matrix. Finally, after the covalent immobilization of fluoresceinamine or n-butyl amine (following the activation with NHS) on the films, domains with relatively low pull-off forces were observed.

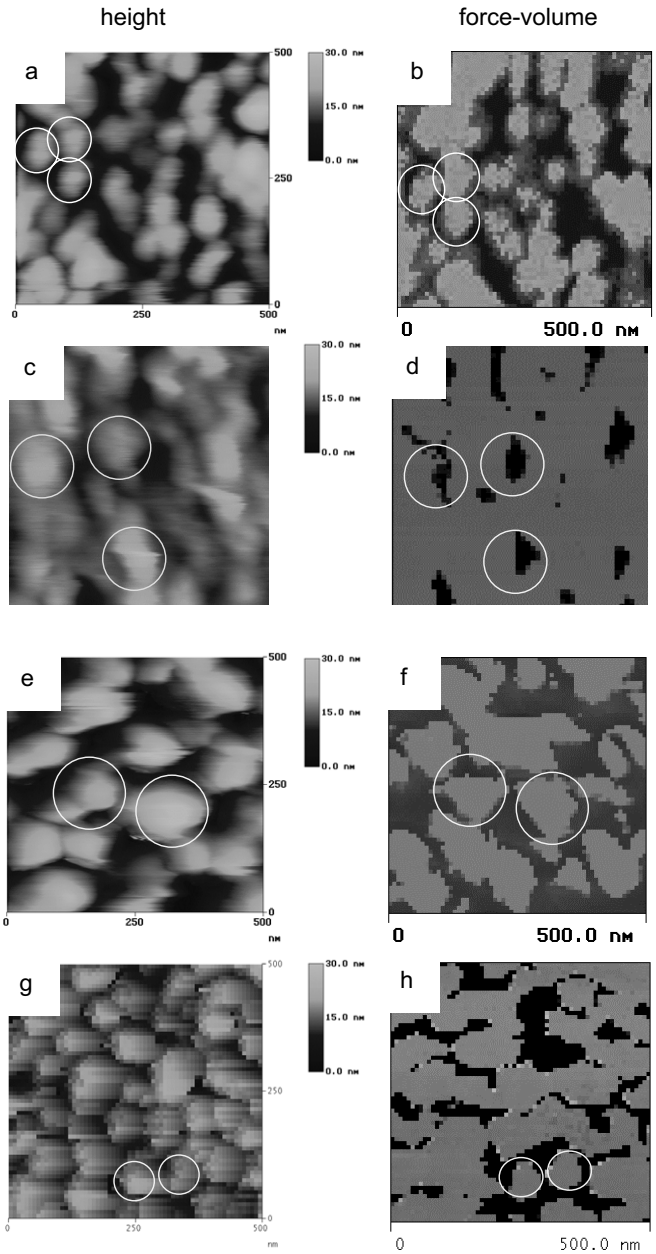

Figure 8.4: (a) AFM height and (b) FV images (500 nm x 500 nm) of the cyclohexane-treated PS_{690}-b-$PtBA_{1210}$ polymer films; (c) AFM height and (d) FV images of the cyclohexane-treated PS-b-PtBA polymer films after hydrolysis; (e) AFM height and (f) FV images of the cyclohexane-treated PS-b-PtBA polymer films after hydrolysis, reactivation by NHS/EDC and grafting of fluoresceinamine; (g) AFM height and (h) FV images of the cyclohexane-treated PS-b-PtBA polymer films after hydrolysis,

reactivation by NHS/EDC and grafting of n-butyl amine. All data has been acquired with a Si_3N_4 probe tip in air. By convention, the bright areas in the FV images correspond to low pull-off forces (several protruding circular areas have been marked with circles to guide the eyes). Slight off-sets between the height and FV images are the result of the sometime unavoidable sequential data acquisition.

Very similar observations were made in AFM friction measurements, as shown in Figure 8.5. While for the unreacted block copolymer films, following the solvent treatment, low friction forces were observed in areas associated with the circular domains of PtBA, the friction forces were higher compared to the PS matrix after hydrolysis with trifluoroacetic acid. After coupling fluoresceinamine (or n-butyl amine), the friction forces of the matrix were large than those observed inside the domains.

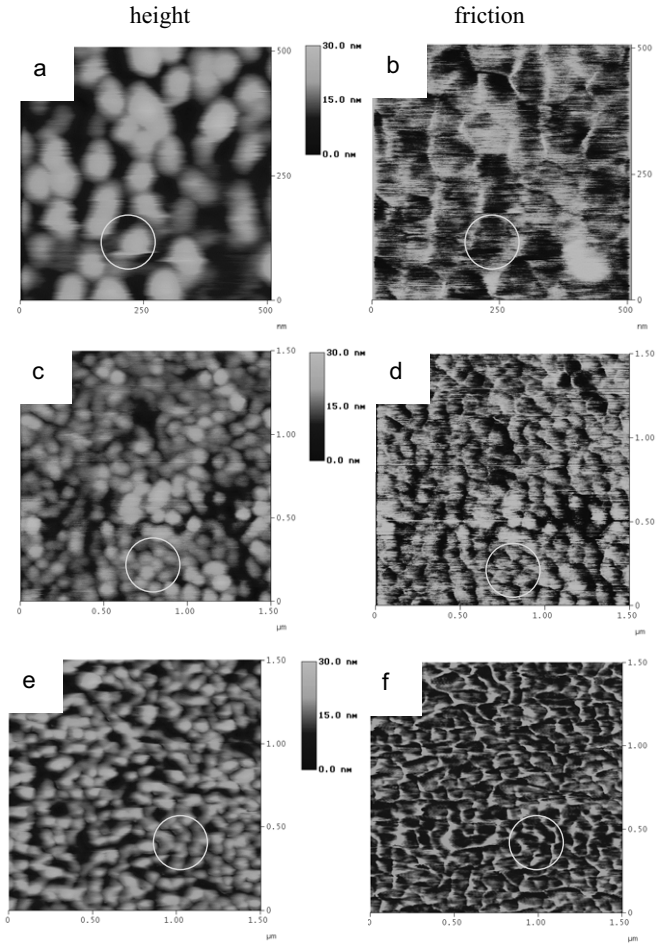

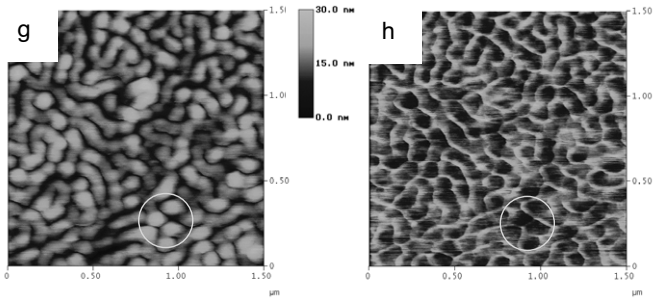

Figure 8.5. Height and friction force images are obtained simultaneously by contact mode AFM. (a) and (b) PS_{690}-b-$PtBA_{1210}$ films after cyclohexane treatment; (c) and (d) Cyclohexane treated PS_{690}-b-$PtBA_{1210}$ with hydrolysis by trifluoroacetic acid (10 min); (e) and (f) hydrolyzed films with fluoresceinamine coupling; (g) and (h) hydrolyzed films with n-butyl amine coupling. Friction forces scale from dark (low friction forces) to bright contrast (high friction forces).

Based on these observations, we attribute the changes in local pull-off and friction forces on the islands (with respect to the matrix) to the different surface composition induced by the chemical modification.[24] PS, as matrix for all the cases, has a surface tension of $\gamma = 40.9$ mN/m.[25] This value is higher than that of the PtBA block ($\gamma = 30.7$ mN/m), but lower than that of the PAA block.[25] Fluoresceinamine and n-butyl amine can be expected to be hydrophobic,[26] thus leading to the lowest surface energy surfaces. Consequently, the changes of pull-off forces F on the islands and domains can be ranked according to this ranking of surface tensions:[27]

$$F(\text{n-butyl amine}) \approx F(\text{fluoresceinamine}) \leq F(\text{PtBA}) < F(\text{PS}) << F(\text{PAA})$$

A more detailed insight into the surface derivatization in this heterogeneous system was obtained from a quantitative analysis of the FV images using a custom-made software. As shown in Figures 8.6 and 8.7, the pull-off force maps were locally not homogeneous.

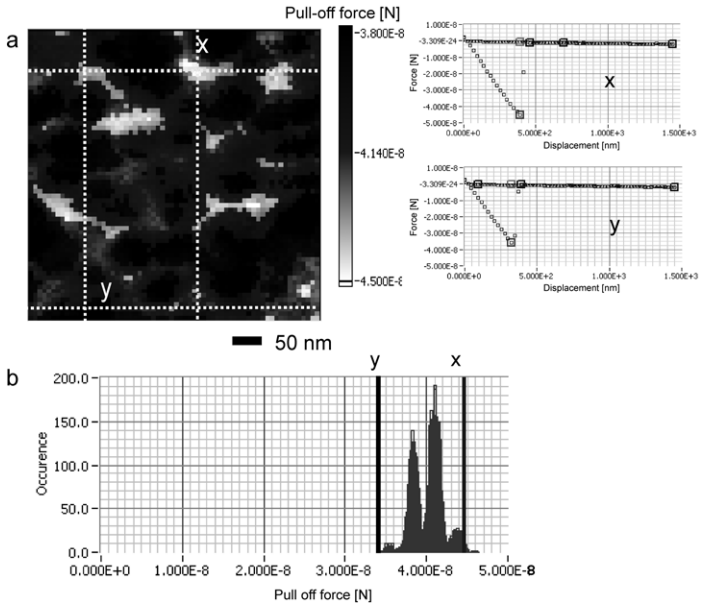

Figure 8.6. (a) Pull-off force map (500 nm x 500 nm, forces increase from dark to bright contrast) and two representative f-d curves (the position of these curves labeled x and y is located at the crossing of the corresponding dotted lines) of cyclohexane-treated PS_{690}-b-$PtBA_{1210}$ polymer films calculated from the FV data, such as shown in Figure 8.4. (b) Pull-off force distribution (again the data points x and y refer to the ones schematically indicated in (a)).

While we observed a multimodal pull-off force distribution (and a qualitatively very similar distribution of the adhesion hysteresis, data not shown) with pull-off forces around 40 nN for the hydrolyzed films, the derivatization with fluoresceinamine inside the PtBA nanodomains led to a broadening of the distribution. In this case the maximum of the distribution was shifted to ~ 7 nN and a long tail was observed towards higher pull-off force values. Also for the fluoresceinamine-derivatized films, the distribution of the adhesion hysteresis looked qualitatively very similar to the pull-off force distribution.

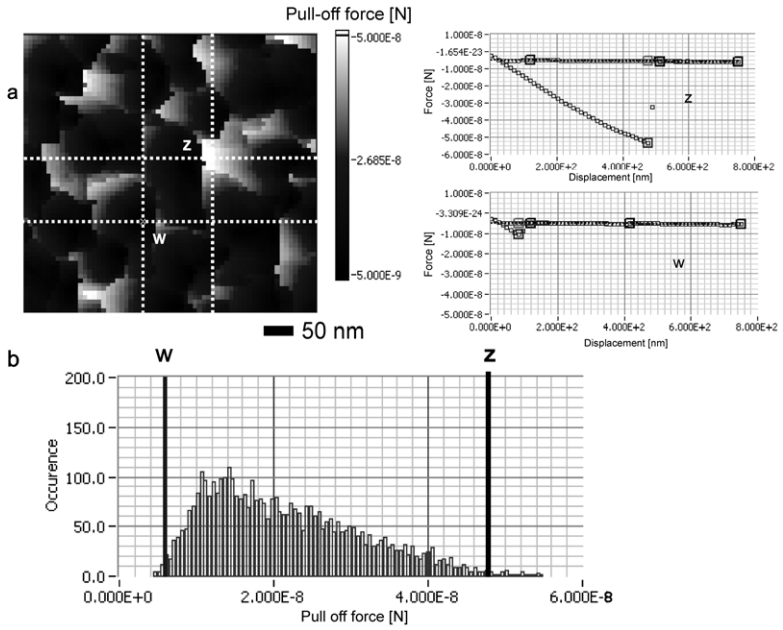

Figure 8.7. (a) Pull-off force map (500 nm x 500 nm, forces increase from dark to bright contrast) and two representative f-d curves (the position of these curves labeled z and w is located at the crossing of the corresponding dotted lines) of cyclohexane-treated PS_{690}-b-$PtBA_{1210}$ polymer films after hydrolysis, activation by NHS/EDC and grafting of fluoresceinamine calculated from the FV data, such as shown in Figure 8.4. (b) Pull-off force distribution (again the data points z and w refer to the ones schematically indicated in (a)).

These pull-off force distributions reflect on the one hand the surface chemistry, i.e. the different relative coverages of the functionalized polymer film surface (PtBA phase vs. PS phase and fluoresceinamine-derivatized areas vs. PS phase, respectively), on the other hand they show the lateral heterogeneity of the different surface chemistries. The differences between PtBA and PS are small, although the highest pull-off force values were observed for the PS matrix (e.g. point x in Figure 8.6), consistent with the higher surface energy of PS compared to PtBA leading to a higher work of adhesion. The covalently attached fluoresceinamine rendered the PtBA nanodomains hydrophobic, thus the low pull-off forces are associated with the fluoresceinamine-rich nanodomains (e.g. point w in Figure 8.7).

All data have been acquired in air using an unmodified, yet chemically distinct, silicon nitride tip. In order to map and evaluate the lateral chemical composition of these films quantitatively, CFM experiments under carefully controlled conditions (incl. drift control) with an increased number of data points averaged in time (for each position) and in plane are required. This kind of analysis is in principle possible, but has not been performed yet.

8.4 Area-Selective Functionalization of Block Copolymer-Based Nanopatterned Platforms

The above mentioned combination of top-down and bottom-up methodologies has been attempted in first feasibility studies that aimed at the area-selective functionalization of the PtBA-b-PS block copolymer platforms.

First, the area-selective immobilization of a protein (BSA) by covalent coupling from solution on solvent treated and subsequently activated / passivated films using reactive microcontact printing (μCP) has been investigated by fluorescence microscopy. The experimental procedure is schematically shown in Figure 8.8a. The solvent treated PS_{690}-b-$PtBA_{1210}$ films were hydrolyzed and then activated with NHS/EDC. By reactive μCP, amino functionalized poly(ethylene glycol) ($PEG_{500}NH_2$) was transferred onto the NHS functionalized surface. Finally, this film was immersed into a buffer solution of BSA (Figure 8.8b). No fluorescence emission of the PEG passivated matrix was detected, while a pattern of circular features with pronounced fluorescence emission was clearly observed. The FV image (Figure 8.8d) provides evidence for a non-uniform surface functionality of the films on the nanometer scale, which is consistent with the notion of domain-selective protein functionalization. On the other hand, BSA can physisorb to a limited extent on PS. This effect was quantified by fluorescence microscopy (Figure 8.8e, f). As can be concluded from the fluorescence emission intensity histograms, the coverage on the activated nanostructured areas is by a factor of 4 - 5 higher compared to PS. Hence, since BSA was found to adsorb only little via physisorption onto PS, the covalent coupling was concluded to occur predominantly selectively inside the 50 nm sized nanodomains. In principle, the non-specific adsorption on the PS areas can be suppressed by masking the exposed PS using PEO-based block copolymer (Pluronics) treatments.[28]

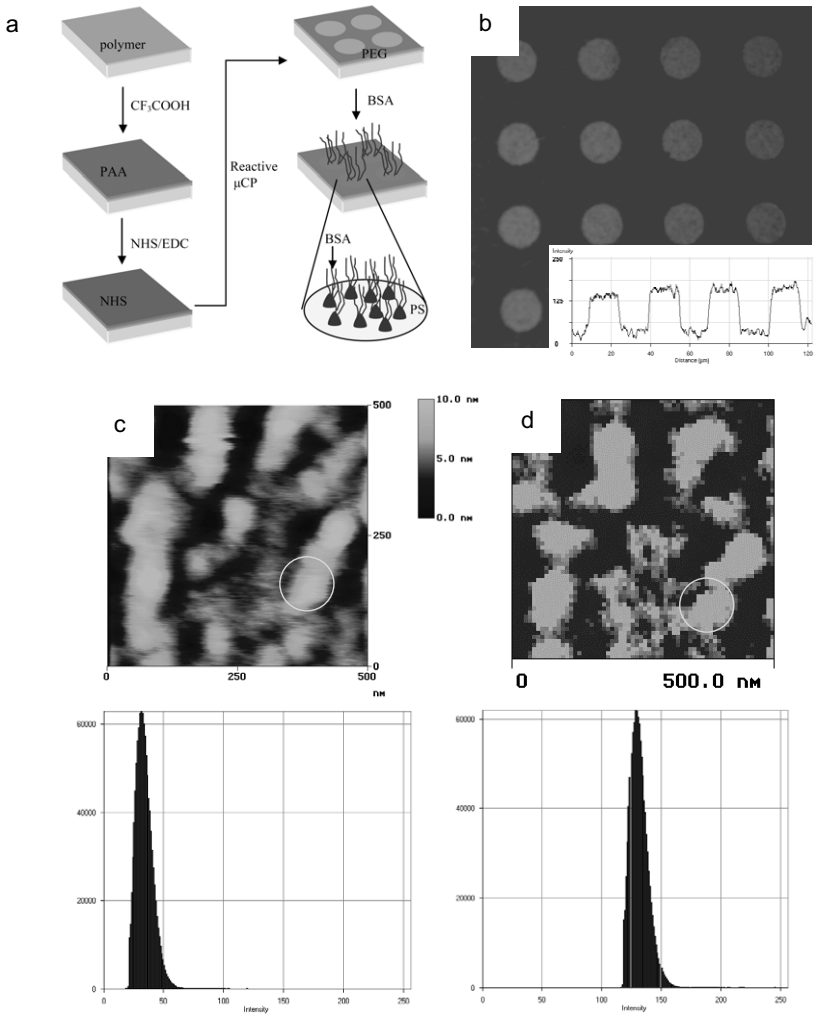

Figure 8.8. (a) Schematic of film fabrication: Solvent treated PS_{690}-b-$PtBA_{1210}$ films were hydrolyzed using CF_3COOH, followed by activation with NHS/EDC. A PEG_{500} blocking layer was transferred on the film by reactive μCP. Finally, dye labeled BSA molecules were backfilled on the PEG pre-patterned film from buffer solution. (b) Corresponding fluorescence micrograph (and cross sectional intensity profile) captured after BSA coupling and thorough rinsing. (c) AFM height and (d) FV images of the cyclohexane-treated PS-b-PtBA polymer films after hydrolysis, reactivation by NHS/EDC and grafting of BSA. The slight off-set between the height and FV images is the result of the sequential data acquisition. By convention, the bright areas in the FV images correspond to low pull-off forces (circular areas have been marked with circles to guide the eyes). Fluorescence emission

intensity histograms for (e) BSA physisorbed on polystyrene and (f) BSA covalently coupled on solvent treated and subsequently activated polymer films.

The fabrication of smaller patterns, in particular on the length scales defined by the domain size and spacing, could not be accomplished by reactive μCP due to the lack of suitable stamps. In addition, it is unlikely that diffusion can be neglected at these length scales (comparing with Chapter 7). To demonstrate the feasibility of a combined scanning probe lithography [29] (top-down) - nanopatterned block copolymer films (bottom-up) approach to realize nanoscale platforms for screening of (bio)molecular interactions, surface reactions, etc., dip pen nanolithography (DPN)[30] was explored on hydrolyzed and NHS activated PS_{690}-b-$PtBA_{1210}$ films.

DPN is a method for directly depositing molecules from an "ink"-coated AFM tip onto a substrate of interest. In analogy to the inked-nib classical writing, this technique uses the AFM tip as a "nib," a chemically well-defined surface as "paper" (usually a solid state substrate), and molecules with a chemical affinity for the surface as the "ink". The patterning process in a DPN experiment comprises two main processes. The first step is molecular transport from the tip to substrate, involving dissolution of ink molecules into the meniscus that spontaneously forms between the tip and substrate. The second step is ink adsorption (physical or chemical) onto the surface, and consequent (mono)layer formation. Both the transport and adsorption of ink molecules often depend on several variables, including temperature, humidity, writing speed of the AFM tip, the physicochemical properties of the ink and surface, among others.

To facilitate the independent analysis and to control the diffusion of the molecular ink,[31,32] generation 5 polyamidoamine (G5 PAMAM) dendrimers were deposited. Each of these dendrimer molecules possess 128 primary amino groups at its periphery. Similar to previously reported work on NHS-functionalized SAMs,[33] the deposited dendrimers were detected by friction mode AFM as low friction areas compared tom the unfunctionalized matrix (Figure 8.9).

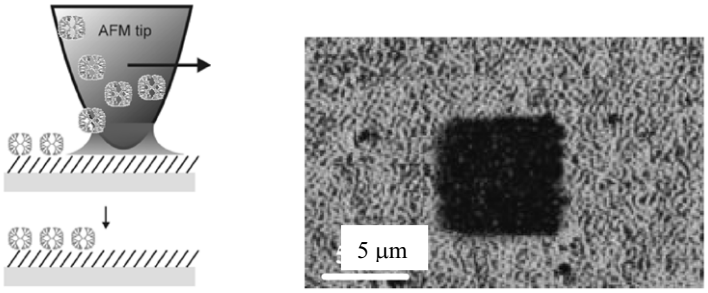

Figure 8.9. Schematic of DPN process and AFM friction force image of square shaped feature of G5 PAMAM dendrimers deposited by DPN on top of a NHS-functionalized PS-b-PtbA film.

Fluorescence labeling of the dendrimers and the subsequent observation of fluorescent patterns helped to ensure that dendrimers were deposited.[31] In addition, for densely covered areas on NHS SAMs, the dendrimers could be directly visualized by AFM.[31] The dendrimers were observed to be bound tightly to the block copolymer matrix and did not diffuse across the surface, suggesting that the coupling is covalent in nature. Using DPN under controlled humidity conditions, structures as small as 150 nm could be deposited by DPN (Figure 8.10). Diffusion experiments, according to the method described by various authors did not show circular features, which implies that the diffusion of G5 PAMAM dendrimers on these reactive platform (or rather dendrimer molecules over each other) is very slow and hence that it should be possible, in the future, to deposit few or even isolated dendrimer molecules to reactive islands obtained by the solvent treatment procedure discussed above.

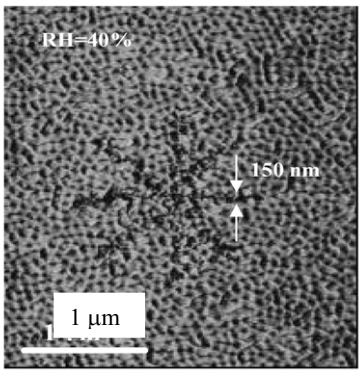

Figure 8.10. AFM friction force image of DPN-patterned G5 PAMAM dendrimers on top of a NHS-functionalized PS-b-PtbA film.

In summary, nanopatterns obtained by a selective solvent treatment-induced film restructuring of PS_{690}-b-$PtBA_{1210}$ films can be deprotected by hydrolysis and derivatized by covalent coupling reactions with a range of amino functionalized (bio)molecules. Combined with reactive microcontact printing and dip-pen nanolithography techniques, it was shown that area-selective functionalization of nanopatterned block copolymer films with biomolecules may become possible in the near future. Therefore the polymer thin film platforms investigated herein will likely provide the opportunity to study a broad variety of surface-mediated biological recognition processes.

8.5 Outlook

As outlined in the introductory chapters, the combination of “bottom-up” self-assembly approaches and “top-down” lithographic and scanned probe based techniques may contribute to the development of future generations of biosensors, genomics and proteomics platforms,[34] fundamental cell biology research,[35] as well as pharmaceutical screening processes and panel immunoassays.[36] The basic aspects of "functional biointerfaces" based on two novel polymeric thin film systems have been tested and the requirements identified have been in large parts successfully implemented. Even though

the rigorous testing using a large range of proteins and different types of cells was not within the scope of this thesis, as were detailed investigations of complementary bioconjugation schemes, such as those summarized in Chapter 2, the concept of combined bottom-up / top-down array approach based on the self-assembly of block copolymers has been shown to be a viable route. Future work certainly needs to address these issues, as well as a range of other open questions, which include the formation of block copolymer platforms that expose the two blocks at the surface, preferentially under conditions of thermodynamic equilibrium. Long range order of the domains, site selective derivatization and analysis and in particular massively parallel processing are further aspects that will require focussed attention, if these approaches are to be developed further. Besides these targeted aspects, the results may contribute to help solving parts of the problems associated with today's DNA and bio chip technologies that are, contrary to common belief, not yet fully established and approved.

8.6 Experimental Section

Materials: PS_{690}-*b*-$PtBA_{1210}$ diblock copolymer was purchased from Polymer Source Company (Dorval, Canada) and was used as received. The molar mass and polydispersity are 202.4 kg/mol and 1.03, respectively. Cyclohexane (Aldrich) and fluoresceinamine (Molecular Probes) were used as received. Bovine serum albumin (BSA) with Alexa Fluor®594 conjugate was bought from Molecular Probes and used as received.

Preparation of Thin Films. Thin polymer films were prepared by spin-coating polymer solutions in toluene (typical concentration between 10 and 20 mg/ml) onto silicon wafers (111) or glass (cover slide from Menzel-Glaser), which were previously cleaned by an oxygen plasma using an Elektrotech PF 340 apparatus (Pressure of O_2: 0.5 Bar; Current: 30 mA). All spin-cast samples were dried at room temperature for 24 hours in vacuum before analysis. The film thickness determined by ellipsometry (details see Chapter 5) was 100 ± 5 nm.

Solvent Treatment of Thin Films. Cyclohexane was used to enrich the surface in PS by placing a cross-linked poly(dimethylsiloxane) (PDMS) slab previously soaked in cyclohexane onto the polymer surface.[22,37] After 3 hrs contact treatment, the PDMS was removed and the samples were stored overnight in vacuum.

Chemical modification. A drop of trifluoroacetic acid (50 µL) was applied on the solvent treated films. The films obtained were activated by immersion in an aqueous solution of 1-ethyl-3-(dimethylamino)-propylcarbodiimide (EDC, 1 M) and N-hydroxysuccinimide (NHS, 0.2 M) for 30 min. The films were immersed inside fluoresceinamine solution (100 µM, PB, pH = 7.4). Then the samples were taken out, rinsed with PB and Milli-Q water, and dried in a stream of nitrogen. Finally, the samples were dried inside a vacuum oven for 1 day before the fluorescence microscopy experiments.

Atomic Force Microscopy (AFM). The contact mode AFM measurements were carried out with a NanoScope III multimode AFM (Digital Instruments / Veeco, Santa Barbara, CA) using a 100 µm scanner and microfabricated silicon tips / cantilevers (Nanosensors, Wetzlar, Germany) in ambient atmosphere (ca. 30 % relative humidity, 24ºC temperature), as described in references 12, 16, and 22. For laterally resolved pull-off force measurements, the AFM was operated in the FV mode using a 10

μm scanner. All FV measurements were performed in air. Arrays of 64 × 64 points^2 (4096 consecutive force – distance measurements) were acquired on at least six different locations on each sample using sizes of 0.5 × 0.5 μm^2 or 1.0 × 1.0 μm^2. DPN was carried out as described in reference[38]

Fluorescence Microscopy: Fluorescence Microscopy. The fluorescence microscopy data was obtained using a Zeiss LSM 510 confocal fluorescence microscope with a BP 500-550 IR filter for fluoresceinamine, as described in Chapter 4.

8.7 References

1 Morkved, T. L.; Lu, M.; Urbas, A. M.; Ehrichs, E. E.; Jaeger, H. M.; Mansky, P.; Russell, T. P. *Science* **1996**, *273*, 931.

2 Albalak, R. J.; Thomas, E. L.; Capel, M. S. *Polymer* **1998**, *38*, 3819.

3 Bodycomb, J.; Funaki, Y.; Kimishima, K.; Hashimoto, T. *Macromolecules* **1999**, *32*, 2075.

4 Reiter, G.; Castelein, G.; Hoerner, P.; Riess, G.; Blumen, A.; Sommer, *J. Phys. Rev. Lett*. **1999**, *83*, 3844.

5 (a) Cheng, J. Y.; Ross, C. A.; Thomas, E. L.; Smith, H. I. Vancso, G. J. *Appl. Phys. Lett*. **2002**, *81*, 3657. (b) Segalman, R. A.; Yokoyama, H.; Kramer, E. J. *Adv. Mater*. **2001**, *13*, 1152.

6 Zehner, R. W.; Lopes, W. A.; Morkved, T. L.; Jaeger, H.; Sita, L. R. *Langmuir* **1998**, *14*, 241.

7 Lopes, W. A.; Jaeger, H. M. *Nature* **2001**, *414*, 735.

8 Morkved, T. L.; Jaeger, H. M.; Grier, D. G.; Witten, T. A. *Appl. Phys. Lett*. **1994**, *64*, 422.

9 Kumar, N.; Hahm, J. *Langmuir* **2005**, *21*, 6652.

10 (a) Kramer, S.; Fuierer, R. R.; Gorman, C. B. *Chem. Rev.* **2003**, *103*, 4367. (b) Wouters, D.; Schubert, U. S. *Angew. Chem. Int. Ed.* **2004**, *43*, 2480. (c) Liu, G. Y.; Xu, S.; Qian, Y. L. *Acc. Chem. Res.* **2000**, *33*, 457.

11 Gong, P.; Grainger, D. W. *Surf. Sci.* **2004**, *570*, 67 and references herein.

12 Schönherr H.; Feng C. L.; Shovsky A. *Langmuir* **2003**, *19*, 10843.

13 Arnold, M.; Cavalcanti-Adam, E. A.; Glass, R.; Blummel, J.; Eck, W.; Kantlehner, M.; Kessler, H.; Spatz, J. P. *Chemphyschem* **2004**, *5*, 383.

14 Deladi, S.; Tas, N. R.; Berenschot, J. W.; Krijnen, G. J. M.; de Boer, M. J.; de Boer, J. H.; Peter, M.; Elwenspoek, M. C. *Appl. Phys. Lett.* **2004**, *85,* 5361.

15 (a) Li, H. W.; Kang, D. J.; Blamire, M. G.; Huck, W. T. S. *Nano Lett.* **2002**, *2*, 347. (b) Li, H. W.; Muir, B. V. O.; Fichet, G.; Huck, W. T. S. *Langmuir* **2003**, *19*, 1963.

16 Feng, C. L.; Vancso, G. J.; Schönherr, H. *Langmuir* **2005**, *21*, 2356.

17 This phenomenon can be exploited for capillary force lithography using a cyclohexane soaked stamp. Sets of lines with repeat distances down to 300 nm lines have been fabricated (no data shown).

18 Elbs, H.; Fukunaga, K.; Stadler, R.; Sauer, G.; Magerle, R.; Krausch, G. *Macromolecules* **1999**, *32*, 1204.

19 (a) Frisbie, C. D.; Rozsnyai, L. F.; Noy, A.; Wrighton, M. S.; Lieber, C. M. *Science* **1994**, *265*, 2071. (b) Noy, A.; Vezenov, D. V.; Lieber, C. M. *Annu. Rev. Mater. Sci.* **1997**, *27*, 381. (c) Thomas, R. C.; Tangyunyong, P.; Houston, J. E.; Michalske, T. A.; Crooks, R. M. *J. Phys. Chem.* **1994**, *98*, 4493. (d) Green, J. B. D.; McDermott, M. T.; Porter, M. D.; Siperko, L. M. *J. Phys. Chem.* **1995**, *99*, 10960. (e) Thomas, R. C.; Houston, J. E.; Crooks, R. M.; Kim, T.; Michalske, T. A. *J. Am. Chem. Soc.* **1995**, *117*, 3830. (f) Akari, S.; Horn, D.; Keller, H.; Schrepp, W. *Adv. Mater.* **1995**, *7*, 549. (g) van der Vegte, E. W.; Hadziioannou, G. *Langmuir* **1997**, *13*, 4357. (h) Sinniah, S. K.; Steel, A. B.; Miller, C. J.; ReuttRobey, J. E. *J. Am. Chem. Soc.* **1996**, *118*, 8925. (i) Werts, M. P. L.; van der Vegte, E. W.; Grayer, V.; Esselink, E.; Tsitsilianis, C.; Hadziioannou, G. *Adv. Mater.* **1998**, *10*, 452. (j) Schönherr, H.; Vancso, G. J. *J. Polym. Sci. B Polym. Phys.* **1998**, *36*, 2483. (k) Schönherr, H.; Hruska, Z.; Vancso, G. J. *Macromolecules* **1998**, *31*, 3679. (l) Schönherr, H.; van Os, M. T.; Förch, R.; Timmons, R. B.; Knoll, W.; Vancso, G. J. *Chem. Mater.* **2000**, *12*, 3689. (m) Schönherr, H.; Hruska, Z.; Vancso, G. J. *Macromolecules* **2000**, *33*, 4532.

20 Kailas, L.; Audinot, J.N.; Migeon, H. N.; Bertrand, P. *App. Surf. Sci*. **2004**, *231*, 289.

21 (a) Vancso, G. J.; Hillborg, H.; Schönherr, H. *Adv. Polym. Sci.* **2005,** *182*, 55. (b) Herrero, M.; Navarro, R.; Garcia, N.; Mijangos, C.; Reinecke, H. *Langmuir* **2005**, *21*, 4425 and references herein.

22 Hillborg, H.; Tomczak, N.; Oláh, A.; Schönherr, H.; Vancso, G. J. *Langmuir* **2004**, *20*, 785.

23 In the so-called force-volume images the pull-off forces can be graphically displayed in a layered image. Pull-off forces larger than a certain value are displayed in a gray scale. As an attractive force has per definition a negative sign, the scaling ranges from dark tones (high pull-off force) to bright tones (low pull-off force).

24 (a) Feldman, K.; Tervoort, T.; Smith, P.; Spencer, N. D. *Langmuir* **1998**, *14*, 372. (b) Johnson, K. L.; Kendall, K.; Roberts, A. D. *Proc. R. Soc. London A* **1971**, *324*, 301. (c) Derjaguin, B. V.; Muller, V. K.; Toporov, Y. P. *J. Coll. Interf. Sci.* **1975**, *53*, 314.

25 *Polymer Handbook*, 3rd ed. Brandrup, J.; Immergut, E. H. John Wiley & Sons: New York, **1989**.

26 Dordi, B.; Pickering, J. P.; Schönherr, H.; Vancso, G. J. *Surf. Sci.* **2004**, *570*, 57.

27 (a) Berger, C. E. H.; van der Werf, K. O.; Kooyman, R. P. H.; de Grooth, B. G.; Greve, J. *Langmuir* **1995**, *11*, 4188. (b) Schönherr H.; Feng C. L.;Tomczak, N; Vancso G. J. *Macromolecular Symposia*. **2005**, *in press*.

28 Hioka, N.; Chowdhary, R.K.; Chansarkar, N.; Delmarre, D.; Sternberg, E.; Dolphin, D. *Can. J. Chem./Rev. can. chim*. **2002**, *80*, 1321.

29 Binnig, G.; Rohrer, H. *Helv. Phys. Acta* **1982**, *55*, 726.

30 (a) Piner, R. D.; Zhu, J.; Xu, F.; Hong, S.; Mirkin, C. A. *Science* **1999**, *283*, 661. (b) Ginger, D. S.; Zhang, H.; Mirkin, C. A. *Angew. Chem. Int. Ed.* **2004**, *43*, 30.

31 Salazar-Nunez, B. M.Sc. thesis, University of Twente, Enschede, The Netherlands, 2005.

32 McKendry, R.; Huck, W. T. S.; Weeks, B.; Florini, M.; Abell, C.; Rayment, T. *Nano Lett.* **2002**, *2, 713.*

33 Degenhart, G. H.; Dordi, B.; Schönherr, H.; Vancso, G. J. *Langmuir* **2004**, *20*, 6261.

34 (a) Macbeath, G.; Schreiber, S. L. *Science* **2000**, *289*, 1760. (b) Mrksich, M.; Whitesides, G. M. *Trends Biotechnol*. **1995**, *13*, 228. (c) Yadavalli, V. K.; Koh, W. G.; Lazur, G. J.; Pishko, M. V. *Sens. Actuators* **2004**, *97*, 290.

35 Kane, R. S.; Takayama, S.; Ostuni, E.; Ingber, D. E.; Whitesides, G. M. *Biomaterials* **1999**, *20*, 2363.

36 MacBeath, G.; Schreiber, S. L. *Science* **2000**, *289*, 1760.

37 Lee, J. N.; Park, C.; Whitesides, G. M. *Anal. Chem.* **2003**, *75*, 6544.

38 Schönherr, H. Salazar, R. B.; Shovsky, A.; Vancso, G.J. *PMSE* **2006**, *in press*.

Summary

The aim of the work described in this Thesis was to investigate interfacial reactions in confinement on ultrathin homopolymer and diblock copolymer films, the immobilization of (bio)molecules and the fabrication of biomolecular patterns by reactive microcontact printing (μCP) on these reactive polymer films. Taking advantage of the microphase separation of diblock copolymer films, the fabrication of nanopatterns was investigated, which could contribute to the future development of a model system that enables one to area-selectively deposit (write) and address (read out) (bio)molecules.

Chapter 2 presented an overview of (bio)reactive surfaces and biointerfaces based on organic and polymeric films, their characterization, as well as surface reactions and patterning of these films. The μCP technique was introduced in detail owing to its central role in this Thesis as a flexible approach for the production of micrometer and sub-micrometer scale patterns. Block copolymers were also discussed as materials used in a "bottom-up" approach to prepare nanometer scale patterns by exploiting the characteristic microphase separation.

In Chapter 3, the effect of the spatial confinement of the reactants on the kinetics of the hydrolysis of poly(*N*-hydroxysuccinimidyl methacrylate) (PNHSMA) and polystyrene-*block*-poly(*tert*-butyl acrylate) (PS_n-b-$PtBA_m$) ultrathin films was systematically investigated. The activation energies determined according to the Arrhenius equation, and in particular the activation entropies calculated according to the transition state theory, revealed that steric crowding in the surface-near region and tightness of the transition state is less pronounced in the polymer films compared to related self-assembled monolayers (SAMs) that expose the same reactive ester groups. Apparent rate constants calculated according to Fourier transform infrared (FTIR) spectroscopy and contact angle (CA) data for both polymer films and SAMs directly demonstrated that the polymer films are characterized by higher reactivity, as well as a higher density of reactive functional groups near and at the polymer surface. However, the reactivity on polymer films was reduced compared to reactivity in solution because of restricted access of reactants and reduced mobility of the ester functional groups in these films. Finally, it was found that polymer film thickness, thermal pre-treatment of the films, block copolymer composition for PS_n-b-$PtBA_m$ and local surface composition did not affect the rate constants.

Spin-coated thin films of PNHSMA were investigated in Chapter 4 as reactive layers for obtaining platforms for biomolecule immobilization with high molecular loading. The surface reactivity of PNHSMA films in coupling reactions with amino-functionalized poly(ethylene glycol) (M_n: 500 g/mol) (PEG_{500}-NH_2) was determined by FTIR spectroscopy, X-ray photoelectron spectroscopy (XPS), fluorescence microscopy and ellipsometry measurements, respectively. The PEG_{500}-NH_2 loading observed was about three times higher for the polymer thin films compared to SAMs of 11,11′-dithiobis(*N*-hydroxysuccinimidyl undecanoate) (NHS-C10) on Au. These data indicate that the

coupling reactions are not limited to the outermost surface layer of the polymer films, but proceed into the surface-near regions of the films. An increased loading was also observed by surface plasmon resonance (SPR) measurements for the covalent immobilization of amino-functionalized probe DNA. Hybridization of fluorescently labeled target DNA was successfully detected by fluorescence microscopy and surface plasmon resonance-enhanced fluorescence spectroscopy (SPFS), thereby demonstrating that thin films of PNHSMA show robustness and comprise an attractive and simple platform for the immobilization of biomolecules with high molecular densities. Finally, the successful application of PNHSMA films as platform for biosensors for pathogen detection was demonstrated using a protein G mediated antibody-based detection of listeria.

The investigation of PS_{690}-b-$PtBA_{1210}$ films and their derivatization to obtain tailored biointerfaces was presented in Chapter 5. Derivatized PS_{690}-b-$PtBA_{1210}$ films showed good stability under a broad range of conditions. Hydrolysis of the reactive *t*-butyl ester groups was performed in trifluoroacetic acid, 3M aqueous HCl, and in the gas phase (HCl). After the subsequent activation with NHS ester groups a variety of amino-functionalized (bio)molecules were covalently immobilized on the previously hydrolyzed surfaces. The reactivity of the PS_{690}-b-$PtBA_{1210}$ films and in particular the controllable loading with amino functionalized PEG_{500}-NH_2 were studied by FTIR and XPS. Subsequently, the immobilization of biologically relevant molecules, such as bovine serum albumin (BSA) and poly(L)lysine (PLL), on PS_{690}-b-$PtBA_{1210}$ films were studied by fluorescence microscopy. To demonstrate possible applications of the PS_{690}-b-$PtBA_{1210}$ based platform as viable biointerfaces, hybridization of target DNA with previously covalently immobilized probe DNA, as well as the interaction of two different types of cells, i.e. K562 and pancreatic cancer cells, on functionalized PS_{690}-b-$PtBA_{1210}$ films were investigated.

In Chapter 6, the fabrication of robust biomolecule microarrays on spin-coated thin films of PNHSMA on oxidized silicon and glass by reactive μCP was described. The approach combines the advantages of activated polymer thin films as coupling layers, characterized by high reactivity and high molecular loading (Chapters 3 and 4), with the versatility and flexibility of soft lithography. The transfer of amino end functionalized PEG_{500}-NH_2 from oxidized poly(dimethyl siloxane) (PDMS) elastomer stamps to PNHSMA films was shown by FTIR spectroscopy, XPS, fluorescence microscopy and ellipsometry measurements to result in covalent coupling and identical grafting densities as reported in Chapter 4 for coupling from solution. The PEG-protected areas effectively inhibited the adsorption of fluoresceinamine, BSA, as well as 25-mer DNA, while the unreacted NHS ester groups retained their reactivity towards primary amino groups. Biomolecule microarrays were thus conveniently fabricated in a 2-step procedure. The hybridization of target DNA to immobilized probe DNA in micropatterns proved the concept of reactive μCP on activated polymer films for obtaining robust patterned platforms for biomolecule immobilization and screening.

Three different lithographic approaches to produce chemical patterns on ultrathin PS_{690}-b-$PtBA_{1210}$ films were introduced in Chapter 7, which were expanded to obtain patterns of biomolecules with

(sub)micrometer feature sizes. In approach (A), PS_{690}-b-$PtBA_{1210}$ films were homogeneously hydrolyzed and subsequently activated with NHS. Fluoresceinamine and BSA were patterned and covalently bound on the activated polymer films in sequential direct molecular transfer steps using reactive μCP. NHS functionalized polymer films were also patterned with PEG_{500}-NH_2 by reactive μCP in approach (B). The PEG layer was used as antifouling layer to prevent the non-specific adsorption of (bio)molecules in the subsequent covalent coupling step of fluoresceinamine and BSA carried out in solution. The area selective immobilization was also successfully demonstrated for 25-mer probe DNA, as shown by the fluorescence microscopic detection of the hybridization of dye-labeled target DNA. In approach (C), the polymer films were firstly locally hydrolyzed with trifluoroacetic acid that was locally applied on the films using acid soaked PDMS stamps. A detailed study of the reactive μCP mechanism led to the conclusion that ink spreading and diffusion must be controlled for faithful pattern transfer, in particular on the sub-μm level. In addition, it was found that patterns with micrometer scale dimensions could be fabricated by using stamps with > 10 μm dimensions by controlling the spreading of trifluoroacetic acid. Thus, ultrahigh density patterns could be conveniently fabricated.

In Chapter 8, nanofabrication and the subsequently selective immobilization of (bio)molecules on reactive PS_{690}-b-$PtBA_{1210}$ ultrathin films were studied. As revealed by AFM and spectroscopic techniques, the surface exposed PtBA islands in a matrix of unreactive PS. The films were then hydrolyzed with trifluoroacetic acid and activated with NHS. The domain selective immobilization of fluoresceinamine on the films was globally analyzed by fluorescence microscopy and was also investigated on the nanometer scale by AFM adhesion force mapping in the force-volume mode. Finally, the area selective functionalization of BSA and polyamidoamine (PAMAM) dendrimers on nanopatterned block copolymer thin films on the micrometer and sub-micrometer scales was carried out by reactive microcontact printing and the dip-pen nanolithography technique, respectively, to yield surfaces that are patterned with (bio)molecules on multiple length scales. Therefore the polymer thin film platforms and patterning approaches investigated herein provide the opportunity to study a broad variety of surface-mediated biological recognition processes in the future.

Samenvatting

In dit proefschrift wordt een overzicht gegeven van het onderzoek dat verricht is naar ruimtelijk begrensde oppervlaktereacties van ultradunne homopolymeer en diblok copolymeer lagen, de immobilisatiereacties van (bio)moleculen en het ontwikkelen van biomoleculaire patronen op reactieve polymeerlagen door middel van microcontact printing (μCP). Gebruikmakend van het feit dat diblok copolymeer lagen fasescheiding op microniveau vertonen, is er onderzoek verricht naar de fabricage van diverse patronen op nanoniveau. Dit onderzoek beoogt een bijdrage te leveren aan de ontwikkeling van een model voor het selectief plaatsen van (bio)moloculen op een oppervlak en de selectieve communicatie met deze (bio)moleculen.

Hoofdstuk 2 geeft een overzicht van de (bio)reactieve oppervlakken voor zowel organische als polymeerlagen, de karakterisering van deze lagen als ook de oppervlakte reacties en de vorming van patronen op nanoniveau. De μCP techniek wordt in detail behandeld, aangezien deze een centrale rol in het proefschrift speelt. Aanleiding hiervoor is het feit dat deze techniek een flexibele benadering voor de fabricage van patronen op micrometer en sub-micrometer niveau vormt. Verder zal ingegaan worden op de rol die blokcopolymeren spelen als interessante materialen voor een "bottom-up" benadering voor het vervaardigen van oppervlakken met patronen op nanometerschaal door gebruik te maken van de karakteristieke fasescheiding.

In Hoofdstuk 3 wordt het effect van reacties in een ruimtelijke begrensde omgeving beschreven aan de hand van de systematische beschrijving van de kinetiek van de hydrolyse van poly(*N*-hydroxysuccinimidyl methacrylaat) (PNHSMA) en dunne lagen van polystyreen-*blok*-poly(*tert*-butyl acrylaat) (PS_n-*b*-P*t*BA_m). De activeringsenergie (bepaald met behulp van de Arrheniusvergelijking) alsmede de aciveringsentropieën (bepaald met behulp van de transition state theorie), laten duidelijk zien dat er sprake is van sterische hindering in de gebieden die zich dicht bij het oppervlak bevinden. In vergelijking met self-assembled monolayers (SAMs) blijkt deze sterische hindering echter minder uitgesproken aanwezig te zijn (als zowel het oppervlak van de polymeerlaag als dat van de SAM dezelfde functionele ester eindgroepen hebben). Reactiesnelheidsconstanten (bepaald met behulp van Fourier tranform infrarood spectroscopie (FTIR)) en contacthoekmetingen voor polymeerlagen en SAMs tonen aan dat de polymeerlaag een duidelijk hogere reactiesnelheid en dichtheid van functionele eindgroepen aan en rond het oppervlak heeft.

De reactiviteit van de polymeerlagen is echter lager wanneer deze vergeleken wordt met dezelfde reactie in oplossing. Dit wordt veroorzaakt door de beperkte toegankelijkheid van het oppervlak voor reactanten en de verminderde mobiliteit van de functionele ester eindgroepen van deze polymeerlagen. Tenslotte kan geconcludeerd worden dat de reactiesnelheidsconstanten niet beïnvloed worden door de dikte van de polymeerlaag, thermische voorbehandeling van deze laag, PS_n-*b*-P*t*BA_m blokcopolymeer samenstelling en de lokale oppervlakte samenstelling.

Dunne PNHSMA lagen (geproduceerd door middel van spin-coating) worden nader beschreven in Hoofdstuk 4. Deze lagen zijn erg geschikt als reactieve oppervlakken voor de immobilisatie van biomoleculen met een hoge graad van moleculaire oppervlaktebedekking. De oppervlakte reactiviteit van PNHSMA lagen in covalente bindingsreacties met amino-gefunctionaliseerd poly(ethyleen glycol) (Mw: 500 g/mol, PEG_{500}-NH_2) is bepaald met behulp van FTIR spectroscopie, X-ray photoelectron spectrocopy (XPS), fluorescentie microscopie en ellipsometrie. Hieruit kan geconcludeerd worden dat de oppervlaktebedekking met PEG_{500}-NH_2 drie keer zo hoog is voor deze polymeerlagen ten opzichte van SAMs van 11,11'-dithiobis(*N*-hydroxysuccinimidyl undecanoaat) (NHS-C10) op goud. Deze gegevens duiden erop dat de koppelingsreactie zich niet beperkt tot het buitenste oppervlak van de dunne laag, maar ook plaatsvindt in gebieden in de buurt van dit oppervlak. Bovendien is met behulp van surface plasmon resonance (SPR) een toename van oppervlaktebedekking voor amino-gefunctionaliseerd "probe DNA" vastgesteld. Hybridisatie van DNA (dat gelabeled was met een fluorescerend molecuul) is daarbij succesvol vastgesteld door middel van fluorescentie microscopie en surface plasmon resonance-enhanced fluorescence microscopy (SPFS). Bovenstaand onderzoek toont aan dat de dunne PNHSMA lagen een robuust en eenvoudig systeem vormen als platform voor de immobilisatie van biomoleculen met een hoogwaardige oppervlaktebedekking op moleculair niveau. Verder werd ook de succesvolle toepassing van PNHSMA lagen als platform voor biosensoren aangetoond. Hiervoor werd gebruik gemaakt van een biosensor opgebouwd uit "proteinG" antilichamen, die de detectie van de darmbacterie Listeria mogelijk maken.

Onderzoek naar PS_{690}-*b*-P*t*BA_{1210} lagen en chemische derivaten daarvan worden beschreven in Hoofdstuk 5. Deze lagen kunnen gebruikt worden voor de productie van speciaal ontwikkelde bio-oppervlakken en hebben verder als kenmerk dat ze een hoge stabiliteit vertonen onder een divers spectrum van omstandigheden. De hydrolyse van de reactieve *tert*-butyl ester groepen is uitgevoerd met behulp van trifluorazijnzuur, 3M HCl en HCl in de gasfase. Na de daaropvolgende activering (met behulp van NHS ester groepen) is het mogelijk om verscheidene amino-gefunctionaliseerde (bio)moleculen covalent te koppelen aan het al eerder gehydrolyseerde oppervlak. De reactiviteit van de PS_{690}-*b*-P*t*BA_{1210} lagen, als ook de gecontroleerde oppervlaktebedekking met PEG-NH_2 zijn bepaald met behulp van FTIR en XPS. Verder werd ook de immobilisatie van biologisch relevante moleculen voor biosensoren, zoals bovine serum albumin (BSA) en poly(L)lysine (PLL), bestudeerd met behulp van fluorescentie spectroscopie.

Om aan te tonen dat PS_{690}-*b*-P*t*BA_{1210} lagen erg geschikt zijn als bio-oppervlakken voor biosensorplatformen, is de hybridisatie van "target DNA" met vooraf geïmmobiliseerd "probe DNA" bekeken. Ook is de interactie tussen deze gefunctionaliseerde polymeerlagen met twee verschillende type cellen, namelijk K562 en kanker cellen (uit de alvleesklier) onderzocht.

In Hoofdstuk 6 wordt de fabricage van robuuste biomoleculaire microarrays op dunne PNHSMA lagen met behulp van "reactive μCP" beschreven. Deze dunne lagen werden ook nu geproduceerd met

behulp van spin-coating op SiO_2- of glassubstraten. “Reactive μCP” combineert de al eerder bepaalde hoge oppervlaktebedekking en reactiviteit (zie ook Hoofdstuk 3 en 4) én de mogelijkheid om geactiveerde polymeerlagen te gebruiken voor covalente bindingsreacties met de diversiteit en flexibiliteit van deze soft lithography methode. De overdracht van PEG_{500}-NH_2 van de elastomere en geoxideerde poly(dimethylsiloxaan) (PDMS) stempel naar de PNHSMA lagen werd onderzocht aan de hand van FTIR, XPS, fluorescentie microscopie en ellipsometrie metingen. Hierbij werden covalente bindingsreacties aangetoond met dezelfde oppervlakte bedekkingsgraad voor koppelingsreacties vanuit oplossing (zie ook Hoofdstuk 4).

De gebieden die met PEG bedekt waren, bleken de adsorptie van fluoresceinamine, BSA als ook 25-mer DNA effectief tegen te gaan, terwijl de niet-gereageerde NHS ester groepen hun functionaliteit behielden ten opzichte van primaire aminogroepen. Biomoleculaire microarrays werden dan ook eenvoudig geproduceerd met behulp van een tweestaps methode. Verder werd aangetoond dat “reactive μCP” een uitstekende methode is voor de fabricage van robuuste platformen voor biomoleculaire immobilisatie en screening. Hiervoor werd de hybridisatie van “target DNA” met geïmmobiliseerde “probe DNA” in micropatronen onderzocht.

In Hoofdstuk 7 worden drie verschillende lithografische benaderingen besproken om chemische patronen op ultradunne PS_{690}-b-$PtBA_{1210}$ lagen te fabriceren. Deze lithografische benaderingen zijn waar nodig aangepast om biomoleculaire patronen op (sub)micrometer niveau te produceren. In aanpak A zijn de PS_{690}-*b*-P*t*BA_{1210} lagen homogeen gehydrolyseerd en vervolgens geactiveerd met behulp van NHS. “Reactive μCP” is gebruikt voor de covalente koppeling van fluoresceinamine en BSA op de geactiveerde polymeerlagen. Ook werden patronen aangebracht op NHS-gefunctionaliseerde polymeerlagen met behulp van “reactive μCP” (aanpak B). Het gevormde PEG-oppervlak werd vervolgens gebruikt om niet-specifieke adsorptie van (bio)moleculen tegen te gaan. Deze laag zorgt er echter ook voor dat er geen reactie optreedt tussen het al eerder gecreëerde PEG-oppervlak en de daaropvolgende covalente koppelingreactie in oplossing van fluoresceinamine en BSA. Ook werd de selectieve immobilisatie van 25-mer DNA succesvol uitgevoerd en onderzocht met behulp van fluorescentie microscopie. In aanpak C werden de polymeerlagen lokaal gehydrolyseerd met een trifluorazijnzuur doordrenkte PDMS stempel.

Uit een gedetailleerd onderzoek naar het mechanisme van “reactive μCP” blijkt dat diffusie en spreiding van inkt goed gecontroleerd dienen te worden tijdens de stempelprocedure om betrouwbare patroonoverdracht te bereiken, vooral op sub-micrometer niveau. Bovendien is gebleken dat patronen met afmetingen op micrometerschaal gefabriceerd kunnen worden met stempels met afmetingen >10 μm door de spreiding van trifluorazijnzuur te controleren.

In Hoofdstuk 8 wordt de nanofabricage en achtereenvolgende selectieve immobilisatie van (bio)moleculen op reactieve en ultradunne PS_{690}-*b*-P*t*BA_{1210} lagen besproken. Hierbij werd cyclohexaan gebruikt als een selectief oplosmiddel en de daaruit resulterende reorientatie van het

oppervlak werd bestudeerd met behulp van atomic force microscopy (AFM). De lagen werden vervolgens gehydroliseerd met trifluorazijnzuur en geactiveerd met NHS. De domeinselectieve immobilisatie van fluoresceinamine op deze lagen werd vervolgens globaal geanalyseerd door middel van fluorescentie microscopie. Verder werd dit fenomeen ook op de nanometerschaal onderzocht met behulp van "AFM adhesion force mapping" in force-volume mode. Tenslotte werd de selectieve functionalisering van BSA en polyamidoamine (PAMAM) dendrimeren uitgevoerd met behulp van respectievelijk "reactive μCP" en dip-pen nanolithography (DPN). Dit leverde oppervlakken met verscheidene patronen en bovendien verschillende interessante patroonafmetingen op. Deze dunne laag polymeerplatformen en de verschillende benaderingen voor het fabriceren van patronen vormen dan ook een interessant onderzoeksgebied voor de toekomstige bestudering van biologische detectie- en herkenningsprocessen op polymeeroppervlakken.

Acknowledgements

Time is flying! Four years will become past soon for me in the Netherlands. I still remember the time when I firstly put my eyes onto Enschede and University of Twente four years ago, I really had a faint idea about them. After four years I cannot imagine a better choice than coming here, a place where I learned very much from a professional and personal perspective. All these things would have not been possible without a number of people, excellent friends and brilliant scientists, whom I have been so fortunate to meet.

First of all, I would like to thank my promoter, Prof. Dr. G. Julius Vancso, for offering me the opportunity pursuing my Ph.D study in MTP group. Dear Julius, thanks a lot for your guidance and fruitful discussion for my research during my last four years. I am so proud to have such invaluable chances to work in your group. Your encouragement makes me feel like so confident for my future. I really appreciate your personal advice and concern on my future.

I would like to thank my daily supervisor Dr. Holger Schönherr. Dear Holger, thanks for your guidance and always being available for discussions. Thanks a lot for the freedom and lively atmosphere you have given to me, where I have enjoyed the collaboration with many people. Thanks for your patience in correcting my papers, posters, and thesis, where I learned a lot from inside about presenting scientific results. Thanks a lot for you teaching me so much how to write and think in English.

In this thesis, there are numerous people who contribute to the research. I firstly own many thanks to Dr. Zhihong Zhang, Dr. Renate Förch and Prof. Wolfgang Knoll (MPIP, Mainz, Germany) for their help in doing SPR experiment and Prof. Qingrong Huang (Department of Food Science, Rutgers University) for fluorescent microscopy experiment described in Chapter 4. I am very grateful to Dr. Maria. F. Garcia-Parajo and Ir. Anita. Bouma (Applied Optics Group, MESA+, University of Twente) and Dr. J. Schnekenburger (University of Münster, Germany) for their collaborative work presented in Chapter 5. I also would like to thank Dr. Henk-Jan van Manen (Biophysical Engineering Group, Faculty of Science and Technology University of Twente))for his help with the fluorescence experiments.

I owe my appreciation to Dr. Mark Hempenius. I still remember you were always so kind and patient to help me since I came here. I learned so much about polymerization from you. Dear Mark, thanks a lot! Appreciative words cannot be enough to thank Ing. Clemens Padberg for his constant help with instruments and computers. I remember you were always so kind and patient to help me to save my laptop, whenever I asked you to help me. I would like to mention all the ladies: Genevieve, Lena, Karin, Cindy, Gerda, Thelma, and Zlata for their kind help during my last four years.

Acknowledgements

It would be impossible to mention all the names of people that have helped me in one way or another. I would like to thank all past and present MTP members during my stay in Twente University: Léon, Maria, Attila, Beata, Barbara, DW, Shan, Eva, Nikodem, Willem-Jan, Giorgio, Nina, Alex, Steffi, Henrik, Anika, Monique, Jing, Marco, Elske, Yujie, Qi, Hui, Inyee, Szczepan, Marina, Eugenia, Edmondo, Denis, Ramon, Joris, Oya, Thomas. Thank you for all the working hours together and unforgettable time that I shared with you.

During these years, many Chinese friends have given me this or that help. We stay together and have a lot of fine during last several years. Dan Liu, Shuying Gu, Jing Yu, Wenbin Hu, Fenghua Meng, Jian Wu, Minshi Li, Wei Chen, Jianjun Zhu, Yi Wei, Boon-hua, Xuemei Li, Xiao Li, Yagang, Zhang, Yu Wang, Zhiyuan Zhong, Shan Zou, Shen Ran, Mao Ye, Li, Yongrong Yang, Yizhi He, Fahong Li, Zheng Zhang, Min Fang, Chunlin Song, Xin Wang, your companion, your help when I needed, and your sharing the wonderfull moments have made all these years more enjoyable.

Finally, and most importantly, I would like to thank my wife Hua Gong, my daughter Yueyue (Yolanda) Feng, and my son Chen (Brian) Feng for their unconditional support and absolute understanding. We spent so much wonderful time together during last four years. Whatever for my experiment, you are always my strongest support behind me. Without your love, support and understanding, it will be not possible to finish this work. In addition, I want to thank my parents, my brothers, and my sisters for their consistent love and support.

冯传良

11. 2005

Publications

Reviewed

Chuan Liang Feng, G. Julius Vancso, Holger Schönherr, "Fabrication of Robust Biomolecular Patterns by Reactive Microcontact Printing on Activated Polymer Films"*, Advanced Functional Materials* 2006, *in press*.

Chuan Liang Feng, Holger Schönherr, G. Julius Vancso, "Interfacial Reactions in Confinement: Kinetics and Temperature Dependence of the Surface Hydrolysis of Polystyrene-b-Poly(tert-butyl acrylate)"*, Langmuir* 2005, *21*, 2356-2363.

Chuan Liang Feng, Zhihong Zhang, Renate Förch, Wolfgang Knoll, G. Julius Vancso, Holger Schönherr, "Reactive Thin Polymer Films as Platforms for the Immobilization of Biomolecules", *Biomacromolecules*, 2005, *6*, 3243-3251.

Holger Schönherr, Geerten H. Degenhart, Barbara Dordi, **Chuan Liang Feng**, Alexander Shovsky, Dorota I. Rozkiewicz, G. Julius Vancso "Organic and Macromolecular Films and Assemblies as (Bio)reactive Platforms: From Model Studies on Structure-Reactivity Relationships to Sub-Micrometer Patterning", *Advances in Polymer Science* 2005, *in press.*

Holger Schönherr, **Chuan Liang Feng**, Nikodem Tomczak, G. Julius Vancso, "Compositional Mapping of Polymer Surfaces by Chemical Force Microscopy Down to the Nanometer Scale: Reactions in Block Copolymer Microdomains", Macromolecular Symposia, 2005, *in press*.

Holger Schönherr, **Chuan Liang Feng**, Alexander Shovsky, "Interfacial Reactions in Confinement (II): Kinetics and Temperature Dependence of Reactions in Self-Assembled Monolayers Compared to Ultrathin Polymer Films"*, Langmuir*, 2003, *19*, 10843-10851.

Chuan Liang Feng, Jian Jin, Yanjie Zhang, Yanlin Song, Lianying Xie, Guirong Qu, Lei Jiang, Daoben Zhu, "Novel Interfacial Photoisomerization of 4-Hydroxy-3′-Trifluoromethyl-Azobenzene on HOPG Studied by STM"*, Surface Science* 2002, *513*, 111-118.

Chuan Liang Feng, Jian Jin, Yanjie Zhang, Yanlin Song, Lianying Xie, Guirong Qu, Yu Xu, Lei Jiang, "Reversible Light-Induced Wettability of Fluorine-Containing Azobenzene Derivative Langmuir-Blodgett Films"*, Surface and Interface Analysis* 2001, 32, 121-124.

Chuan Liang Feng, Yanjie Zhang, Jian Jin, Yanlin Song, Lianying Xie, Guirong Qu, Lei Jiang, Daoben Zhu, "Wettability of Photoresponsive Fluorine-Containing Azobenzene Polymer in Langmuir-Blidgett Films"*, Langmuir* 2001, *19*, 4593-4597.

Chuan Liang Feng, Jian Jin, Yanjie Zhang, Yanlin Song, Lianying Xie, Guirong Qu, Yu Xu, Lei Jiang, "Self-Assembled Films of Azobenzene Derivative on Liquid/Solid Interface Studied by STM"*, Journal of Electron Microscopy Society,* 2001, *20*, 569-572.

Unreviewed

Holger Schönherr, **Chuan Liang Feng,** G. Julius Vancso, *Polymer Preprints* 2006, *in press*.

Holger Schönherr, **Chuan Liang Feng**, Alexander Shovsky, Geerten H. Degenhart, Barbara Dordi, Zhihong Zhang, Renate Förch, Wolfgang Knoll, G. Julius Vancso, *ACS*, *Polymer Material Science Engineering* 2004, *90*, 147-148.

Holger Schönherr, **Chuan Liang Feng**, Alexander Shovsky, *ACS*, *Polymer Material Science Engineering.* 2003, *89*, 250-251.

Submitted

Chuan Liang Feng, Guirong Qu, Yanlin Song, Lei Jiang, Daoben Zhu. "*Structure Characterization of Azobenzene-Containing Langmuir-Blodgett Films"* 2005*, submitted.*

To be submitted

Chuan Liang Feng, G. Julius Vancso, Holger Schönherr, "*Reactive μCP on Ultrathin Block Copolymer Films: Sub-μm molecular Patterning"*.

Chuan Liang Feng, G. Julius Vancso, Holger Schönherr, "*Reactive μCP on Ultrathin Block Copolymer Films: Investigation of the μCP Mechanism and Applications to Sub-μm (Bio)molecular Patterning"*.

Chuan Liang Feng, G. Julius Vancso, Holger Schönherr, "*Tailored Biointerfaces via Derivatization of Polystyrene-b-Poly(tert-butyl acrylate) Thin Films"*.

Curriculum Vitae

Chuanliang Feng was born on September 4, 1972 in Henan province, P. R. China. He started his study in department of chemistry, Henan Normal University in 1992. After he received his BS degree in 1996, he worked as a teacher in Xinxiang 25th School. Two years later, he went to Institute of Chemistry, Chinese Academy of Sciences and joined the research group of Prof. Dr. Lei Jiang to continue his study as a master student. With the thesis entitled "Controllable Wettability of Interface Materials Under Light", He graduated in 2001. In the same year, he joined Material Science and Technology of Polymer Group In University of Twente, the Netherlands, as a Ph.D student under the supervision of Prof. Dr. G. Julius Vancso and Dr. Holger Schönherr. His Ph.D research subjects were to investigate interfacial reactions in confinement on ultrathin homopolymer and diblock copolymer films, the immobilization of (bio)molecules and the fabrication of biomolecular patterns by reactive microcontact printing (μCP) on these reactive polymer films. From December 18, 2005, he will work in the research group of Prof. Wolfgang Knoll (Max Planck Institute for Polymer Research Material Science, Mainz, Germany) as a postdoctoral researcher.